

# **NEGATIVE REGULATION OF THE JAK/STAT SIGNALLING PATHWAY IN INFLAMMATORY ARTHRITIS**

**ALICIA DERRAC SORIA**

A thesis submitted to Cardiff University  
in candidature for the degree of  
Doctor of Philosophy

June 2020

“One must, from time to time, attempt things that are beyond one’s capacity.”

— Pierre-Auguste Renoir



## Acknowledgements

---

Getting to the end of my PhD has been perhaps more rewarding than I could have ever imagined (despite submitting in the time of Covid-19), and I am hugely grateful to so many wonderful individuals for their contribution throughout this whole process, without whom this thesis would have never been possible.

First and foremost, I would like to thank my supervisor Prof Simon Jones for taking me on as a Research Assistant and for making it possible for me to pursue a PhD alongside. Thank you, Simon, for your incredible support and insight, honest advice and invaluable guidance during this journey. I genuinely admire the trustful atmosphere in your research group. I would also like to thank my co-supervisor Dr Gareth Jones; thanks for always being there when needed, for your immeasurable patience and for being able to look on the bright side of my data. Special acknowledgements go to Dr Xiao Liu; thank you, Tommy, for welcoming me into the lab, and for starting what it later became my PhD project. This thesis simply wouldn't exist without you.

Thank you to every past and present member of the Simon & Gareth Jones' research group, who made my time in the lab a truly unique life experience. To Dr Anna Cardús, thank you for your constant encouragement inside and outside the lab, for being one of the pillars of the group and for always looking out for us. To Dr Jason Twohig, thank you for making the lab meetings so stimulating, for your scientific and artistic feedback and for all the discussions in the office on immunology and life. To Dr Robert Jenkins, thanks for your kindness, constructive advice and for bringing gossip to the office! To Dr David Hill, thanks for all the i.a. injections and for leaving me your RNA-seq legacy; I owe you a lot. To Ben, my writing-up officemate, thanks for your thoughtfulness and generosity, particularly on the bioinformatic side. To Aisling, thank you for being such a great colleague and amazing friend, for being a shoulder to cry on when things went wrong and for those precious moments listening to each other rant. It's been a pleasure to share this PhD craziness with you! To Dr Javier Uceda (1992 – 2018), thanks for all the fun and optimism you brought to all of us and for making the lab and the office a better place. You were taken suddenly and way too soon, but your radiant energy is ever with me, brightening the darkest of days.

To Dr Robert Andrews, thanks for all your help and patience with bioinformatic analyses, and for bringing songs, laughter and your wit into the office. To Dr Katherine Tansey, for teaching me everything I know about R, and to Dr Barbara Szomolay for spending your time clustering and analysing my data. To Dr Catherine Naseriyan and Dr Ann Kift-Morgan (CBS, Cardiff University) for sorting my cells. Everyone from the Tenovus building with whom I shared lunch conversations and all the members of the Spanish-language ('racist') coffee group deserve a thanks for distracting me from my PhD and making my time in work more enjoyable.

I would also like to acknowledge my collaborators from outside of Cardiff University: Prof Nigel J. Stevenson (Trinity College Dublin), Prof Hua Yu and Assoc Prof Martin Kortylewski (City of Hope, California), Prof Jürgen Scheller and Dr Jens Moll (HHU, Düsseldorf) and Prof Costantino Pitzalis and Dr Myles Lewis (The William Harvey Research Institute, Queen Mary University of London). Special gratitude goes out to Versus Arthritis and Wellcome Trust for funding my PhD and to the William Morgan Thomas, the British Society of Immunology (BSI) and the Milstein travel awards which enabled my travel to international conferences to present my research. I would also like to thank Prof Matthias Eberl, Prof Ernest Choy and Dr You Zhou, for taking the time to read my annual progress reports and providing feedback during the appraisals; and to Prof Iain McInnes (University of Glasgow), Dr James Harker (Imperial College London) and Prof Susan Wong, for kindly agreeing to be on my viva examination panel.

Finally, in the non-science category, the people who reminded me that there were more important things in life than failed experiments. All my friends in Cardiff, back home and around the world, thanks for being there over the years, making it all worthwhile; an essential part of this thesis belongs to you all. To my family, thanks for knowing exactly when to tell me what I wanted to hear when I wanted to hear it the most. I couldn't have achieved this without your unconditional love and enduring support. And last, but definitely not least, to Alex. I am forever indebted to science for crossing our paths together. Thank you for hiding me away under your arm when the world got tough and for always having faith in me.

Alicia Derrac Soria  
June 2020

## Summary

---

**Background** — Rheumatoid arthritis (RA) is one of the most common forms of autoimmune disease, affecting about 1% of the population and causing chronic inflammation that primarily affects the joints. Cytokines that signal via the Janus kinase (JAK)/signal transducer and activator of transcription (STAT) signalling pathway are major drivers of synovitis in patients with RA and contribute to the rapid progression of the disease. Biological agents targeting the cytokine interleukin (IL)-6, its receptor system or downstream pathway have revolutionised the treatment of immune-mediated diseases and can induce drug-free remission. However, RA is a highly heterogeneous and complex disease and consequently, around 40% of patients do not respond to current frontline biologics. This has raised the need for alternative therapeutic strategies or precision medicine approaches that improve treatment decisions for RA patients. My thesis aimed to investigate the action of novel therapeutic modalities that target the IL-6 receptor system or downstream signalling cassette to improve understanding of the underlying inflammatory processes that drive synovitis.

**Results** — Exploiting three novel classes of IL-6/STAT3 inhibitors, I have interrogated their mode of action in *in vitro* model systems and animal models of synovitis. (1) Using histopathology and RNA-sequencing of the inflamed synovium, I demonstrated that an anti-cancer therapy (CpG-*Stat3*siRNA) improved arthritis outcome, altered the balance of STAT1/STAT3 signalling and reduced the incidence of ectopic lymphoid-like structures in synovitis. (2) I also used a virus-derived SOCS3 modulator peptide that suppresses STAT3 activity through the induction of SOCS3. This agent was shown to block pathogenic T-helper (Th)17 cell differentiation *in vitro* and reduced disease pathology in mice with antigen-induced arthritis. (3) Blocking of IL-6 trans-signalling pathway with engineered inhibitors (cs-130Fc) based on regulatory domains of the sgp130 receptor proved efficacy over other related therapy variants (e.g., olamkicept) in inhibiting STAT3-driven Th17 cell expansion *in vitro*. In a final approach, I also examined the biology of genes that are suppressed by IL-6 and IL-27 in CD4<sup>+</sup> T-cells. These factors might have immune-protective function in synovitis, and initial studies are presented on the identification of CRTAM as one such factor and its inflammatory regulation in mouse synovitis.

**Conclusions** — These studies showcase how JAK/STAT signalling through the IL-6 receptor cassette may be controlled at multiple levels and further demonstrate how investigations into their mode of action help to unearth new understanding of IL-6 biology in RA.

## PUBLICATIONS

### In preparation

**Derrac Soria A**, Liu X, Cossins BC, Hill DG, Andrews R, Szomolay B, Cardus Figueras A, Yu H, Kortylewski M, Jones GW, Jones SA. *Therapeutic targeting of the latent transcription factor STAT3 in inflammatory arthritis*.

**Derrac Soria A**<sup>\*</sup>, Liu X<sup>\*</sup>, Cardus Figueras A, Twohig JP, Andrews R, Jenkins BJ, Thompson C, Choy E, Lewis MJ, Pitzalis C, Jones GW, Jones SA. *CRTAM is regulated by IL-6 and IL-27 in inflammatory arthritis*. <sup>\*</sup> These authors contributed equally to this work.

### Under review

Heise D, Dambietz C, Hansen S, Akbarzadeh M, Waetzig GH, **Derrac Soria A**, Jones SA, Dvorsky R, Ahmadian MR, Scheller J, Moll JM. *Selective inhibition of IL-6 but not IL-11 trans-signalling by chimeric soluble gp130 (cs-130)*. **Science Signaling**. [Impact factor; IF 6.481]

### 2020

Lucchesia D, Coleby R, Pontarini E, Prediletto E, Rivellese F, Hill DG, **Derrac Soria A**, Jones SA, Humphreys I, Nurhan S, Anwar T, Pitzalis C, Jones GW, Bombardieri M. *Impaired IL-27 mediated control of CD4<sup>+</sup> T cells function impacts on ectopic lymphoid structures formation in patients with Sjögren's syndrome*. **Arthritis & Rheumatology**. [Impact factor; IF 9.002]

### 2019

Twohig JP<sup>\*</sup>, Cardus Figueras A<sup>\*</sup>, Andrews R, Wiede F, Cossins BC, **Derrac Soria A**, Lewis MJ, Townsend MJ, Millrine D, Li J, Hill DG, Uceda Fernandez J, Liu X, Szomolay B, Pepper CJ, Taylor PR, Pitzalis C, Tiganis T, Williams NM, Jones GW and Jones SA. *Activation of naïve T-cells re-tunes STAT1 signalling to deliver unique cytokine responses in memory CD4<sup>+</sup> T-cells*. **Nat Immunol**. [Impact factor; IF 23.530]. <sup>\*</sup> These authors contributed equally to this work.

### 2016

Catar R, Witowski J, Zhu N, Lucht C, **Derrac Soria A**, Uceda Fernandez J, Chen L, Jones SA, Fielding CA, Rudolf A, Topley N, Dragun D, Jörres A. *IL-6 Trans-Signaling Links Inflammation with Angiogenesis in the Peritoneal Membrane*. **JAm Soc Nephrol**. [Impact factor; IF 8.547]

## PRESENTATIONS AND SCIENTIFIC CONFERENCES

**Oral Presentation** — *Therapeutic targeting of the latent transcription factor Stat3 in inflammatory arthritis.* **Derrac Soria A**, Liu X, Cossins BC, Hill DG, Andrews R, Szomolay B, Yu H, Kortylewski M, Jones GW, Jones SA. Cardiff University Infection and Immunity Annual Meeting 2019, Cardiff City Stadium, Cardiff, UK. November 2019.

**Image Presentation** — 2<sup>nd</sup> prize winner of the Images of Research Event. Doctoral Academy, Cardiff University. December 2018.

**Oral Presentation** — *Negative regulation of JAK/STAT signalling pathway in inflammatory arthritis.* Cardiff University Infection and Immunity Seminar Series: final year PhD students. School of Medicine, Cardiff University. December 2018.

**Poster Presentation** — *Negative regulation of CRTAM by IL-6 and IL-27 in inflammatory arthritis.* **Derrac Soria A**, Liu X, Cardus Figueras A, Twohig JP, Andrews R, Jenkins BJ, Jones GW, Jones SA. Cardiff University Infection and Immunity Annual Meeting 2018, Cardiff City Stadium, Cardiff, UK. November 2018.

**Posters (2) Presentation** — (1) *Negative regulation of CRTAM by IL-6 and IL-27 in inflammatory arthritis.* **Derrac Soria A**, Liu X, Cardus Figueras A, Twohig JP, Andrews R, Jenkins BJ, Jones GW, Jones SA. (2) *Therapeutic targeting of the latent transcription factor STAT3 in inflammatory arthritis.* **Derrac Soria A**, Liu X, Cossins B, Andrews R, Szomolay, Yu H, Kortylewski M, Jones GW, Jones SA. 6th Annual Meeting of the International Cytokine & Interferon Society (ICIS), Westin Boston Waterfront, Boston, USA. October 2018.

**Oral Presentation** — *Evaluation of novel treatment strategies for Inflammatory Arthritis: novel STAT3 blockers.* Arthritis Research UK ARUK visit to Cardiff University. February 2018.

**Oral Presentation** — *Playing with the fire of inflammation.* 3 Minute Thesis (3MT). 32<sup>nd</sup> Annual Schools of Medicine and Dentistry Postgraduate Research Day, Cardiff. January 2018.

**Poster Presentation** — *A virus-derived peptide from the P7 protein of Hepatitis C virus blocks experimental arthritis through induction of SOCS3.* **Derrac Soria A**, Wubben R, Bloemenkamp L, Stevenson NJ, Jones GW, Jones SA. Cardiff University Infection and Immunity Annual Meeting 2017, Wales Millennium Centre, Cardiff, UK. November 2017. \*

\*Received 'Peter Tomasec prize for an outstanding poster presentation' Award

# Abbreviations

---

## A

<i>A. actinomycetemcomitans</i>	<i>Aggregatibacter actinomycetemcomitans</i>
aa	Aminoacid
Ab	Antibody
AC	Adenylate cyclase
ACPAs	Anti-citrullinated protein antibodies
ACR	American College of Rheumatology
Actb	Actin beta
ADAM	Adamalysin and desintegrin-associated metalloprotease
Ahr	Aryl hydrocarbon receptor
AI	Arthritic index
AIA	Antigen-induced arthritis
AID	Activation-induced cytidine deaminase
Akt/PKB	Protein kinase B
ANOVA	Analysis of variance
APC	Antigen presenting cell
APRIL	A proliferation-inducing ligand
ATAC-seq	Assay for transposase-accessible chromatin-seq
ATP	Adenosine triphosphate

## B

BAFF	B-cell activating factor
Bcl6	B-cell lymphoma 6
BCR	B-cell receptor
BLAST	Basic local alignment search tool
BLyS	B lymphocyte stimulator
bp	Base pair
BSA	Bovine serum albumin

## C

CADM1	Cell adhesion molecule 1
CAML	Calcium modulating ligand
CCL	Chemokine (C-C motif) ligand
CCP2	Cyclic citrullinated peptide 2
CCR	Chemokine (C-C motif) receptor
CD	Cluster of differentiation
CDAI	Clinical disease activity index
cDNA	Complementary DNA
CFA	Complete Freund's adjuvant
ChIP	Chromatin immunoprecipitation
CIA	Collagen-induced arthritis
CIS	Cytokine-induced STAT inhibitor
CLB	Cell lysis buffer
COOH	Carboxylic acid

CpG ODN	Short single-stranded synthetic DNA containing cytosine and guanine triphosphate deoxynucleotides linked through a phosphodiester
CpG site	DNA region where a cytosine and a guanine deoxynucleotides are separated by only one phosphate group
CRP	C-reactive protein
CRTAM	Cytotoxic and regulatory T-cell molecule/ Class-I MHC-restricted T-cell associated molecule
cs	Chimeric soluble
Ct	Threshold cycle
CTL	Cytotoxic T-lymphocyte
CTLA4	CTL antigen 4
CXCL	Chemokine (C-X-C motif) ligand
CXCR	Chemokine (C-X-C motif) receptor

**D**

DAB	3,3'-diaminobenzidine
DAMP	Danger-associated molecular pattern
DAPI	4',6-diamidino-2-phenylindole
DAS28	Disease activity scores
DC	Dendritic cell
DEGs	Differentially expressed genes
DKK1	Dickkopf WNT signalling pathway inhibitor 1
DMARDs	Disease modifying anti-rheumatic drugs
DMSO	Dimethyl sulfoxide
DNA	Deoxyribonucleic acid
dNTP	Deoxynucleotide
DPX	Distyrene Plasticizer Xylene
DRE	DNA regulatory element
DUSP	Dual specificity protein phosphatase

**E**

E	Error component
EAE	Experimental autoimmune encephalomyelitis
EBI3	Epstein-Barr virus-induced gene 3
ECM	Extracellular matrix
EDTA	Ethylenediaminetetraacetic acid
ELISA	Enzyme-linked immunosorbent assay
ELS	Ectopic lymphoid-like structure
Eomes	Eomesodermin
EPH	Elute, prime, fragment high
ERK	Extracellular signal-regulated kinase
ESR	Erythrocyte sedimentation rate
EULAR	European league against rheumatism

**F**

F	Phenylalanine
Fab	Fragment antigen-binding
FACS	Fluorescence activated cell sorting

FBS	Foetal bovine serum
Fc	Fragment crystallisable
FC	Fold change
FDA	Food and drug administration
FDC	Follicular DC
FDR	False discovery rate
FF	gp130 <sup>F/F</sup> mice
FGF	Fibroblast growth factor
FITC	Fluorescein isothiocyanate
FLS	Fibroblast-like synoviocyte
FoxP3	Forkhead box P3
FPKM	Fragments per kilobase of transcript per million mapped reads
FSC-A	Forward scatter-area
FSC-H	Forward scatter-height

**G**

G	Gauge
GFP	Green fluorescent protein
GM-CSF	Granulocyte-macrophage colony-stimulating factor
gp130	Glycoprotein 130
GRZB	Granzyme B
GWAS	Genome-wide association studies

**H**

H <sub>2</sub> O	Water
H <sub>2</sub> O <sub>2</sub>	Hydrogen peroxide
H <sub>2</sub> SO <sub>4</sub>	Sulphuric Acid
HAT	Histone acetyltransferase
HCl	Hydrochloric acid
HCV	Hepatitis C virus
HEPES	4-(2-hydroxyethyl)-1-piperazineethanesulfonic acid
HEV	High endothelial venules
HGF	Hepatocyte growth factor
HIES	Hyper IgE syndromes
HIV	Human immunodeficiency virus
HLA	Human leukocyte antigen
HRP	Horseradish peroxidase

**I**

i.a.	Intraauricular
i.p.	Intraperitoneal
IC50	Half maximal inhibitory concentration
ICAM-1	Intracellular adhesion molecule 1
ICS	Intracellular cytokine staining
ID	Identification
IF	Immunofluorescence
IFN-γ	Interferon-gamma



Ig	Immunoglobulin
IHC	Immunohistochemistry
IL	Interleukin
IL-23R	IL-23 receptor
IL-27R	IL-27 receptor
IL-6R	IL-6 receptor
IL2RA	IL-2 receptor alpha chain
IL6ST	IL-6 signal transducer
ILC	Innate lymphoid cells
IMDM	Iscoe's modified dulbecco's medium
IP	Immunoprecipitation
IPA	Ingenuity pathway analysis
IPDB	IP dilution buffer
IPEB	IP elution buffer
IPWB	IP wash buffer
IRF	Interferon regulatory factor
iTreg	Inducible Treg
<b>J</b>	
JAK	Janus-activated kinase
<b>K</b>	
K <sup>+</sup>	Positively charged potassium ion
kDa	Kilodalton
KO	Knock-out
<b>L</b>	
LHS	Left hand side
LiCl	Lithium chloride
LN <sub>s</sub>	Lymph nodes
LPS	Lipopolysaccharides
LT	Lymphotoxin
LTβR	Lymphotoxin beta receptor
LTi	Lymphoid tissue inducer
LTo	Lymphoid tissue organiser
<b>M</b>	
mAb	Monoclonal antibody
MACS	Magnetic activated cell sorting
MAPK	Mitogen-activated protein kinase
mBSA	Methylated BSA
MHC	Major histocompatibility complex
miR	Micro RNA
MMP	Matrix metalloproteinases
mRNA	Messenger RNA
MT	Methyl transferase
MTX	Methotrexate
MW	Molecular weight

**N**

N	Total number of units
NaCl	Sodium chloride
NaHCO <sub>3</sub>	Sodium bicarbonate
NaN	Not a number
NECL	Nectin-like proteins
NFκB	Nuclear factor - κB
NGS	Next generation sequencing
NICE	National Institute of Clinical Excellence (NICE)
NK	Natural killer
NLB	Nuclear lysis buffer
NLR	NOD-like receptor
NOD	Nucleotide-binding oligomerisation-domain protein
NSAID	Non-steroidal anti-inflammatory drugs
nTreg	Natural Treg

**O**

OA	Osteoarthritis
OD	Optical density
ODN	Oligodeoxynucleotide
OVA	Ovalbumin

**P**

p	Population
<i>P. gingivalis</i>	<i>Porphyromonas gingivalis</i>
p7	Protein 7
PAD	Peptidyl arginine deiminase
PAMP	Pathogen-associated molecular pattern
PBS	Phosphate buffered saline
PCR	Polymerase chain reaction
PD-1	Programmed cell death-1
PDB	Protein data bank
PFM	Position frequency matrix
PIAS	Protein inhibitor of activated STATs
PKA	Protein kinase A
PMA	Phorbol 12-myristate 13-acetate
PMSF	Phenylmethylsulfonyl fluoride
PNAd	Peripheral node addressin
PPL	Project licence
PRDM1	Positive regulatory domain 1
PRR	Pattern/pathogen recognition receptor
PTP	Protein tyrosine phosphatase
PWM	Position weight matrix
pY	Tyrosine phosphorylated

**Q**

QC	Quality control
qPCR	Quantitative PCR

**R**

R	Programming language and free software environment for statistical computing and graphics
R <sup>2</sup>	Correlation coefficient

RA	Rheumatoid arthritis
RAG	Recombination activating gene
RANKL	Receptor activator for NFκB ligand
RASF	RA synovial fibroblasts
RBC	Red blood cell
RCGD-423	Regulator of cartilage growth and differentiation-423
RF	Rheumatoid factor
RHS	Right hand side
RIN	RNA integrity number
rm	Recombinant mouse
RNA	Ribonucleic acid
RNA-Seq	RNA-Sequencing
RORγt	Retinoic acid-related receptor orphan gamma-T
ROS	Reactive oxygen species
RPMI	Roswell park memorial institute medium
rRNA	Ribosomal RNA
RTK	Receptor tyrosine kinases

## S

s.b.	Subcutaneous
SD	Standard deviation
sdAb	Single domain Ab
SDAI	Simplified disease activity index
SDS	Sodium dodecyl sulphate
SEM	Standard error of the mean
Seq	Sequencing
sgp130	Soluble gp130
SH2	Src homology 2
sIL-6R	Soluble IL-6R
siRNA	Small interfering RNA
SLE	Systemic lupus erythematosus
SLOs	Secondary lymphoid organs
SOCS	Suppressor of cytokine signalling
SP1	Specificity protein 1
SPAG16	Sperm associated antigen 16
SPF	Specific pathogen free
SSC-A	Side scatter-area
STAT	Signal transducer and activator of transcription

## T

T	Treatment component
T1D	Type 1 diabetes
TACI	Transmembrane activator and CAML interactor
TBS	Tris buffered saline
TBS/T	TBS/Tween 20
TCCR	T-cell cytokine receptor
TCR	T-cell receptor
TE	Tris EDTA
TEV	Tobacco etch virus
TF	Transcription factor
TFBS	TF-binding sites
Tfh	T-follicular helper

TGF- $\beta$	Transforming growth factor beta
Th	T-helper
TLRs	Toll-like receptors
Tm	Melting temperature
TMB	3,3',5,5'-tetramethylbenzidine blue
TNF	Tumour necrosis factor
TNFAIP3	TNF alpha induced protein 3
Tr1	Type 1 Tregs
Treg	Regulatory T-cell
TRIS	Tris(hydroxymethyl)aminomethane
TSS	Transcriptional start site
TYK	Tyrosine kinase
<b>U</b>	
UCSC	University of California Santa Cruz
<b>V</b>	
V(D)J	Variable, diversity, joining
VAS	Visual analogue scale
VCAM-1	Vascular cell adhesion molecule 1
VEGF	Vascular endothelial growth factor
<b>W</b>	
WHRI	The William Harvey Research Institute
WT	Wild-type
<b>Y</b>	
Y	Tyrosine residue
YAP	Yes-associated protein
<b>Z</b>	
ZEB1	Zinc finger E-Box binding homeobox 1

All units of measure and their abbreviations used in this thesis follow the International System of Units unless otherwise specified.

# Table of contents

---

<b>1</b>	<b>INTRODUCTION.....</b>	<b>1</b>
<b>1.1</b>	<b>The immune system in health and disease.....</b>	<b>1</b>
1.1.1	Overview of the inflammatory immune response .....	1
1.1.1.1	<i>Innate Immunity.....</i>	<i>1</i>
1.1.1.2	<i>Adaptive Immunity.....</i>	<i>4</i>
1.1.2	Autoimmunity .....	8
<b>1.2</b>	<b>Rheumatoid arthritis .....</b>	<b>8</b>
1.2.1	Assessment of disease activity .....	9
1.2.2	Genetic, environmental and epigenetic risk factors .....	10
1.2.3	Mechanisms of disease initiation and progression .....	11
1.2.4	Pathogenesis .....	14
1.2.4.1	<i>The synovium .....</i>	<i>14</i>
1.2.4.2	<i>Cytokine and signalling networks.....</i>	<i>21</i>
1.2.5	Ectopic lymphoid-like structures.....	24
1.2.5.1	<i>Disease heterogeneity in Rheumatoid Arthritis.....</i>	<i>24</i>
1.2.5.2	<i>Secondary lymphoid organogenesis.....</i>	<i>26</i>
1.2.5.3	<i>Mechanisms of ELS development.....</i>	<i>26</i>
1.2.6	Therapy options: past, present and future .....	28
<b>1.3</b>	<b>JAK/STAT signalling pathway in RA.....</b>	<b>30</b>
1.3.1	JAK/STAT signalling pathway.....	30
1.3.1.1	<i>The STAT transcription factors .....</i>	<i>32</i>
1.3.1.2	<i>SOCS proteins: primary negative regulators of JAK/STAT activation .....</i>	<i>34</i>
1.3.1.3	<i>STAT3 and SOCS3 in RA.....</i>	<i>35</i>
1.3.2	Interleukin-6.....	36
1.3.2.1	<i>The IL-6 receptor complex.....</i>	<i>36</i>
1.3.2.2	<i>Classical and trans-activation of IL-6 receptor signalling.....</i>	<i>37</i>
1.3.2.3	<i>IL-6 in innate and adaptive immunity .....</i>	<i>39</i>
1.3.3	Interleukin-27 .....	40
1.3.3.1	<i>The IL-27 receptor complex .....</i>	<i>40</i>
1.3.4	Relation of IL-6 and IL-27 in inflammatory arthritis .....	41
<b>1.4</b>	<b>Therapeutic approaches for RA.....</b>	<b>42</b>
1.4.1	Cytokine blockers .....	43
1.4.2	Lymphocyte-targeting agents .....	44
1.4.2.1	<i>B-cell directed therapy .....</i>	<i>44</i>
1.4.2.2	<i>T-cell directed therapy .....</i>	<i>46</i>

1.4.3	Small molecule inhibitors of signal transduction pathways .....	48
1.4.3.1	<i>JAK inhibitors</i> .....	48
1.4.3.2	<i>Other small molecular inhibitors</i> .....	49
1.4.4	In vivo models for inflammatory arthritis .....	50
<b>1.5</b>	<b>Project aims .....</b>	<b>52</b>
<b>2</b>	<b>MATERIAL AND METHODS .....</b>	<b>53</b>
<b>2.1</b>	<b>Cell culture .....</b>	<b>53</b>
2.1.1	Buffers and media for cell culture.....	53
2.1.2	Isolation, culture and Th17 differentiation of murine naïve CD4 <sup>+</sup> T-cells .....	54
2.1.2.1	<i>Preparation of murine splenocytes</i> .....	54
2.1.2.2	<i>MACS sorting of CD4<sup>+</sup> T-cells</i> .....	54
2.1.2.3	<i>Isolation of naïve CD4<sup>+</sup> T-cell by flow cytometric cell sorting</i> .....	55
2.1.2.4	<i>In vitro generation of murine Th17 cells</i> .....	55
2.1.2.5	<i>Inhibition of in vitro Th17 cultures</i> .....	55
2.1.3	Cell Counting .....	58
2.1.4	Cryopreservation and thawing .....	58
<b>2.2</b>	<b>Flow Cytometry .....</b>	<b>58</b>
2.2.1	Cell surface staining .....	59
2.2.2	Intracellular cytokine staining (ICS) assay .....	59
<b>2.3</b>	<b><i>In vivo</i> experiments .....</b>	<b>60</b>
2.3.1	Mouse strains.....	60
2.3.2	Murine antigen-induced arthritis (AIA) .....	62
2.3.2.1	<i>Administration of Stat3-targeted therapies during AIA</i> .....	62
2.3.2.2	<i>CpG-Stat3siRNA Oligonucleotide Hybridisation</i> .....	64
2.3.3	Collection of serum from blood .....	64
2.3.4	Isolation of synovial tissue .....	64
2.3.5	Isolation of inguinal lymph nodes .....	65
<b>2.4</b>	<b>Histological analysis .....</b>	<b>65</b>
2.4.1	Preparation of knee joints for histology.....	65
2.4.2	Haematoxylin, fast green and safranin O staining .....	66
2.4.3	Histological assessment of arthritis.....	66
2.4.4	Immunohistochemistry (IHC) .....	70
2.4.4.1	<i>Immunofluorescence (IF)</i> .....	71
<b>2.5</b>	<b>Enzyme-linked immunosorbent assay (ELISA) .....</b>	<b>72</b>
2.5.1	Detection of inflammatory cytokines by ELISA .....	72
2.5.2	mBSA-specific antibody response by ELISA.....	73
<b>2.6</b>	<b><i>In silico</i> identification of transcription factor-binding sites (TFBSs).....</b>	<b>73</b>
<b>2.7</b>	<b>Chromatin immunoprecipitation (ChIP) – qPCR .....</b>	<b>74</b>

2.7.1	Buffers and reagents used for ChIP .....	74
2.7.2	Chromatin Immunoprecipitation (ChIP) .....	74
2.7.2.1	Cross-linking and sonication of genomic DNA.....	75
2.7.2.2	Immunoprecipitation.....	76
2.7.2.3	DNA purification and qPCR.....	76
2.7.2.4	Primer design .....	77
<b>2.8</b>	<b>RNA expression analysis .....</b>	<b>78</b>
2.8.1	RNA extraction .....	78
2.8.2	cDNA synthesis.....	79
2.8.3	Quantitative Real-Time Polymerase Chain Reaction (qPCR) .....	79
<b>2.9</b>	<b>Transcriptomic profiling of synovium.....</b>	<b>80</b>
2.9.1	Input RNA quality control.....	81
2.9.2	Removal of ribosomal RNA .....	81
2.9.3	Library preparation .....	81
2.9.4	Read mapping strategy .....	83
2.9.5	Differential gene expression analysis.....	83
2.9.6	Evaluation of duplicated reads.....	84
2.9.7	Data visualisation and interpretation.....	87
2.9.7.1	Heatmaps.....	87
2.9.7.2	Venn diagrams .....	87
2.9.7.3	Volcano plots.....	87
2.9.7.4	2D Scatter plots.....	87
2.9.7.5	Alluvial diagrams.....	87
2.9.7.6	Ingenuity Pathway Analysis .....	88
2.9.7.7	K-means clustering.....	88
2.9.7.8	Molecular visualisation .....	88
<b>2.10</b>	<b>Statistical data analysis .....</b>	<b>89</b>
<b>3</b>	<b>EVALUATION OF CPG-STAT3SIRNA THERAPY IN DIFFUSE AND LYMPHOID-RICH SYNOVITIS .....</b>	<b>90</b>
<b>3.1</b>	<b>Background .....</b>	<b>90</b>
<b>3.2</b>	<b>Aims .....</b>	<b>93</b>
<b>3.3</b>	<b>Results .....</b>	<b>94</b>
3.3.1	TLR9-expressing cells are present in synovial tissue .....	94
3.3.2	CpG-Stat3siRNA treatment improves arthritis severity <i>in vivo</i> .....	96
3.3.3	Experimental validation of Stat3 silencing by CpG-Stat3siRNA in AIA .....	100
3.3.4	CpG-Stat3siRNA treatment alters the transcriptomic profile of the inflamed synovium .....	101
3.3.5	Identification of CpG-Stat3siRNA-regulated genes during active synovitis .....	104
3.3.6	K-means clustering to identify temporal patterns of regulation.....	108
3.3.7	Canonical pathway analysis of genes that change in response to CpG-Stat3siRNA.....	115

3.3.8	STAT3 inhibition reduces cell metabolism and bone remodelling-associated pathways in diffuse-like synovitis .....	117
3.3.9	CpG- <i>Stat3</i> siRNA triggers interferon and Th1 pathways in diffuse-like synovitis .....	119
3.3.10	CpG- <i>Stat3</i> siRNA treatment results in downregulation of RhoA signalling and genes involved in the pathogenesis of RA in lymphoid-rich synovitis .....	121
3.3.11	CpG- <i>Stat3</i> siRNA alters the STAT1/STAT3 balance in inflammatory arthritis .....	123
3.3.12	Synovial ectopic lymphoid-like structures are reduced by CpG- <i>Stat3</i> siRNA therapy .....	126
<b>3.4</b>	<b>Discussion .....</b>	<b>129</b>
<b>4</b>	<b>THERAPEUTIC TARGETING OF STAT3-DRIVEN RESPONSES THROUGH THE PHARMACOLOGICAL INDUCTION OF SOCS3 EXPRESSION .....</b>	<b>135</b>
<b>4.1</b>	<b>Background .....</b>	<b>135</b>
<b>4.2</b>	<b>Aims .....</b>	<b>136</b>
<b>4.3</b>	<b>Results .....</b>	<b>137</b>
4.3.1	Arthritis severity and synovial infiltration are diminished by SOCS3-inducing peptide in experimental arthritis .....	137
4.3.2	Local administration of SOCS3-inducing peptide does not significantly affect systemic mBSA-specific antibody titres in AIA mice .....	142
4.3.3	SOCS3 reduces STAT3 activity and the number of synovial infiltrating T-cells .....	143
4.3.4	SOCS3-inducing peptide selectively prevents differentiation of Th17 cells .....	146
<b>4.4</b>	<b>Discussion .....</b>	<b>149</b>
<b>5</b>	<b>THERAPEUTIC TARGETING OF IL-6 TRANS-SIGNALLING BY CHIMERIC SOLUBLE GP130 (CS-130).....</b>	<b>152</b>
<b>5.1</b>	<b>Background .....</b>	<b>152</b>
<b>5.2</b>	<b>Aims .....</b>	<b>155</b>
<b>5.3</b>	<b>Results .....</b>	<b>156</b>
5.3.1	Design of miniaturised sgp130 variants .....	156
5.3.2	cs-130Fc variants inhibit Th17 cell differentiation in a dose-dependent manner .....	158
5.3.3	Potency-enhancing mutations in sgp130 do not show any improvement in inhibitory selectivity towards IL-6 trans-signalling.....	164
5.3.4	Comparison of the effect of all the different cs-130Fc variants in preventing Th17 cell differentiation in <i>vitro</i> murine T-cell cultures.....	166
<b>5.4</b>	<b>Discussion .....</b>	<b>167</b>
<b>6</b>	<b>NEGATIVE REGULATION OF CRTAM BY IL-6 AND IL-27 IN INFLAMMATORY ARTHRITIS</b>	<b>169</b>
<b>6.1</b>	<b>Background .....</b>	<b>169</b>
<b>6.2</b>	<b>Aims .....</b>	<b>172</b>
<b>6.3</b>	<b>Results .....</b>	<b>173</b>
6.3.1	Exploring the regulation of inflammatory synovitis by IL-27 and IL-6 in AIA .....	173
6.3.2	CRTAM expression during active arthritis is associated with disease severity .....	175
6.3.3	Synovial CRTAM is predominantly expressed in CD3 <sup>+</sup> CD4 <sup>+</sup> joint infiltrating T-cells.....	177



6.3.4	IL-6 and IL-27 inhibit CRTAM expression on naïve CD4 <sup>+</sup> T-cells .....	181
6.3.5	STAT3 signalling plays a major role in regulating CRTAM expression .....	185
6.3.6	CRTAM and its transcriptional repressor, ZEB1, colocalise in the inflamed synovium of AIA mice .....	189
6.3.7	CRTAM and ZEB1 exhibit a negative correlation in inflammatory arthritis.....	191
6.3.8	STAT3 interacts with <i>Zeb1</i> to regulate <i>Crtam</i> expression .....	192
6.3.9	CRTAM is expressed in human synovial pathology and correlates with indices of synovial pathology in patients with RA. ....	196
<b>6.4</b>	<b>Discussion .....</b>	<b>201</b>
<b>7</b>	<b>GENERAL DISCUSSION .....</b>	<b>206</b>
<b>7.1</b>	<b>Summary of work .....</b>	<b>206</b>
<b>7.2</b>	<b>Future perspectives for rheumatoid arthritis immunotherapy .....</b>	<b>209</b>
7.2.1	The context-dependent nature of cytokine action and the relevance to therapy.....	209
7.2.2	Safety and strategies for the optimal use of biologics in RA.....	211
7.2.3	Towards personalised therapies .....	213
7.2.3.1	<i>Identification of predictive biomarkers .....</i>	<i>213</i>
7.2.3.2	<i>Population-wide studies – how do you classify a patient with complex disease?.....</i>	<i>216</i>
<b>7.3</b>	<b>Concluding remarks.....</b>	<b>218</b>
<b>8</b>	<b>APPENDIX .....</b>	<b>219</b>

## List of figures

---

Figure 1.1 Interplay between innate and adaptive immunity. ....	2
Figure 1.2 Schematic structure of an antibody molecule and the T-cell receptor. ....	6
Figure 1.3 Initiation and progression of RA. ....	13
Figure 1.4 Citrullination of peptidyl arginine by peptidyl arginine deiminase (PAD). ....	14
Figure 1.5 Structure and pathology of the synovium. ....	16
Figure 1.6 Effector Th cell differentiation. ....	19
Figure 1.7 Joint pathology in RA and ELSs structure. ....	25
Figure 1.8 Secondary lymphoid organogenesis and ELS structure development. ....	27
Figure 1.9 Alignment of the JAK-STAT family members with associated cytokines. ....	31
Figure 1.10 Key components of the Jak-STAT signalling pathway. ....	32
Figure 1.11 Different mechanisms of IL-6 receptor signalling. ....	38
Figure 1.12 The IL-27 receptor complex. ....	41
Figure 1.13 Currently approved cytokine blockers for the treatment of RA. ....	44
Figure 1.14 Currently approved lymphocyte-targeting agents for the treatment of RA. ....	46
Figure 1.15 Abatacept mechanism of action. ....	47
Figure 1.16 Mode of action of Tofacitinib. ....	49
Figure 2.1 Gating strategy for sorting naïve CD4+ T-cells by flow cytometry. ....	57
Figure 2.2 STAT3 signalling in <i>gp130<sup>Y757F:Y757F</sup></i> and WT mice. ....	61
Figure 2.3 Timeline for the general antigen-induced arthritis mouse model. ....	63
Figure 2.4 Histology of mouse knee joints. ....	67
Figure 2.5 Histological assessment of AIA. ....	69
Figure 2.6 The basic principle of immunohistochemistry on tissue samples. ....	71
Figure 2.7 Diagram of the ChIP-qPCR workflow. ....	75
Figure 2.8 Sonication of genomic DNA for ChIP. ....	76
Figure 2.9 Workflow of RNA-seq library preparation. ....	85
Figure 2.10 Cluster generation during Illumina HiSeq 4000 sequencing. ....	85
Figure 2.11 Sequencing by synthesis using Illumina HiSeq 4000. ....	86
Figure 3.1 Structure and mechanism of action of the CpG-Stat3siRNA conjugate. ....	92
Figure 3.2 TLR9 is expressed in the joints of WT and <i>Il27ra<sup>-/-</sup></i> mice with AIA. ....	95
Figure 3.3 CpG-Stat3siRNA reduces the inflammatory component in early arthritis. ....	97
Figure 3.4 CpG-Stat3siRNA decreases synovial infiltrate, pannus formation and cartilage/bone erosion in established arthritis. ....	98

Figure 3.5 CpG- <i>Stat3</i> siRNA conjugate is the only compound having a significant impact on AIA outcome compared to controls. ....	99
Figure 3.6 CpG- <i>Stat3</i> siRNA inhibits the transcriptional activity of <i>Stat3</i> . ....	100
Figure 3.7 The inflamed synovium of CpG- <i>Stat3</i> siRNA-treated mice show different transcriptional profiles compared to AIA untreated and healthy mice.....	101
Figure 3.8 CpG- <i>Stat3</i> siRNA changes global gene expression in the inflamed synovium of mice. ....	103
Figure 3.9 Dynamics of CpG- <i>Stat3</i> siRNA-mediated gene expression.....	105
Figure 3.10 Common CpG- <i>Stat3</i> siRNA-induced genes across AIA timeline and genotypes are associated with innate and adaptive immune responses and inflammation.....	106
Figure 3.11 Identification of genes that change in response to CpG- <i>Stat3</i> siRNA therapy. ....	107
Figure 3.12 Mathematical determination of the optimal number of clusters for the synovial transcriptome.....	108
Figure 3.13 K-means clustering analysis of the synovial transcriptome during the time course of AIA and as a response to CpG- <i>Stat3</i> siRNA in WT mice.....	111
Figure 3.14 K-means clustering analysis of the synovial transcriptome during the time course of AIA and as a response to CpG- <i>Stat3</i> siRNA in <i>Il27ra</i> <sup>-/-</sup> mice. ....	112
Figure 3.15 Comparison of canonical pathways linked to individual clusters in WT and <i>Il27ra</i> <sup>-/-</sup> mice with AIA and the impact of CpG- <i>Stat3</i> siRNA intervention.....	114
Figure 3.16 Comparison of diseases and functions are linked to individual clusters in WT and <i>Il27ra</i> <sup>-/-</sup> mice and the impact CpG- <i>Stat3</i> siRNA intervention. ....	115
Figure 3.17 Canonical pathway analysis of genes switching pattern of expression as a response to CpG- <i>Stat3</i> siRNA.....	116
Figure 3.18 Reduced expression of cell metabolism and bone and cartilage remodelling genes in WT mice treated with CpG- <i>Stat3</i> siRNA.....	118
Figure 3.19 STAT1-dependent Th1 and IFN pathways are increased in WT mice treated with CpG- <i>Stat3</i> siRNA.....	120
Figure 3.20 CpG- <i>Stat3</i> siRNA inhibits expression of RhoA signalling and immune cell genes involved in RA in <i>Il27ra</i> <sup>-/-</sup> mice.....	122
Figure 3.21 STAT3-regulated gene expression decreases, while STAT1-associated gene expression is upregulated in WT mice in response to treatment. ....	124
Figure 3.22 STAT3-regulated gene expression decreases, while STAT1-associated gene expression is upregulated in <i>Il27ra</i> <sup>-/-</sup> mice, in response to treatment. ....	125
Figure 3.23 CpG- <i>Stat3</i> siRNA treated mice show fewer ectopic lymphoid-like structures. ....	127
Figure 3.24 ELS-associated genes are downregulated in the presence of CpG- <i>Stat3</i> siRNA.....	128
Figure 4.1 Experimental design for SOCS3-inducing peptide in <i>vivo</i> experiment. ....	138
Figure 4.2 Joint swelling is partially reduced in mice treated with SOCS3-inducing peptide. ....	139
Figure 4.3 SOCS3-inducing peptide distinctly reduces synovial infiltration and general disease activity in experimental arthritis. ....	140

Figure 4.4 No adverse local inflammatory effects are observed in response to SOCS3-inducing peptide or control peptide administration in mice. ....	141
Figure 4.5 SOCS3-inducing peptide does not significantly diminish adaptive immune responses in mice at day 3 of AIA.....	142
Figure 4.6 SOCS3-inducing peptide decreases the proportion of CD3 <sup>+</sup> T-cells and STAT3 activity in the inflamed synovium. ....	144
Figure 4.7 pY-STAT3 co-localisation with CD3 <sup>+</sup> T-cells in inflamed synovium treated with SOCS3-inducing peptide. ....	145
Figure 4.8 Gating strategy for CD4 <sup>+</sup> IL17A <sup>+</sup> T-cells identification using flow cytometry. ....	147
Figure 4.9 SOCS3-inducing peptide blocks Th17 cell differentiation in vitro. ....	148
Figure 5.1 Structure of the human IL-6/IL-6R/gp130 complex.....	154
Figure 5.2 Schematic illustration of sc-130 variant design. ....	157
Figure 5.3 Increasing IL-6 concentration and adding anti-IL-2 magnifies Th17 cell expansion, while IL-27 inhibits it. ....	159
Figure 5.4 The fusion protein sgp130Fc is able to suppress the proliferation of Th17 cells in a dose-dependent manner <i>in vitro</i> .....	160
Figure 5.5 cs-130Fc inhibits Th17 cell formation in a dose-dependent manner <i>in vitro</i> . ...	161
Figure 5.6 cs-130 inhibits Th17 cell formation in a dose-dependent manner <i>in vitro</i> .....	162
Figure 5.7 Inactivating cs-130Fc variants did not affect Th17 differentiation <i>in vitro</i> .....	163
Figure 5.8 Affinity-enhancing mutation did not improve the inhibitory capacity of cs-130Fc variants.....	165
Figure 5.9 Summary of the Th17 cells inhibitory capacity of cs-130Fc variants <i>in vitro</i> .....	166
Figure 6.1 Microarray data analysis showing downregulated genes upon IL-6 stimulation. ....	170
Figure 6.2 Joint histopathology of AIA in WT, <i>Il27ra</i> <sup>-/-</sup> and <i>Il6ra</i> <sup>-/-</sup> mice. ....	174
Figure 6.3 CRTAM is expressed in the joints of mice with AIA and correlates with synovial pathology. ....	176
Figure 6.4 <i>Crtam</i> and its binding molecule, <i>Cadm1</i> are expressed in the inflamed joint, but <i>Cadm1</i> shows no dependency on IL-6 or IL-27 control. ....	177
Figure 6.5 Gating strategy for the characterisation of CRTAM secreting cells within the inflamed synovium of mice with AIA by flow cytometry.....	178
Figure 6.6 Joint-infiltrating CD3 <sup>+</sup> CD4 <sup>+</sup> cells are the main CRTAM expressing cells in the synovium at day 3 and day 10 post arthritis induction. ....	180
Figure 6.7 The proportion of CD3 <sup>+</sup> CD4 <sup>+</sup> CRTAM <sup>+</sup> is increased at day 10 post arthritis induction as well as in the synovium of <i>Il-27ra</i> <sup>-/-</sup> mice in both time points. ....	181
Figure 6.8 Gating strategy for CD4 <sup>+</sup> CRTAM <sup>+</sup> T-cells identification using flow cytometry..	182
Figure 6.9 CRTAM expression peaks at 18 hours after TCR activation in naïve CD4 <sup>+</sup> T-cells from WT mice and is regulated by IL-6 and IL-27 <i>in vitro</i> .....	183
Figure 6.10 CRTAM expression peaks at 18 hours after TCR activation in naïve CD4 <sup>+</sup> T-cells from <i>Il6ra</i> <sup>-/-</sup> and <i>Il27ra</i> <sup>-/-</sup> mice and is regulated by IL-6 and IL-27 <i>in vitro</i> . ....	184

Figure 6.11 CRTAM expression peaks at 18 hours after TCR activation in naïve CD4 <sup>+</sup> T-cells from <i>gp130<sup>F/F</sup></i> mice and is regulated by STAT3.....	186
Figure 6.12 CRTAM expression peaks at 18 hours after TCR activation in naïve CD4 <sup>+</sup> T-cells from <i>gp130<sup>F/FStat3+/-</sup></i> mice and is regulated by STAT3. ....	188
Figure 6.13 STAT3 activation by both IL-6 and IL-27 leads to inhibition of CRTAM gene expression .....	189
Figure 6.14 Spatial relationship of CRTAM and ZEB1 in the inflamed synovium of AIA mice. ....	190
Figure 6.15 Negative correlation between CRTAM and ZEB1 in inflammatory arthritis. ....	191
Figure 6.16 STAT3-binding sites are associated with transcriptional repressor of CRTAM, ZEB1.....	195
Figure 6.17 CRTAM expression is present at higher levels in RA synovium than OA. ....	197
Figure 6.18 Association of CRTAM with rheumatoid arthritis in human studies. ....	199
Figure 6.19 Negative association between CRTAM and ZEB1 in patients with RA.....	200
Figure 6.20 A model of the regulation of CRTAM by a network of signalling and transcriptional pathways.....	204
Figure 7.1 Visual summary of the research content within this thesis. ....	207
Figure 7.2 Summary of the main disease-modifying antirheumatic drugs for RA treatment .....	216
Figure 8.1 Flow cytometry gating strategy to determine purity of naïve CD4 <sup>+</sup> T-cells.....	219
Figure 8.2 Promoter sequence of <i>Crtam</i> and negative regulator <i>Zeb1</i> .....	220
Figure 8.3 Quality of sequencing determined by FastQC report.....	221
Figure 8.4 Association of CRTAM, ZEB1 and CADM1 with RA in human studies.....	224

## List of tables

---

Table 2.1 The composition of buffers and cell culture media used throughout this thesis.	53
Table 2.2 The list of nanobodies and concentrations used in Th17 cell differentiation assays.....	56
Table 2.3 The list of antibodies used for flow cytometry staining in this thesis. ....	59
Table 2.4 Scoring criteria for histological assessment of joint pathology in AIA.....	68
Table 2.5 The composition of IHC buffers used throughout this thesis. ....	70
Table 2.6 The list of antibodies used for immunohistochemistry. ....	72
Table 2.7 The composition of buffers and reagents used for ChIP. ....	74
Table 2.8 General guidelines for primer design. ....	78
Table 2.9 Custom-designed primers for ChIP-qPCR. ....	78
Table 3.1 Sign test and Wilcoxon signed-rank test in clusters from WT genes. ....	109
Table 3.2 Sign test and Wilcoxon signed-rank test in clusters from <i>Il27ra</i> <sup>-/-</sup> genes.....	110
Table 6.1 Summary table of all over-represented TFBS motifs in the promoter region of ZEB1. ....	193
Table 6.2 Summary table of the first 10 over-represented TFBS motifs in the promoter region of CRTAM based on relative score.....	194
Table 8.1 Summary table of all over-represented TFBS motifs in the promoter region of CRTAM based on relative score. ....	222

# 1 Introduction

---

## 1.1 The immune system in health and disease

### 1.1.1 Overview of the inflammatory immune response

The body is protected from exogenous agents (e.g., infections by viruses, bacteria and archaea, fungi or parasites) and endogenous threats (e.g., malignantly transformed cells) by a variety of effector cells and molecules that together make up the immune system. However, host defence and surveillance is only one component of the immune system's overall function, and its activities also contribute to physiological processes such as development, metabolism, maintenance of tissue homeostasis and repair, and mental wellbeing <sup>1</sup>. Immunity is not a simple circuit involving few types of immune cells but a multi-layered, dynamic network of interlocking subsystems that form one of the most complex and important frontiers of scientific enquiry we know <sup>2</sup>. This remarkably sophisticated biological system has evolved to sense and interpret changes in environmental cues and is capable of dealing with a massively diverse collection of constantly evolving pathogens by discriminating between foreign entities and the host's own tissues. However, the delivery of these activities are delicately controlled and if inappropriately regulated, can lead to chronic pathologies and cancer <sup>3</sup>. The immune response is divided into two interconnected subsystems termed innate and adaptive immunity. These systems determine the speed and duration of the immune response, dictate the types of effector cells involved, and fine-tune the specificity of the host defence. Recent research shows that the boundaries between innate immune response and adaptive immunity are more blurred than initially believed, and their actions are closely intertwined to ensure a highly coordinated response to infection, trauma or injury <sup>4</sup> (**Figure 1.1**).

#### 1.1.1.1 *Innate Immunity*

Innate immune responses represent the first barrier of fast-acting defence against infectious organisms. Plants and some animals, such as insects, rely exclusively on innate defences, a highly conserved ancestral system designed to contain and neutralise infections <sup>5</sup>. Mechanical and chemical defences operate continuously as the body is exposed on a daily basis to viruses and bacteria in the environment. For example, mucosal surfaces produce a

variety of antimicrobial proteins that act as natural antibiotics to prevent microbes from penetrating the body. At the same time, a diverse community of commensal bacteria inhabits mucosal and epidermal surfaces in humans and are beneficial to the host <sup>6</sup>. However, if the normal barrier function of the epithelia at these surfaces is compromised, these microbes can become pathogenic.

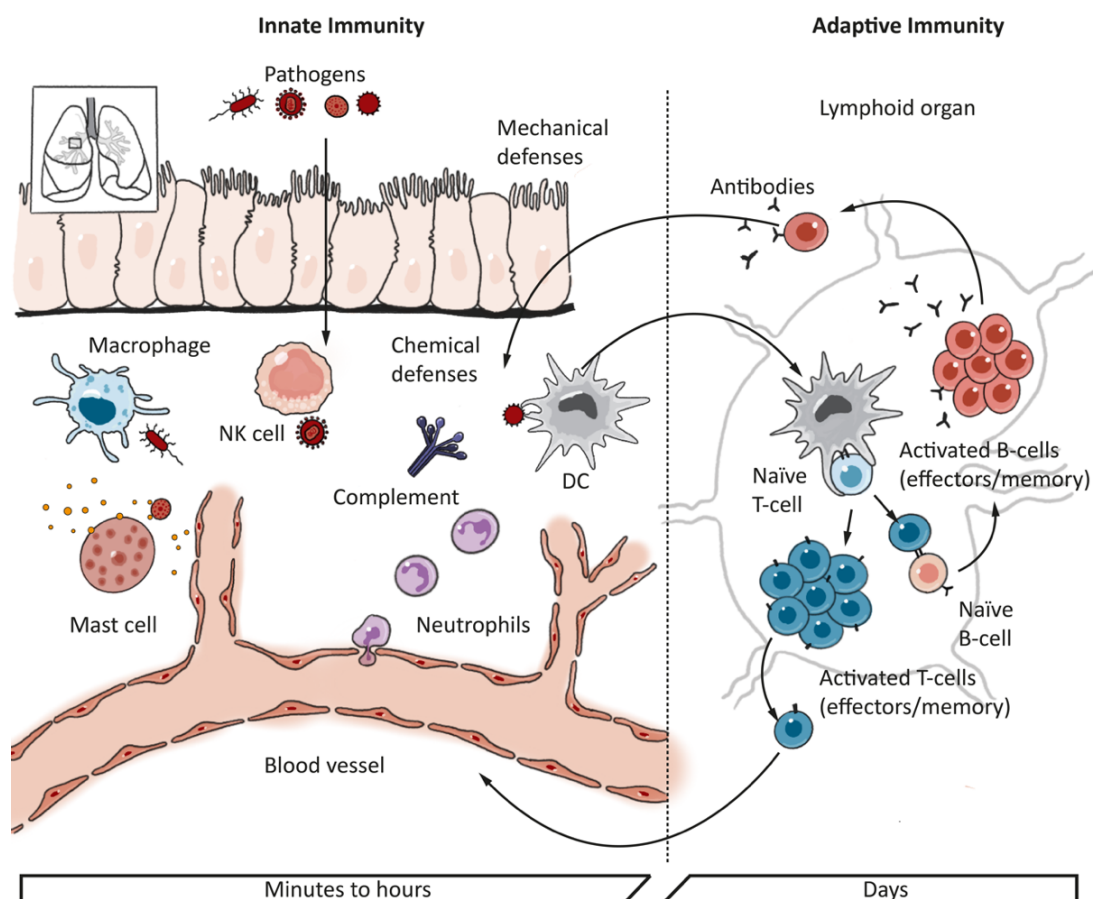


**Figure 1.1 Interplay between innate and adaptive immunity.**

The first level of defence is the anatomic barrier provided by the body's epithelial surfaces. Second, various chemical and enzymatic systems, including complement, act as an immediate antimicrobial barrier near these epithelia. If epithelia are breached, nearby innate lymphoid cells (e.g., macrophages, NK cells, neutrophils) can coordinate a rapid cell-mediated defence. If the pathogen overcomes these barriers, the slower-acting defences of the adaptive immune system are brought to bear. In the lymph nodes, dendritic cells present pathogen-derived antigens to naïve and central memory T-cells, leading to stimulation of pathogen-specific cells. T-cells provide help to B-cells, inducing the production of antibodies that directly neutralise pathogens and lead to additional targeting of innate responses. NK, natural killer; DC, dendritic cell.



Consequently, the innate immune system responds immediately by recognition of conserved motifs found in the pathogens as well as a number of other indicators of cell stress or death <sup>7</sup>. The cells responsible for detecting these pathogens or the damage induced by them are phagocytic myeloid cells such as tissue-resident macrophages, neutrophils and other polymorphonuclear leukocytes, Langerhans cells and dendritic cells (DCs). These sensor cells are equipped with a limited number of pathogen recognition receptors (PRRs) <sup>8,9</sup> that recognise simple molecules and regular patterns of molecular structure known as (i) danger-associated molecular patterns (DAMPs), induced in response to endogenous stress (e.g., K<sup>+</sup>, ions, uric acid or ATP), and (ii) pathogen-associated molecular patterns (PAMPs), which are molecular components unique to bacteria, viruses, fungi and parasites <sup>10</sup>. Such PAMPs include mannose-rich oligosaccharides, peptidoglycans, and lipopolysaccharides of the bacterial cell-wall (LPS), as well as unmethylated CpG or double-stranded RNA <sup>11</sup>. Each of these microbial components has become highly conserved during microbial evolution, making them excellent targets for recognition by the immune system. Some PRRs are transmembrane proteins, such as the Toll-like receptors (TLRs) that detect PAMPs (and certain DAMPs) derived from extracellular bacteria or bacteria taken into vesicular pathways by phagocytosis <sup>12</sup>. Other PRRs are cytoplasmatic proteins, such as the NOD (nucleotide-binding oligomerisation-domain protein)-like receptors (NLRs), and the leucine-rich repeat-containing receptors, among others <sup>13</sup>. Some NLRs detect intracellular bacterial invasion, viral infections and biological allergens and induce the inflammasome complex, which leads to caspase-1-dependent processing and secretion of members of the interleukin 1 (IL-1) family of cytokines, IL-1 $\beta$  and IL-18 <sup>14,15</sup>. The inflammasome is also involved in recognition of non-pathogen stimuli such as self-generated DAMPs (e.g., cholesterol crystals in cardiovascular disease, uric acid crystals in gout) <sup>16</sup>.

Local inflammation and the phagocytosis of invading bacteria can also be triggered by the activation of the complement system, designed to instruct leukocyte recruitment and activation, flag pathogens for immune attack, and promote pathogen killing <sup>17</sup>. Bacterial surfaces can activate the complement system, inducing a cascade of proteolytic reactions that coat the microbes with fragments of specific serum proteins of the complement system. Microbes coated in this way (termed opsonisation) are recognised by specific complement receptors on macrophages and neutrophils, taken up by phagocytosis, and destroyed. Neutrophils also attempt to kill the invading agents by releasing the toxic contents of their granules, which include reactive oxygen species (ROS) and reactive nitrogen species,

proteinase 3, cathepsin G and elastase, having possible unavoidable collateral damage to host tissues <sup>18</sup>. Additionally, natural killer (NK) cells play an important role in the early innate response to viral infections, before the adaptive immune response has developed <sup>10</sup>.

Pathogens are not the only causative agents of tissue and cell damage. During cellular stress, trauma and its associated tissue damage, inflammation and necrotic cell death, self-derived host molecules (DAMPs) are produced in large quantities in order to activate repair mechanisms and restore homeostasis <sup>19</sup>. Acidosis, hypoxia, extracellular matrix (ECM) reorganisation, and tissue remodelling follow in order to combat the stressors. Thus, DAMPs play a role in correcting the altered physiological state, but in excess, the resultant intracellular signalling can induce the elaboration of inflammatory mediators which are also DAMP generators, forming a vicious loop and creating a pro-inflammatory state <sup>20</sup>.

Activation of PRRs on sensor cells serves to amplify the immune response by the production of inflammatory mediators, including chemokines, cytokines, vasoactive amines, eicosanoids and products of proteolytic cascades, which recruit cells from the blood into infected tissues, a process known as inflammation, that helps destroy the pathogen <sup>21</sup>. Inflammation increases the flow of lymph, which carries microbes or innate cells, such as DCs, bearing their antigens, from the infected tissue to nearby lymphoid tissues, such as the spleen and lymph node, where the adaptive immune response is initiated.

#### 1.1.1.2 *Adaptive Immunity*

Innate immune responses occur rapidly on exposure to an infectious organism while adaptive immunity is learned or acquired more slowly, in days to weeks <sup>7</sup>. However, the adaptive immune system is capable of eliminating infections more efficiently because of exquisite specificity of antigen recognition by its lymphocytes and generating immunological memory. In contrast to a limited repertoire of receptors expressed by innate immune cells, lymphocytes express highly specialised antigen receptors that collectively possess a vast repertoire of specificity. This enables the adaptive immune system to respond to virtually any pathogen and effectively focus resources to eliminate pathogens that have evaded or overwhelmed innate immunity. But the adaptive immune system interacts with, and relies on cells of the innate immune system for many of its functions <sup>21</sup>.

The adaptive arm of immunity consists of antigen-specific lymphocytes: B-cells and T-cells. This basic principle of lymphocyte differentiation is observed in all jawed vertebrates (e.g.,

mammals), but it was already present in jawless vertebrates (e.g., lampreys) <sup>22</sup>. Both B-cells and T-cells derive from common lymphoid progenitors of haematopoietic stem cells in the bone marrow, and B-cell and T-cell differentiation occurs in primary lymphatic organs: the bone marrow and thymus for B-cells and T-cells respectively. B-cells and T-cells are distinguished by the structure of the antigen receptor that they express, the B-cell receptor (BCR) and its soluble form (immunoglobulins), and the T-cell receptor (TCR) (**Figure 1.2**). Antibodies and T-cell receptors are composed of constant and variable regions that provide distinct functions.

The antibody molecule consists of two identical heavy chains and two identical light chains with variable and constant regions. Proteolytic cleavage by papain cuts the antibody molecule on the amino-terminal side of the disulphide bonds that link the two heavy chains, releasing the two arms of the antibody molecule as two identical fragments that contain the antigen-binding activity or Fab fragments, and one Fc fragment (fragment crystallisable), which is the part of the antibody molecule that interacts with effector molecules and cells <sup>21</sup>. The T-cell receptor is composed of two chains: the TCR  $\alpha$  and  $\beta$  chains in the case of  $\alpha\beta$  T-cells, which are the most abundant and best characterised human T-cell subset; and the TCR  $\gamma$  and  $\delta$  chains, expressed by  $\gamma\delta$  T-cells, which are considered 'unconventional' and represent 1-10% of circulating T-cells. These chains are expressed as part of a complex with the invariant CD3 chain molecules. The large repertoire of both T-cell and B-cell receptors is acquired by rearrangement of the variable (V), diversity (D), and joining (J) gene segments by a multistep process called V(D)J recombination. The enzyme pair RAG1 and RAG2 at the end of V(D)J genes, selectively targets recombination signal sequences <sup>23–25</sup>. In fact, RAG- deficient mice completely lack mature B-cells and T-cells, highlighting the importance of these enzymes in adaptive immunity <sup>26</sup>. The V(D)J recombination is a random mechanism unique to antigen-specific receptors on B-cells and T-cells that allows adaptive immune responses against a virtually limitless array of antigens, including molecules encoded by the host. Thus, cells that recognise self-antigens must be removed by negative selection before they enter circulation to avoid unwanted self-reactive receptors (autoimmunity) that can result in chronic inflammation.

Adaptive immune responses are initiated when B-cells or T-cells encounter antigens in the secondary lymphoid organs (SLOs) – the lymph nodes, spleen, and mucosal lymphoid tissues. Mature naïve lymphocytes are continually recirculating through these tissues, to which

pathogen-derived antigens are carried from sites of infection, primarily by DCs. DCs are crucial for the initiation of adaptive immune responses as they process the captured antigens and convert proteins to peptides that are presented on major histocompatibility complex (MHC) molecules and recognised by T-cells through a TCR<sup>27</sup>. In humans, MHC molecules are encoded within the Human leukocyte antigen (HLA) locus. When a T-cell first encounters an antigen that its receptor can bind, it proliferates and differentiates into one of several different functional types of effector T lymphocytes.

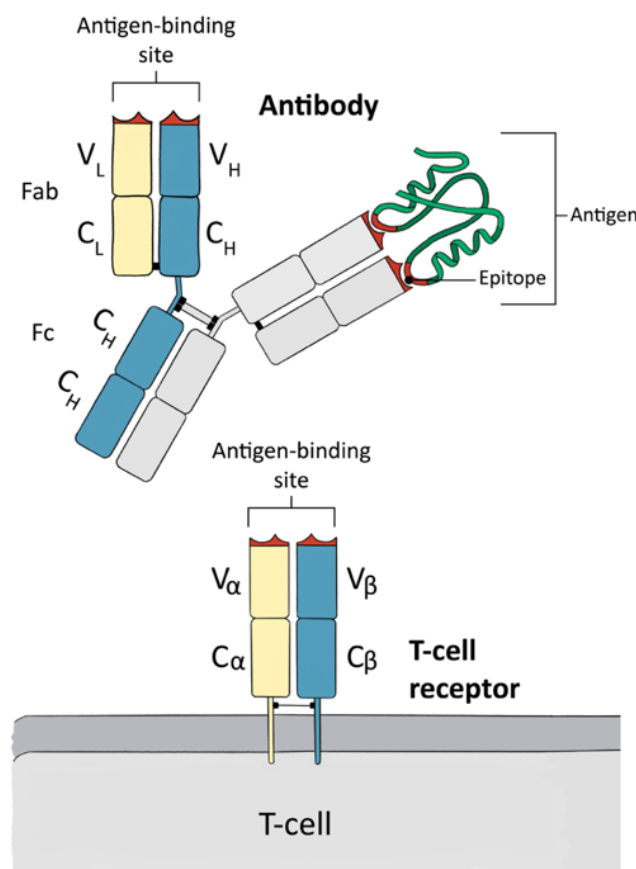


**Figure 1.2 Schematic structure of an antibody molecule and the T-cell receptor.**

The Fab fragment of an antibody molecule is a disulphide-linked heterodimer, each chain of which contains one immunoglobulin C domain and one V domain. The T-cell receptor is also a disulphide-linked heterodimer, with each chain containing an immunoglobulin C-like domain and an immunoglobulin V-like domain. The juxtaposition of the V domains forms the site for antigen recognition. Most antigens are larger than the sites on the antibody or antigen receptor to which they bind, being the epitope the small portion of the antigen's molecule structure that is recognised. Fab, fragment antigen-binding; Fc, fragment crystallisable, C, constant; V, variable.

When effector T-cells subsequently detect antigen, they can manifest three broad classes of activity: (i) Cytotoxic T-cells ( $CD8^+$ ), that kill other cells that are infected with viruses or other intracellular pathogens bearing the antigen; (ii) Helper T-cells ( $CD4^+$ ), that provide signals, often in the form of specific cytokines that activate the functions of other cells, such as B- cell production of antibodies and macrophage killing of engulfed pathogens; (iii) Regulatory T- cells, that suppress the activity of other lymphocytes and help to limit excessive or sustained immune activation <sup>21</sup>. The *MHC* genes encode two homologous types of proteins, MHC molecules of class-I (MHC-I), which present peptide antigens to  $CD8^+$  cytotoxic T-cells, and class-II (MHC-II), which present peptides to  $CD4^+$  helper T-cells. To become activated, T- cells require both initial TCR activation (termed 'signal 1') and interaction of co-stimulatory molecules CD80 (B7-1), CD86 (B7-2) and CD40, expressed on antigen-presenting cells (APCs) that bind CD28 and CD40 ligand (CD40L) on T-cell respectively that will initiate T-cell proliferation (termed 'signal 2'). Finally, the presence of soluble cytokine signal may determine the differentiation state of the T-cell (termed 'signal 3', see **Figure 1.6**) <sup>28</sup>.

Activation of B-cells usually requires not only antigen, which binds to the B-cell receptor (comprising a membrane-bound immunoglobulin – typically monomeric IgM or IgD) but also the cooperation of activated T-follicular helper (Tfh) cells. When they recognise a peptide:MHC class II complex on the B-cell surface, Tfh cells deliver additional signals that include the expression of CD40 ligand and the production of various important cytokines (e.g., IL-21, IL-6 TGF- $\beta$ , IFN- $\gamma$  and IL-4). This results in the expression of activation-induced cytidine deaminase (AID) which promotes class-switching and somatic hypermutation within the antigen-binding site in order to increase the affinity and diversity of antibodies <sup>29</sup>. In the germinal centres, B-cells proliferate and differentiate into plasma cells that promote antigen-specific responses. These are the effector form of B-cells, and they secrete antibodies that have the same antigen specificity as the plasma cell's BCR. Whilst early antibody production comprises pentameric IgM, the cytokine network established as part of the inflammatory processes promotes antibody class-switching to tailor the immune response to a specific antigenic challenge. Here, class-switching involves a genetic rearrangement of the antibody constant region of the immunoglobulin heavy chain in order to generate antibodies with different effector functions. There are five immunoglobulin (Ig) isotypes – IgM, IgG, IgD, IgA and IgE. Thus, lymphocytes activated by antigen give rise to

clones of antigen-specific effector cells that mediate the adaptive response in a process known as clonal selection <sup>30</sup>.

Some of the B-cells and T-cells activated by antigen will differentiate into memory cells, the lymphocytes that are responsible for the long-lasting immunity that can follow exposure to disease or vaccination <sup>31</sup>. Memory cells will readily differentiate into effector cells on a second exposure to their specific antigen <sup>21</sup>. I discuss the role of each of the T-cell subsets in the context of rheumatoid arthritis in **Section 1.2.4.1**.

### **1.1.2 Autoimmunity**

There are three major areas in which the immune system can cause pathology: genetic immune deficiency syndromes in which there is inability of one or more components of the immune system to respond in a protective fashion to immune challenge, auto-inflammatory conditions driven by DAMPs, and autoimmunity arising from aberrant antibody targeting of host tissues and cells <sup>32</sup>. The failure to discriminate self from nonself is commonly called ‘a breach of tolerance’ and is the starting point for autoimmune disease. Human autoimmune diseases arise out of intricate interactions between genetic and environmental factors that accumulate over time until the appearance of clinical symptoms. While underlying adaptive immunity alterations have been considered for decades, the pathogenic role of innate immunity in many of these diseases is also becoming evident <sup>33</sup>. Traditionally, autoimmune diseases were considered to be rare, but following meticulous epidemiological studies, have now been demonstrated to affect 3-5% of the global population. There are almost 100 different autoimmune diseases, some of which are organ-specific, as in type 1 diabetes (T1D), or widely expressed, as in systemic lupus erythematosus (SLE) or rheumatoid arthritis (RA), leading to the appearance of autoantibodies and/or autoreactive T-cells <sup>32</sup>. Importantly, while organ-specific, systemic immune responses mean that organ-specific autoimmunity is also linked to multi-morbidities. As my work addresses the modulation of the JAK/STAT signalling pathway for the treatment of inflammatory arthritis, the rest of my thesis will focus on this autoimmune disease in particular.

## **1.2 Rheumatoid arthritis**

Rheumatoid arthritis (RA) is a clinically heterogeneous autoimmune disease that results in chronic inflammation of the synovial membrane and causes pain, swelling and stiffness in

the joints <sup>34</sup>. However, it should be considered a syndrome that includes extra-articular manifestations such as systemic comorbidities – e.g., cardiovascular complications, anaemia, fatigue, alterations in sleep, mood and often psychological conditions, including depression. A hallmark of RA is the presence of autoantibodies such as rheumatoid factor (RF) and autoantibodies against citrullinated peptides (ACPAs), which are associated with more severe joint damage and increased mortality <sup>34</sup>. It is the most frequent inflammatory arthritis worldwide, affecting 0.5 - 1% of the adult global population, predominantly women, and it can cause severe joint damage, loss of function and disability <sup>35</sup>. Although RA may present at any age, it occurs most commonly in individuals between the age of 45 and 65 years, and the peak incidence for women occurs earlier than for men <sup>36</sup>. RA prevalence also varies between ethnicities, with the highest reported in Native American population <sup>37</sup>. Moreover, geographical differences such as a lower prevalence in southern Europe have been reported, although studies are limited <sup>38</sup>. While not fatal, there is evidence of a gap in mortality between individuals with RA and the general population. This mortality gap is mainly attributed to high prevalence of cardiovascular risk factors associated with the disease <sup>39</sup>. A prospective analysis of the Nurse's Health Study reported that women with RA had an increased risk of total mortality compared with those without RA <sup>40</sup>. With current treatment strategies, premature mortality is no longer observed <sup>41</sup>, yet RA still associates with higher mortality rates, as shown in recent cohorts studies <sup>42</sup>. The disease is complex and involves environmental factors that trigger disease in genetically susceptible individuals. In later sections, I discuss the main genetic risk factors believed to influence the development and course of RA.

### **1.2.1 Assessment of disease activity**

The pathogenesis of RA is complex, and while soluble markers including RF, ACPA and C- reactive protein (CRP) predict disease onset, current biomarkers are unable to reliably predict the rate and severity of disease, and the response to biological drug intervention. Assessment of clinical disease activity is currently the best method to identify the stage of disease and response to therapy in patients with RA <sup>43</sup>. Disease activity is assessed using the Disease Activity Scores (DAS28) as an observational clinical measure of joint pathology <sup>44</sup>. As its name indicates, DAS28 considers the number of swollen and tender joints out of 28 examined and is combined with measures of systemic markers of inflammation such as the erythrocyte sedimentation rate (ESR) and serum CRP levels, and personal assessment of

health, in order to calculate an overall disease activity score. For example, a patient with a DAS28 score of less than 2.6 is in remission; a score greater than or equal to 2.6 and less than 3.2 indicates low activity, and a score greater than 5.1 indicates high disease activity<sup>45</sup>. In clinical trials, the clinical response is usually measured using the American College of Rheumatology (ACR) score, which helps determine response to treatment by judging of disease improvement as opposed to measuring disease activity. An improvement of 20% (ACR20) is the minimal required response and means that there is a 20% improvement in tender or swollen joint counts, a reduction in overall assessment of RA and reduction in serum markers of inflammation. Similarly, an ACR50 and ACR70 response indicate a 50% and 70% improvement respectively<sup>46</sup>. Boolean Scores, simplified and clinical disease activity indexes (SDAI, CDAI) avoid CRP measures in determining disease remission and can be useful in cases where, due to drugs like tocilizumab, disease scores are heavily skewed by the impact on CRP<sup>47</sup>.

### 1.2.2 Genetic, environmental and epigenetic risk factors

Family history has long been recognised as one of the strongest risk factors for developing RA<sup>48</sup>. Although twin studies have estimated a relatively high heritability (40-60 %) in patients who are positive for ACPAs, they also demonstrated that non-coding factors play an important role in susceptibility<sup>48,49</sup>. Genome-wide association studies (GWAS) have characterised more than hundred loci significantly associated with risk and progression of RA, the most common being the human leukocyte antigen (*HLA*)-*DRB1*, which encodes a specific amino acid motif in the peptide-binding groove (QKRAA), called 'the shared epitope'<sup>50</sup>. Other genetic loci that predict susceptible to RA are linked to genes involved in cytokine signalling and sensitivity (e.g., *STAT4*, *IL12RA*, *TYK2*, *IRF5*, *IRF8*), lymphocyte receptor activation threshold (e.g., *PTPN22*)<sup>51</sup>, altered stimulatory pathways (e.g. *CD28*, *CD40*), immune checkpoint receptor expressed on activated T-cells (e.g., *CTLA4*, *PRDM1*), and innate immune activation (e.g., *TNFAIP3*)<sup>52</sup>. Interestingly, genetic variations in *IL6ST* (encoding gp130) and *IL6R* are common in patients with RA<sup>53</sup>. In addition to susceptibility, *IL2RA*, *DKK1*, *GRZB*, *MMP9* and *SPAG16* have also been associated with RA severity<sup>54</sup> and a single nucleotide polymorphism in *IL27* (encoding IL-27p28) was linked to more advanced disease<sup>55</sup>.

As mentioned before, studies have shown that women are twofold to threefold more likely to develop RA than men<sup>56</sup>. The higher frequency of RA among women than among men is



poorly understood, but it is partly attributed to the stimulatory effects of oestrogen on the immune system. Furthermore, women have an earlier disease onset and are more likely to have been negative for RF and have lower titres of ACPAs compared to men<sup>57</sup>. Interestingly, while RA risk increases in nulliparous women, pregnancy is often associated with disease remission. Nevertheless, the role of hormonal factors in the pathogenesis and development of RA remains controversial<sup>58</sup>. In addition to mature effector T-cell function, the generation and maintenance of central tolerance (involving appropriate selection of T-cells in the thymus and B-cells in the bone marrow) and of peripheral tolerance (dependant on appropriate regulatory T-cell function) can contribute to an over-reactive immune system<sup>59</sup>.

The outcome of RA is also influenced by environmental factors such as tobacco smoking, which promotes the citrullination of proteins and doubles the risk of disease in smokers compared with non-smokers. Other environmental risk factor includes silica exposure, infectious agents, vitamin D deficiency, obesity and changes in the microbiota, although studies for some of these factors are not very robust<sup>58</sup>. Finally, one of the ways in which individuals may respond to environmental exposure is through changes in epigenetics<sup>60</sup>. The term epigenetics is often used to described regulatory mechanisms that do not involve changes in the nucleotide sequence, regardless of whether such imprinting is strictly heritable<sup>61</sup>. Methylated positions, altered histone acetylation, DNA methylation and microRNAs represent epigenetic aspects that could promote genetic risk in RA<sup>34</sup>.

### **1.2.3 Mechanisms of disease initiation and progression**

The disease process may be characterised as having a predisposing genotype upon which environmental and genetic factors operate to promote 'preclinical RA'. During this period, there is no clinical evidence of disease activity, but some patients may have markers in the blood that denote autoimmunity (e.g., ACPA, RF); an early inflammatory phase that includes clinical manifestations that may or may not be accompanied by a confirmed diagnosis of RA (early RA); a destructive phase that includes erosions and disease progression; and an ongoing phase accompanied by hyperplasia and irreversible joint destruction (established RA)<sup>62</sup> (**Figure 1.3**).

The mechanisms that lead to a breach of tolerance in RA are poorly defined but probably arise at a systemic immune regulatory level, in aberrant thymic selection or peripheral tolerance. One of the fundamental elements in the initiation of the disease process is the

presence of specific autoantibodies, such as RF and ACPAs<sup>58</sup>. RF was the first autoantibody identified for RA, and it was later found to be directed to the Fc portion of IgG. In addition, RF and IgG join to form immune complexes that contribute to the disease process. Since then, numerous additional autoantibodies have been characterised in sera of patients of RA recognising autoantigens such as type 2 collagen (particularly in oxidised form), glucose- 6- phosphate isomerase and proteoglycans, contributing to pathogenesis<sup>63</sup>. Moreover, the identification of these additional autoantibodies has been used to establish mouse models to investigate disease mechanism in RA (e.g., CIA and K/BxN mouse models)<sup>64</sup>.

Citrullination or deimination is the conversion of the amino acid arginine in a protein into the amino acid citrulline, which is not one of the twenty standard amino acids encoded by DNA in the genetic code. Instead, enzymes known as peptidyl arginine deiminases convert arginine residues to citrulline residues<sup>65</sup> (**Figure 1.4**). Up to 70% of patients with RA are found to be anti-cyclic citrullinated peptides (CCP2) positive with high specificity<sup>66</sup>. Stressors like cigarette smoke, for example, can act on cells in mucosal sites and promote the post- translational conversion of the amino acid arginine to citrulline in a range of proteins, including intracellular proteins (such as histones) and matrix proteins (e.g., fibronectin, collagen, fibrinogen, enolase and vimentin)<sup>67</sup>. The microbiota also plays a role in the induction of citrullination. For example, *P. gingivalis*, linked with bacterial periodontal disease, expresses a peptidyl arginine deiminase (PAD) that enzymatically controls citrullination to promote ACPA generation<sup>68</sup>. A similar citrullination reaction is also triggered by a bacterial toxin derived from *A. actinomycetemcomitans*. This Gram-negative bacterium is associated with localised aggressive periodontitis and secretes an acylated protein toxin termed leukotoxin-A, which promotes membranolysis and cell death in host immune cells. This process drives hypercitrullination of RA autoantigens in human neutrophils, and exposure to *A. actinomycetemcomitans* is a significant risk factor for disease onset in patients carrying HLA-DRB1<sup>69</sup>.

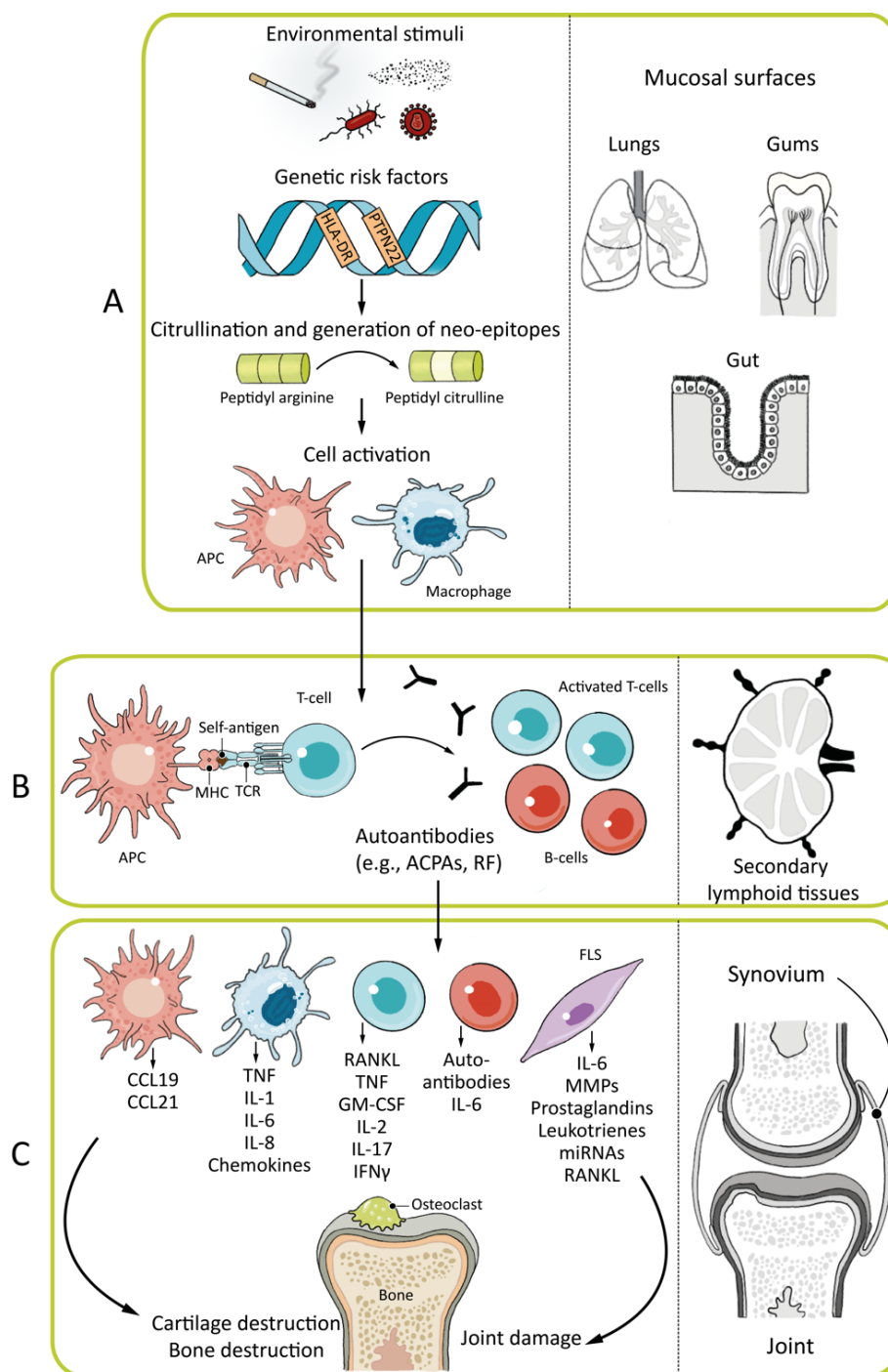


**Figure 1.3 Initiation and progression of RA.**

**(A)** Environmental stimuli and specific HLA haplotypes contribute to post-translational modifications, such as citrullination, carbamylation, sialylation or acetylation, in the mucosa, and initiate the production of neo-epitopes that can be recognized by the adaptive immune system. **(B)** These altered peptides are presented by APCs and activate an adaptive immune response in lymphoid tissues and elicit autoantibody formation. **(C)** Stromal cells (FLS), APCs and macrophages can be activated locally and produce a range of inflammatory factors. Paracrine and autocrine actions of cytokines, along with persistent, adaptive immune responses, can perpetuate the disease and ultimately lead to cartilage and bone destruction. APC, antigen-presenting cell; FLS, fibroblast-like synoviocyte; TNF, tumour necrosis factor; GM-CSF, granulocyte-macrophage colony-stimulating factor; IFN- $\gamma$ , interferon-gamma; MMPs, matrix metalloproteinases; RANKL, receptor activator for N $\kappa$ B ligand.

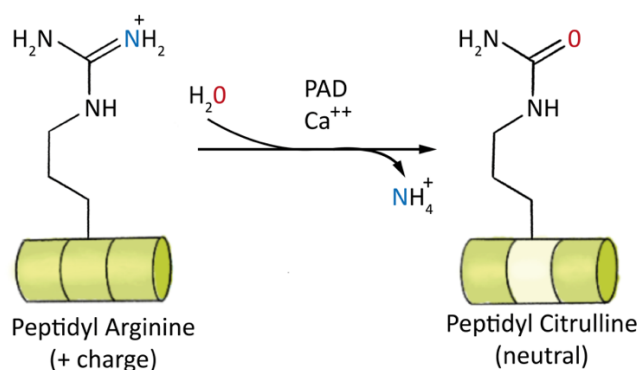


**Figure 1.4 Citrullination of peptidyl arginine by peptidyl arginine deiminase (PAD).**

Other mechanisms of protein modification (post-translational modifications like acetylation, sialylation or non-enzymatic carbamylation) are also likely to turn self-proteins into targets for autoantibody generation <sup>70</sup>. These altered peptides bind to MHC protein heterodimers, especially those containing the previously mentioned shared epitope (QKRAA), leading to antigen presentation, which in turn stimulate B-cells to synthesise a range of antibodies that recognise self-antigens, including RF (targeting IgGs) and ACPAs (targeting citrullinated proteins) <sup>65,71</sup>. The presence of circulating autoantibodies (seropositivity) can be detected up to 10 years before diagnosis, with an increase of their concentration and epitope diversity over time and is associated with more severe joint damage and increased mortality. Thus, they can be used not only as a diagnostic marker but also as a prognostic marker <sup>72</sup>. Importantly, the presence of ACPAs alone is not sufficient to cause disease onset; an additional immunological challenge (e.g., immune complex formation, complement activation or microvascular insult), triggered by an adverse infection or environmental factor, is likely required to initiate autoimmune reactions and clinical synovitis characterised by increased vascular permeability and the synovial infiltration of inflammatory cells <sup>73</sup>.

## 1.2.4 Pathogenesis

### 1.2.4.1 The synovium

Although RA is a systemic disease that can affect organs and areas of the body other than the joints, the synovial membrane or synovium is the major target tissue of inflammation (termed synovitis). Why RA localises predominantly in joints and not in other parts of the body is still poorly understood. The synovium produces synovial fluid which provides a lubricated surface that enables the cartilage surfaces to operate with a low frictional

coefficient <sup>74</sup>. In addition, the synovial fluid supplies essential nutrients to the cartilage since this tissue lacks its own blood supply, and removes the waste products from the cells within the cartilage <sup>75</sup>. A healthy synovial membrane is a relatively delicate structure with an intimal lining that covers the non-articulating surfaces of synovial joints. The intimal lining is composed of macrophage-like synoviocytes and fibroblast-like synoviocytes (FLS), while the sublining, a loose connective tissue that lies beneath the intimal lining, is composed of fibroblasts, adipocytes, blood vessels and scattered immune cells <sup>58</sup> (**Figure 1.5**). This architecture lacking epithelial cells, a basement membrane, tight junctions or desmosomes, probably contributes to the accumulation of immune complexes, bacterial cell walls, and other material in the synovium <sup>76</sup>. The joint forms a dynamic environment that is subject to constant minor trauma by movement. As a result, continual remodelling of the articular cartilage and adjacent bone and its careful regulation are necessary in order to maintain self-repair and homeostasis <sup>74</sup>.

The intimal lining thickens (synovial hyperplasia) due to an increase and activation of both macrophage-like synoviocytes and FLS <sup>74</sup>. Macrophage-like synoviocytes produce an array of pro-inflammatory cytokines, including IL-1, IL-6, tumour necrosis factor (TNF) and others. These cytokines activate FLS and release IL-6 and large amounts of proteases, most notably matrix metalloproteases (e.g., collagenases, stromelysins and ADAM family members), as well as small bioactive lipid mediators (e.g. prostaglandins and leukotrienes) <sup>58</sup>. Several other cell types (adaptive immune cells) infiltrate and accumulate in the synovial sublining such as T-cells, B-cells, plasma cells, antigen-presenting follicular dendritic cells, macrophages and mast cells <sup>58</sup>. Angiogenesis accompanies this immune cell accumulation, increasing leukocyte migration, and the synovial tissue transforms into an invasive and destructive front of synovial tissue attached to the articular surface, called pannus, which ultimately can result in cartilage and bone destruction <sup>74</sup>. Bone erosion is generally due to maturation and activation of osteoclasts (bone-resorbing cells) by receptor activator of nuclear factor -  $\kappa$ B (RANK; also known as TNFRSF11A) ligand (RANKL; also known as TNFSF11) produced by T- cells, together with TNF, IL-6 and IL-1 produced by macrophages and FLS in the synovial lining (**Figure 1.3C**). In the accompanying Sections below, I will discuss in more detail the most abundant cell populations within the RA synovium.

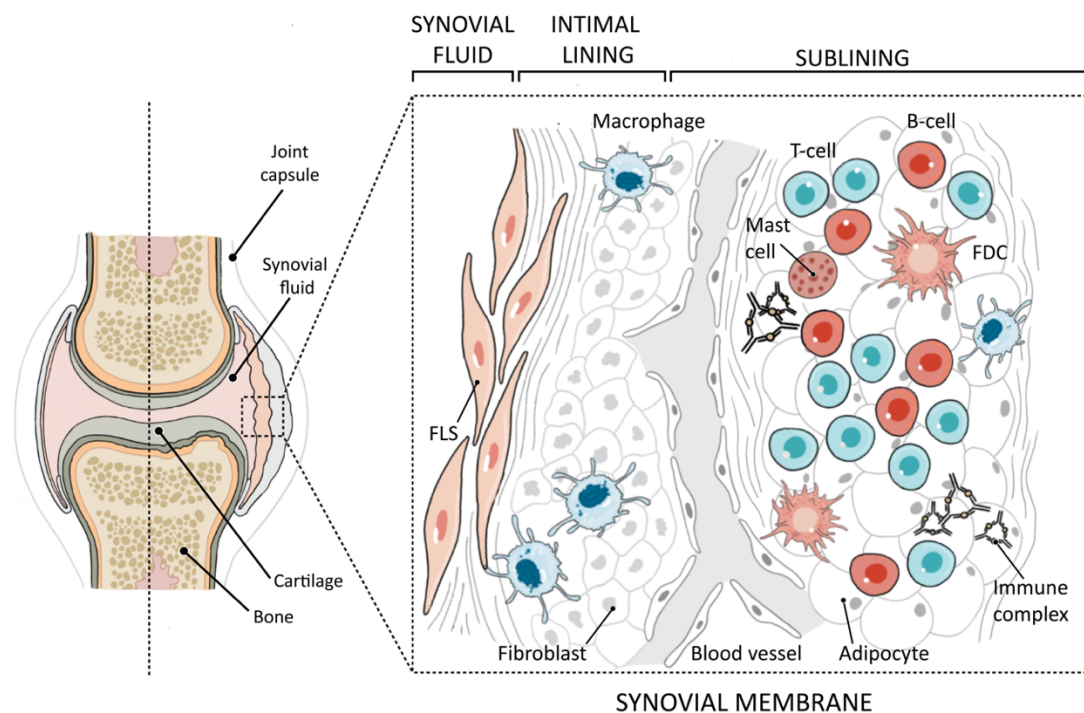


**Figure 1.5 Structure and pathology of the synovium.**

Diagram comparing a normal (left) and arthritic joint (right). The arthritic synovial membrane comprises an intimal lining characterised by thickening due to an increase of macrophage-like synoviocytes and fibroblast-like synoviocytes (FLS), and a sublining composed of fibroblasts, adipocytes, blood vessels and scattered immune cells, where T-cells, B-cells, immune complexes, antigen-presenting follicular dendritic cells (FDC), macrophages and mast cells infiltrate and accumulate contributing to inflammation of the area. The cells within the intima produce extracellular matrix molecules and mediate the production and clearance of synovial fluid. FLS, fibroblast-like synoviocyte; FDC, follicular dendritic cell.

**Fibroblast-like synoviocytes (FLS).** The origin of the expanding FLS population is uncertain, but they are thought to have emerged from FLS precursors found in the synovium or migrated from mesenchymal stem cells from the circulation that multiplied due to an imbalance between proliferation, survival and death <sup>76</sup>. Cadherin-11 was identified as a relatively unique surface marker mainly present on intimal FLS <sup>77</sup>, and these cadherin-11- positive FLS are the dominant destructive cell type for cartilage, as they produce RANKL, TNF, IL-6, IL-1 and proteases, most notably MMPs (e.g. collagenases and stromelysins), as well as small-molecule mediators (e.g. prostaglandins and leukotrienes) <sup>78</sup>, and can potentially migrate from joint to joint to propagate disease <sup>79</sup>. FLS also express specific patterns of microRNAs that could contribute to their activated phenotype <sup>80</sup>. Thus, the phenotype of FLS is aggressive in RA, as cells have inherent invasive qualities not observed in other fibroblasts from, for example, patients with osteoarthritis (OA), a joint disorder

caused mainly by mechanical factors with little inflammatory involvement <sup>76,81</sup>. The complexity and diversity of the fibroblast population in RA has been more recently elucidated through the use of single-cell RNA sequencing which identified different fibroblast subsets based on the expression patterns of multiple markers that localised to specific regions in the synovium and showed differential roles: erosive processes (FAP $\alpha$ <sup>+</sup> THY1<sup>-</sup>) vs maintaining inflammation (FAP $\alpha$ <sup>+</sup> THY1<sup>+</sup>) <sup>81,82</sup>.

**T-cells.** Although the origin of peripheral tolerance defects remains unclear, disruption in peripheral T-cell tolerance has been postulated as a mechanism contributing to RA pathogenesis <sup>59</sup>. About half of the sublining cells are CD4<sup>+</sup> memory T-cells, which either directly infiltrate the joint in response to inflammatory chemokines or are generated locally within the inflamed synovium as part of germinal centre reactions triggered by the presence of synovial ectopic lymphoid-like structures (ELS), which are presented in 15-20% of RA patients. These lymphocyte-rich structures are often highly organised and drive B-cell maturation, proliferation and differentiation into antibody-producing cells (discussed in more detail in **Section 1.2.5**). Naïve CD4<sup>+</sup> T-cells differentiate into diverse phenotypes of effector subsets with defined cytokine signatures. This is achieved by programmed alterations of gene expression regulated by structural changes in chromatin. Th1 cells differentiate in the presence of IL-12, express T-bet and produce interferon- $\gamma$  (IFN- $\gamma$ ), helping with immunity against intracellular parasites <sup>83</sup>; Th2 cells are differentiated by IL-4, express GATA3 and secrete IL-4, IL-5 and IL-3, having a role in fighting helminth infections <sup>84</sup>; Th17 cells are induced in response to transforming growth factor- $\beta$  (TGF $\beta$ ), IL-6, IL-23, and IL-1 $\beta$ , express the transcription factor ROR $\gamma$ t, and lead to the production of IL-17A, IL-17F, IL-22 and IL-21, to provide immunity against extracellular bacteria and fungi <sup>85,86</sup>; Tfh cell differentiation is dependent on IL-6 and IL-21, induce the expression of Bcl6 and upregulate the expression CXCR5 and IL-21, supporting the generation of high-affinity antibodies by B-cells <sup>87-89</sup>; Regulatory T-cells (Tregs) limit effector T-cell responses, support immune tolerance and maintain homeostasis. These suppressor T-cells are released from the thymus as a distinct lineage (termed natural regulatory T-cells; nTreg) or are induced (inducible regulatory T-cells; iTreg) in response to TGF- $\beta$ , which promotes expression of the transcriptional regulator FoxP3 and the release of IL-10 <sup>90</sup> (**Figure 1.6**).

A less well-defined Th subset is Th22, which can be promoted by IL-6 and TNF- $\alpha$ , along with the help of DCs, and is characterised by the secretion of IL-22 and TNF- $\alpha$ , but not IFN- $\gamma$ , IL-4



or IL-17<sup>90</sup>. Previous studies suggest that Th22 cells play important roles in certain inflammatory skin disorders and were elevated in the bone marrow of patients with RA in comparison to OA patients, correlating with disease severity and promoting osteoclast differentiation<sup>91</sup>. Moreover, IL-9-producing type 2 innate lymphoid cells (ILC2s) have been recently identified as the mediators of a molecular and cellular pathway that orchestrates the resolution of inflammatory arthritis. Here, patients with RA in remission exhibited high numbers of IL-9<sup>+</sup> ILC2s in joints and the circulation<sup>92</sup>. Nevertheless, the definitions of T-helper subsets are not absolute. There are ever-expanding numbers of recently discovered T-cell subsets such as Tr1<sup>93</sup>, Th3<sup>94</sup>, Th9<sup>95,96</sup>, Th22<sup>91</sup> (mentioned above), as well as examples of phenotypic plasticity between defined T-cell subsets in both mice and humans<sup>93,97,98</sup>. Recent findings suggest that lineage differentiation may be reversible under certain conditions, with specific cell surface markers identified that may indicate the former phenotype<sup>99</sup>. Many of these subsets also have innate counterparts thought to be evolutionarily linked to these T-cell subsets (e.g., ILC3s and Th17 cells and the already mentioned IL-9 producing ILC2s, among others)<sup>100</sup>. Thus, understanding the sequential generation, balance and the diverse effector characteristics displayed by T-helper subsets within the joint is central to the development of autoimmunity.

Th1 cell frequency and elevated IFN- $\gamma$  production are elevated in RA, suggesting a dominant Th1-driven disease over Th2. Th17 are thought to be pivotal in the development of autoimmune diseases and notably in RA, where they drive arthritic bone destruction in mice and human<sup>101</sup>. However, whether RA is prevalently Th1-or Th17-mediated is still unclear<sup>102</sup>, although recent research has shown that Th17 cells initiate and mediate chronic inflammation and are associated with ELS development in RA<sup>100,103,104</sup>. Importantly, human Th17 cells, as mentioned before, are unstable and can shift to a Th1 profile suggesting a high degree of plasticity inherent to Th17 cells and therefore, a very complex and dynamic relationship between T-cell subsets<sup>102</sup>. Some studies cite a failure of Treg-cell activity, whereas others suggest that pathogenic T-cells can become refractory to regulation<sup>105</sup>. Additionally, a published study has shown that arthritic synovial fibroblast promoted FoxP3<sup>+</sup> CD4<sup>+</sup> T-cells conversion into Th17-like cells, that produced IL-17A and RANKL, and contributed to disease progression in a model of collagen-induced arthritis (CIA)<sup>106</sup>. Tfh cells upregulate the expression of CXCR5, which directs their recruitment to B-cell zones within lymphoid organs and class-switching<sup>107</sup>.



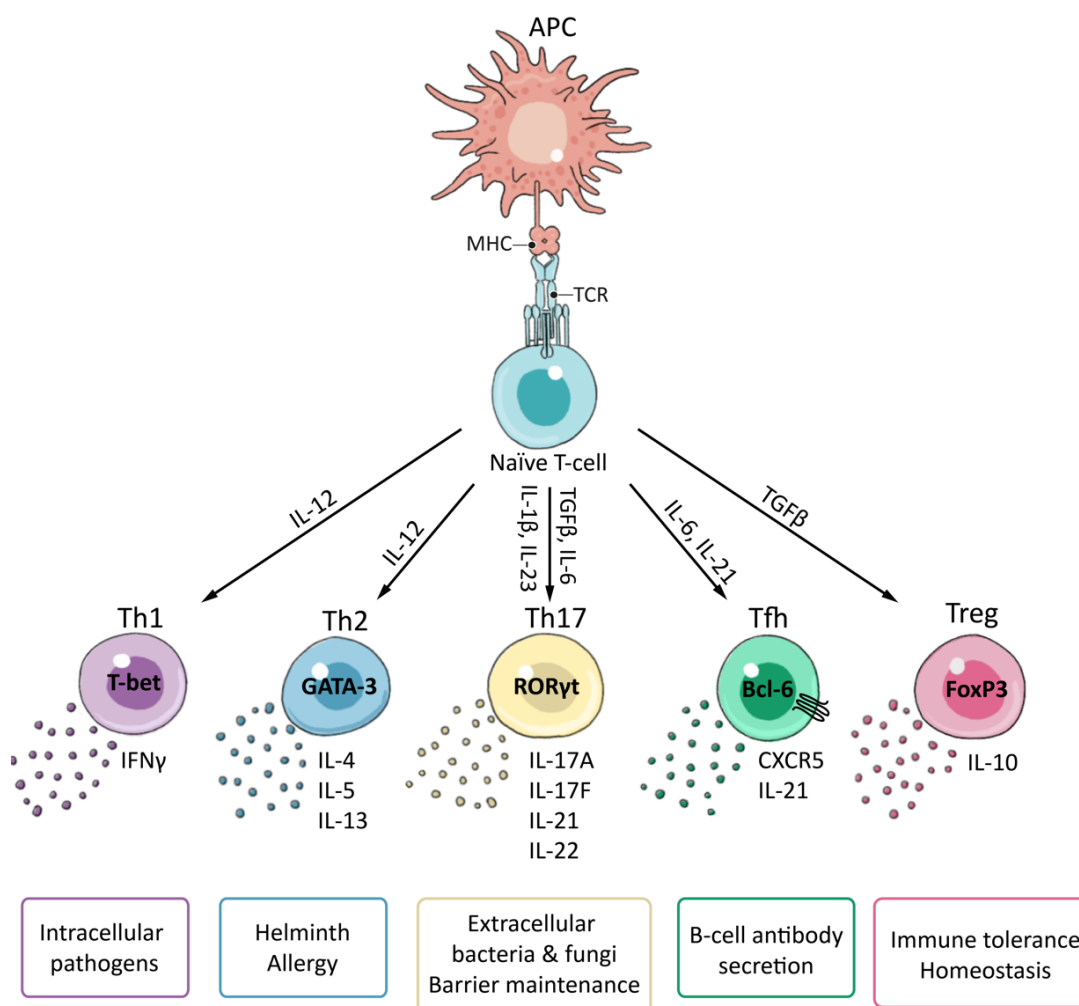


**Figure 1.6 Effector Th cell differentiation.**

Upon encountering antigen presented by antigen-presenting cells (APCs), naïve CD4<sup>+</sup> T-cells differentiate into effector subsets – T helper (Th)1, Th2, Th17, T follicular helper (Tfh) and regulatory T (Treg) cells (among others) that are characterised by their cytokine production, expression of transcription factors, chemokine receptors, and immune regulatory functions. APC, antigen-presenting cell; MHC, major histocompatibility complex; TCR, T-cell receptor.

Finally, CD8<sup>+</sup> T-cells, which represent a population of cytotoxic lymphocytes (CTLs) that are able to induce targeted killing of both infected and malignant cells<sup>108,109</sup>, are increasingly gaining interest in RA. A number of studies provide evidence that autoreactive CD8<sup>+</sup> T-cells can accumulate with duration of disease in the peripheral blood and synovial fluid and be involved in aggravating pathologic responses in rheumatoid synovitis. However, their role in the disease remains to be fully clarified<sup>110</sup>.

**B-cells.** B-cells, plasmablasts and plasma cells are also present in the synovium. Their importance in RA pathology is illustrated by the effectiveness of B-cell depletion therapies

(see **Section 1.4.2.1**), and it is now clear that they play multiple roles in the rheumatoid disease process <sup>111</sup>. In addition to their classical role as producers of autoantibodies (including RF and ACPAs), B-cells are central to the activation of CD4<sup>+</sup> T-cells in synovial tissue, and their depletion disrupts the production of proinflammatory cytokines and RANKL, which support osteoclastogenesis and joint pathology within the inflamed synovium<sup>112,113</sup>. B-cells have also been implicated in the process of ectopic lymphoid organogenesis <sup>114</sup>. Studies of immunoglobulin gene rearrangements and the relevant tissue enzyme expression associated with ectopic germinal centres suggest that autoantibody-producing cells (including those that produce IgG, IgM and IgA isotypes), undergo affinity maturation in the tissue <sup>107</sup>. This indicates an ongoing immune response to native or altered peptides <sup>115</sup>. Nevertheless, the relative contribution of these synovial pathways to the general pathogenesis is obscure, as the largest proportion of affinity maturation takes place before clinical disease onset <sup>116</sup>.

**Macrophages.** Monocytes circulate in the bloodstream, are produced by the bone marrow from precursors called monoblasts (bipotent cells that differentiated from haematopoietic stem cells), and when they move into tissues throughout the body, they differentiate into macrophages <sup>21</sup>. Macrophages are among the most abundant cell types within the inflamed synovium. Indeed, synovial sublining macrophage infiltration can be used as a biomarker for response to treatment as it directly correlates with clinical scores for local disease activity and progression of joint damage <sup>117</sup>. As previously outlined, macrophages play an important role in the pathogenesis of RA by helping induce inflammation, producing many inflammatory mediators (such as proinflammatory cytokines, chemoattractants and metalloproteinases) that activate other cells (such as FLS, T-cells and DCs) and recruit them into the synovium <sup>58</sup>.

Additionally, **antigen-presenting follicular dendritic cells** and **mast cells** are scattered across the synovial sublining and **neutrophils** are oddly absent. Some studies suggest that distinct pathotypes of synovial histology that include inflammatory versus non-inflammatory patterns are associated with clinical phenotype or response to targeted agents <sup>74</sup> (see **Sections 1.2.5.1** and **1.4**).

#### 1.2.4.2 Cytokine and signalling networks

The cytokine network is central to the pathogenesis of RA and contributes to the pro-inflammatory environment linked with the development of synovitis and joint damage. Here, cytokines produced by stromal tissue cells and inflammatory cells within the synovium affect cellular proliferation, differentiation and survival and adopt paracrine, autocrine or juxtacrine mechanisms to maintain inflammation in RA. For instance, macrophages release cytokines that activate adjacent FLS, T-cells and DCs; these cells, in turn, produce additional cytokines that can stimulate other cells in the joint environment <sup>34</sup>. Cytokines control cellular phenotype, localisation, activation status and longevity in the synovial and lymphoid microenvironments <sup>118</sup>.

Two pivotal pro-inflammatory cytokines in RA pathophysiology are TNF- $\alpha$  and IL-6, and their importance is clearly depicted by the accumulation of clinical advantages following their inhibition <sup>119,120</sup>. TNF- $\alpha$  mediates the activation, adhesion and migration of leukocytes as well as the activation of stromal cells, endothelium and chondrocytes within the synovium <sup>121</sup>. TNF- $\alpha$  promotes pain processes, angiogenesis, MMP and chemokine production, and together with RANKL, contributes to the activation and effector function of osteoclasts <sup>122</sup>. The wider benefits of clinical studies using TNF- $\alpha$  -blocking therapies indicate that TNF- $\alpha$  is also involved in other functions such as altering cognition, depression and fatigue, alterations in lipid metabolism, glucose tolerance, and changes in vascular endothelial function and repair <sup>123</sup>. Although IL-6 has similar effects to those of TNF- $\alpha$  in the local synovial environment (e.g., cholesterol elevations and composition, anaemia – linked with hepcidin regulation and iron metabolism), IL-6 is a lymphokine that affects the survival, proliferation, differentiation and effector properties of T-cells and B-cells and therefore drives the acute-phase response in response to inflammation <sup>124</sup>. Furthermore, IL-6 has an essential immunoregulatory role in adaptive immunity, acting at a checkpoint in the differentiation of naïve T-cells towards proinflammatory Th17 or Treg cell phenotype with a probable role in early disease and the development of cardiovascular comorbidities <sup>125,126</sup>. Importantly, the ADACTA trial revealed that monotherapy is better with tocilizumab (IL-6 blocker) than adalimumab (TNF- $\alpha$  inhibitor), showing that IL-6 intervention works in patients that are intolerant to methotrexate and therefore reflecting the action of IL-6 as a lymphokine <sup>127</sup>. Another difference with TNF- $\alpha$  is that IL-6 can signal via classic- and trans-signalling pathways, with the *trans* pathway facilitated by circulating soluble IL-6 receptor (sIL-6R) and

widespread expression of the co-receptor gp130 (see **Section 1.3.2**). Results of clinical studies suggest, however, heterogeneity in the disease and imply that the activity of additionally cytokines are responsible for perpetuating inflammation <sup>128</sup>.

Several members of the IL-1 family, including IL-1- $\alpha$ , IL-1- $\beta$ , IL-1RA, IL-18, IL-33 and IL-36, are present and functionally active within the arthritic synovium <sup>129,130</sup>. IL-1, for example, acts in synergy with TNF and mediates effector pathways like prostanoid synthesis and activation of FLS and chondrocytes. IL-1 also propitiates acute inflammatory responses, facilitating the differentiation of IL-17-producing T-cells and innate immune cells <sup>131</sup>. The inflammasome component NLRP3 is found to be an important platform responsible for the maturation and secretion of IL-1 via caspase-1 activity and has also been involved in the pathogenesis of RA. Indeed, IL-1 inhibition was shown to be very successful in blocking inflammatory disease symptoms in patients with a gain-of-function mutation in *NLRP3* gene. However, as we will see later in **Section 1.4.1**, therapeutic inhibition of IL-1 has not been successful for RA in the clinic compared to other biologics <sup>132</sup>. Type I interferons (IFNs) are also broadly present and functionally active in the synovium and peripheral blood leukocytes in RA and are associated with immune regulation by modulating leukocyte subsets. Granulocyte-macrophage colony-stimulating factor (GM-CSF) drives the differentiation of macrophages, neutrophils and dendritic cells to an inflammatory phenotype, promoting downstream cytokine release, prostanoid synthesis and enhanced cellular activation <sup>133</sup>. GM-CSF inhibitors have shown to produce rapid and clinically meaningful effects in RA similar to those observed using TNF blockade, highlighting a regulatory role for this pathway in the synovial response <sup>134</sup>.

The proinflammatory T-cell cytokine, IL-17A, has multiple overlapping functions with both TNF $\alpha$  and IL-6 <sup>135,136</sup>. IL-17A, at the same time, promotes the release of other proinflammatory cytokines such as TNF, IL-6, IL-1 and GM-CSF; chemokines such as CXC-chemokine 8 and CC-chemokines 2 and 3; and MMPs. It has also shown to help angiogenesis and osteoclast activation, and its expression correlates with disease activity and tissue damage <sup>135</sup>. Along with other growth factors, IL-17A upregulates anti-apoptotic genes and works as a recruitment and survival factor for FLSs, B-cells and T-cells, supporting germinal centre formation <sup>137</sup>. IL-17 and IL-22 are also linked to the early development of RA through the posttranslational modification of autoantibodies (sialylation) <sup>138</sup>. Furthermore, previous studies from our group have demonstrated that IL-17A is required for the development of functional ELS <sup>139</sup>. These observations have prompted the development of

biologics targeting IL-17A. However, conflicting results are reported for RA, resulting in a high degree of heterogeneity in response, whereas IL-17 inhibitors are more effective in some inflammatory immune diseases such as psoriasis<sup>140</sup>. This is possibly due to the cytokine pleiotropy and redundancy<sup>123</sup>. For example, some studies suggest blockade of IL-17 activity in combination with anti TNF- $\alpha$  therapy to achieve a more successful and stable response<sup>141</sup>. Interestingly, GM-CSF, which is a Th17-associated cytokine, is showing promise for the treatment of RA, as previously noted<sup>133</sup>.

IL-23 is crucial for the stabilisation of IL-17 expression and for promoting Th17 pathogenicity and induce autoimmune tissue inflammation<sup>141</sup>. IL-23 is a proinflammatory cytokine member of the IL-12 family that induces expression of its own receptor (IL-23R), creating a positive feedback loop that enhances IL-23 expression<sup>142</sup>. Belonging to the same cytokine family, there is IL-12, which is also a predominantly pro-inflammatory cytokine involved in Th1 cell development, and IL-35, which is, on the contrary, immunoregulatory. IL-35 has recently been found to be involved in important mechanisms for natural Tregs and in the generation of Treg cells including a population that does not express FoxP3, IL-10 or TGF- $\beta$  (iTreg cells)<sup>123</sup>. Finally, IL-27, also a member of the IL-6/IL-12 family, is a lymphokine that controls responses in T-cells and B-cells, often opposing the action of IL-6 and inhibiting Th17 differentiation (anti-inflammatory role), however, in certain settings IL-27 can promote Th1 cell expansion<sup>143</sup>. (This cytokine and its interaction with IL-6 in RA will be discussed in more detail in **Section 1.3.3**).

Besides the previously mentioned role of IL-21 as a differentiation factor for Th17 cells, IL-21 is an adaptive response cytokine produced by these cells, with downstream effects on Tfh cells, DCs, NK cells, osteoclasts and B-cells<sup>144</sup>. IL-11 has also shown to regulate many anti-inflammatory outcomes in arthritis, which sustained clinical trials with recombinant IL-11<sup>145</sup>. Additionally, IL-7 and IL-15 are cytokines essentially involved in homeostasis whose increased expression has been reported in various autoimmune diseases, including RA, and IL-15 particularly has been associated with proinflammatory roles in T-cell and NK-cell activation and with promoting crosstalk between T-cells and macrophages in RA synovitis<sup>146</sup>. These cytokines are antiapoptotic and co-stimulatory, usually supporting T-cell expansion and activation of memory T-cells, yet they could also promote autoreactivity, as shown recently; by sensitising the TCR to subthreshold stimuli, possibly including autoantigens, and simultaneously favouring pro-inflammatory pathways<sup>147</sup>. Finally, when

stimulated with ACPAs, osteoclasts produce high levels of IL-8, which is involved in driving neutrophil recruitment to the synovial fluid and activating and triggering subsequent responses during early disease <sup>148</sup>.

## 1.2.5 Ectopic lymphoid-like structures

### 1.2.5.1 *Disease heterogeneity in Rheumatoid Arthritis*

Recent progress in synovial tissue acquisition from patient joints through minimally invasive ultrasound-directed small-needle synovial biopsy, combined with histopathological assessment of joint inflammation, have allowed a better understanding of the high heterogeneity of RA synovitis <sup>74</sup>. Synovitis in inflammatory arthritis can be broadly classified into three distinct pathotypes based on the cellular and molecular signatures of inflammation: (i) follicular or lymphoid-rich, where immune cells, mainly B-cells, can be found spatially grouped into follicular structures (30-40% of patients); (ii) diffuse or myeloid-rich, where immune cells are randomly distributed within the synovial sublining; (iii) pauci-immune or fibroblast-rich, where only few infiltrating immune-cells, predominantly CD68<sup>+</sup> monocytes, are detected (60-70% diffuse and pauci-immune combined) <sup>107,149,150</sup> (**Figure 1.7A**). Importantly, follicular and diffuse patterns of synovitis are not necessarily mutually exclusive, and individual tissues may feature variable levels of diversity or overlap <sup>151</sup>. In addition, these different forms of synovitis affect the rate of disease progression, severity and response to therapy <sup>128,152,153</sup>. Advances in the field of transcriptomics are providing a more detailed picture of these pathotype subsets, and consequently, they are being renamed to reflect the overlap seen at a molecular level but not evidenced at the cellular (histological) level (e.g., fibroblastic pauci-immune, lympho- myeloid and macrophage-rich diffuse-myeloid pathotype) <sup>154</sup>.

In follicular synovitis, immune-cell follicular-structures may acquire features of secondary lymphoid organs (SLOs) such as peripheral node addressin positive (PNAd<sup>+</sup>) high endothelial venules (HEVs), T-cell and B-cell segregation with active germinal centres (GCs), and CD21<sup>+</sup> follicular dendritic cell (FDC) networks. These structures are defined as ectopic lymphoid-like structures (ELS), also referred to as tertiary lymphoid organs (TLOs) or tertiary lymphoid-like structures (TLS) <sup>150</sup>, and therefore they may also be able to generate antigen-specific responses and drive adaptive immune reactions <sup>155</sup> (**Figure 1.7B**). These local autoantibody responses have been linked with disease exacerbation and also influence the clinical

response to mainstream biologics (e.g. anti-TNF $\alpha$  inhibitors)<sup>155</sup>. Unlike SLOs that develop during embryogenesis, ELS are not encapsulated, and instead, they are induced in response to inflammatory stimuli, having the potential to develop in any tissue where persistent inflammation features. However, why and how these structures develop at these sites is currently unknown but secondary lymphoid organogenesis is used as a model for ELS development due to their resemblance<sup>156</sup>.

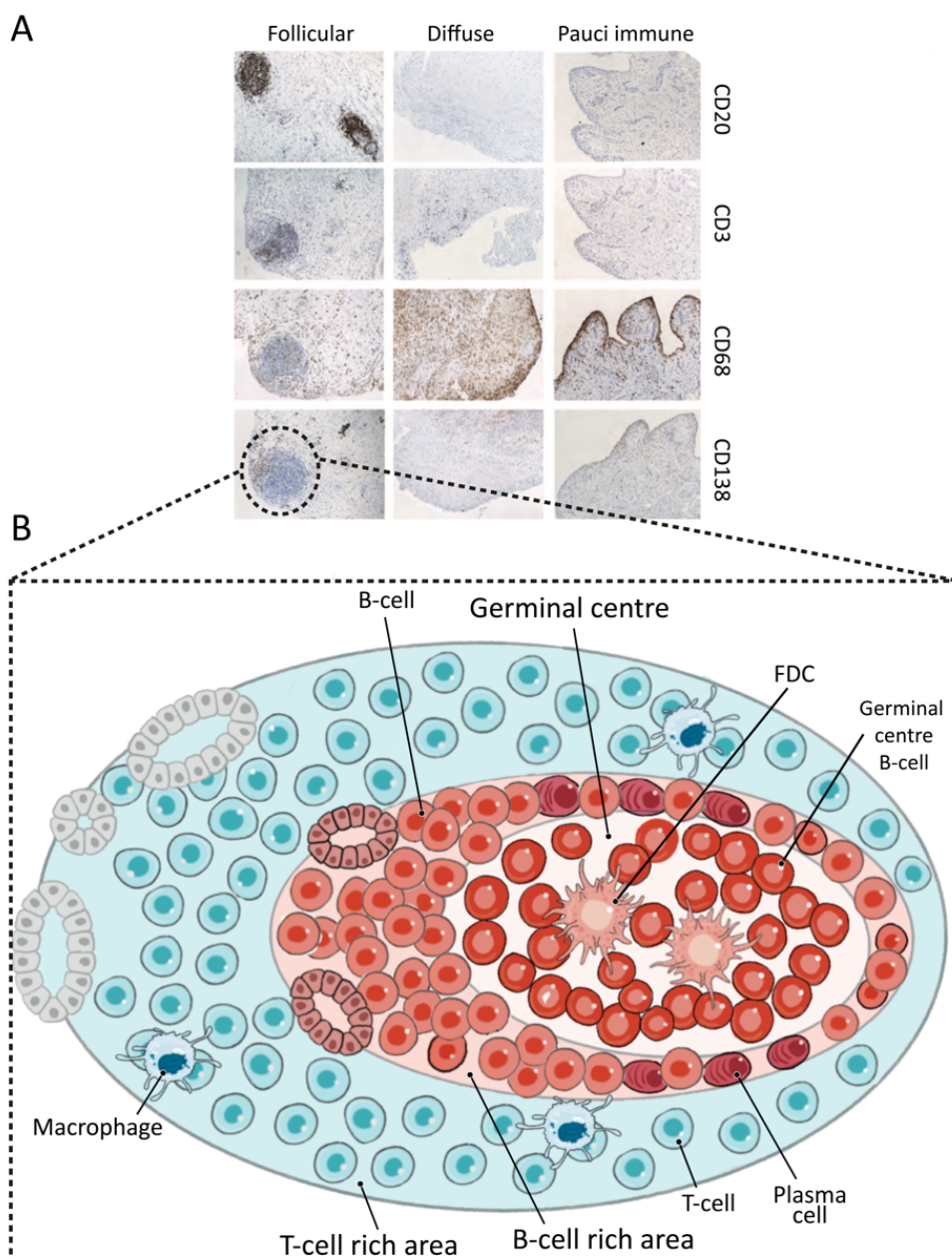


**Figure 1.7 Joint pathology in RA and ELSs structure.**

(Legend continues on the following page)



**(A)** Immunohistochemical staining for CD20 (B-cells), CD3 (T-cells), CD68 (macrophages) and CD138 (plasma cells). Synovial inflammation can include diffuse leukocyte infiltrates (diffuse or myeloid-rich), contain follicular aggregates of lymphocytes (follicular) or have low infiltration of immune cells (pauci immune). Adapted from Pitzalis *et al.* 2013. **(B)** Schematic illustration of ELSs showing similar characteristics of secondary lymphoid organs: segregation of T- cells and B-cells into separate areas; development of high endothelial venules (HEVs) and presence of follicular dendritic cells (FDCs) and hypermutated and class-switched plasma cells.

#### 1.2.5.2 Secondary lymphoid organogenesis

SLO development occurs at pre-determined sites of lymph node development during embryogenesis when haematopoietic-derived CD3<sup>+</sup> CD4<sup>+</sup> CD45<sup>+</sup> lymphoid tissue inducer (LTi) cells interact with mesenchymal-derived lymphoid tissue organiser (LTo) <sup>157</sup>. Briefly, LTi cells receive activating signals from mesenchymal organiser cells in the presence of CXCL13, IL-7 and RANKL, and express the chemokine receptor CXCR5 and IL-7R, which results in their accumulation at these sites <sup>158</sup>. Consequently, LTi cells secrete lymphotoxin (LT)  $\alpha\beta$  which stimulates stromal LTo cells to produce the homeostatic chemokines (CXCL13, CXCL12, CCL21, and CCL19) initiating the recruitment of haematopoietic cells into organised lymphoid structures <sup>156</sup>. Expression of adhesion molecules, including intracellular adhesion molecule 1 (ICAM-1) and vascular cell adhesion molecule 1 (VCAM-1) by LTo cells further supports leukocyte recruitment <sup>159</sup>, and the release of vascular endothelial growth factor (VEGF), fibroblast growth factor (FGF), and hepatocyte growth factor (HGF) promotes the development of high endothelial venules (HEVs) <sup>160</sup>. Stromal LTo cells also differentiate into cell lineages (e.g., FDCs) which create stromal cellular migration. SLOs are sites for T-cell activation and differentiation (e.g., into Th1, Th2, Th17, and Tfh cells), and Tfh cells promote the development and maintenance of germinal centres and interact with B-cells to generate high-affinity antibodies and homeostatic chemokines (**Figure 1.8A**).

#### 1.2.5.3 Mechanisms of ELS development

The mechanisms of ELS development share many similarities with those of SLO development. However, ELS are neither encapsulated nor developmentally pre-programmed. Instead, they are inducible structures that form in response to inflammatory trigger at sites of inflammation <sup>156</sup>. In addition, conventional germinal centres are better at excluding autoreactive B-cells than ectopic germinal centres; therefore ELS may serve as sites for establishing or propagating autoreactivity to local joint antigens <sup>156</sup>. While both structures rely on homeostatic chemokines and lymphoneogenic cytokines, ELS



development can occur in the absence of LTi cells. Immune cells can substitute for LTi cells as the main orchestrator of ELS formation, and activated resident stromal cells respond phenotypically like LTo cells <sup>156</sup>. These stromal cells (e.g. synovial fibroblasts) are able to produce homeostatic chemokines, including CXCL12, and influence the composition and activity of ELS <sup>161</sup>. The plasticity of T-cells may contribute to ELS formation through the acquisition of Tfh-like effector characteristics that promote B-cell activities such as active class-switching and autoantibody generation within the inflamed synovium (**Figure 1.8B**). Indeed, active germinal centres in ELS found in synovium of RA patients express activation-induced cytidine deaminase (AID) <sup>107</sup>.

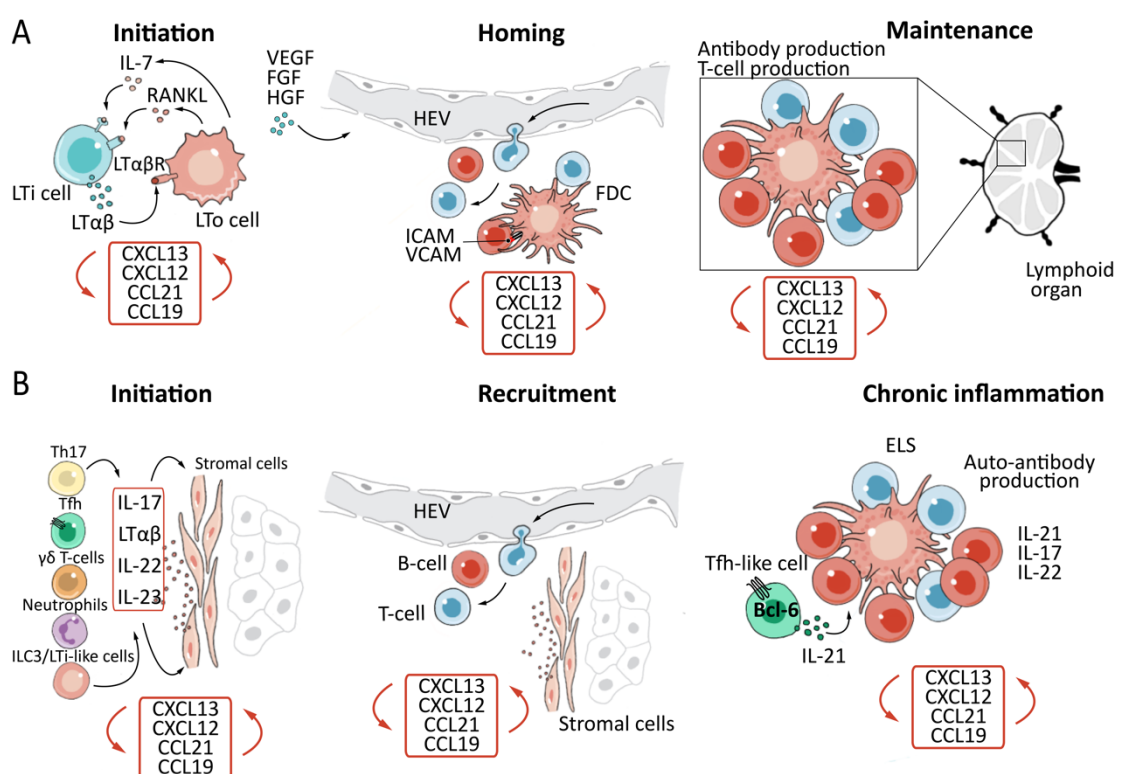


**Figure 1.8 Secondary lymphoid organogenesis and ELS structure development.**

**(A)** Secondary lymphoid organs (SLOs) formation takes place during embryogenesis at pre-programmed sites and is mediated through the interaction between LTi cells, which secrete LT $\alpha\beta$ , with LTo cells to produce homeostatic chemokines (CXCL12, CCL19 and CCL21). This generates the recruitment and spatial organisation of cells into lymphoid organs, and the release of VEGF, FGF, and HGF from LTo cells that promotes the development of high endothelial venules (HEVs). LTo cells can also differentiate into follicular dendritic cells (FDCs) that stimulate expression of adhesion molecules to further support leukocyte recruitment. **(B)** Ectopic lymphoid-like structures (ELS) usually develop in the synovium with follicular pathology. Immune cells can replace LTi cells, and the release of effector molecules can induce stromal cells to produce homeostatic chemokines involved in the recruitment and spatial organisation of cells into ELS. LTI, lymphoid tissue inducer; LTo, lymphoid tissue organiser; VEGF, vascular endothelial growth factor; FGF, fibroblast growth factor; HGF, hepatocyte growth factor; ICAM, intracellular adhesion molecule; VCAM, vascular cell adhesion molecule.

T-helper cells and their effector cytokines, particularly Th17 cells and IL-17, have recently shown to be fundamental initiators of ELS development in RA <sup>162</sup>. Studies in a murine model of inflammatory arthritis performed by our group showed that elevated levels of IL-21, derived from either Th17 or Tfh cells, were observed in synovial tissue that featured ELS, demonstrating an implication of this cytokine in ELS regulation <sup>104</sup>. Additionally, innate leukocyte subsets such as neutrophils and innate lymphoid cells (ILCs) have also been associated with ELS development. ILC3s share many effector characteristics with Th17 cells, including ROR $\gamma$ t expression, the chemokine receptor CCR6, secretion of IL-17, IL-22, and GM-CSF, and responsiveness to IL-23 and aryl hydrocarbon receptor (Ahr) ligands <sup>156</sup>. A recent study from my own laboratory identified IL-27 as an inhibitor of ELS development in inflammatory arthritis, where *Il27ra*<sup>-/-</sup> mice developed exacerbated inflammatory arthritis characterised by an increase in leukocyte infiltration, synovial exudate and homeostatic chemokine expression <sup>104</sup>. Besides, when translating these observations into the human setting, levels of IL-27 in synovial tissue from patients with RA correlated inversely with ELS development <sup>104</sup> (see **Section 1.3.3**). Thus, it is proposed that the development of ELS in autoimmunity, including RA, is detrimental and contributes to the perpetuation of the immune response.

### 1.2.6 Therapy options: past, present and future

While there is currently no cure for RA, the ongoing treatment strategy aims to achieve drug- free disease remission, or at the very least, a low disease activity state, which restricts inflammation, normalises physical function, and improves the overall quality of life for patients <sup>58</sup>. Importantly, remission also prevents progression of joint damage <sup>163</sup>. Early diagnosis and prompt initiation to effective therapy are key factors in the treatment of patients with RA, and the sooner treatment begins, the more effective the therapeutic response is likely to be <sup>119</sup>. This has been facilitated by the development of reliable instruments for clinical assessment that can be used for research and clinical practice (e.g., ultrasound, X-rays) <sup>58,164</sup> and early treatment adaptation in a treat-to-target-approach (based on tight monitoring of disease activity and change of managements if a treatment end-point is not reached) <sup>47,165</sup>. Lastly, biological agents have entered the field of RA, providing the best effectiveness in combination with methotrexate <sup>166</sup>. Consequently, the outcome of RA has had a dramatic improvement over the past twenty years.

Prior to the introduction of corticosteroids in the 1950s<sup>167</sup>, traditional therapies were largely limited to agents such as non-steroidal anti-inflammatory drugs (NSAIDs), that although they provided symptomatic relief, they did not slow disease progression<sup>34</sup>. The approval by the Food and Drug Administration (FDA) of the synthetic disease-modifying anti-rheumatic drug (DMARD) methotrexate (MTX) as a therapy for RA did not arrive until 1988. Rheumatologists have since learned how to use this immunosuppressant optimally, and this drug has become the therapeutic anchor for managing RA today<sup>168</sup>. Indeed, both American College of Rheumatology (ACR) and the European League Against Rheumatism (EULAR) management recommendations suggest starting treatment with MTX plus short term glucocorticoids upon diagnosis. If disease activity does not diminish, patients may receive a different synthetic DMARD and only when all these conventional therapies fail; biological DMARDs are then prescribed<sup>169</sup>.

In the mid-1990s, a major turning point took place in the treatment of RA, with the introduction of therapies that block the actions of specific cytokines or immune regulators (biological DMARDs), also called biologic agents<sup>119</sup>. Later on, more biologics were introduced; these therapies include (i) TNF-blocking agents such as the neutralising anti-TNF monoclonal antibodies (mAb) infliximab<sup>170</sup>, adalimumab and golimumab; the polyethylene glycol-linked mAb fragment certolizumab pegol; and the soluble TNF receptor-2-IgG-Fc fusion protein etanercept; (ii) IL-6 receptor (IL-6R) blocking monoclonal antibody tocilizumab<sup>171</sup>, (iii) the anti-CD20 B-cell-depleting monoclonal antibody rituximab<sup>172</sup>, (iv) the T-cell activation inhibitor abatacept, which is a fusion of recombinant cytotoxic T lymphocyte antigen 4 (CTLA-4) and IgG1, (v) and the IL-1 receptor antagonist anakinra. Furthermore, second-generation agents are now emerging in early-stage clinical development, including anti-IL-17 monoclonal antibodies (secukinumab and ixekizumab), the IL-17 receptor-blocking monoclonal antibody brodalumab, and alternative IL-6 blocking strategies (olokizumab, clazakizumab, sarilumab, siltuximab, olamkicept). In addition, selective small-molecule inhibitors of the JAK/STAT pathway (tofacitinib, baricitinib and ruxolitinib) and spleen tyrosine kinase (fostamatinib) have recently been approved<sup>119</sup>. The combination of all the previously described advances has considerably improved treatment outcomes for the majority of patients<sup>173</sup>. However, not all patients can achieve low disease activity, let alone remission. For example, approximately 40% of patients show poor responses to anti-TNF- $\alpha$  therapy and improved treatment decisions are still required<sup>174–176</sup>.

In addition to reducing articular inflammation in patients with RA, biologic agents also improve indices of systemic inflammation or disease-associated co-morbidities (e.g., anaemia, fatigue, osteoporosis, cardiovascular risk and depression) and lead to an overall improvement health-related quality of life assessments<sup>119</sup>. My work is focused around the current spectrum of immunotherapies that engage the IL-6/gp130/STAT3 signalling axis (discussed in **Section 1.4**); therefore, I will first introduce the role of IL-6 and JAK/STAT signalling pathway in RA in the following section.

### 1.3 JAK/STAT signalling pathway in RA

Transmembrane receptors enable cells to sense and interpret signals and changes in environmental cues. At the cellular level, these signals are generally received by a myriad of cell-surface receptors, causing cells to alter their metabolism in many different ways<sup>177</sup>. Over the past decades, extensive research has permitted a general understanding of many individual pathways of signal transduction that connect events at the cell surface directly to gene activation<sup>178</sup>. As discussed above, the hierarchical dominance of cytokines during RA development is dynamic and often depends on disease duration. However, the key pro-inflammatory cytokines involved in the pathogenesis of the disease comprise TNF, IL-6, IL-1 and GM-CSF<sup>123</sup>. The dramatic success of clinical targeting of these cytokines using biologic therapies has led to substantial interest in therapeutic targeting their transcription factors and signalling pathways. These include the Janus activated kinase (JAK) and signal transducers and activator of transcription (STAT) signalling pathway and GTPase Ras, nuclear factor (NF)- $\kappa$ B pathway and mitogen-activated protein kinase (MAPK) cascades. Description of the former pathways is, however, beyond the scope of this Introduction, and has been amply discussed elsewhere<sup>179–182</sup>. Here I will focus on the JAK/STAT signal pathway in the context of RA, which is also perhaps one of the pathways best understood out of those mentioned above.

#### 1.3.1 JAK/STAT signalling pathway

The JAK/STAT signalling pathway is an elegant, poised transmembrane receptor-to-nucleus communication system. A wide variety of cytokines, colony-stimulating factors, and hormones employ this mode of signal transduction. Upon receptor-ligand engagement, the correspondent receptor cassette dimerises and activates receptor-associated JAK proteins. The mammalian JAK family comprises four members named JAK1, JAK2, JAK3, and TYK2,

which are selectively employed by different receptor systems <sup>183</sup>. The dimerisation or clustering of receptor signalling chains brings the JAKs into close proximity, causing their tyrosine phosphorylation and regulation of kinase activity. The activated JAKs then phosphorylate the intracellular tail of their receptors, thereby creating docking sites that are recognised by SH2 domains found in latent, cytoplasmatic STAT transcription factors (**Figure 1.9**). For example, IL-6-JAK-mediated phosphorylation promotes the recruitment and activation of STAT1, STAT3 and, to a lesser extent, STAT5 <sup>184</sup>, which in turn dimerise and translocate to the nucleus where they directly bind DNA and regulate gene expression (**Figure 1.10A**). JAK/STAT signalling through gp130 is strictly controlled at many steps through distinct mechanisms. Key regulators include the protein inhibitor of activated STATs (PIAS), the suppressors of cytokine signalling (SOCS) and members of the CIS ('cytokine-inducible SH2-domain-containing') family of cytokine receptor inhibitors, which act to limit IL-6 signalling <sup>184</sup>. Finally, the clinical relevance of the JAK/STAT pathway has also been evidenced by the existence of several disorders of primary immunodeficiency that are linked to known mutations of JAKs and STATs (e.g., Hyper IgE (HIES) or Job's syndromes, mucocutaneous candidiasis, mycobacterial infection) <sup>185</sup>.

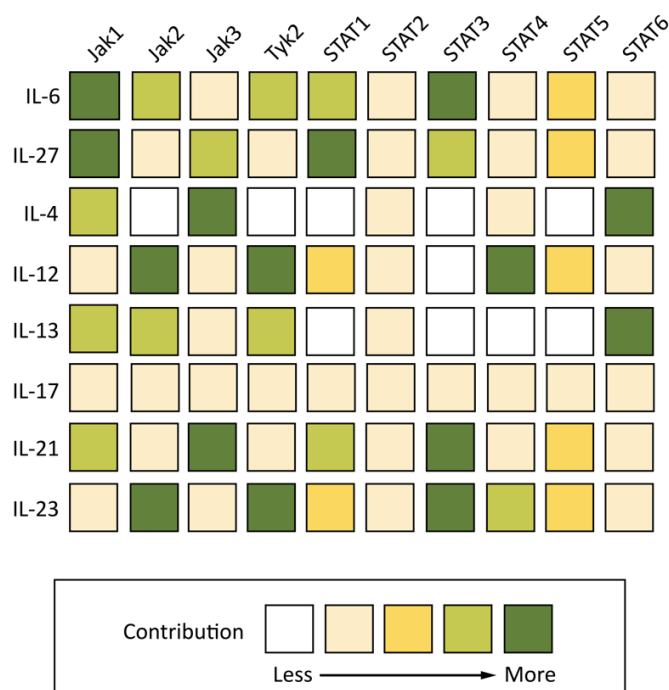


**Figure 1.9 Alignment of the JAK-STAT family members with associated cytokines.**

The four Jaks (Jak1, Jak2, Jak3, Tyk2) are selectively bound to and therefore mediate signalling for various cytokine receptors; and different cytokines also have a propensity to activate certain STATs, as indicated. The heat map depicted above details how individual cytokines contribute to specific members of the JAK/STAT signalling pathway. (Adapted from O'Shea *et al.*, 2013 and Hunter & Jones, 2015).

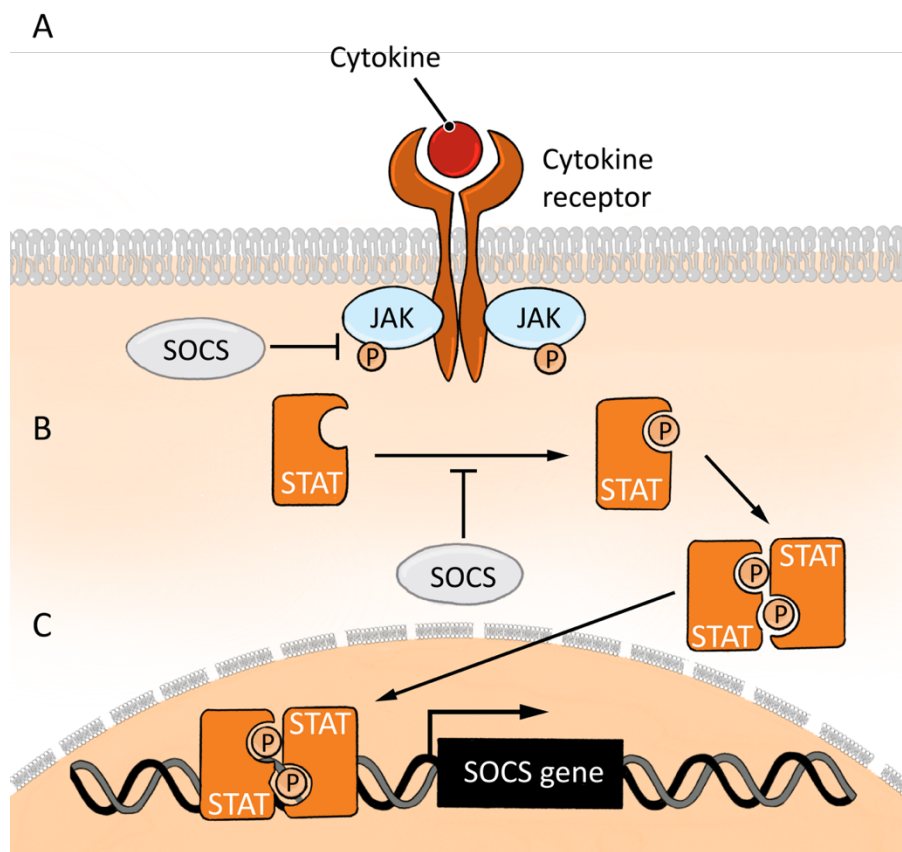


**Figure 1.10** Key components of the Jak-STAT signalling pathway.

**(A)** When a cytokine engages its receptor, JAKs become activated and phosphorylate each other, as well as the intracellular tail of their receptors. This creates a docking site for STATs, which are now able to bind to the cytoplasmic domain of the receptor. **(B)** The STATs, in turn, are phosphorylated and activated, which allows them to dimerise and translocate to the nucleus, where it can directly bind DNA and regulate gene expression. **(C)** SOCS genes are induced by activated STATs, and SOCS proteins inactivate JAK/STAT pathway by inhibition of JAK kinase activity and/or promoting degradation of the signalling complex.

#### 1.3.1.1 The STAT transcription factors

STAT transcription factors are latent cytoplasmic proteins that form homodimers upon activation, due to a specific homotypic interaction between domains present at the amino termini of the individual STAT proteins. Following IL-6 binding to the IL-6 $\alpha$ /gp130 complex, STAT proteins are recruited (Jak-mediated) to the cytokine/receptor complex via the SH2 domain where they become phosphorylated. This recruitment leads to a rearrangement, in which the phosphotyrosine of each STAT protein bind to the SH2 domain of the other STAT, forming a configuration that can directly engage DNA regulatory elements (DREs) and thereby control the transcription of associated genes <sup>186</sup> (**Figure 1.10B**). Although IL-6

activates both STAT1 and STAT3, IL-6 has often been equated with activating STAT3, whereas IL-27 mostly activates STAT1<sup>187,188</sup>. Notably, a study by Hirahara and colleagues indicated that STAT3 is responsible for the overall transcriptional output driven by both IL-6 and IL-27, whilst STAT1 is the major driver of specificity<sup>189</sup>. Likewise, IL-6 and IL-10 employ STAT3 as their main signalling component, but their downstream cellular effects are clearly different, as evidenced by their respective pro-inflammatory and anti-inflammatory activities in myeloid cells<sup>186</sup>. However, there are more than 60 cytokines that signal via seven different STATs (1-4, 5a, 5b, and 6) and the mismatch in numbers means that many cytokines activate the same STATs and the action of cytokines probably represents the combinatorial participation of multiple STATs<sup>189</sup>.

In addition to nearby DREs such as promoters, STATs frequently localise distant from protein-encoding genes such as enhancers (regions of DNA that promote gene expression via protein activators)<sup>190</sup>. Therefore, STATs engage with distal DREs and regulate enhancer activity and/or epigenetic status of associated genes by means of physical interaction with histone acetyltransferases (HATs) (e.g., p300) or methyltransferases (MTs) (e.g., EZH2), or directly instruct far non-coding loci (e.g., miRNAs). STAT-regulated DREs are commonly studded with several binding sites that tend to attract more than one STAT, generating overlaps, and co-localise with those of other transcription factors<sup>186</sup>. Thus, STATs can physically interact with other transcription factors or transcriptional regulators (e.g., glucocorticoid receptor, SP1-like transcription factors) to control gene expression<sup>186</sup>.

Since signalling by these receptors depends on tyrosine phosphorylation, dephosphorylation of the receptor complex by tyrosine phosphatases is one way that cells can terminate signalling. A variety of tyrosine phosphatases have been implicated in the dephosphorylation of cytokine receptors, JAKs, and STATs. These include protein phosphatases such as dual-specificity protein phosphatases (DUSPs) and protein tyrosine phosphatases (PTPs) which have the capacity to modify the way particular T-cell subsets sense and interpret common cytokine cues<sup>191,192</sup>. For example, PTPN2 and PTPN11 control the phosphorylation of STAT1 in fibroblasts<sup>193</sup>, and PTPN22 and PTPN2 control STAT1 phosphorylation in response to IL-6 in memory or activated CD4<sup>+</sup> T-cells<sup>194</sup>.

The discovery of new Th cell subsets is linked with the identification of significant roles for STAT transcription factors in the differentiation towards the specific effector characteristics of these diverse populations<sup>195</sup>. Furthermore, novel technology platforms including



next- generation sequencing methods and proteomic approaches also allow extensive views of STAT action while insights from GWAS identify genetic risk loci in genes linked with JAK proteins, STAT transcription factors or downstream targets in human pathology<sup>195</sup>

#### 1.3.1.2 *SOCS proteins: primary negative regulators of JAK/STAT activation*

Suppressor of cytokine signalling (SOCS) intracellular, cytokine-inducible proteins are the most thoroughly studied regulators of JAK/STAT signalling. The SOCS family of proteins has eight members: CIS (cytokine-inducible SH2 domain protein) and SOCS1-SOCS7<sup>196</sup>. This group of proteins shares a central SH2 domain, a conserved carboxy-terminal SOCS box and an amino-terminal domain of variable length and sequence<sup>197</sup>. SOCS proteins are generally expressed at low levels in unstimulated cells and become rapidly induced by cytokines, growth factors, chemokines and pathogenic components, thereby inhibiting JAK/STAT signalling and forming a classic negative-feedback loop<sup>198</sup> (**Figure 1.10C**). The SH2 domain of SOCS1 and SOCS3 binds directly to tyrosine-phosphorylated JAKs, resulting in the direct inhibition of JAK activity. However, once SOCS3 is recruited to receptors via high-affinity binding sites, such as gp130, it binds to and inhibits the catalytic activity of JAK1, JAK2 and TYK2<sup>199</sup>.

Both SOCS1 and SOCS3 also compete for the acquisition of phosphorylated cytokine receptor tyrosine residues, thereby blocking STAT binding. Furthermore, the involvement of SOCS proteins in the degradation of signalling proteins through the ubiquitin-proteasome pathway via interaction with their SOCS box has also been suggested<sup>197</sup>. Compared to other SOCS family members, the SOCS box of SOCS1 and SOCS3 binds with lower affinity to the E3 ligase protein, Cullin-5, revealing their differential mechanism of action<sup>200</sup>. Among the SOCS family, SOCS1 and SOCS3 are the best characterised in their inhibition of JAK/STAT signalling, and both have essential roles in the regulation of immune functions. SOCS3 is a well-characterised regulator of STAT3 activation in response to several cytokines, including those in the gp130-containing IL-6 receptor family, although it can also inhibit other STATs<sup>201</sup>. SOCS3 has an important regulatory role in innate immune regulation (e.g., during infection) and adaptive immunity (e.g., T-cell activation and polarisation), however here I will specifically focus on its role in inflammatory arthritis.



### 1.3.1.3 *STAT3 and SOCS3 in RA*

IL-6/gp130 signalling through STAT3 plays an integral role in the progression of inflammatory arthritis. In 1995, Wang *et al.* reported activated STAT3, but not STAT1, in cells isolated from the synovial fluid of patients with RA <sup>202</sup>, and synovial fluid from RA patients induced STAT3 activation in monocytes <sup>203</sup>. A study conducted by my colleagues indicated a role for STAT3 in directing leukocyte infiltration within the inflamed joint during repeated episodes of monoarticular arthritis <sup>204</sup>. Furthermore, mice expressing mutant gp130 (generated by known-in mutation of *Il6st*) that is unable to bind SOCS3, display more sustained signalling via STAT1 and STAT3 and develop exacerbated inflammation <sup>204,205</sup>. Similarly, genetic overexpression of the SOCS3 in experimental models of disease has shown that negative regulation of STAT3 activity leads to substantive improvements in inflammatory conditions, including synovitis <sup>206,207</sup>. A recent study provided evidence that STAT3 promotes inflammation and joint erosion in a mouse model of arthritis <sup>208</sup>. Furthermore, the presence of synovial ELS has been linked with enhanced STAT3 activity, and in previous studies from my laboratory, significant pY-STAT3 staining was found within the joint, although not exclusively restricted to synovial ELS <sup>104</sup>. More recently, a study in mice showed that a haploinsufficiency of the *Ptpn2* gene was associated with the pathogenic conversion of Treg cells into Th17 cell during inflammatory arthritis, where exacerbated synovitis was also linked with heightened STAT3 activity and the development of ELS <sup>209</sup>.

Studies delivering SOCS3 as a therapeutic approach in models of arthritis have shown reduction in IL-6 production and arthritis severity <sup>206</sup>. Additionally, high expression of SOCS3 in splenic APCs led to decreased production of IL-6 and TNF- $\alpha$ , but heightened production of the immune-modulatory cytokine IL-10 and consequent protection against inflammatory arthritis <sup>210</sup>. Interestingly, in the absence of SOCS3, the effects of IL-6 are altered to resemble those of IL-10, which is a potent inhibitor of macrophages and dendritic cells <sup>207,211,212</sup>. Moreover, deletion of SOCS3 in endothelial and hematopoietic cells was linked to severe IL-1-dependent inflammatory arthritis, featured by an increase in bone destruction and neutrophil synovial infiltrate <sup>213</sup>. This absence of SOCS3 enhanced T-cell and macrophage activation, leading to upregulation of IL-17 and IL-6 and an uncontrolled, detrimental STAT3 signal transduction <sup>213</sup>. In addition, Van de Loo *et al.* showed that SOCS3 mRNA and protein are increased in human pathological chondrocytes, suggesting that SOCS3 dysregulates normal chondrocyte function, and therefore, play an important role in the development of

cartilage pathology observed in RA patients <sup>214</sup>. Together, these findings reveal the significant role SOCS3 and STAT3 play in RA progression and emphasise that signal inhibition of STAT transcription factors, especially STAT3 (see **Chapter 3**), by SOCS3 could be an effective strategy in the treatment of RA (see **Chapter 4**).

### 1.3.2 Interleukin-6

IL-6 represents a keystone cytokine in inflammation and is implicated in many pathologic features of RA, driving disease progression and supporting the maintenance of immunological reactions. Although it was first identified for its ability to regulate the acute phase response and support the activation and expansion of T-cell populations and differentiation of B-cells <sup>215</sup>, IL-6 has now been attributed hormone-like characteristics that influence the neuroendocrine system, neurological behaviour, lipid and iron metabolism, vascular disease, insulin resistance and mitochondrial activities <sup>118,216</sup>. While almost all immune and stromal cells produce IL-6 mainly in response to IL-1 $\beta$  and TNF, IL-6 expression is also induced by other cytokines (e.g., GM-CSF, IL-17), prostaglandins, adipokines, stress responses and other TLRs agonists <sup>212</sup>. Therefore, while IL-6 is a pleiotropic cytokine with a protective role in many infections, the same activities can be key to the propagation and maintenance of chronic inflammation, including RA <sup>212</sup>.

#### 1.3.2.1 *The IL-6 receptor complex*

IL-6 signalling relies on the IL-6 receptor complex, which is composed of an 80-kDa type 1 cytokine  $\alpha$ - receptor subunit (IL-6R; also known as CD126), and a universally expressed 130- kilodalton (kDa) signal-transducing  $\beta$ -receptor-subunit (gp130; also known as CD130; encoded by *IL6ST*) <sup>217–219</sup>. In order to be fully functional, the IL-6 receptor requires formation of an IL-6–IL-6R–gp130 complex that is clustered into a dimer structure <sup>220</sup>. While IL-6R expression is restricted to hepatocytes, leukocytes and megakaryocytes, gp130 is expressed ubiquitously <sup>221</sup>. In fact, other cytokines such as IL-11, IL-27, oncostatin-M, ciliary neurotrophic factor, leukaemia inhibitory factor and cardiotrophin-1, also share this gp130 transducing co-receptor <sup>143,216</sup>. Once the IL-6 receptor complex is engaged, there are multiple downstream events that allow IL-6 to mediate its different effects.

### 1.3.2.2 Classical and trans-activation of IL-6 receptor signalling

IL-6 signalling via the membrane-bound IL-6R subunit (only in cells that express it), in partnership with gp130, is a mechanism termed as ‘classical’ IL-6R receptor signalling, whilst IL-6 ‘trans-signalling’ refers to a process in which a soluble form of IL-6R (sIL-6R) binds secreted IL-6 to form a complex that increases the circulating half-life of IL-6 and promotes its bioavailability<sup>221,222</sup> (**Figure 1.11**). This soluble form of the IL-6R can be produced by proteolytic cleavage of the extracellular domain by the enzyme adamalysin and disintegrin-associated metalloproteases (ADAM)-17 and ADAM-10, or by differential splicing of the *IL6ra* gene to produce a protein lacking the membrane anchor region<sup>223</sup>. Therefore, since any gp130-expressing cell can achieve responsiveness to IL-6, IL-6 trans-signalling broadens the cell types that can respond to IL-6. It has been suggested that these distinct signalling mechanisms coordinate differing biological outcomes. For example, classical IL-6 receptor signalling is to be more centrally involved in processes affecting tissue homeostasis, metabolism and acute phase responses<sup>212</sup>, while IL-6 trans-signalling is important for the recruitment and apoptosis of leukocytes, the maintenance of the effector function of T-cells, and the inflammatory activation of stromal tissues<sup>224,225</sup>. Naïve, effector memory and central memory T-cells all express IL-6 receptor, but their response to IL-6 differs depending on whether they have previously experienced TCR activation<sup>194</sup>. Additionally, CD4<sup>+</sup> T cells recovered from sites of disease typically lack IL-6R but remain responsive to IL-6 trans-signalling<sup>212</sup>.

A soluble form of gp130 (sgp130) is also released by cells generated by alternative splicing of the *IL6st* trans-signalling and to a lesser extent by proteolytic cleavage<sup>226</sup>. Although sgp130 does not bind IL-6 or IL-6R alone, sgp130 interacts with the IL-6–sIL-6R complex to block IL-6 trans-signalling, and IL-11 trans-signalling too; although the biology of the latter pathway is less clear<sup>227</sup>. Biochemical studies have shown that sgp130 has no effect on classical IL-6 receptor signalling and has a limited effect on other gp130-activating cytokines (for example, IL-27 responses are unaffected by sgp130)<sup>212</sup>. Alternatively, IL-6 signal transduction can be induced by a third mechanism, namely IL-6 trans-presentation or “cluster signalling” that occurs when membrane-bound IL-6:IL-6R complexes on transmitter cells activate gp130 receptors on neighbouring receiver cells and activate signal transduction through sgp130 dimerisation<sup>228,229</sup>. The participation of these models of receptor signalling in health and disease means that inhibitors that target IL-6 or the cognate IL-6R or selectively

block IL-6 trans-signalling are in development. A variation of these novel blockers using nanobodies and their implications in disease will be discussed in **Chapter 5**.

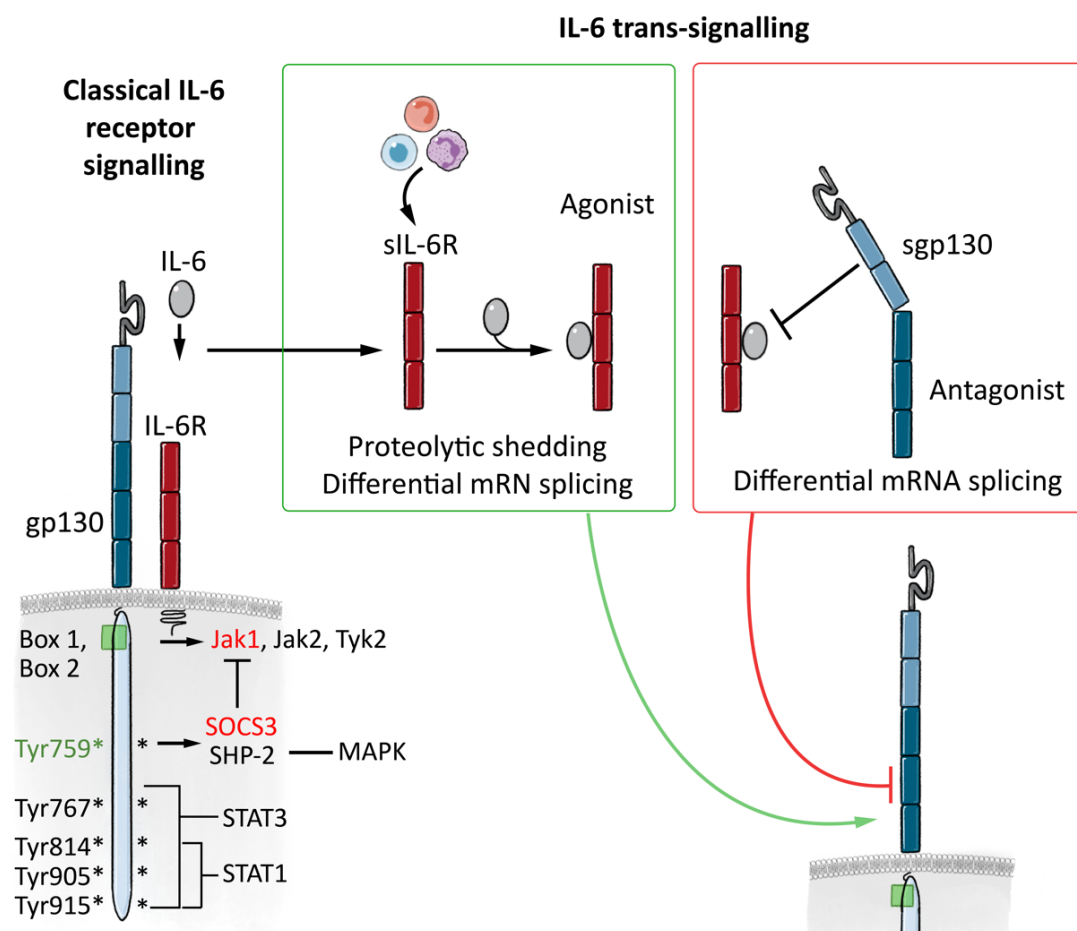


**Figure 1.11 Different mechanisms of IL-6 receptor signalling.**

Classical IL-6 receptor signalling takes place in cells expressing a non-signalling receptor IL-6R, that binds IL-6; and the signal-transducing receptor for IL-6 and its related family members, the gp130 subunit. On the other hand, IL-6 trans-signalling allows IL-6 to act on cells that lack IL-6R, by binding to a soluble form of IL-6R that is released from the cell surface of infiltrating neutrophils, monocytes and T-cells, by proteolysis and splicing of IL6R mRNA, forming an agonistic complex that signals through gp130. IL-6 trans-signalling is antagonised by sgp130. Both modes of IL-6 receptor signalling lead to gp130 activation of Jak proteins, which can phosphorylate several tyrosine residues in the carboxy-terminal of the cytoplasmic tail of gp130. This phosphorylated tyrosine serves as docking sites for the recruitment and activation of STAT1, STAT3 and the mitogen-activated protein kinase (MAPK) cascade. Tyr759 is crucial for docking of the tyrosine phosphatase SHP-2 and the cytokine receptor signalling inhibitor SOCS3, acting as negative regulators of gp130-STAT signalling. (Adapted from Hunter & Jones, 2015).

### 1.3.2.3 *IL-6 in innate and adaptive immunity*

An essential role for IL-6 in innate immunity is revealed by the identification of an ancestral IL-6-like cytokine system in *Drosophila melanogaster*<sup>230</sup>. Particularly, unpaired-3 (IL-6-like), when induced as a response to bacterial infection, forms a signalling network with domeless (gp130-like), hopscotch (Drosophila homolog of mammalian Jak) and marelle (a Drosophila homolog of a STAT protein; also called stat92E) to promote innate immunity<sup>212,230</sup>. In addition, IL-6 is linked to mononuclear phagocytes, the complement system and pattern-recognition receptors<sup>212</sup>.

IL-6 modulates almost every aspect of the innate system, including the accumulation of neutrophils at sites of infection or trauma through the control of granulopoiesis<sup>212</sup>. IL-6 trans-signalling in stromal tissue cells, enabled by these infiltrated neutrophils, inhibits expression of chemokines CXCL1, CXCL8 and CX3CL1, promotes release of CXCL5, CXCL6, CCL2 and CCL8 as well as ICAM-1 and VCAM-1. Moreover, IL-6 also mediates neutrophil apoptosis<sup>231</sup>, and consequently, *Il-6*<sup>-/-</sup> mice display a heightened and prolonged neutrophil accumulation<sup>232</sup>. IL-6 inhibits pro-inflammatory cytokine release and promotes an alternatively activated macrophage phenotype associated with wound healing, coordinating anti-inflammatory activities that are essential for resolution of inflammation<sup>233,234</sup>. IL-6 also promotes IL-10 production in T-cells, again balancing pro-anti-inflammatory behaviours<sup>235</sup>. Taken together, IL-6 has context-dependent pro-inflammatory effects that ensure competent host defence and yet prevent excessive tissue damage.

Conversely, IL-6 also shapes adaptive immunity, having an important role in driving chronic inflammation. Here, IL-6 plays pivotal roles in both lymphocyte proliferation and survival, and the coordination of lymphocyte differentiation into defined lymphoid subsets<sup>212</sup>. As noted before, IL-6 promotes commitment to the Tfh cell lineage through induction of *Bcl6* and control of IL-21 activity, supporting B-cell responses and class-switching and therefore, acting as a principal link between T-cell and B-cell responses<sup>87,89,236</sup>. However, given the complexity of IL-6 signalling, it is not clear if blockade of IL-6 in RA affects pre-existing Tfh B-cell populations in ELS<sup>212</sup>. IL-6 is required for the differentiation of IL-17-secreting CD4<sup>+</sup> or CD8<sup>+</sup> cells. IL-6 activation of STAT3 in naïve CD4<sup>+</sup> T-cells in the presence of the morphogen TGF- $\beta$  results in the expression of ROR $\gamma$ t and expansion of Th17 cells that secrete IL-17A and IL-17F as their signature cytokines<sup>86,237–239</sup>. Conversely, IL-6 inhibits the expansion of Foxp3<sup>+</sup> Treg cells and at sites of inflammation can reprogram regulatory T-cells to adopt alternate

effector cytokine characteristics<sup>240</sup>. The function and implications of Tfh and Treg cells in RA have been previously described in **Section 1.2.4.1**. Lastly, the fact that *Il6*<sup>-/-</sup> mice show protection in experimental models of inflammatory arthritis<sup>241,242</sup> and other inflammatory diseases further demonstrates the crucial role of IL-6 in chronic inflammation.

### 1.3.3 Interleukin-27

The IL-6-related family member IL-27 is increasingly acknowledged for its effects on cellular proliferation, lymphocyte differentiation and the inhibition of IL-2 and certain IL-6 regulated outcomes<sup>143</sup>. IL-27 is a heterodimeric cytokine consisting of an Epstein-Barr virus-induced gene 3 (EBI3) subunit and an IL-27p28 (also known as IL-30) subunit<sup>243</sup>. Initially described as a proinflammatory cytokine, IL-27 was characterised by its ability to promote and maintain the proliferative survival of IFN- $\gamma$ -secreting Th cells<sup>187,243–245</sup>. However, subsequent studies revealed that IL-27 elicits various immunosuppressive actions and can restrict the development of T-cell-driven response through inhibition of IL-2<sup>143,246</sup>. These anti-inflammatory properties are mainly attributed to the ability of IL-27 to promote distinct Th cell populations, such as Treg and Type-1 regulatory T (Tr1)-cells, that express IL-10<sup>247,248</sup>. Furthermore, IL-27 has emerged as a potent negative regulator of Th17 cell development<sup>249</sup>.

#### 1.3.3.1 *The IL-27 receptor complex*

Like all IL-6 family cytokines, IL-27 signals through binding its cognate receptor IL-27R $\alpha$  (also termed WSX-1 or T-cell cytokine receptor (TCCR)), which is limited primarily to monocytes, lymphocytes and osteoclasts, and the receptor gp130<sup>250</sup>. However, unlike IL-6, IL-27 uses only a classical IL-27 receptor system comprising IL-27R $\alpha$  and gp130 (**Figure 1.12**). Moreover, although both IL-6 and IL-27 receptor activation leads to signalling through STAT1 and STAT3, IL-27 is the only IL-6-related cytokine family to predominantly signal through activation of STAT1<sup>250</sup>. Consequently, both cytokines elicit common and distinct biological effects regulating innate and adaptive immunity; IL-27 often opposing the action of IL-6 regarding T-cell mediated pathology.

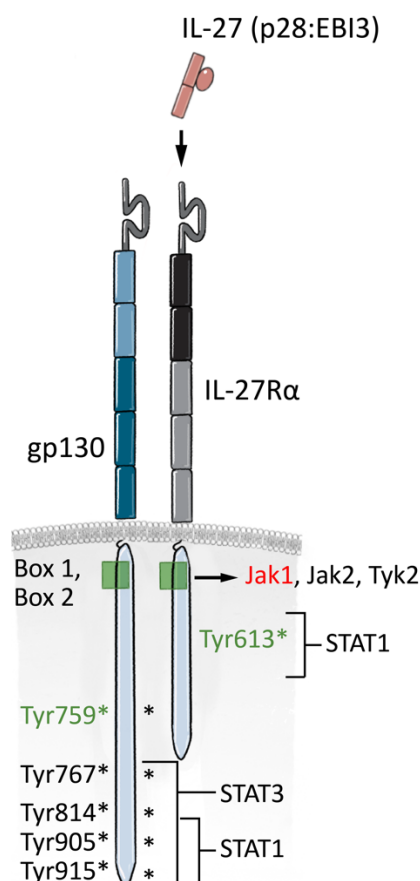


**Figure 1.12 The IL-27 receptor complex.**

IL-27 is composed of two subunits: IL27p28 and EBI3 and is mainly produced by myeloid cells (macrophages, monocytes and dendritic cells). IL-27 signals through binding its cognate receptor, IL-27R $\alpha$ , which is expressed in lymphocytes, monocytes and osteoclasts; in partnership with the signal-transducing co-receptor, gp130. Like IL-6, IL-27 predominantly signals through STAT1 and STAT3, although IL-27 has a preferential activation of STAT1.

### 1.3.4 Relation of IL-6 and IL-27 in inflammatory arthritis

The lymphokines IL-6 and IL-27 have an important role in shaping synovial pathology. Here, their activities also result in contrasting inflammatory outcomes that impact the initiation, maintenance and severity of joint disease<sup>143</sup>. As mentioned before, *Il6*<sup>-/-</sup> mice display a protected phenotype with reduced synovial leukocyte infiltration, and erosive joint damage in models of inflammatory arthritis<sup>204,241,242,251</sup> and RA patients show high levels of IL-6 in the synovial fluid<sup>252</sup>. Conversely, IL-27 deficiency is linked with the development of a more severe form of synovitis and enhanced adaptive immune responses, reflected by an increase in effector CD4<sup>+</sup> T-cells and antibody responses<sup>104</sup>. For example, *Il27ra*<sup>-/-</sup> mice presented enhanced mBSA-specific titres, and synovial T-cell infiltrate with the presence of ELS in response to antigen-induced arthritis<sup>104</sup>. Similarly, patients with follicular disease, where ELS are observed, displayed decreased expression of IL-27 compared to patients with diffuse synovitis<sup>104</sup>. Importantly, IL-27RA was highly expressed in cells localised at ELS, in the follicular form of synovitis. Thus, a lack of IL-27 signal may support the development of a follicular form of synovitis that is linked with severe disease and poor responses to biological

therapy<sup>128,153,253</sup>. More recently, I have contributed to studies showing that these inhibitory actions extend to ELS inflamed salivary glands with clinical features reminiscent of another rheumatological condition – Sjogren’s syndrome<sup>254</sup>. Local expression of IL-17 and IL-21 was linked to ELS development in antigen-induced arthritis<sup>104</sup>, and effector cytokines associated with Th17 cells, such as IL-17F, IL-21, IL-23, IL-22, have also been involved in synovial lymphoid neogenesis in clinical RA<sup>255</sup>. Moreover, In CIA mouse models, systemic administration of IL-27 resulted in reduced incidence of disease and histological paw score. This was associated with reduced collagen-specific antibody titres and decreased serum levels of IL-6 and IL-17<sup>256</sup>. Hence, while cytokines such as IL-6 and IL-21, can facilitate ELS development in inflammatory arthritis, IL-27 is a negative regulator of ELS.

IL-6 and IL-27 also have an effect on stromal tissue responses to inflammation. For instance, IL-6 and IL-27 contribute significantly to bone remodelling, where a disparity between bone formation and resorption leads to bone destruction in inflammatory arthritis<sup>257,258</sup>. IL-27 inhibits RANKL-mediated activation of nuclear factor kappa-B ligand (RANKL) in osteoclast precursors<sup>259</sup>. IL-27 also restrains the production of RANKL in activated CD4<sup>+</sup> T-cells<sup>260</sup>. Furthermore, a recent study linked IL-27 to pain, which may be relevant to pain in RA, which is a priority RA research area, and consequently, showed potential for IL-27 to span immunomodulation and pain treatment<sup>261</sup>. In conclusion, both IL-6 and IL-27 cytokines assist in the control of synovitis and associated changes in cartilage and bone erosion. These anti-inflammatory properties, together with the inhibitory control of effector Th17-type responses by IL-27, suggest that an IL-27 supplementation intervention may offer a therapeutic strategy for RA (discuss later in **Section 1.4.1**).

## 1.4 Therapeutic approaches for RA

The design and application of biological drugs for RA have been of considerable interest for several decades. Due to the breadth and pace of development of this field, a truly exhaustive review of all this literature is beyond the scope of this introduction. Here, I will instead introduce the current biologic agents and future prospects in RA that are relevant to my own studies. Some expansion of this background will be provided in the introduction to specific results chapters. In this respect, small molecule inhibitors of signal transduction pathways will be discussed in **Chapters 3** and **4**, while cytokine blockers will be the focus of **Chapter 5**.



### 1.4.1 Cytokine blockers

The recognition of cytokines as primary targets for therapy led to the development of cytokine inhibitors for the treatment of RA. Biologic agents that target TNF $\alpha$  or IL-6 have had a major impact on the management of RA <sup>262,263</sup>, whereas IL-1 $\beta$  blocker (anakinra) has been of limited application in treating RA and is considered effective in conditions where the inflammasome is a central feature of the pathology (such as gout and various inflammatory syndromes) <sup>264</sup>. The roles of other IL-1 family members, such as IL-33, IL-36 $\alpha$ , IL-36 $\beta$ , IL-36 $\psi$ , IL-37 and IL-38 and their potential usefulness as therapies or therapeutic targets, are still being investigated in preclinical studies <sup>265</sup>. In the future, recombinant forms of the newer members of the IL-1 family should be developed for use in clinical trials <sup>265</sup>.

Because of the overlap and interplay between cytokines that drive synovial inflammation, the traditional view of a defined cytokine hierarchy has been altered and therefore switching from TNF $\alpha$  to IL-6 inhibitors in RA patients might be appropriate when TNF $\alpha$  inhibitor therapy fails <sup>119</sup>. Indeed, the intracellular signalling mechanisms activated by these cytokines are different: TNF $\alpha$  mainly operating through NF $\kappa$ B and extracellular signal-regulated kinase (ERK) signalling pathways <sup>266</sup> while as previously discussed, IL-6 signals through the JAK/STAT pathway <sup>124</sup>. However, neither of these pathways are exclusive to IL-6 and TNF $\alpha$ ; various other cytokines and pattern recognition molecules signal through NF $\kappa$ B (including IL-1 $\beta$ , IL-17 and Toll-like receptors) <sup>267</sup> or STAT transcription factors (for example, IL-10, IL-21, IL-23). Some of which are now considered potential therapeutic targets for clinical intervention in RA (e.g., secukinumab, IL-10, IL-21 and IL-23) <sup>268</sup>.

To date, five unique anti-TNF agents have been clinically developed, approved, and are used in rheumatology practice (etanercept, infliximab, adalimumab, certolizumab and golimumab), one IL-1 $\beta$  blocker (anakinra) is currently being used, although with limited success; and there are only two IL-6 inhibitors available for routine management of RA (tocilizumab and sarilumab) (**Figure 1.13**), with other four in Phase III clinical trials (sirukumab, olokizumab, clazakizumab and vobarilizumab). However, the success of IL-6 blocking therapies has incited the development of a number of alternative drugs that target different structural domains of IL-6 or its receptor <sup>216</sup> (discussed in **Chapter 5**). For example, a sgp130Fc fusion protein (olamkicept), which targets IL-6 bound to the IL-6R <sup>143</sup>. Additionally, several newer biologic agents targeting other cytokines associated with RA pathology are under clinical development. For example, IL-17 (gold standard therapy now

for psoriasis and spondyloarthropathies), is targeted by secukinumab and ixekizumab <sup>269</sup> and its receptor by brodalumab <sup>270</sup>, and the p40 subunit common to both IL-12 and IL-23 is targeted by ustekinumab <sup>271</sup>. These cytokines are centrally involved in the programming of early innate and adaptive immune responses, including, the differentiation and commitment of naive CD4<sup>+</sup> T-cells into effector T-cell populations <sup>272</sup>. Moreover, mavrilimumab is a monoclonal antibody that targets GM-CSF, which in addition to haematopoiesis, has important immunoregulatory functions <sup>273</sup>. The monoclonal antibody showed convincing efficacy and good tolerability in a large Phase II trial in RA, and further development in phase III is anticipated <sup>273</sup>. Finally, denosumab is a human monoclonal IgG2 antibody that inhibits bone resorption by binding and inhibiting the receptor activator of the NF- $\kappa$ B ligand, RANKL <sup>274</sup>. In summary, cytokine inhibitors have revolutionised therapeutics for RA and other inflammatory musculoskeletal diseases by offering unparalleled efficacy and favourable safety profiles as well as changing the economic perspectives in rheumatology.

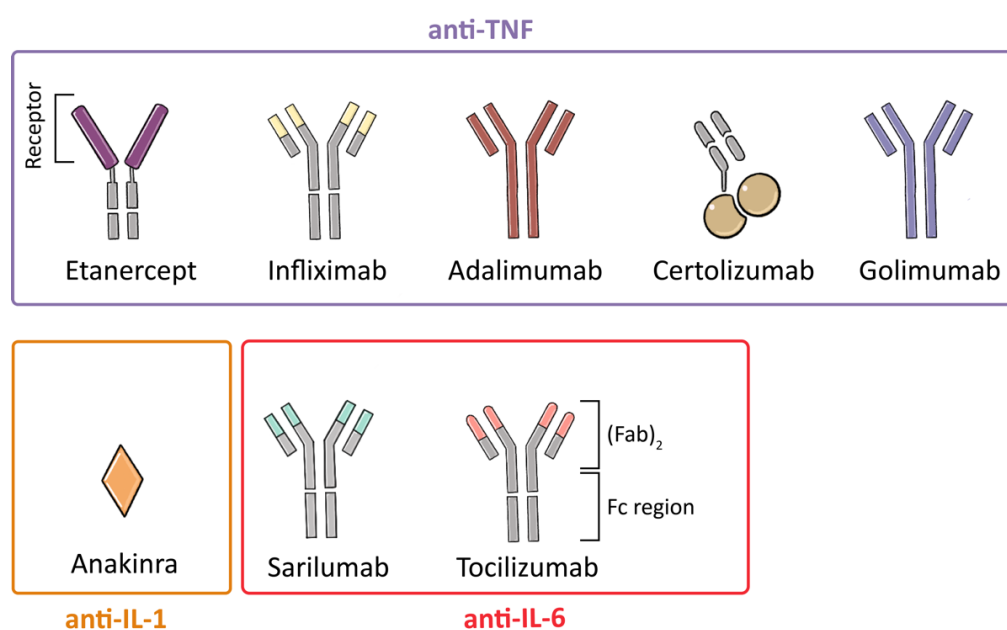


Figure 1.13 Currently approved cytokine blockers for the treatment of RA.

## 1.4.2 Lymphocyte-targeting agents

### 1.4.2.1 B-cell directed therapy

B-cells have numerous roles in autoimmunity, involving antigen presentation, secretion of inflammatory and immunoregulatory mediators (such as cytokines), production of autoantibodies, and modulation of lymphoid organization within inflammatory sites.

Rituximab is the most successful B-cell-directed therapeutic strategy that is currently in clinical practice (**Figure 1.14**). It is a chimeric monoclonal antibody directed against the CD20 molecule, which is present in all mature B-cells but not expressed by antibody-secreting plasma cells <sup>275</sup>. On binding to CD20, rituximab triggers cell death through antibody-mediated cellular cytotoxicity; following infusion of rituximab complete depletion of B-cells from the peripheral blood that can be documented within a matter of days <sup>172</sup>. Although all treated patients experience profound depletion of circulating peripheral B-cells, only 60% of these patients respond clinically <sup>276,277</sup>. Furthermore, in patients who are either RF or ACPA positive (or both), rituximab seems to be more effective <sup>278</sup>. Despite the rapid biologic effect of the treatment, the onset of clinical action was somewhat slower, and studies demonstrate that rituximab is more effective in combination with MTX <sup>279</sup>. Currently, rituximab is approved for use in patients with RA who have previously failed anti-TNF therapy, although in practice it is also used in patients where anti-TNF $\alpha$  is considered less desirable <sup>280</sup>.

Apart from rituximab, several other B-cell directed biologics have been developed over the years, although none are currently approved for the treatment of RA. The anti-CD20 monoclonal antibodies ocrelizumab <sup>281</sup>, veltuzumab <sup>282</sup>, and ofatumumab <sup>283</sup>, are in phase II and early phase III clinical trials. However, ocrelizumab has been shown to have side effects such as severe infections that have led to termination of trial programs <sup>284</sup>. Epratuzumab is another B-cell therapy that targets CD22, and instead of depleting B-cells, it downregulates their activity and is currently being tested for the treatment of systemic lupus erythematosus (SLE) <sup>285</sup>. Several strategies, aside from B-cell depletion that inhibit B-cell growth and development have been developed. For example, some biologics target B-cell activating factor (BAFF) also known as TNF ligand superfamily 13b and B lymphocyte stimulator (BLyS); the proliferation-inducing ligand (APRIL) also known as TNF ligand superfamily member 13. BAFF and APRIL are proteins recognised by a cell surface receptor called transmembrane activator and CAML interactor (TACI) <sup>119</sup>. Belimumab (directed against soluble forms of BAFF) had only minor effects in RA <sup>286</sup> but was approved for the treatment of SLE. Atacicept (TACI-Fc fusion protein) has also been examined in phase II clinical trials in RA <sup>287</sup>. Two-phase II clinical trials of atacicept recruited over 500 patients with RA in total and failed to demonstrate any significant efficacy. Similarly, belimumab is not moving forward in further clinical trials <sup>288</sup>. Finally, another anti-BAFF, tabalumab, also had modest efficacy in RA <sup>289</sup> but is not being developed further.

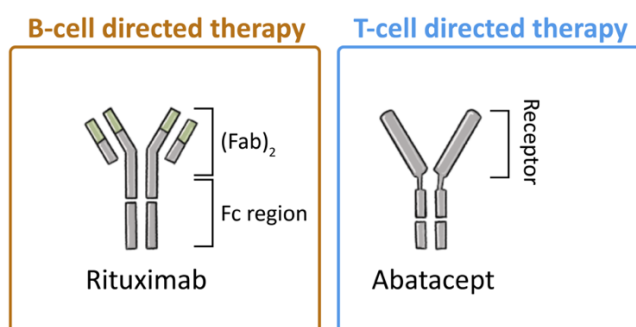


**Figure 1.14** Currently approved lymphocyte-targeting agents for the treatment of RA.

#### 1.4.2.2 T-cell directed therapy

The first biologics to be tested for RA were directed at T lymphocytes. At present, the only successful approach directed at T-cells is through targeting co-stimulation. T-cell negative regulatory signals can be initiated through membrane receptors, following the binding of cognate ligands, either soluble or membrane-bound <sup>21</sup>. These inhibitory receptors, also known as 'checkpoints', counterbalance the T-cell activation state. For example, cytotoxic T-lymphocyte antigen 4 (CTLA-4), is considered a master regulator of peripheral T-cell tolerance *in vivo* <sup>290</sup>. The physiologic role of CTLA-4 is believed to be the termination of T-cell activation and the prevention of excessive inflammation. Abatacept is a construct of the naturally occurring CTLA-4 coupled to an IgG framework designed to block the interaction of CD28 with CD80 or CD86, which is present on APCs, and therefore antagonise T-cell coactivation <sup>291</sup> (**Figures 1.14 & 1.15**). Extensive data from phase III and phase IV trials have confirmed that abatacept has good clinical efficacy in the treatment of RA in different stages of the disease, comparable to anti-TNF- $\alpha$  therapy <sup>292</sup>, however, the exact mode of action in RA is still not understood.

Abatacept has shown to suppress ROS, which contributes to the inflammatory properties of RA, by preventing T-cell interactions with synovial fibroblasts <sup>293</sup>. Another study revealed that abatacept significantly reduced the levels of IFN- $\gamma$  expression and the overall inflammatory status of the synovium without disrupting cellular homeostasis in patients with RA, for whom TNF-blocker therapy had failed <sup>291</sup>. Changes in the number of circulating subsets of CD4<sup>+</sup> and CD8<sup>+</sup> Treg cells and a consequent enhanced regulatory function have also been reported in a small case series, after abatacept therapy <sup>294</sup>. In murine models of arthritis, abatacept was evidenced to inhibit T-cell activation and proliferation as well as reduce the migration of T-cells into B-cell follicles, limiting the breach of self-tolerance <sup>295</sup>.

Alternative approaches to inhibiting abnormal T-cell activation in RA, include anti-CD4 antibodies 4162W9477<sup>296</sup>, keliximab<sup>297</sup>; anti-CD3 antibodies otelexizumab, teplizumab, foralumab and visilizumab<sup>298,299</sup>; and anti-CD52 antibody alemtuzumab. However, the outcomes from these therapies have been less impressive than abatacept. Despite RA heterogeneity, a number of spontaneous or induced models of RA showed that Treg cells are able to slow down or stop the clinical progression of this disease. Treg cell-based immunotherapy is at present restricted to animal models. For example, adoptive transfer of CD25<sup>+</sup> regulatory T-cells in CIA proved to be an effective treatment as it prevented and almost ceased arthritis progression<sup>300</sup>. Further, in a model of proteoglycan-induced arthritis in mice, CD4<sup>+</sup> CD25<sup>+</sup> Foxp3<sup>+</sup> Treg cells were able to suppress arthritis<sup>301</sup>.

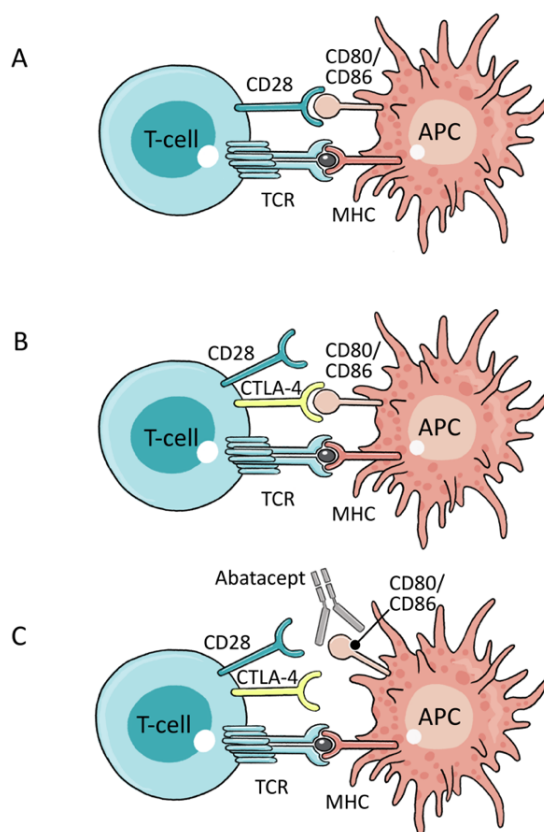


**Figure 1.15 Abatacept mechanism of action.**

**(A)** T-cell activation requires both cognate interactions between the TCR and an antigenic peptide presented by the class I or II MHC molecule on the surface of an APC, and a second co-stimulatory signal, for example, the binding of CD28 on the T-cell surface to CD80/86 on the surface of the APC. **(B)** After 24-48 hours, the expression of CTLA4 is upregulated on the activated T-cell, which has higher affinity for CD80/86 than CD28 and therefore, provides a control signal that terminates T-cell activation. **(C)** Abatacept (CTLA4Ig) strongly binds CD80/86, thereby disrupting the second signal to the T-cell and preventing or interfering with T-cell activation. APC, antigen-presenting cell, MHC, major histocompatibility complex, TCR, T-cell receptor.

### 1.4.3 Small molecule inhibitors of signal transduction pathways

#### 1.4.3.1 *JAK inhibitors*

In recent years, a novel class of DMARD has emerged as an oral treatment for inflammatory disorders such as RA, psoriasis, inflammatory bowel disease, and the prevention of organ transplant rejection. Among them, several inhibitors of JAK proteins (collectively termed jakinibs) have been developed as potential treatments for RA and currently only one is approved (tofacitinib), while several others are in clinical development. JAK family kinases (JAK1, JAK2, Tyk2, and JAK3) are ubiquitous intracellular regulators with a crucial role in driving chronic inflammation in RA (See **Section 1.3.1**). IL-2, IL-4, IL-7, IL-9, IL-15, and IL-21 belong to the  $\gamma$ -chain cytokine family, and commonly mediate lymphocyte activation, proliferation, and survival through the activation of JAK3, while JAK2 governs colony-stimulating factors, erythropoietin, and cytokines comprising the IL-6/IL-12, IL-10, and IL-3/IL-5 families, and JAK1 regulates interferon activities <sup>119</sup>.

Tofacitinib binds to and competitively inhibits the kinase domains of JAK1, JAK3 and to a lesser extent JAK2 (**Figure 1.16**). Several phase III trials over the last years have shown that tofacitinib is effective for RA, as monotherapy or in combination with MTX, reporting significant amelioration of disease activity, improvements in functional status and prevention of structural joint disease in patients. Subsequently, tofacitinib has been approved, on a regimen of 5 mg twice daily, by the FDA for the treatment of moderate and severe RA, in patients who are intolerant or unresponsive to MTX <sup>144</sup>. Moreover, an extended-release version of tofacitinib that uses osmotic delivery to enable once-daily dosing has also been approved by the FDA for the treatment of RA <sup>302</sup>. Ruxolitinib, a potent inhibitor of JAK1 and JAK2, have shown encouraging preliminary results <sup>216</sup>. Baricitinib is a first-generation jakinib, structurally related to ruxolitinib, that selectively blocks JAK1 and JAK2. Extensive data from phase III trials have also demonstrated its long-term safety and efficacy, showing clinically significant improvements in disease activity, structural damage and patient-reported outcomes. Nevertheless, its approval by the FDA is currently in process. Other JAK inhibitors are in earlier-phase trials, such as peficitinib, which blocks multiple JAKs and has achieved clinical responses similar to other jakinibs, yet with worsen adverse effects <sup>144</sup>.

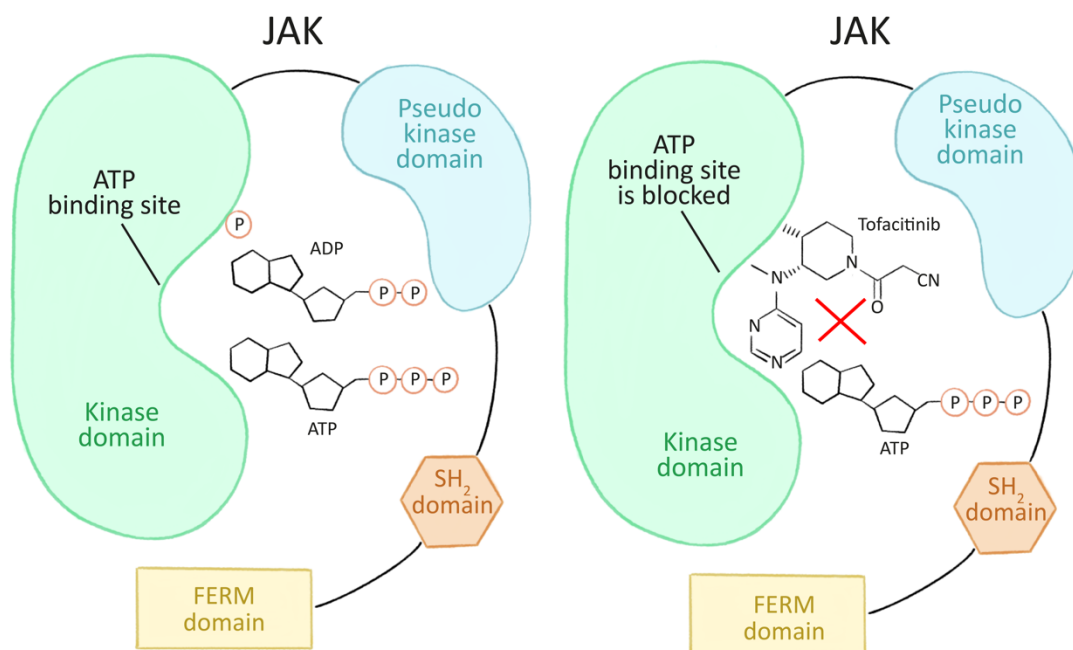


**Figure 1.16 Mode of action of Tofacitinib.**

Janus kinases contain several domains; the kinase domain is responsible for phosphorylation. This occurs when ATP binds to the ATP-binding site and releases its phosphate, which can then be used to phosphorylate JAKs and cytokine receptors. Tofacitinib competitively inhibits the ATP-binding site and therefore the kinase activity of JAK3. (Adapted from O'Shea *et al.* 2015).

#### 1.4.3.2 Other small molecular inhibitors

Several small-molecule designer drugs have been developed to mimic cytokine-cytokine receptor engagement or to modulate intracellular mechanisms linked to membrane gp130 or JAK/STAT signalling<sup>303</sup>. For example, regulator of cartilage growth and differentiation-423 (RCGD-423) promotes a transient activation of gp130 dimerisation and signalling<sup>304</sup>. Other modalities that interfere with gp130 signalling include madindoline-A, the small-molecule inhibitor SC144 and the synthetic oxazolidinone derivative LMT-28<sup>303</sup>. Since STATs are crucially involved in signal transduction and are often triggered within the context of malignancy, substantial effort has been made for more than two decades to develop STAT inhibitors. As opposed to JAKs, whose kinase domains display an evident pharmacological target, STATs do not possess intrinsic catalytic activity and thus, are a more challenging objective. Oligonucleotide-based STAT transcription factor inhibitors, which silence the genomic expression of STAT genes, are the most well-developed approach (e.g., AZD9150, which targets STAT3)<sup>305</sup>, and small molecules, inhibitory peptides and small interfering RNAs that target STAT transcription factors are also undergoing clinical trials<sup>306</sup> (See **Chapter 3**).

Moreover, natural chemical blockers of STAT3 activity (e.g., curcumin and capsaicin) are also considered promising therapies for RA <sup>303</sup>. Small-molecule inhibitors of receptor tyrosine kinases (RTKs), a class of growth-factor and hormone receptors whose genes are prone to gain-of-function mutations associated with STAT-driven malignancy are also being tested for the treatment of RA and others inflammatory pathologies <sup>307</sup>. Additionally, due to its regulatory role in the JAK/STAT signalling pathway (**Section 1.3.1.2**), the transient nature of SOCS expression is currently being addressed to ensure therapeutic effectiveness <sup>201</sup> (See **Chapter 4**).

Biologic agents have brought major therapeutic advances to the treatment of patients with RA as they are generally effective, well-tolerated and safe by the majority of patients <sup>119</sup>. Their modes of action and class-specific adverse effects are different, and although some of the possible side effects (e.g., risk of infections, malignancy, administration reactions) apply to all these compounds, some conditions that affect patients selection and management within these categories seem to be specific to particular biologic treatments <sup>308</sup>. The impact of cytokine-network modulation on systemic homeostatic processes – such as mood, fatigue, depression, infection and cardiovascular risk – and haematologic processes, is also an important aspect of biologic intervention <sup>119</sup>. In addition to reducing articular inflammation in patients with RA, biologic agents can reduce systemic inflammation and improve health-related quality of life by effecting control of the acute-phase response and fatigue <sup>119</sup>. However, over a million patients with RA have been successfully treated, and a better perspective on the risk of harm and its management has become part of good clinical practice <sup>121</sup>. Furthermore, a novel trial design might allow biologic combinations to be evaluated scientifically and systematically. These novel treatments and therapeutic strategies are needed to make disease remission a possibility for most patients with RA.

#### **1.4.4 In vivo models for inflammatory arthritis**

Finally, clinical testing on humans can only begin after a pre-clinical phase (involving laboratory studies in vitro and in vivo), which is required for the experimental drug to be considered safe and effective. Whilst a certain amount of testing can be carried out by means of in vitro experiments and computer modelling, animal testing is an obligatory stage in the process of obtaining regulatory approval for new drugs and therapies. Moreover, animal models are not only key for success in clinical translation, but also necessary to advance medical and biological knowledge. Models of inflammatory arthritis are extensively used to



investigate pathogenic mechanisms governing inflammation-driven joint damage. Despite limitations that apply to all animal models of human disease, *in vivo* mouse models of inflammatory arthritis have been instrumental in identifying pathogenic mediators, immune cell subsets and stromal cell responses that determine disease onset, progression and severity. Two commonly used models include antigen-induced arthritis (AIA) and collagen-induced arthritis (CIA). These offer unique advantages for modelling different aspects of human disease: CIA involves breach of immunological tolerance resulting in systemic auto-antibody-driven arthritis, while AIA results in local resolving inflammatory flares that mimic the flares of disease seen in clinical RA, and articular T-cell-mediated damage (See **Section 2.3.2** for a detailed description of this model). Development of AIA is dependent on CD4<sup>+</sup> T-cells, and the kinetics of synovial leukocyte infiltration are highly reproducible. Additionally, the C57BL/6 strain of mice described in **Section 2.3.1** is highly susceptible to mBSA AIA, which has facilitated the study of individual immune pathways and functions using transgenic and gene deficient mice<sup>309</sup>. Thus, AIA serves as the perfect model to investigate molecular mechanisms underpinning arthritis progression linked with RA and provides a pre-clinical testing ground for novel biological therapies, including cytokine blockers and small molecule inhibitors of the JAK/STAT signalling pathway such as those utilised in this thesis.

## 1.5 Project aims

RA affects around 1% of the global adult population and is a systemic autoimmune disease of synovial joints. At present, there is no known cure yet for RA, but current therapies are broadly aimed at restricting inflammation and show considerable efficacy, allowing many patients to achieve remission. However, approximately 40% of patients do not respond to current frontline biologics, due, in part, to the high heterogeneity of the disease. My thesis mainly focuses on therapeutic intervention of the JAK/STAT signalling pathway utilising novel approaches, by targeting either the cytokine receptor or the downstream intracellular signalling.

- In **Chapter 3**, studies focused on the therapeutic targeting of the latent transcription factor STAT3 in experimental arthritis. Here, I hypothesised that re-positioning an anti-cancer therapy (CpG-*Stat3*siRNA), which utilises a novel siRNA delivery technology to silence STAT3 gene in TLR9-expressing cells, may have therapeutic potential to treat inflammatory arthritis. *In vivo* investigations tested the efficacy of CpG-*Stat3*siRNA in antigen-induced arthritis as judged by histopathology and computational analysis of optimised RNA-seq of the inflamed synovium.
- The aim of **Chapter 4** was to investigate the potential of SOCS3 induction as a target for RA therapy. I hypothesised that synovial induction of SOCS3 in response to a peptide derived Hepatitis Virus-C (p7-derived peptide), could result in improved disease outcome in antigen-induced arthritis, by indirectly targeting STAT3.
- In **Chapter 5**, experiments aimed to use novel IL-6 trans-signalling inhibitors by fusion of a minimised sgp130 variant to an IL-6:sIL-6R complex-binding nanobody. My hypothesis was that these new sgp130 variants would have inhibitory capacity of STAT3-driven Th17 cell expansion *in vitro*, due to their smaller size and improved efficacy.
- In **Chapter 6**, I hypothesised that CRTAM (CD355), an important molecule in regulating T-cell effector characteristics that has also been implicated in various inflammatory and pathogenic processes, could be involved in controlling synovitis, by reason of being downregulated in activated naïve CD4<sup>+</sup> T-cells as a response to IL-6 and IL-27. The main goal was to investigate the negative regulation of *Crtam* by IL-6 and focus on the potential role CRTAM may play in the context of inflammatory arthritis.

## 2 Material and Methods

### 2.1 Cell culture

#### 2.1.1 Buffers and media for cell culture

All reagents and buffers, with the exception of those supplied as part of commercial kits, used for T-cell culture are listed in **Table 2.1**. All buffers and cell media were sterile filtered using 0.2  $\mu\text{m}$  syringes or bottle top filters (Stericup, Merck Millipore), stored at 4 °C and used within 30 days after preparation. All chemicals were purchased from Life Technologies (Thermo Fisher Scientific) unless otherwise stated.

<i>Media and reagents</i>	<i>Composition</i>
Supplemented RPMI	RPMI-1640 10% (v/v) Heat-Inactivated Foetal Bovine Serum (FBS) 100 U/mL Penicilin, 100 $\mu\text{g/mL}$ Streptomycin 2 mM L-Glutamine 1 mM Sodium Piruvate 50 $\mu\text{M}$ $\beta$ -mercaptoethanol
Supplemented IMDM	IMDM already containing 4 mM L-Glutamine and 25 mM HEPES 10% (v/v) FBS 100 U/mL Penicilin 50 $\mu\text{M}$ $\beta$ -mercaptoethanol
Freezing buffer	90% (v/v) FBS 10% (v/v) DMSO (Dimethyl sulphoxide)
MACS buffer	DPBS (no calcium, no magnesium) 0.5% (w/v) Bovine Serum Albumin (BSA) 2 mM EDTA
FACS buffer	DPBS (no calcium, no magnesium) 0.5% (w/v) Bovine Serum Albumin (BSA) 5 mM EDTA 7.5 mM Sodium Azide

**Table 2.1** The composition of buffers and cell culture media used throughout this thesis.

## 2.1.2 Isolation, culture and Th17 differentiation of murine naïve CD4<sup>+</sup> T-cells

### 2.1.2.1 *Preparation of murine splenocytes*

Mice were dissected, and the whole spleen extracted into supplemented RPMI (**Table 2.1**) prior to homogenisation. A single-cell suspension was prepared by homogenising spleen through a sterile 40 µm cell strainer (Greiner Bio-one), using the plunger of a sterile 2 mL syringe (BD Biosciences). Recovered cells were washed, resuspended in red blood cell (RBC) lysis buffer (BioLegend) and incubated on ice for 1 minute, to lyse red blood cells. Supplemented RPMI was added to equilibrate the pH of the buffer and the extracted cells pelleted by centrifugation. (All centrifugation steps were conducted for 5 minutes at 4 °C, 400 xg).

### 2.1.2.2 *MACS sorting of CD4<sup>+</sup> T-cells*

CD4<sup>+</sup> T-cells were isolated from murine splenocytes, using a magnetic-activated cell sorting (MACS) CD4<sup>+</sup> T-cells Isolation Kit (Miltenyi Biotec). Magnetic bead isolation was conducted according to the manufacturer's instructions and yielded a highly enriched population of CD4<sup>+</sup> T-cells (typically > 90%). Briefly, cells were first washed with MACS buffer and then resuspended in 40 µL of MACS buffer per 10<sup>7</sup> cells prior to the magnetic labelling step. CD4<sup>+</sup> T-cells were recovered by negative selection, incubating cells with 10 µL per 10<sup>7</sup> cells of a cocktail of biotin-conjugate monoclonal antibodies against CD8a, CD11b, CD11c, CD19, CD45R (B220), CD4b (DX5), CD105, MHC-class II and Ter-119 and TCR γ/δ for 5 minutes at 4 °C. Cells were subsequently incubated for 10 minutes at 4 °C with 20 µL per 10<sup>7</sup> cells of anti-biotin monoclonal antibodies conjugated with MicroBeads. The cell suspension was applied to in a magnetic separator and a LS positive selection column (Miltenyi Biotec). The column was washed three times with MACS buffer and the enriched CD4<sup>+</sup> T-cell fraction collected as flow-through. MACS buffer was kept on ice at all times, and the centrifugation was performed at 4 °C to prevent bead internalisation. Potential cell clumps or fatty material that would block the column were removed by passing the cell suspension through a 0.22 µm filter.

### 2.1.2.3 Isolation of naïve CD4<sup>+</sup> T-cell by flow cytometric cell sorting

Naïve CD4<sup>+</sup> T-cells were obtained from enriched CD4<sup>+</sup> T-cells by flow cytometry cell sorting. In brief, CD4<sup>+</sup> T-cells were adjusted to  $2 \times 10^7$  cells/mL in MACS buffer and treated with 4 µg/mL rat anti-mouse CD16/CD32 (Fc block; clone 2.4G2, BD Biosciences) for 15 minutes at 4 °C to prevent non-specific binding and help reduce background fluorescent staining. Cells were immune-labelled for 30 minutes at 4 °C in the dark using cell surface marker fluorochrome-conjugated antibodies (diluted 1:200) against CD4, CD25, CD44, and CD62L (**Table 2.3; Section 2.2.1**). Flow cytometric cell sorting was performed using a BD FACS Aria II (BD Biosciences). CD4<sup>+</sup> T-cells were gated based on forward, and side scatter profiles and analysed for the exclusion of doublets. Naïve CD4<sup>+</sup> T-cells were identified at those cells displaying CD4<sup>+</sup>CD25<sup>-</sup>CD44<sup>lo</sup>CD62L<sup>hi</sup> characteristics. The representative gating strategy is shown in (**Figure 2.1**). T-cell subset purity was > 90% (see **Appendix Figure 8.1** for an example of the purity strategy used).

### 2.1.2.4 In vitro generation of murine Th17 cells

Naïve CD4<sup>+</sup>CD25<sup>-</sup>CD44<sup>lo</sup>CD62L<sup>hi</sup> T-cells ( $1 \times 10^5$  cells/well) were cultured in Nunclon delta surface 96-well U-shape bottom plates (Thermo Fisher Scientific) in supplemented RPMI or IMDM <sup>104,310</sup>. For TCR activation, cells were co-stimulated with plate-bound anti-CD3 (1 µg/mL anti-CD3; clone 145-2C11, R&D systems) added the previous day and incubated at 4 °C overnight, and soluble anti-CD28 (5 µg/mL; clone 37.51, eBioscience). Cytokines were included at the following concentrations to promote differentiation of naïve CD4<sup>+</sup> T-cells into a defined Th17 lineage: TGF-β (1 ng/mL), IL-6 (20 ng/mL) and IL-23 (20 ng/mL). All recombinant mouse cytokines were purchased from R&D Systems. Cells were grown at 37 °C with 5% CO<sub>2</sub> for 4 days before phenotypic characterisation by flow cytometry (**Section 2.2**).

### 2.1.2.5 Inhibition of in vitro Th17 cultures

Naïve CD4<sup>+</sup> T-cells were recovered and activated under Th17 polarising conditions as previously described. To test the efficacy of SOCS3-inducing peptide (SOCS3 P) against Th17 cell differentiation, cultures were incubated with or without 200 ng/mL SOCS3 P or control P7-derived scrambled peptide. Culture medium and inhibitor were replenished on a daily basis for 4 days. These peptides were derived from the Hepatitis C virus (HCV) P7 protein

and kindly provided by Dr Nigel Stevenson (Trinity College Dublin, Ireland) (see **Chapter 4**). Conversely, to test the inhibitory properties of miniaturised sgp130 variants (cs-130) against the IL-6:sIL-6R complex (that block IL-6 trans-signalling), cultures were incubated with or without varying doses of each modality (see **Table 2.2**). Recombinant gp130-based fusion proteins were kindly provided by Prof Jürgen Scheller and Dr Jens Moll (Heinrich Heine Universität, Düsseldorf, Germany) (see **Chapter 5**). Intracellular staining for IL-17A and IFN- $\gamma$  was performed as described in **Section 2.2.2**.

<i>Compounds</i>	sgp130Fc	cs-130Fc	cs-130	C <sub>GFP</sub> S-130Fc	CS- <sup>130190K/F191E</sup> Fc
<i>MW in g/mol</i>	240000	157000	52000	153000	157000
<i>nM</i>	<i>ng/mL</i>	<i>ng/mL</i>	<i>ng/mL</i>	<i>ng/mL</i>	<i>ng/mL</i>
10	2400	1570	520	1530	1570
1	240	157	52		
0.1	24	15.7	5.2		
0.01	2.4	1.57	0.52		
0.001	0.24	0.157	0.052		

**Table 2.2** The list of nanobodies and concentrations used in Th17 cell differentiation assays.

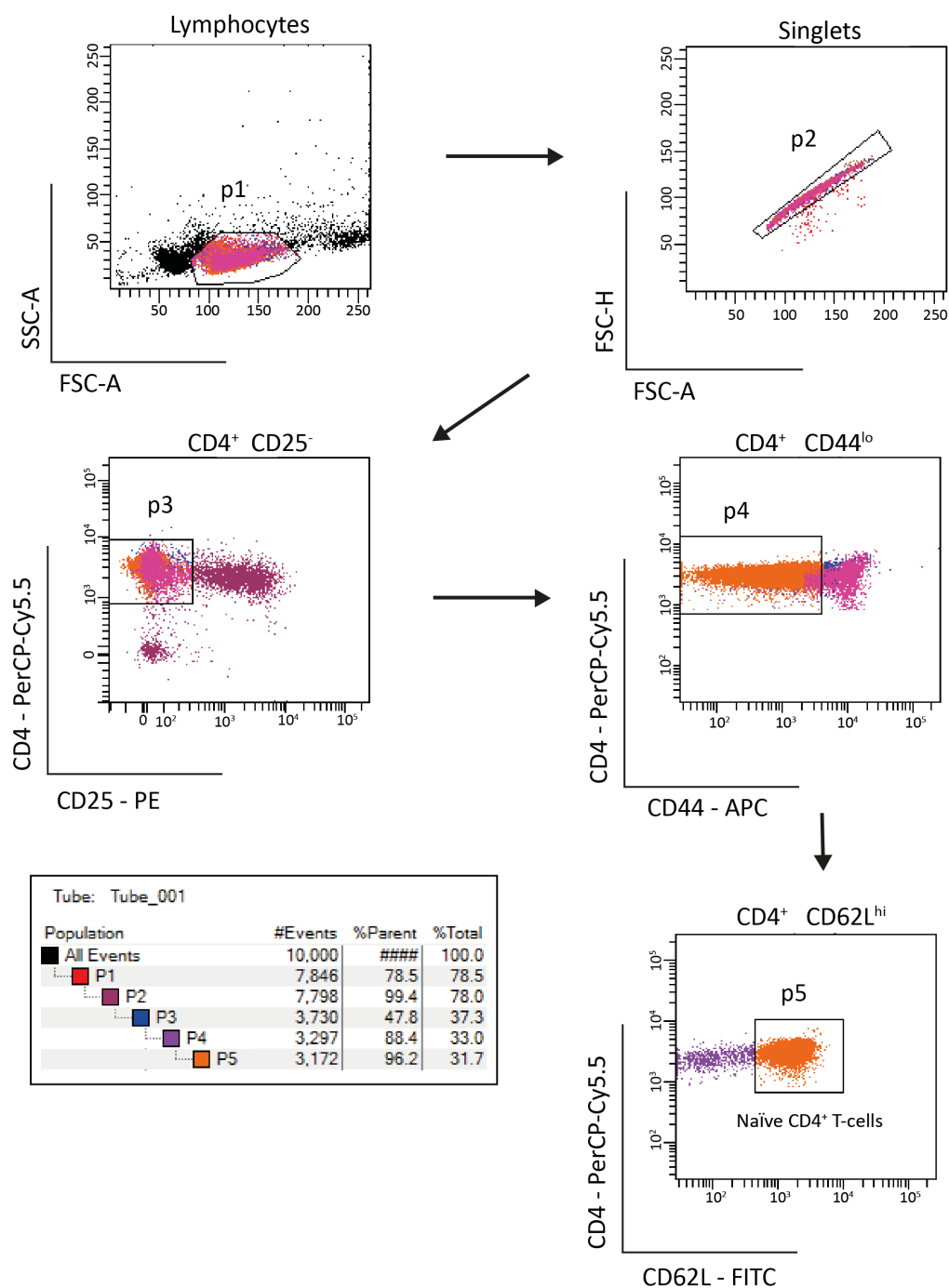


**Figure 2.1 Gating strategy for sorting naïve CD4<sup>+</sup> T-cells by flow cytometry.**

Cells were gated based on characteristic forward and side scatter profiles of lymphocytes (p1), followed by exclusion of doublets to avoid multiple cells being acquired at the same time (p2). Naïve T-cells were identified as: CD4<sup>+</sup>CD25<sup>-</sup> (p3), CD4<sup>+</sup>CD25<sup>-</sup>CD44<sup>lo</sup> (p4), and finally CD4<sup>+</sup>CD25<sup>-</sup>CD44<sup>lo</sup>CD62L<sup>hi</sup> (p5). SSC-A – side scatter-area; FSC-A – forward scatter-area; FSC-H – forward scatter-height.

### 2.1.3 Cell Counting

Cells were resuspended in supplemented RPMI, 10  $\mu$ L of cell suspension was mixed with 10  $\mu$ L of 0.4% (w/v) Trypan Blue solution (Sigma Aldrich). The resulting mixture was applied to a haemocytometer, and live cells were counted based on trypan blue exclusion according to the following formula: average viable cell count from two 16-squared grids x 2 (dilution factor) x  $10^4$  = number of viable cells/mL.

### 2.1.4 Cryopreservation and thawing

For cryopreservation, recovered cells from murine spleens (**Section 2.1.2.1**) or lymph nodes (**Section 2.3.5**) were resuspended in freezing buffer (**Table 2.1**) and then moved to internally threaded cryogenic vials (Nunc) and stored at -80 °C using a controlled rate freezing device (Mr Frosty, Nalgene). For thawing, cells were removed from the freezer and thawed in a water bath at 37 °C. The thawed cells were seeded into a 96 well plate (Greiner Bio-One) and used as single fluorochrome-stained cellular controls to provide negative and positive populations to establish compensation parameters in flow cytometry (**Section 2.2**).

## 2.2 Flow Cytometry

Analysis was performed as described previously <sup>204</sup>. Samples were acquired on a BD FACSCanto II flow cytometer (BD Biosciences) using the FACSDiva software (BD Biosciences). Data analysis was conducted using FlowJo Version 10 (Tree Star Inc, US). Between each incubation step and wash, cycle cells were isolated by centrifugation at 600 xg for 3 minutes. To quantify the number of cells per sample, cell counting beads (Life Technologies) were used according to the manufacturer's instructions. A detailed description of each antibody used is listed in **Table 2.3**.



<i>Target</i>	<i>Species</i>	<i>Fluorochrome</i>	<i>Clone</i>	<i>Isotype</i>	<i>Manufacturer</i>
CD3	Hamster anti-mouse	PE Cy7	145-2C11	IgG	BioLegend
CD4	Rat anti-mouse	efluor 450 PerCP Cy 5.5	RM4-5	IgG2a	eBioscience
CD25	Rat anti-mouse	PE	PC61.5	IgG1	eBioscience
CD44	Rat anti-human/mouse	APC	IM7	IgG2b	eBioscience
CD62L	Rat anti-mouse	FITC	MEL-14	IgG2a	eBioscience
CD8a	Rat anti-mouse	PerCP Cy 5.5	53-6.7	IgG2a	eBioscience
$\gamma\delta$ TCR	Hamster anti-mouse	APC	eBioGL3	IgG	eBioscience
NK1.1	Mouse anti-mouse	FITC	PK136	IgG2a	eBioscience
IL17A	Rat anti-mouse	PE Alexa Fluor 647	TC11-18H10.1	IgG1	BD Biosciences BioLegend
IFN $\gamma$	Rat anti-mouse	efluor 450 FITC	XMG1.2	IgG1	Invitrogen eBioscience
CD355/CRTAM	Rat anti-mouse	PE	11-5	IgG2a	BioLegend

**Table 2.3** The list of antibodies used for flow cytometry staining in this thesis.

### 2.2.1 Cell surface staining

Cells were washed in FACS buffer (**Table 2.1**) and resuspended in Zombie Aqua live/dead stain (BioLegend) in PBS for 5 minutes in the dark for dead cell exclusion, before surface staining. Alternatively, Live/Fix Viability Dye eFluor 450 (eBioscience) was used. Non-specific staining caused by antibody binding to Fc receptors was prevented by incubating cells in 4  $\mu$ g/mL rat anti-mouse CD16/CD32 (Fc block; clone 2.4G2, BD Biosciences) for 15 minutes at 4 °C. Cells were then incubated for 20 minutes at 4 °C in the dark, with fluorochrome- conjugated antibodies specific to cell surface receptors (**Table 2.3**) at a working dilution of 1/200 in FACS buffer. They were then washed twice in FACS buffer and finally resuspended in 200  $\mu$ L of PBS. Cells were kept on ice in the dark (or fixed with CellFix, BD Biosciences) until flow cytometric analysis.

### 2.2.2 Intracellular cytokine staining (ICS) assay

Intracellular cytokine staining (ICS) was used to detect T-cell subsets with defined effector cytokine profiles. Because intracellular cytokines are typically expressed at low levels in

resting cells, cells were stimulated with 50 ng/mL PMA (Phorbol 12-myristate 13-acetate) and 500 ng/mL ionomycin (calcium ionophore) to enhance effector cytokine production. Monensin (3  $\mu$ M) treatment was used to increase the accumulation of the target cytokine within the cytoplasm by blocking intracellular transport at the Golgi apparatus. Cells were incubated for 4 hours at 37 °C, before live/dead staining, Fc block and labelling of cell markers as described in **Section 2.2.1**. Following surface staining, cells were fixed and permeabilised using Cytofix/Cytoperm™ (BD Biosciences) as described in the manufacturer's instruction booklet. Permeabilised cells were then incubated with anti-cytokine fluorochrome-conjugated antibodies (**Table 2.3**) for 30 minutes on ice at a working dilution of 1/200. Cells were subsequently washed twice, resuspended in CellFix™ (BD Biosciences) and stored overnight at 4 °C in the dark prior to analysis by flow cytometry and data analysis (see **Section 2.10**).

## 2.3 *In vivo* experiments

### 2.3.1 Mouse strains

Experiments were undertaken in adult (8-12-week-old) male wild-type, *Il27ra*<sup>-/-</sup>, *Il6ra*<sup>-/-</sup>, *gp130*<sup>Y757F:Y757F</sup> and *gp130*<sup>Y757F:Y757F</sup>: *Stat3*<sup>+/-</sup> C57BL/6 mice. Inbred wild-type mice were purchased from Charles River UK. IL-27R deficient mice (*Il27ra*<sup>-/-</sup>) were originally sourced from The Jackson Laboratory (line B6N.129P2-*Il27ra*<sup>tm1Mak</sup>/J) and bred and maintained at Cardiff University<sup>245</sup>. These mice were generated using a targeting vector designed to replace a genomic fragment containing an exon encoding a portion of the extracellular fibronectin type III domain of the IL-27R with a neomycin resistance cassette. *Il27ra*<sup>-/-</sup> mice are healthy and fertile, and there are no significant differences in gross or radiographic findings or in body or organ weights compared to wild-type mice<sup>245</sup>. Inbred *Il6ra*<sup>-/-</sup> were generated at GlaxoSmithKline (Stevenage, UK) using a conventional replacement vector to disrupt exons 4, 5 and 6, which encode the structural regions important for IL-6 recognition<sup>310</sup>. Both *gp130*<sup>Y757F:Y757F</sup> (*gp130*<sup>F/F</sup>) and *gp130*<sup>F/F</sup> bearing a monoallelic ablation of *Stat3* (*gp130*<sup>F/F</sup>:*Stat3*<sup>+/-</sup>) mice were generated in Ludwig Institute for Cancer Research (Australia) and have been extensively characterised as previously described<sup>311,312</sup>. At the molecular level, *gp130*<sup>F/F</sup> mice have a phenylalanine (F) knock-in substitution of the cytoplasmic tyrosine (Y) residue at position 757 within the intracellular domain of gp130.

This disrupts the negative feedback imposed on gp130 by SOCS3, and therefore, these mice have hyperactivation of STAT3 (**Figure 2.2**). Compound  $gp130^{F/F}:Stat3^{+/-}$  mice were generated by crossing  $gp130^{F/F}$  mice with  $Stat3^{+/-}$  mice, resulting in genetically reduced levels of gp130-dependent STAT3 activation<sup>312</sup>. These heterozygous mice display a seemingly normal phenotype since complete germline inactivation of STAT3 ( $Stat3^{-/-}$ ) results in early embryonic lethality<sup>313</sup>. While the level of gp130-dependent STAT3 activation had been genetically reduced, STAT1 and gp130 expression remained unaffected<sup>311,312</sup>. Mice were bred and housed under specific-pathogen-free (SPF) conditions at the Hudson Institute of Medical Research (Australia). Experiments were performed in accordance with and approved by, the Monash Medical Centre 'A' Monash University Animal Ethics Committee. All experiments were endorsed by the UK Home Office - approved project licenses PPL 30/2928 (2015-2017) and PB3E4EE13 (2017-2019), with consideration of the 3 R's (Replace, Reduce, Refine)<sup>314</sup>.

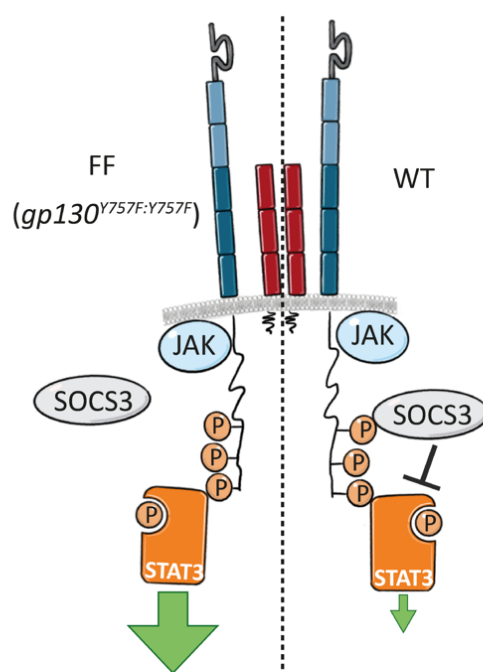


**Figure 2.2** STAT3 signalling in  $gp130^{Y757F:Y757F}$  and WT mice.

In  $gp130^{F/F}$  mice (left), there is a substitution of tyrosine 757 for a phenylalanine in the intracellular domain of gp130 that disrupts the binding of SOCS3 and leads to a loss of negative feedback inhibition on STAT3 activity. Thus, these mice have hyperactivation of STAT3 (indicated by the size arrow) compared to normal STAT3 activation in WT mice (right).

### 2.3.2 Murine antigen-induced arthritis (AIA)

Antigen-induced arthritis (AIA) was established as previously described<sup>309,315</sup>. Briefly, 8- 12- week-old male mice were immunised (s.c) with 100  $\mu$ L methylated bovine serum- albumin (mBSA) (1 mg/mL) emulsified in an equal volume of Complete Freund's Adjuvant (CFA). To prepare this emulsion, CFA was forcefully mixed with mBSA solution using a glass syringe and an 18-gauge (G) blunt fill needle, and this process was repeated until a white and stable emulsion was generated. Mice were then inoculated in the right flank using a 1 mL syringe and 25G needle. At the same time, mice also received 160 ng of heat- inactivated *Bordetella pertussis* toxin in 100  $\mu$ L of PBS as a single intraperitoneal injection (1 mL syringe, 25G needle) (all from Sigma-Aldrich), to prime the immune response. One week later, mice were reimmunised with an identical subcutaneous administration of mBSA/CFA into the left flank. Twenty-one days after the initial immunisation, inflammatory arthritis was induced by intra-articular administration of 10  $\mu$ L mBSA (10 mg/mL) into the knee joints using a 29G insulin syringe. Animals were monitored daily for well-being and clinical signs of arthritis development by measuring knee joint diameters using a POCO 2T micrometre (Kroeplin). At indicated time points post arthritis inductions animals were killed using the schedule 1 method of rising concentration of CO<sub>2</sub>, followed by cervical dislocation to confirm death.

#### 2.3.2.1 Administration of Stat3-targeted therapies during AIA

Murine AIA was established as described in **Section 2.3.2**. To examine the activities of STAT3 *in vivo*, two different intervention strategies were developed: (1) On disease induction, mice were treated with either a SOCS3-inducing peptide derived from hepatitis C virus (SOCS3P) or a control peptide sequence (P7). Both were administered (i.a.) at a final concentration of 0.01 mg/mL (see **Chapter 4**). (2) Alternatively, mice were treated (i.a.) with CpG-Stat3siRNA (0.125 nmol/ $\mu$ L) (**Figure 2.3**). Control joints received CpG, single-stranded CpG-Stat3siRNA or single-stranded CpG-Stat3siRNA non-hybridised (see **Chapter 3**). Knee joints (**Section 2.4.1**) and blood (**Section 2.3.3**) were recovered and processed for further analysis.

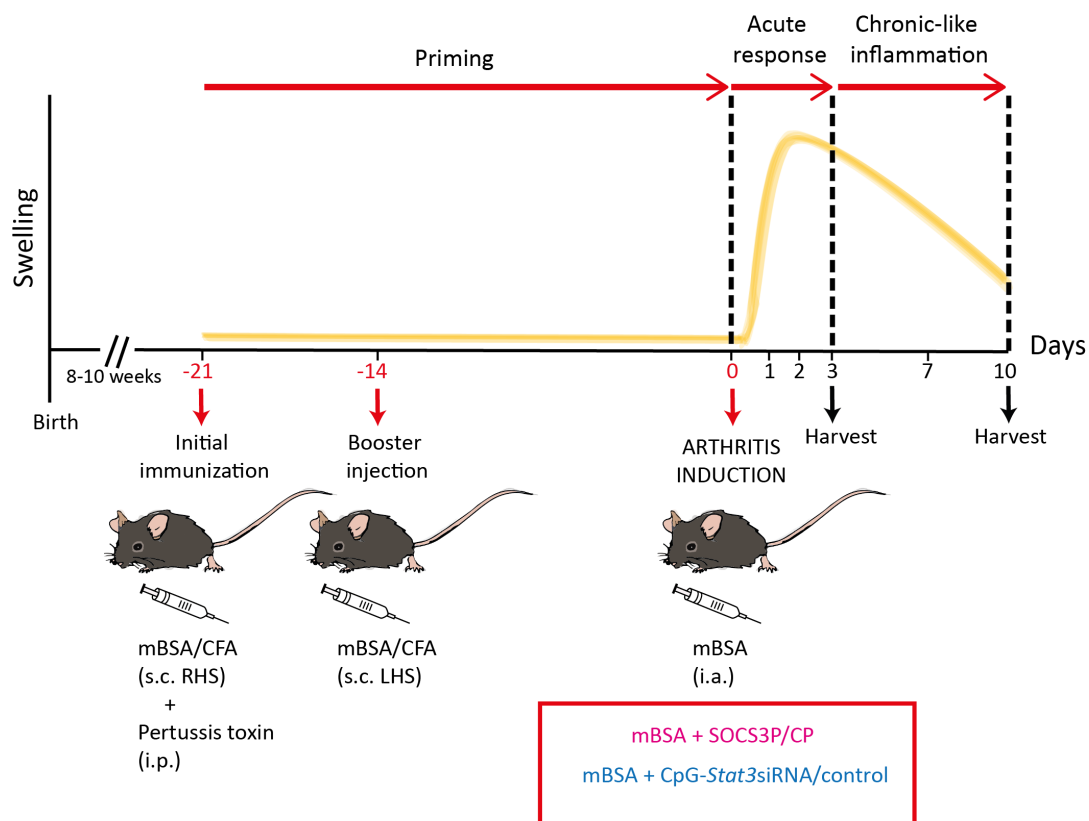


**Figure 2.3 Timeline for the general antigen-induced arthritis mouse model.**

The priming of the immune response towards mBSA in the absence of synovitis occurs from day -21 until day 0 (mBSA-specific immune response). Inflammatory arthritis is initiated by intraarticular administration of mBSA into the knee joint. The followed acute response is characterised by an early T-cell response and the infiltration of innate leukocyte populations, including neutrophils and inflammatory macrophages. The chronic-like inflammation phase is marked by a prominent effector T-cell response within the joint and regions of B-cell infiltration. Arrows indicate days of antigen/adjuvant and *Bordetella pertussis* toxin challenge, routes of administration to induce AIA, and days of harvest. Joint swelling is measured on days 0, 1, 2, 3 and 10 post arthritis induction. The different colours show the two different interventions used in this thesis during AIA, administered on disease induction (day 0), via intra-articular injection. In pink, mBSA + SOCS3-inducing peptide (SOCS3P) or mBSA + control P7-derived peptide sequence. In blue, mBSA + CpG-Stat3siRNA or mBSA + controls: CpG, single-stranded CpG-Stat3siRNA and single-stranded CpG-Stat3siRNA non-hybridised. CFA, complete Freund's adjuvant; mBSA, methylated BSA; RHS, right hand side; LHS, left hand side; i.p., intraperitoneal injection; s.c., subcutaneous injection; i.a., intraarticular injection.

### 2.3.2.2 *CpG-Stat3siRNA Oligonucleotide Hybridisation*

CpG-Stat3siRNA was kindly provided by Professor Hua Yu and Associated Professor Marcin Kortylewski (City of Hope, USA). The oligonucleotide design and synthesis have been previously described<sup>316</sup>. Briefly, each 50 nmol oligonucleotide was dissolved in 250 µL of DNase/RNase free water at 37 °C for 5-7 minutes. The resulting single-stranded sequences were next hybridised with complementary sense strands of siRNAs by heating to 80 °C for one minute and then promptly transferred to a 37 °C water bath for 1 hour. Samples were mixed by gentle vortex before a brief centrifugation and aliquoting for storage.

### 2.3.3 Collection of serum from blood

Total blood volume was collected from mice by cardiac puncture (1 mL syringe, 25G needle). Whole blood was added to a 1.5 mL sterile tube and incubated at room temperature for 30 minutes to allow coagulation. Samples were centrifuged (2,000 xg, 10 minutes, 4 °C) and the straw-colour serum fraction carefully transferred to a sterile tube and stored at -80 °C using a controlled rate freezing device (Mr Frosty, Nalgene). After 24h, cells were moved to a storage box at -80 °C for long term use.

### 2.3.4 Isolation of synovial tissue

The harvest and dissection of the inflamed synovium were conducted as described previously<sup>317</sup>. To extract joint-infiltrating leukocytes, samples were placed into supplemented RPMI medium, on ice. After collection, the synovial tissue underwent an enzymatic digestion using 1 mg/mL Collagenase Type IV (Worthington Biochemicals) in supplemented RPMI at 37 °C for 1-2 hours. Tubes were gently vortexed every 15 minutes. Finally, cells were carefully passed through a 40 µm cell strainer to remove tissue debris, washed (400 xg, 5 minutes), and resuspended in supplemented RPMI medium before analysis by flow cytometry (**Section 2.2.1**).

Alternatively, inflamed synovial tissue was immediately placed into *RNA/later* (Ambion) and stored at -80 °C for transcriptomic and qPCR analysis. Prior to the extraction of total RNA, synovial tissues were removed from *RNA/later* and weighed, as it is essential to use the correct amount of starting material to obtain sufficient RNA yield and purity (a maximum

amount of 30 mg can generally be processed without affecting RNA quality). Total RNA was extracted by homogenising in 600  $\mu$ L of RLT buffer (Qiagen) before purifying RNA as outlined in **Section 2.8.1**.

### **2.3.5 Isolation of inguinal lymph nodes**

Inguinal lymph nodes were recovered and gently passed through a sterile 40  $\mu$ m cell strainers (Greiner Bio-one) to obtain a single-cell suspension. Cells were then either cryopreserved (**Section 2.1.4**) or resuspended in supplemented RPMI medium and seeded in 96-well U-bottom plates to be used as single-stained cell controls for flow cytometry analysis (**Section 2.2**)

## **2.4 Histological analysis**

### **2.4.1 Preparation of knee joints for histology**

Entire knee joints were collected by dissection and cutting the bones proximal (femur) and distal (tibia and fibula) to the knee. After removing the skin and excess muscle, knees were then dissected free of skin and excess muscle and fixed in 10% (v/v) neutral buffered formal saline (pH 7.4) at 4 °C for 3 days. Following fixation, knee joint bones were decalcified in either formic acid (**Table 2.5**) at 4 °C for approximately a week, or EDTA decalcification solution (**Table 2.5**) for approximately two weeks, with the decalcification solution being changed twice weekly. The decalcification solution was chosen based on the type of staining performed and speed of process required. Formic acid is generally the quickest method; however, EDTA chelation preserves DNA better and is preferable for most of immunohistochemical staining protocols. Joints were X-rayed using a Kodak FX-Pro imaging system to confirm complete decalcification (**Figure 2.4A**). Fixed and decalcified joints were then processed and embedded in paraffin using HistoCore PEARL and Arcadia H instruments from Leica Biosystems. Parasagittal serial sections of 7  $\mu$ m thickness were cut using a Leica RM2235 rotary microtome (**Figure 2.4B**). To ensure strong adherence to the glass slides, samples were baked at 60 °C for approximately 6 hours.

### 2.4.2 Haematoxylin, fast green and safranin O staining

Rehydration and dewaxing were achieved by passing the tissue sections through three changes of xylene and decreasing concentrations (100%, 90% and 70%) of absolute ethanol for 3 minutes each, followed by 5 minutes in distilled water. Sections were then stained in haematoxylin, fast green and safranin O to assess pathology and for evaluation of bone and cartilage erosion. Briefly, sections were placed in Harris Haematoxylin (VWR International Ltd) for 5 minutes. Excess stain was removed under running tap water, and the sections transferred to 0.01% (w/v) fast green for 5 minutes. Samples were dipped briefly in 1% (v/v) acetic acid and incubated in 0.2% (w/v) safranin-O for 5 minutes. After staining, sections were sequentially dehydrated in 70% (v/v), 90% (v/v) and 100% absolute ethanol (3 minutes each) and cleared by three changes of xylene. Coverslips were placed onto stained slides using DPX mountant (Sigma) and left to dry overnight prior to histological analysis and archiving. Sections were visualised using a Leica DM 2000 microscope and Leica Application Suite v4.9 software.

### 2.4.3 Histological assessment of arthritis

Histological sections of knee joints were evaluated by two independent observers, blinded to the experimental groups<sup>104,204,309</sup>. They scored the sections for synovial exudate, sub-synovial inflammation, synovial hyperplasia and cartilage/bone erosion (**See Table 2.4**). Regions of the synovium stained with haematoxylin indicated synovial cellular infiltration, whilst proteoglycan staining safranin-O was used to identify erosion of the articular cartilage (**Figure 2.5**). The combined aggregate score of all parameters is presented as an arthritis index (AI) of disease activity.



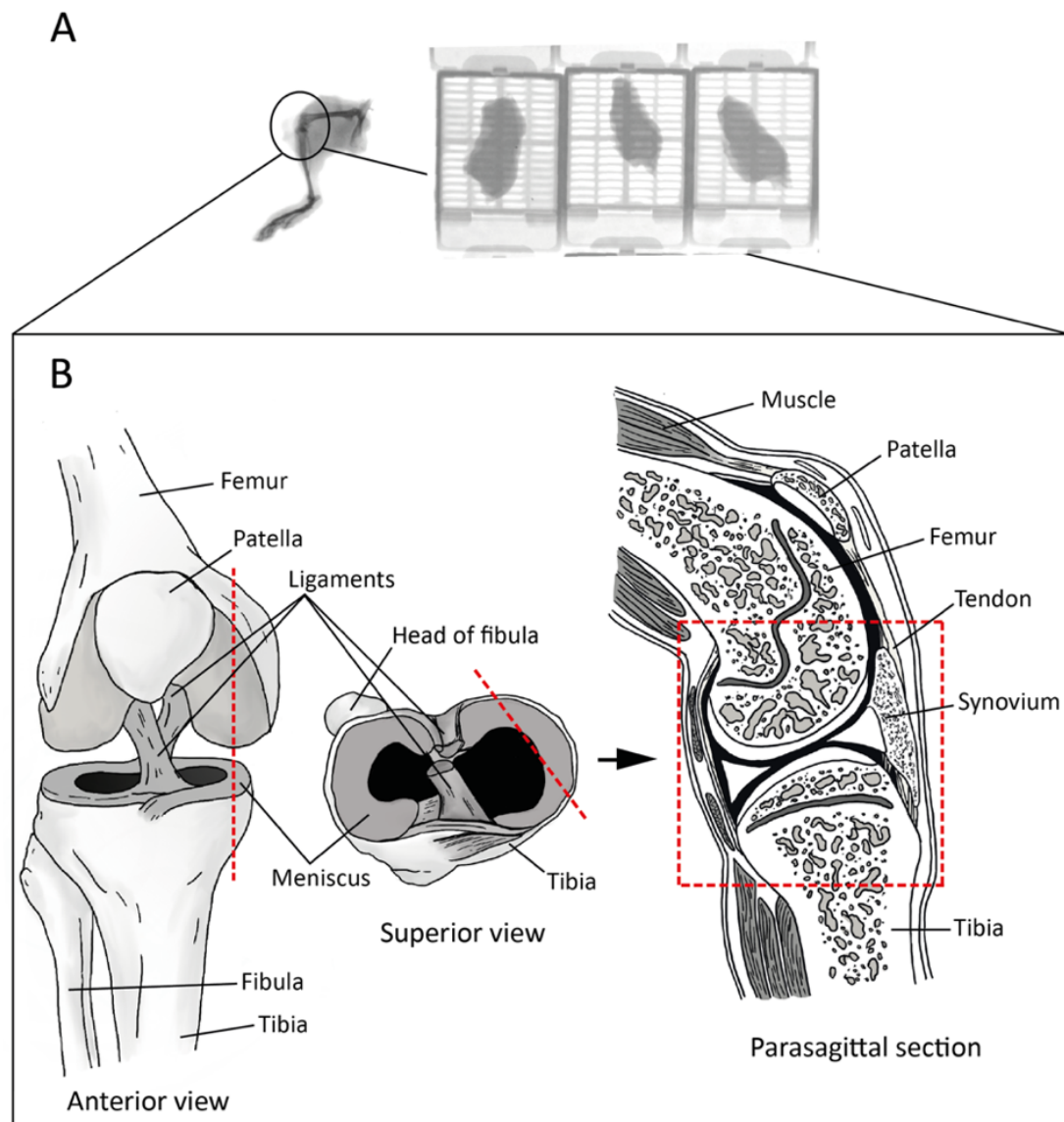


**Figure 2.4 Histology of mouse knee joints.**

**(A)** X-ray images of formalin-fixed mouse knees from an AIA experiment. A whole leg showing the presence of calcified bone can be seen on the left. Images on the right show knees (in histology cassettes) following EDTA or formic acid decalcification. Images captured using a Kodak FX-Pro imaging system (Settings: Exposure, 30; f-stop, 4.96; FOV, 200; focal plane, platen). **(B)** Diagram of anterior, superior and parasagittal views of the mouse knee joint. The red dotted lines indicate where the sections were cut.

*Synovial Infiltrate*

- 
- 0 Normal (adipose tissue appears normal - no infiltrate)
  - 1 Focal inflammatory infiltrates, adiposity hardly affected (10% inflammatory cells, 90% adipose tissue)
  - 2 Focal inflammatory infiltrate equals adiposity (50% inflammatory cells, 50% adipose tissue)
  - 3 Random inflammatory infiltrates dominating cellular histology (70% inflammatory cells, 30% adipose tissue)
  - 4 Substantial inflammatory infiltrate with severe loss of adiposity (90% inflammatory cells, 10% adipose tissue)
  - 5 Ablation of adiposity due to inflammatory infiltrate (100% inflammatory cells, 0% adipose tissue)

*Synovial Exudate*

- 
- 0 Normal
  - 1 Evidence of inflammatory cells in space
  - 2 Moderate numbers of inflammatory cells in space, with evidence of fibrin deposits
  - 3 Substantial number of inflammatory cells with large fibrin deposits

*Synovial Hyperplasia & Pannus Formation*

- 
- 0 Normal (1-3 layers thick)
  - 1 Over three layer thick synovial and evidence of thickening and/or invasion of joint space
  - 2 Over three layer thick synovial lining "creeping" over cartilage surfaces and/or finger-like processes into joint space
  - 3 Over three layer thick synovial showing substantial covering of cartilage surfaces with evident cartilage loss

*Cartilage/Bone Erosion*

- 
- 0 Normal
  - 1 Detectable loss of cartilage detected by Safranin O staining
  - 2 Detectable erosion of underlying bone by pannus activity
  - 3 Pannus has destroyed a significant part of the bone

**Table 2.4 Scoring criteria for histological assessment of joint pathology in AIA.**

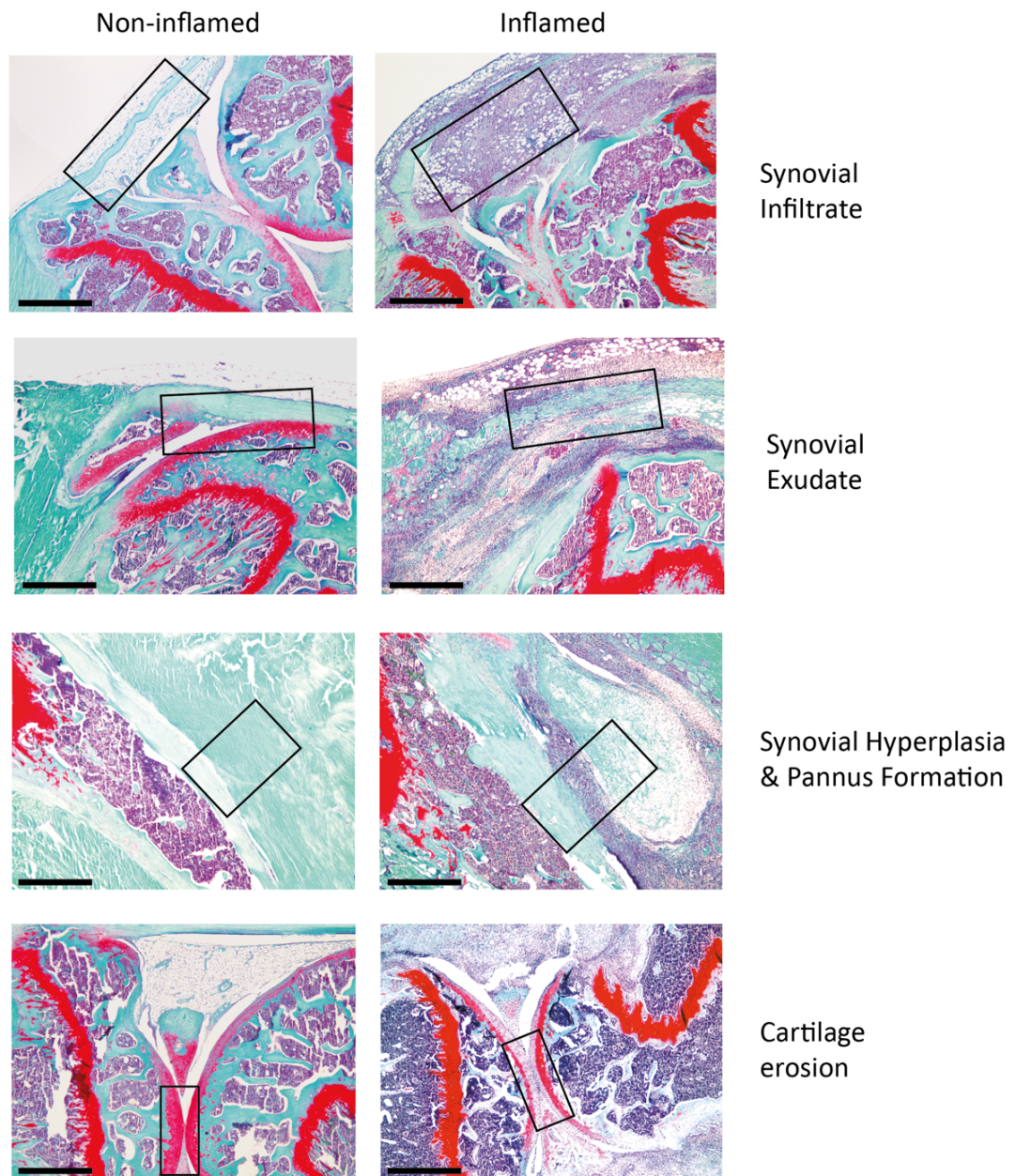


**Figure 2.5 Histological assessment of AIA.**

Haematoxylin, fast green and safranin O staining of knee joints at day 10. From top to bottom, boxes highlight areas of synovial infiltrate, synovial exudate, synovial hyperplasia and pannus formation and cartilage erosion. Scale bars: 600  $\mu$ m.

## 2.4.4 Immunohistochemistry (IHC)

All buffers, with the exception of those supplied as part of commercial kits, used for immunohistochemistry are listed in **Table 2.5**.

<i>Buffer</i>	<i>Composition</i>
EDTA decalcification solution	0.5 M EDTA, 4% formaldehyde, pH 8.0
Formic acid decalcification solution	10% (v/v) formic acid, 2% (w/v) formaldehyde, pH 8.0
Sodium Citrate Buffer	10 mM Sodium Citrate, 0.05% Tween 20, pH 6.0
Tris Buffered Saline with Tween 20 (TBS/T)	0.05 M Tris Base, 0.9% (w/v) NaCl, 0.05% Tween 20, pH 8.4
Tris Buffered Saline (TBS)	0.05 M Tris Base, 0.9% (w/v) NaCl, 0.05%, pH 8.4

**Table 2.5** The composition of IHC buffers used throughout this thesis.

Sections were dewaxed and rehydrated, as stated in **Section 2.4.2**. Lymphocyte and cell-surface markers were detected in paraffin sections using antibodies listed in **Table 2.6**. Antigen unmasking was performed by heating sections in 10 mM citrate buffer (**Table 2.5**) containing 0.05% (v/v) Tween-20 at 95 °C for 40 minutes. For F4/80 staining, antigen retrieval was performed by incubating with 0.05% (v/v) Trypsin-EDTA at 37 °C for 30 minutes. Slides were allowed to cool to room temperature for 20 minutes before endogenous peroxidase activity was blocked using 3% (v/v) H<sub>2</sub>O<sub>2</sub>. Sections were incubated in serum appropriate to the secondary antibody before primary antibody incubations. Primary antibodies (**Table 2.6**) were incubated overnight at 4 °C, in TBS/T (**Table 2.5**). Immuno- labelling of defined antigens was detected using biotinylated secondary antibodies (**Table 2.6**) specific to the primary antibody. Visualisation of antibody labelling was performed using the Vectastain ABC kit and the 3,3'-diaminobenzidine (DAB) chromogen staining kit (Vector Laboratories) following the manufacturer's protocols. DAB is oxidised by hydrogen peroxide in a reaction catalysed by an avidin-conjugated horseradish peroxidase (HRP) diluted in TBS (**Table 2.5**). The oxidised DAB forms a localised brown precipitate that can be visualised using light microscopy (**Figure 2.6**). Slides were counterstained with Harris haematoxylin for 1 minute and dehydrated, cleared and mounted as in summarised in

**Section 2.4.2.** Sections were visualised using Leica DM 2000 microscope and Leica Application Suite v4.9 software. The Leica QWin microscope imaging software was used to quantify positive staining, based on the number of brown DAB-positive pixels detected in the area of staining.

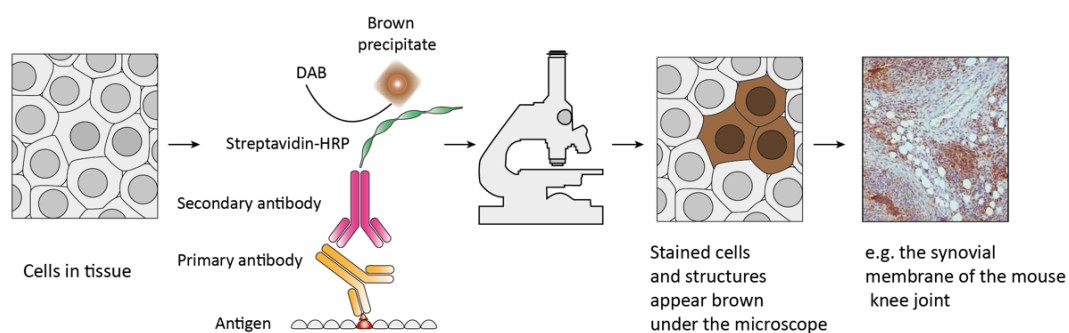


**Figure 2.6** The basic principle of immunohistochemistry on tissue samples.

#### 2.4.4.1 Immunofluorescence (IF)

The following technique is a specialised type of IHC, which uses a fluorochrome-conjugated streptavidin or antibodies to visualise antigen detection by fluorescent microscopy. Briefly, paraffin-embedded sections were unwaxed and rehydrated before antigen unmasking by incubating in 10 mM sodium citrate buffer (95 °C, 40 minutes) (See **Table 2.5**; **Section 2.4.4**). Immuno-labelling was performed as described in **Section 2.4.4** and was detected using a streptavidin-APC (BioLegend) conjugated diluted 1/200 in TBS (**Table 2.5**). Tissue sections were incubated for 1 hour at room temperature in the dark, and after washing in TBS, sections were stored in the dark prior to analysis. Sections were mounted with ProLong Gold Antifade Mountant with DAPI (4',6-diamidino-2-phenylindole). Images were collected using a Zeiss Apotome microscope and analysed using ImageJ software.

<i>Target</i>	<i>Primary Antibody</i>	<i>Clone</i>	<i>Working Concentration</i>	<i>Manufacturer</i>	<i>Secondary Antibody</i>	<i>Working dilution</i>	<i>Manufacturer</i>	<i>Serum</i>
CD3	Rabbit anti-human	Polyclonal	3 µg/ml	Dako	Biotinylated swine anti-rabbit	1/200	Dako	Swine
F4/80	Rat anti-mouse	Cl:A3	2 µg/ml	Bio-Rad	Biotinylated rabbit anti-rat	1/200	Dako	Rabbit
pY-STAT3	Rabbit anti-mouse	D3A7	0.83 µg/ml	Cell Siganlling	Biotinylated goat anti-rabbit	1/200	Vector Laboratories	Goat
CRTAM	Rabbit anti-mouse	Polyclonal	2 µg/ml	Abcam	Biotinylated swine anti-rabbit	1/200	Dako	Swine
TLR9	Rabbit anti-human	Polyclonal	2 µg/ml	Abcam	Biotinylated swine anti-rabbit	1/200	Dako	Swine
ZEB1	Goat anti-mouse	Polyclonal	4 µg/ml	Santa Cruz Biotechnology	Donkey anti-goat CFL-488	1/200	Santa Cruz Biotechnology	Donkey

**Table 2.6 The list of antibodies used for immunohistochemistry.**

## 2.5 Enzyme-linked immunosorbent assay (ELISA)

### 2.5.1 Detection of inflammatory cytokines by ELISA

ELISA was performed to detect T-cell activation to a range of stimuli, by measuring the concentration of secreted inflammatory cytokines, according to manufacturer's instructions (Duoset mouse ELISA kits, R&D Systems). In brief, half area flat-bottom 96-well plates (assay plate) (Corning, Inc.) were coated with a capture antibody (1.5 µg/mL in PBS) and incubated overnight at room temperature. The following day, the assay plates were washed 3x with wash buffer (0.05 % Tween-20 in PBS) using an automated plate washer then blocked with reagent diluent (1% BSA in PBS) for at least 1 hour at room temperature. After blocking, plates were washed, and cell culture supernatants (200 µL volumes) were added to individual wells. Recombinant protein standards (diluted in reagent diluent) were used to generate a standard curve for quantification of cytokine concentrations. After 2 hours of incubation at room temperature, plates were washed, and detection antibody was added and incubated at room temperature for another 2 hours. After incubation and washing, streptavidin-horseradish peroxidase (HRP) was added. Following 20 minutes at room



temperature in the dark, plates were washed again, and the chromogenic peroxidase substrate 3,3',5,5'-tetramethylbenzidine blue (TMB; KPL Inc.) was added, and the reaction stopped with 1.8 M Sulphuric Acid (H<sub>2</sub>SO<sub>4</sub>), once the initial colour reaction had peaked. The optical density (OD) of each well as measured at 450 nm in a FLUOstar Omega plate reader (BMG Labtech).

### 2.5.2 mBSA-specific antibody response by ELISA

Antigen-specific responses to mBSA were determined by measuring mBSA-specific IgG titres in serum (see **Section 2.3.3**), and it has been previously described<sup>104,204</sup>. Serum antibody titres to mBSA were determined by coating half area flat bottom 96 well plates with mBSA diluted in PBS (5µg/mL) and incubated overnight at room temperature. Non-specific binding sites were blocked with 5% (v/v) milk extract and Tween-20 for 1 hour. Wells were washed 3x with wash buffer prior to the addition of sera (diluted 1/1000) in PBS containing milk extract and Tween-20. Assay plates were incubated for 2 hours at room temperature. ELISA was performed as described in **Section 2.5.1**. The assay detection was however modified and included the use of HRP-conjugated goat anti-mouse IgG (0.5 mg/mL, 2 hours, Dako) and 3,3',5,5'-tetramethylbenzidine blue substrate (TMB; KPL Inc.). Absorbance was measured at 450 nm in FLUOstar Omega plate reader (BMG Labtech).

## 2.6 *In silico* identification of transcription factor-binding sites (TFBSs)

Transcription factors (TFs) target specific consensus DNA binding motifs within the genome where they regulate the control of target gene expression<sup>318</sup>. DNA regions at which TFs bind are defined as TF-binding sites (TFBSs) and can be identified *in vivo* by methods such as chromatin immunoprecipitation (ChIP) (see **Section 2.7.2**) or *in vitro* by methods based on binding of large pools of DNA fragments<sup>319</sup>. JASPAR (<http://jaspar.genereg.net>) is among the most popular and longest maintained open-access databases of position frequency matrices (PFMs) and predicts TF binding sequences within a given gene promoter sequence (See **Section 2.7.2.4** for details regarding how to find promoter sequences from genome databases)<sup>320</sup>. A PFM summarises experimentally determined DNA sequences bound by an individual transcription factor by counting the number of occurrences of each nucleotide at each position within aligned TFBSs. These can be converted into position weight matrices (PWMs), used for scanning genomic sequences<sup>321</sup>.

## 2.7 Chromatin immunoprecipitation (ChIP) – qPCR

### 2.7.1 Buffers and reagents used for ChIP

All reagents and buffers, with the exception of those supplied as part of commercial kits, used for ChIP are listed in **Table 2.7**. All chemicals were purchased from Life Technologies (Thermo Fisher Scientific) unless otherwise stated.

<i>Buffer</i>	<i>Composition</i>
Cell lysis buffer (CLB)	10 mM Tris-HCL, 10 mM NaCl, 0.2% (v/v) NP-40, 10 mM Sodium butyrate, 50 µg/mL PMSF, 1 µg/mL Leupeptin
Nuclear lysis buffer (NLB)	50 mM Tris-HCL, 10 mM EDTA, 1% SDS, 10 mM Sodium butyrate, 50 µg/mL PMSF, 1 µg/mL Leupeptin
IP dilution buffer (IPDB)	20 mM Tris-HCL, 10 mM EDTA, 1% SDS, 10 mM Sodium butyrate, 50 µg/mL PMSF, 1µg/mL Leupeptin
IP wash buffer (IPWB) 1	20 mM Tris-HCL, 50 mM NaCl, 2 mM EDTA, 0.1% Triton X-100, 0.1% (w/v) SDS
IP wash buffer (IPWB) 2	10 mM Tris-HCL, 250 mM LiCl, 1 mM EDTA, 1% (v/v) NP-40, 1% (v/v) Deoxycholic acid
TE	10 mM Tris-HCL, 1mM EDTA, pH 8
IP elution buffer (IPEB)	NaHCO <sub>3</sub> , SDS

**Table 2.7** The composition of buffers and reagents used for ChIP.

### 2.7.2 Chromatin Immunoprecipitation (ChIP)

STAT1 and STAT3 Chromatin Immunoprecipitation (ChIP) was performed as previously described <sup>189</sup>. Briefly,  $1 \times 10^7$  cells/mL CD4<sup>+</sup> naïve T-cells per condition (sorted as previously outlined in **Section 2.1.2.3**) were placed in Nunclon delta surface 12-well bottom plates (ThermoFisher Scientific) at a density of  $5 \times 10^6$  cells/well. In a plate previously incubated at 4 °C overnight with anti-CD3 (1 µg/mL anti-CD3; clone 145-2c11, R&D systems), cells were incubated in the presence of soluble anti-CD28 (5 µg/mL; clone 37.51, eBioscience), with either IL-6 (20 ng/mL), IL-27 (10 ng/mL) or no cytokines in supplemented RPMI for 6 hours (**Table 2.1**). **Figure 2.7** is a diagram of the ChIP-qPCR workflow.



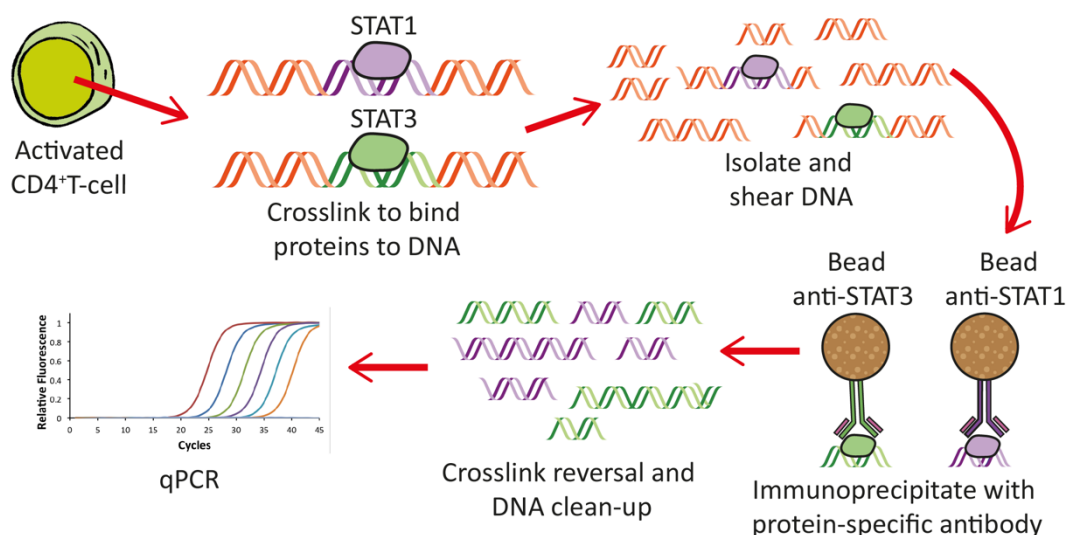


**Figure 2.7** Diagram of the ChIP-qPCR workflow.

### 2.7.2.1 Cross-linking and sonication of genomic DNA

After 6 hours co-incubation at 37 °C, cells were collected and washed with serum-free RPMI medium. Protein-DNA complexes were cross-linked by incubating the cells with 270  $\mu$ L 38% (v/v) formaldehyde for 10 minutes at room temperature. The formaldehyde was quenched by incubating with 1M Glycine (pH 8.0) for 5 minutes at room temperature. Cells were then washed with cold PBS and the cell pellet resuspended in 1 mL of Cell Lysis Buffer (CLB) (**Table 2.7**) before been transferred to a 1 mL tube and left on ice for 10 minutes. After another wash to recover the cell nuclei, supernatant was carefully removed, and cell pellet resuspended in 275  $\mu$ L of Nuclei Lysis Buffer (NLB) (**Table 2.7**). To shear the DNA-protein complexes into fragments, immunoprecipitation dilution buffer (IPDB) (**Table 2.7**) was added, and samples were sonicated using a Bioruptor Plus sonication device (Diagenode). Sonication efficiency was checked with a 20  $\mu$ L sample of chromatin treated with 1.4  $\mu$ L 5M NaCl, 2.6  $\mu$ L H<sub>2</sub>O and 1  $\mu$ L Proteinase K at 65 °C for 1-2 hours, by visualisation on an agarose gel (**Figure 2.8**). For ChIP qPCR assays, the optimal size range of chromatin should be between 150-600 bp, as larger chromatin fragments can negatively influence data quality.

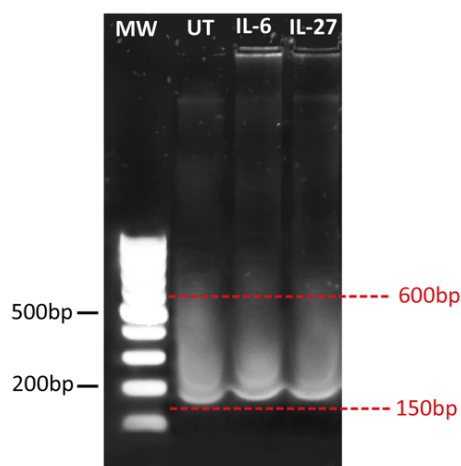


**Figure 2.8 Sonication of genomic DNA for ChIP.**

Untreated, +IL-6, +IL-27 samples were sonicated using a Bioruptor Plus (Diagenode), amplitude: 20%, no. of burst: 30 seconds, allowing samples to cool between bursts. Sonication efficiency was checked by visualisation on agarose gel. The left lane shows the 100 bp DNA molecular weight marker (MW), loaded as size standard. Optimal DNA size range for ChIP analysis was achieved.

### 2.7.2.2 Immunoprecipitation

For IP, Pierce Protein A/G magnetic beads (Invitrogen) were briefly pre-blocked in PBS, then incubated with chromatin samples at room temperature for 2 hours on a rotating wheel, after coupling samples with 5  $\mu$ g of anti-STAT1 (sc-592, Santa Cruz Biotechnology) or anti-STAT3 (sc-482, Santa Cruz Biotechnology) polyclonal antibodies or isotype-specific IgG control antibodies overnight. Beads were washed 5 minutes each with rotation at 4 °C with IPWB1, IPWB2 and TE, using Eppendorf LoBind microcentrifuge tubes (Sigma-Aldrich). After adding 10  $\mu$ L 10% (w/v) SDS, 6  $\mu$ L of 5M NaCl and 2  $\mu$ L RNaseA, tubes were incubated at 65 °C for 2-4 hours.

### 2.7.2.3 DNA purification and qPCR

The DNA was then purified using a DNA clean-up column (Zymo Research), according to manufacturer's instructions, and quantified with Qubit fluorometer. The quality of transcription factor enrichment by immunoprecipitation was confirmed by ChIP-qPCR for STAT transcription factor binding motifs in the promoter regions of *Irf1* and *Socs3*. To minimise systematic biases in the downstream data, an input reference control sample (chromatin taken before ChIP) was used to correct genomic copy number variations, sonication-induced fragmentation bias and chromatin accessibility. Taqman custom assays were designed as described in **Section 2.7.2.4**. (oligonucleotide primer sequences to the promoter region of *Zeb1*, *Irf1* and *Socs3* are shown in **Table 2.9**), and qPCR performed using a QuantStudio 12K Flex Real-Time PCR System as outlined in **Section 2.8.3**. Specific

enrichment was normalised by subtracting the IgG control values from those derived for the input and antibody-specific immunoprecipitation samples. Values were expressed as  $2^{\Delta\Delta CT}$ .

#### 2.7.2.4 Primer design

The sequence of murine genes of interest was determined using Ensembl software (<http://www.ensembl.org/index.html>) and the promoter sequence (**Appendix Figure 8.2**) was subsequently retrieved by identifying the transcriptional start site (TSS) or first exon, as these promoter sequences typically reside immediately upstream from the genomic regions. BLAT-UCSC Genome Browser (<http://genome.ucsc.edu/cgi-bin/hgBlat>) was used to confirm that the promoter sequence matched verified UCSC annotations. Moreover, the presence of CpG islands within the putative sequence motif was used to further substantiate the mapping of TFBS. Part of the promoter sequence was then pasted into the source input box of Primer3Plus (<http://primer3plus.com/cgi-bin/dev/primer3plus.cgi>). Under general settings, “pick hybridisation probe” was selected to show the internal oligonucleotide, and a product size range of 50-100 was chosen before pressing “pick primers”. Forward and reverse primers were then checked using BLAT-UCSC Genome Browser, by performing an “*In silico* PCR”. All the designed primers in this thesis met the guidelines for an efficient primer design established by Taqman (**Table 2.8**) before generation by Invitrogen. All custom designed primers used for ChIP-qPCR are listed in (**Table 2.9**).

<i>Parameters</i>	<i>Criteria</i>
	58 - 60 °C
Melting temperature (T <sub>m</sub> )	Taqman probe T <sub>m</sub> should be 10 °C higher than the primer T <sub>m</sub> The T <sub>m</sub> of both primers should be equal
Length	15 - 30 base pairs (bp)
GC Content	Ideally 30 - 80%
GC Clamp	The total number of Gs and Cs in the last five nucleotides at the 3' end of the primer should not exceed two
Amplicon Length	Ideally 50-150 bp Should not exceed 400 bp
Runs and Repeats	Should not have runs of identical nucleotides (especially four or more consecutive Gs) G+C content should be more Cs than Gs, and not a G at the 5' end.
Genomic DNA Avoidance	In the cDNA preparation, it is preferable to have primers spanning exon-exon junctions.

**Table 2.8 General guidelines for primer design.**

<i>Gene</i>	<i>Forward Primer</i>	<i>Reverse Primer</i>
<i>Zeb1 Promoter</i>	CAAAGTGCGCAACTCGTC	TCCTAGGCCAGGTTGAGC
<i>Irf1 Promoter</i>	CCTTCGCCGCTTAGCTCTAC	CCCACTCGGCCTCATCATT
<i>Socs3 Promoter</i>	CTCCGCGCACAGCCTTT	CCGGCCGGTCTTCTTGT

**Table 2.9 Custom-designed primers for ChIP-qPCR.**

## 2.8 RNA expression analysis

### 2.8.1 RNA extraction

Total RNA from synovial tissue (**Section 2.3.4**) and *in vitro* T-cells cultures *in vitro* (**Section 2.1.2.4**) was extracted using the RNEasy Mini Kit (Qiagen) according to the manufacturer's instructions. For recovery of RNA from synovial tissue, total RNA was extracted by homogenising in 600  $\mu$ L of RLT buffer (Qiagen) supplemented with 1% (v/v)  $\beta$ -mercaptoethanol, per 20 mg of tissue using a D1000 handheld homogeniser (Benchmark scientific). For T-cells, the cell pellet was resuspended with 250  $\mu$ L of RLT buffer supplemented with 1% (v/v)  $\beta$ -mercaptoethanol for lysis. Genomic DNA was then eliminated by passing through an on-column DNaseI digestion column (Qiagen), an equal volume of 70% (v/v) ethanol was added to the recovered flow-through fraction. RNA was then bound onto the RNEasy MinElute spin column, washed and finally eluted with 20-30  $\mu$ L of RNase-free water. The quality and quantity of eluted RNA were determined using a Nanodrop 2000 spectrophotometer (ThermoFisher scientific) by measuring optical absorbances at 230, 260 and 280 nm and the determination of A260/280 and A260/230 ratios for the assessment of, using absorbance measurements at 320 nm, 260 nm and 280 nm, to detect contaminating proteins and phenols respectively. RNA was stored at -80 °C or used directly for cDNA synthesis. All the procedures that involved RNA handling were conducted in a clean, RNase-free space designated within the laboratory, and filtered tips and RNA-free reagents were used throughout the procedures to ensure no degradation of the samples and to prevent contamination.

### 2.8.2 cDNA synthesis

Total RNA reverse transcription into cDNA was performed using a Precision nanoScript 2 Reverse Transcription Kit (Primerdesign) using random oligonucleotide primers according to the manufacturer's instructions. Samples and reagents were kept on ice at all times. RNA samples were thawed at room temperature. For all reactions, 1 µg of total RNA was used. The following mix was prepared for each sample:

Reagent	1 reaction
RNA (up to 2µg)	X µL
Oligo-dT primer	1 µL
RNAse/DNAse free water	X µL
Final volume	10 µL

The reaction tubes were placed in a thermal cycler and incubated at 65 °C for 5 minutes, then immediately transferred to ice for the annealing step. The following master mix for n reactions was prepared and 10 µL added to each tube for the extensions step:

Reagent	1 reaction
NanoScript 4X Buffer	5 µL
dNTP mix 10 mM	1 µL
RNAse/DNAse free water	3 µL
nanoScript2 enzyme	1 µL
Final volume	10 µL

In a thermal cycler, the tubes were incubated at 42 °C for 20 minutes, then heat-inactivated at 75 °C for 10 minutes and finally cDNA samples were store at -20 °C until use.

### 2.8.3 Quantitative Real-Time Polymerase Chain Reaction (qPCR)

Gene expression was quantified by qPCR using TaqMan Gene Expression Assay (Applied Biosystems) in a barcoded MicroAmp Optical 384-well reaction plate (Applied Biosystems). The qPCR reaction was prepared, as shown below:

Reagent	1 reaction
TaqMan Fast Advanced Master Mix	5 µL
TaqMan primer	0.5 µL
cDNA	1 µL
RNAse/DNAse free water	3.5 µL
Final volume	10 µL

and amplified and acquired using the Fast protocol in the QuantStudio 12K Flex Real-Time PCR system (Applied Biosystems). A list with the Taqman probes from Thermofisher used for qPCR is shown below:

<i>Gene</i>	<i>Species</i>	<i>Assay ID</i>
<i>Socs3</i>	Mouse	Mm00545913_m1
<i>Irf1</i>	Mouse	Mm01288580_m1
<i>Crtam</i>	Mouse	Mm00490300_m1
<i>Zeb1</i>	Mouse	Mm00495564_m1
<i>Cadm1</i>	Mouse	Mm00457551_m1
<i>Stat3</i>	Mouse	Mn01219775_m1
<i>Actb</i>	Mouse	Mm01205647_g1

Data were analysed using a comparative threshold cycled (Ct) method<sup>322,323</sup>. A Ct value is the number at which the signal of the reporter crosses a set threshold in the exponential phase of amplification. Thus, Ct is inversely related to the amount of amplicon or target gene present in the sample. Ct values for genes of interest are then standardised against an internal housekeeping control, whose expression is known to remain unaltered within the experimental conditions. Here, relative mRNA expression was determined using the Ct method and normalised to the housekeeping gene *Actb*.

## 2.9 Transcriptomic profiling of synovium

RNA-seq methodologies were used for the evaluation of CpG-*Stat3*siRNA therapeutic outcome in an experimental model of inflammatory arthritis (**Section 2.3.2.1**) (see **Chapter 3**). The method utilised for RNA-seq of mouse synovium used in this thesis had been previously optimised by my colleague Dr David Hill (Cardiff University). **Figure 2.9** provides a schematic representation of the experimental workflow described in this section.

### 2.9.1 Input RNA quality control

For RNA-sequencing (RNA-seq) of mouse synovium, RNA was extracted as outlined in **Section 2.8.1**. The assessment of RNA integrity is a critical first step in obtaining meaningful gene expression data. The quality and integrity of the purified total RNA were determined using a Nanodrop 2000 spectrophotometer (Thermo Fisher Scientific) and an Agilent 2100 Bioanalyser using an RNA Nano Kit (Agilent Technologies) following manufacturer's instructions. Samples were then selected based on their Integrity Number (RIN), which is the ratio of the 18S and 28S ribosomal subunits (rRNA). This value plays an important role in determining the level of sample degradation and therefore is an indicator of the quality of the RNA. RIN values over 8 were considered sufficient for library preparation (**Figure 2.9 – 1**). Libraries were prepared with 0.5 – 1 µg of total RNA from each sample.

### 2.9.2 Removal of ribosomal RNA

Ribosomal RNA (rRNA) was removed from samples using a polyA capture method adopting a Dynabeads mRNA Direct Kit (Ambion). All protocol steps were conducted according to the manufacturer's instructions. This isolation method relies on base pairings between the polyadenylated (polyA) tail at the 3' end of most mRNA, and the oligo (dT)<sub>25</sub> residues covalently coupled to the surface of the magnetic Dynabeads. Thus, only mRNA from RNA species that are not polyadenylated are positively selected. The efficiency of rRNA-depletion was confirmed on an Agilent 2100 Bioanalyser using an RNA Pico kit (Agilent Technologies) following manufacturer's instructions (**Figure 2.9 – 2**).

### 2.9.3 Library preparation

Libraries were prepared using the TruSeq Stranded Total RNA Library Prep Kit (Illumina) following the manufacturer's instructions. Five biological replicates were used for each genotype at day 3, and six replicates for each genotype at day 10, in line with ENCODE guidelines regarding the optimal replicates required for statistical validation<sup>324,325</sup>. Each step of the library is detailed below:

*Fragmentation of RNA.* For the HiSeq 4000 platform, fragment sizes should fall within the range between approximately 260 to 280 bp (**Figure 2.9 – 6**). Purified mRNA was fragmented

by adding EPH (elute, prime, fragment high) Mix to samples and heating to 94 °C for 6 minutes.

*Synthesis of cDNA.* Double-stranded cDNA was generated by reverse transcription reaction using a SuperScript III reverse transcriptase (Invitrogen) followed by a cleaning step using Agencourt AMPure XP beads (Beckman Coulter). These magnetic beads are coated with carboxyl groups that, in the presence of salt, bind to DNA to remove any impurities.

*3' Ends Adenylation.* To optimise the ligation of adapter sequences to cDNA fragments, a single 'A' nucleotide was introduced to the COOH-terminal sites.

*Adapter ligation.* Sequencing adapters were then annealed to the purified 3'-ends-adenylated-cDNA. These adapters add distinct sequences to the 5' and 3' ends of each strand in the genomic fragment, serving as barcodes to identify samples when pooled and preparing to generate sequencing libraries complementary to the amplification primers on the flow cell. (**Figure 2.10**). This was followed by another washing using AMPure XP beads, that selectively bind to DNA fragments 100 bp and larger, removing non-ligated adapters, and select a size-range of sequencing library appropriate for cluster generation. This selective binding depends on the accuracy of the volumetric ratio of salt to DNA, that was optimised for binding the correct sized fragments for sequencing.

*PCR amplification and library quantification.* Purified cDNA fragments that had adapter molecules on both ends were then selectively enriched to amplify the amount of DNA in the library for accurate quantification, using PCR. A further magnetic bead purification using AMPure XP beads was utilised after the amplification. Libraries were validated, as recommended by Illumina, on an Agilent 2100 Bioanalyser, using a high sensitivity DNA kit (Agilent Technologies) following the manufacturer's instructions. Final cDNA libraries were quantified by qPCR using DNA of known concentrations as directed in the KAPA Library Quantification Kit (KAPA Biosystems). Libraries were diluted to a final concentration of 10 pM and combined into a single pool. The pooled libraries were sequenced across multiple lanes, in order to remove bias derived from sequencing on different lanes, using a HiSeq 4000 (Illumina) and pair-end sequencing (**Figure 2.11**). Libraries were finally sequenced to have greater than 30 million mapped reads, agreeing on ENCODE guidelines<sup>325</sup>.



### 2.9.4 Read mapping strategy

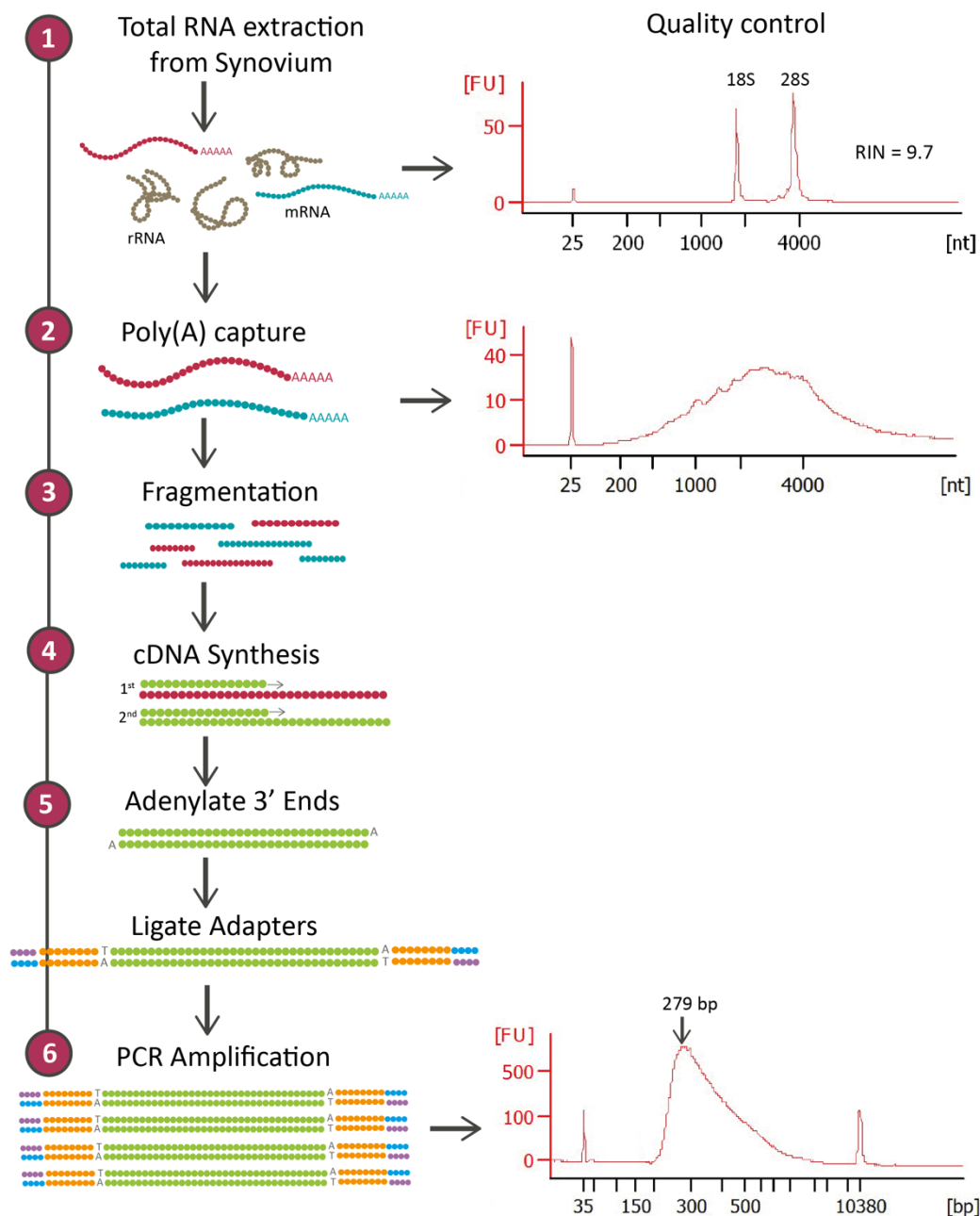
Raw sequencing files (fastq files) were trimmed in order to remove adapter sequences and low-quality reads, as these would affect mapping to the genome. To verify the quality of the sequencing reads, datasets were tested using fastQC software (Babraham Institute, <https://www.bioinformatics.babraham.ac.uk/projects/fastqc/>). All sequencing reads were mapped to a reference genome (mm10/gb38.90) using STAR software. STAR can align spliced sequences of any length with moderate error rates and can detect annotated and novel splice junctions. Duplicate reads were identified and marked using Picard (Broad Institute, <https://broadinstitute.github.io/picard/>) and further analysis performed to assess the quality of the libraries (e.g. number of reads, percentage duplication). The alignment of sequences to specific genes was determined using the featureCounts software. An example of the quality of sequencing determined by FastQC report is provided in the **Appendix, Figure 8.3**.

### 2.9.5 Differential gene expression analysis

Differential gene expression analysis was performed using the DESeq2 package (Bioconductor) to identify significantly regulated gene changes across the course of the disease as a response to therapeutic intervention. Analysis combined newly generated datasets derived from CpG-*Stat3*siRNA treated WT and *Il27ra*<sup>-/-</sup> mice with AIA (performed at day-3 and day-10 post disease onset) and archived RNA-seq datasets previously obtained from WT and *Il27ra*<sup>-/-</sup> mice with AIA (unpublished data generated by Dr David Hill). Genes selectively controlled in response to arthritis onset were identified by comparison to RNA-seq datasets generated from the synovial tissues of healthy control WT and *Il27ra*<sup>-/-</sup> mice without AIA. Firstly, normalised read counts were calculated, which accounts for the different depth in sequencing between individual samples. The fragments per kilobase of transcript per million mapped reads (FPKM) were then calculated from the normalised counts, which corrects the number of reads to account for variation in gene lengths. Since analysis was focused on identifying changes in the same gene in different conditions, the normalised counts were used to calculate fold expression changes and statistical analysis unless otherwise stated.

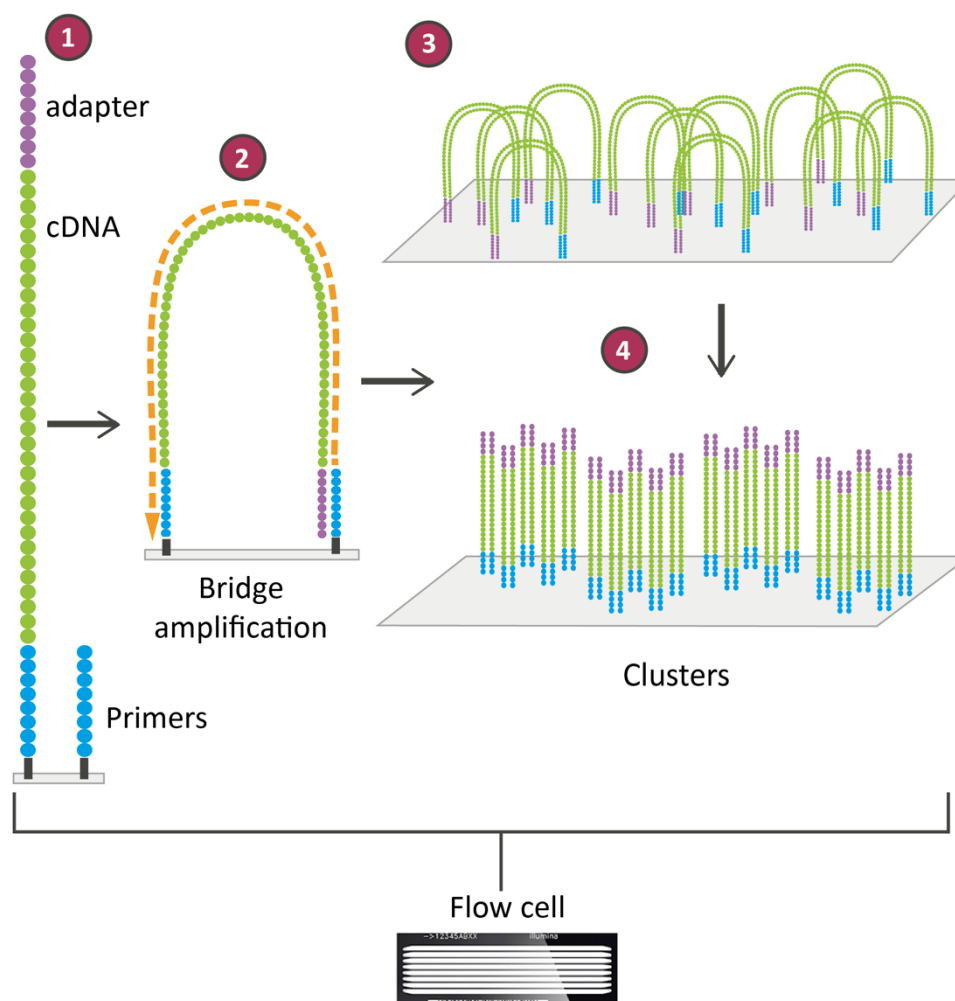
### 2.9.6 Evaluation of duplicated reads

To minimise the potential impact of erroneous duplicate reads that may bias the gene expression analysis within the data set, the R package dupRadar (Bioconductor) was used<sup>326</sup>. This package identifies the number of duplicates per gene assigned using Picard and compares this against the fold change in gene expression as determined using the DESeq2 package (see **Section 2.9.4**).



**Figure 2.9 Workflow of RNA-seq library preparation.**

(1) First, total RNA was extracted from the synovium and quality control was performed as indicated in representative bioanalyser trace of total RNA extraction from mouse synovium. (2) A poly(A) capture method was used to isolate mRNA from rRNA, and quality control was performed as indicated in representative bioanalyser after ribosomal depletion. (3) RNA was fragmented into suitable sizes for sequencing before a (4) reverse transcription reaction was utilised to form cDNA and (5) 3' ends were adenylated in preparation for ligation to unique adapters which served as barcodes to enable multiplexing of samples, as well as primers for amplification on the flow cell. (6) cDNA libraries were finally amplified before being quantification and sequencing.

**Figure 2.10 Cluster generation during Illumina HiSeq 4000 sequencing.**

(1) The surface of the Illumina flow cell is coated with a lawn of primers that are complementary to the adapters ligated on the cDNA library. (2) Priming occurs as the opposite end of a ligated fragment bends over to another complementary oligo on the surface. (3) This technology is called bridge amplification, and it is used to generate clusters of hundreds of identical strands of DNA. (4) Repeated denaturation and extension cycles result in localised amplification of single molecules into millions of unique, clonal clusters across the flow cell.

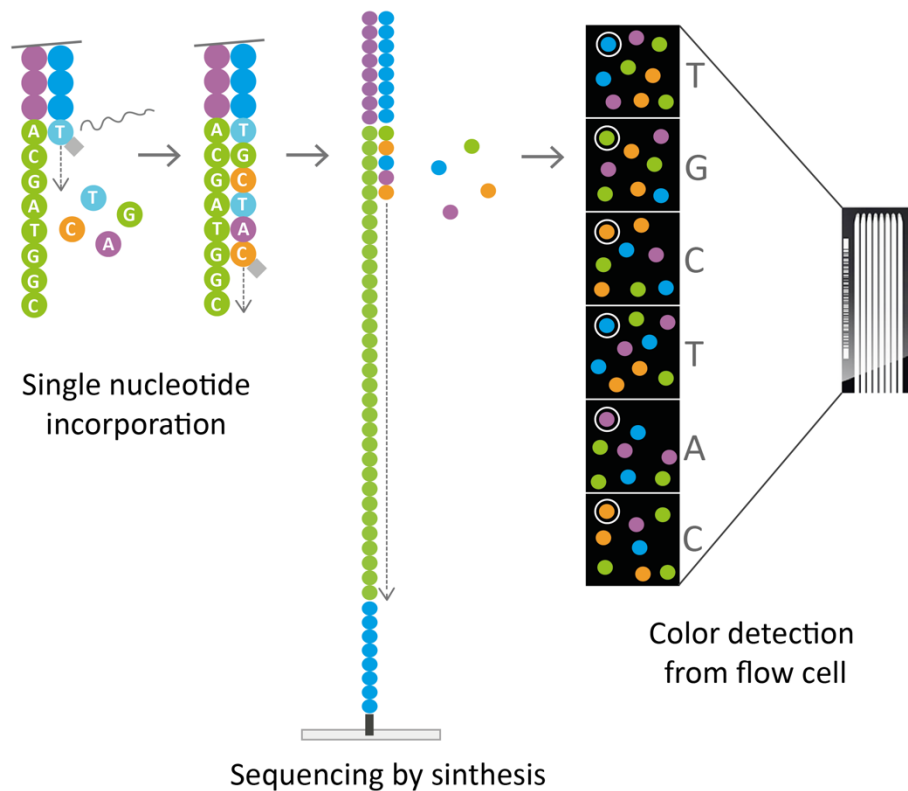


**Figure 2.11 Sequencing by synthesis using Illumina HiSeq 4000.**

Sequencing is determined by a reversible termination method. Each of the four dNTPs is fluorescently labelled with a different dye and modified by a terminator group. During each sequencing cycle, a single labelled nucleotide is added to the nucleic acid chain, and the fluorescent dye is identified through laser excitation and imaging, then enzymatically cleaved to allow the next round of incorporation to obtain the full sequence.

## 2.9.7 Data visualisation and interpretation

### 2.9.7.1 *Heatmaps*

Heatmaps were generated using Genesis software or the online tool Morpheus available from the Broad Institute. Heatmap visualisations were based on a  $\log_2$  fold change ( $\log_2FC$ ) in gene regulation as compared to a healthy control joint (naïve) or an inflamed joint (AIA). Genes clustered according to time point or mouse genotype, as indicated in the associated Figure Legend. All data sets were hierarchically clustered using one minus Pearson correlation coefficient.

### 2.9.7.2 *Venn diagrams*

Venn diagrams were used to visualise the number of genes sharing common or distinct patterns of regulation between different conditions (as described in accompanying Figure Legends). Plots were generated using the VennDiagram package (CRAN).

### 2.9.7.3 *Volcano plots*

To illustrate the distribution of induced and suppressed genes, data sets were visualised by using Volcano plots. Data were expressed as a  $\log_2$  fold change ( $\log_2FC$ ) against the  $\log_{10}$  of the adjusted *p-value* using the ggplot2 package (tidyverse). 2D scatter plots were made using ggplot2 packages (tidyverse)

### 2.9.7.4 *2D Scatter plots*

2D Scatter plots ( $\log_2FC$  vs  $\log_2FC$ ) were created using tidyverse and ggplot2 packages. Data were expressed as a  $\log_2$  fold change ( $\log_2FC$ ) for each condition as compared to a naïve control.

### 2.9.7.5 *Alluvial diagrams*

Alluvial diagrams were generated using networkD3 and alluvial packages (CRAN) and were used to identify groups of genes that change pattern of expression as a response of treatment.

#### 2.9.7.6 *Ingenuity Pathway Analysis*

Molecular pathways analysis adopted Ingenuity Pathway Analysis (IPA; Qiagen) to identify canonical pathways, upstream regulators and functions and diseases associated with differentially regulated genes between treated and untreated joints across genotypes and the time course of AIA. Relevant pathways were determined by their p-value.

#### 2.9.7.7 *K-means clustering*

To identify genes displaying common patterns of gene regulation across the time course of the disease model, RNA-seq datasets were analysed using Genesis software to group genes based on K-means clustering. The optimal number of clusters was determined using statistical tests (Davies-Bouldin Index, Silhouette and Gap values) (as outlined in **Chapter 3**) and was performed in collaboration with Dr Barbara Szomolay (Cardiff University). These methods provide a statistical measure of how individual genes behave in response to inflammation). A low value observed with the Davies-Bouldin index reveals a more optimal number of clusters in the data<sup>327</sup>. Conversely, a higher value predicted by the Silhouette and Gap methods indicates that genes displaying a similar profile of expression are appropriately grouped into clusters that share common patterns of regulation<sup>328,329</sup>.

#### 2.9.7.8 *Molecular visualisation*

PyMOL 2.0 is a free cross-platform molecular graphics system software and was used in **Chapter 6** to visualise the 3D molecular structure of the human IL-6/IL-6R/gp130 complex using a PDB code 1P9M. Every molecular model (atomic coordinate file) in the Protein Data Bank (PDB) - a database for the three-dimensional structural data of large biological molecules such as proteins and nucleic acids - has a unique accession or identification code (4 characters in length)<sup>330</sup>.

## 2.10 Statistical data analysis

Figures and statistical analysis were made using GraphPad Prism 7 software (GraphPad Software Inc., La Jolla, USA) or RStudio (RStudio Inc.) unless otherwise stated. Student's t-test was used to determine statistical significance when comparing two experimental groups that distributed normally (Gaussian distribution). Alternatively, for data that were not normally distributed a Mann-Whitney U-test was performed. To identify statistical significance between multiple groups for normally distributed data, a one-way ANOVA with Turkey's multiple comparison test was used. Where experimental groups were compared across multiple time points, a two-way ANOVA was used with a Bonferroni post-test. A  $P < 0.05$  was considered statistically significant. Graphs are presented as mean  $\pm$  standard error of the mean (SEM) unless indicated otherwise. For *in vivo* analysis, where pilot data was available, the appropriate sample size for experimental groups was determined by statistical power analysis using G\*Power (<http://www.gpower.hhu.de/>)<sup>331,332</sup>. For *in vivo* studies where no preliminary data was available, pilot experiments were performed using small group sizes calculated in accordance with the resource equation<sup>333</sup>:

$$E = N - T$$

Where E must be between 10 and 20, N = total number of animals, T = number of treatments/groups

## 3 Evaluation of CpG-Stat3siRNA therapy in diffuse and lymphoid-rich synovitis

---

### 3.1 Background

Synovitis in inflammatory arthritis is highly heterogeneous, affecting the rate of disease progression, severity and response to therapy. In this regard, joint inflammation can be broadly classified into three distinct pathotypes based on the cellular and molecular signatures of inflammation: pauci-immune (or fibroblast-rich), diffuse (myeloid-rich) and follicular (lymphoid-rich)<sup>149,150</sup>. Although recent advances in targeted therapeutic strategies have enhanced the clinical management of RA, patients often display an inadequate response to certain biological drugs. Thus, there is a pressing need to understand the mechanisms responsible for disease heterogeneity and to identify those patients who are likely to benefit from specific therapies. For example, patients with follicular synovitis often present with a severe form of disease and remain a challenging group for treatment<sup>107,128,153,154,334</sup>. Patients with this form of synovitis show histological features of ELS that contribute to disease activity. Understanding the inflammatory events that lead to ELS development, maintenance and activity within the inflamed synovium may ultimately improve the diagnosis, stratification and treatment of this type of pathology.

Cytokines that signal via the JAK/STAT signalling pathway are determining factors during inflammatory arthritis. More specifically, the activity of STAT3 is intrinsically linked with the development of synovitis in patients with RA and contributes to the rapid progression of the disease<sup>204,212</sup> (discussed in more detail in **Chapter 1, Section 1.3.1.3**). It is well established that STAT3 is not only active in autoimmunity but is also overexpressed and persistently activated in a wide diversity of solid and hematologic cancers, enhancing tumour cell proliferation and survival, inflammation and is associated with poor prognosis<sup>335–338</sup>. Cytokine-targeting therapies have revolutionised the treatment of immune-mediated diseases<sup>339</sup>; some biologics (e.g., the interleukin-6 receptor blocker tocilizumab) and small molecule inhibitors (e.g., tofacitinib, which blocks Janus kinases that regulates STAT activation) are used in the treatment of inflammatory arthritis and inhibit STAT3 activity as



part of their mode of action<sup>212,216</sup>. However, these are non-specific for STAT3, do not selectively target cell types responsible for disease progression and frequently elicit adverse contraindications.

In this Chapter, I utilised a novel anti-cancer therapy (CpG-*Stat3*siRNA), to develop an alternate strategy that specifically inhibits STAT3 signalling in inflammatory cells. CpG-*Stat3*siRNA is a synthetically engineered STAT3 small interfering (si) RNA linked to an endosomal Toll-like receptor (TLR)-9 agonistic immunostimulatory unmethylated CpG oligonucleotide<sup>316</sup> (**Figure 3.1A**). TLR9 recognises pathogen-associated molecular pattern molecules (PAMPs) in unmethylated CpG containing DNA of bacterial and viral origin and has been extensively studied<sup>340</sup> (see **Section 1.1.1.1**). Thus, CpG-*Stat3*siRNA targets STAT3 driven outcomes in TLR9<sup>+</sup> cells, such as DCs and other myeloid cell populations.

CpG-*Stat3*siRNA has been previously shown considerable efficacy in cancers such as myeloid leukaemia, melanoma and lung cancer when used *in vivo*, where silencing of STAT3 lead to activation of tumour-associated immune cells and ultimately to potent antitumour immune responses<sup>316,341–344</sup> (**Figure 3.1 B**). Both unconjugated siRNAs and CpG oligonucleotides targeting TLR9 have also been tested in the clinic, showing no toxicity and completing Phase I and Phase II trials of certain cancers<sup>343–345</sup>. Thus, CpG-*Stat3*siRNA, as a cancer therapy, has a unique mode of action involving two mechanisms – a targeted inhibition of STAT3 and an adjunct antitumour response triggered by CpG signalling through engagement of the TLR9 innate sensing system.

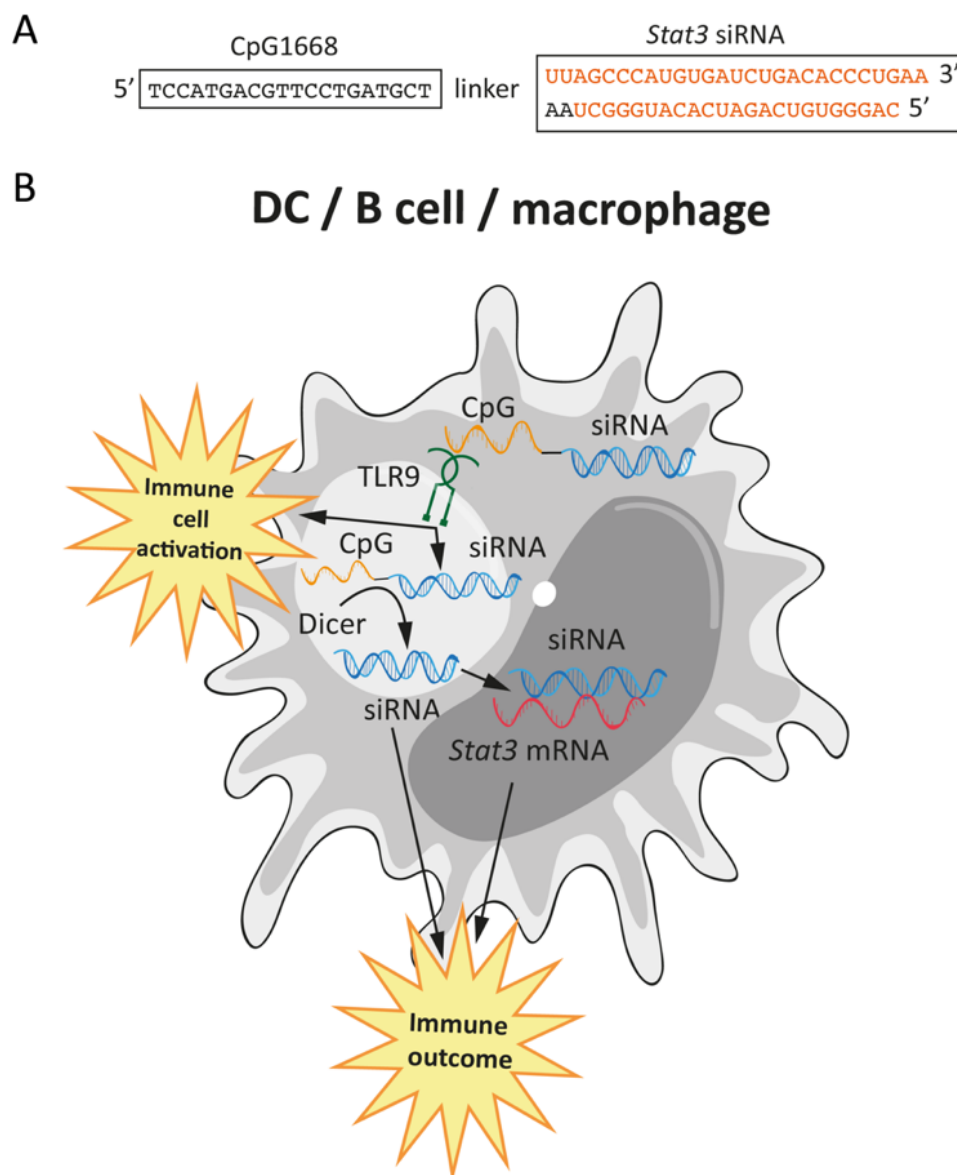


**Figure 3.1 Structure and mechanism of action of the CpG-Stat3siRNA conjugate.**

**(A)** Sequence of the CpG-linked mouse *Stat3* siRNA conjugate (CpG1668 - *Stat3* siRNA). CpG1668 single-stranded oligonucleotide was coupled to the antisense strand of double-stranded *Stat3* siRNA, using a carbon chain linker. **(B)** The CpG oligonucleotide component binds to endosomal toll-like receptor 9 (TLR9) on dendritic cells (DCs), B-cells and macrophages to initiate a cascade of innate and adaptive immune responses in the cell and to efficiently internalised the conjugate. Within the cell, the dicer enzyme cleaves the siRNA from CpG, allowing the siRNA to bind and silence *Stat3* mRNA, upregulating the cell's ability to initiate a Th1-type immune response.

## 3.2 Aims

Since STAT3 is a potential therapeutic target for RA, it was hypothesised that selective inhibition of JAK/STAT signalling, and more specifically directly targeting of STAT3, would provide a novel therapeutic approach for the treatment of inflammatory arthritis. In the next Chapter, I took a similar approach inhibiting JAK/STAT signalling by indirectly upregulating SOCS3 instead.

The overall aim of this study, which was carried out in collaboration with Prof Hua Yu and Assoc Prof Marcin Kortylewski (City of Hope, California – expertise on CpG-*Stat3*siRNA therapy in cancer), was to explore the applicability of CpG-*Stat3*siRNA technology as a siRNA delivery platform to treat indications other than cancer, including inflammation and autoimmunity. Therefore, this study represents the first attempt to reposition this novel anti-cancer therapy, that activates the innate immune system through TLR9 while also inactivating STAT3, in the context of inflammatory arthritis. The objectives of the study were to:

- Investigate the efficacy and mode of action of CpG-*Stat3*siRNA in experimental arthritis (AIA) by evaluating synovial histopathology.
- Explore holistic gene changes in synovial tissue at day-3 and day-10 post-AIA as a response to CpG-*Stat3*siRNA treatment, using computational analysis of optimised RNA-seq methodologies.
- Evaluate transcriptional events controlled by STAT1 and STAT3 and identify signatures controlled by STAT1/STAT3 cross-regulation.
- Determine whether CpG-*Stat3*siRNA disrupts formation, maintenance and functional properties of ELS by addressing the responses to therapy in two forms of synovitis, where WT and *Il27ra*<sup>-/-</sup> mice are used as models of diffuse and lymphoid-rich disease respectively.

### 3.3 Results

#### 3.3.1 TLR9-expressing cells are present in synovial tissue

The use of IL-27 receptor deficient mice is one of the approaches that allows for the development of a more chronic form of AIA and also facilitates the investigation of discrete synovial pathotypes. *Il27ra*<sup>-/-</sup> mice lack regulatory cytokine IL-27, resulting in synovitis featuring ectopic lymphoid-like follicles, a histopathological characteristic seen in RA patients with severe synovitis and inferior responses to biological treatment. My laboratory is uniquely placed to compare the responses to therapy in two forms of synovitis – diffuse (WT) and lymphoid-rich (*Il27ra*<sup>-/-</sup>) and determine whether CpG-*Stat3*siRNA disrupts formation, maintenance and functional properties of ELS associated with lymphoid-rich synovitis<sup>104</sup>.

Our collaborators at City of Hope (California, USA) successfully generated a CpG-*Stat3*siRNA therapy with antitumour activities as a response to silencing *Stat3* in TLR9<sup>+</sup> cells, which enhances antitumor immune responses *in vivo*<sup>316,346</sup>. The distribution of TLR9 expression in murine leukocyte subsets is widely known, being primarily localised in intracellular compartments of DCs, macrophages and B-cells<sup>347</sup>. Lymphoid-rich synovitis in RA is associated with the development of synovial ELS, characterised by the presence of T-cells, B-cells and follicular dendritic cells (FDCs)<sup>104,155</sup>. Although FDCs are not classic DCs (as they are of mesenchymal origin), studies have demonstrated that FDCs are also equipped with TLRs including TLR2 and TLR4<sup>348</sup>. However, TLR9 expression in FDCs has not been yet described. Moreover, TLR9<sup>+</sup> cells have been shown to be present in RA synovial fibroblasts (RASf)<sup>349</sup> and synovial-infiltrated monocytes<sup>350</sup>. Therefore, we first evaluated the expression of TLR9 in the inflamed synovium of mice with AIA prior to testing the efficacy of CpG-*Stat3*siRNA in experimental arthritis.

Here, antibody detection of TLR9 in the inflamed synovium of mice with AIA by IHC confirmed TLR9 expression in both WT and *Il27ra*<sup>-/-</sup> mice with AIA (**Figure 3.2A**). Consistent with our previous work, exacerbated inflammatory arthritis in *Il27ra*<sup>-/-</sup> mice was associated with an increased infiltration of CD3<sup>+</sup> T-cells (**Figure 3.2B**). However, the presence of TLR9<sup>+</sup> cells did not share a similar relationship with the degree of synovitis, where a comparable

degree of TLR9 staining was observed in inflamed joints from AIA-challenged WT and *Il27ra*<sup>-/-</sup> mice (**Figure 3.2C**).

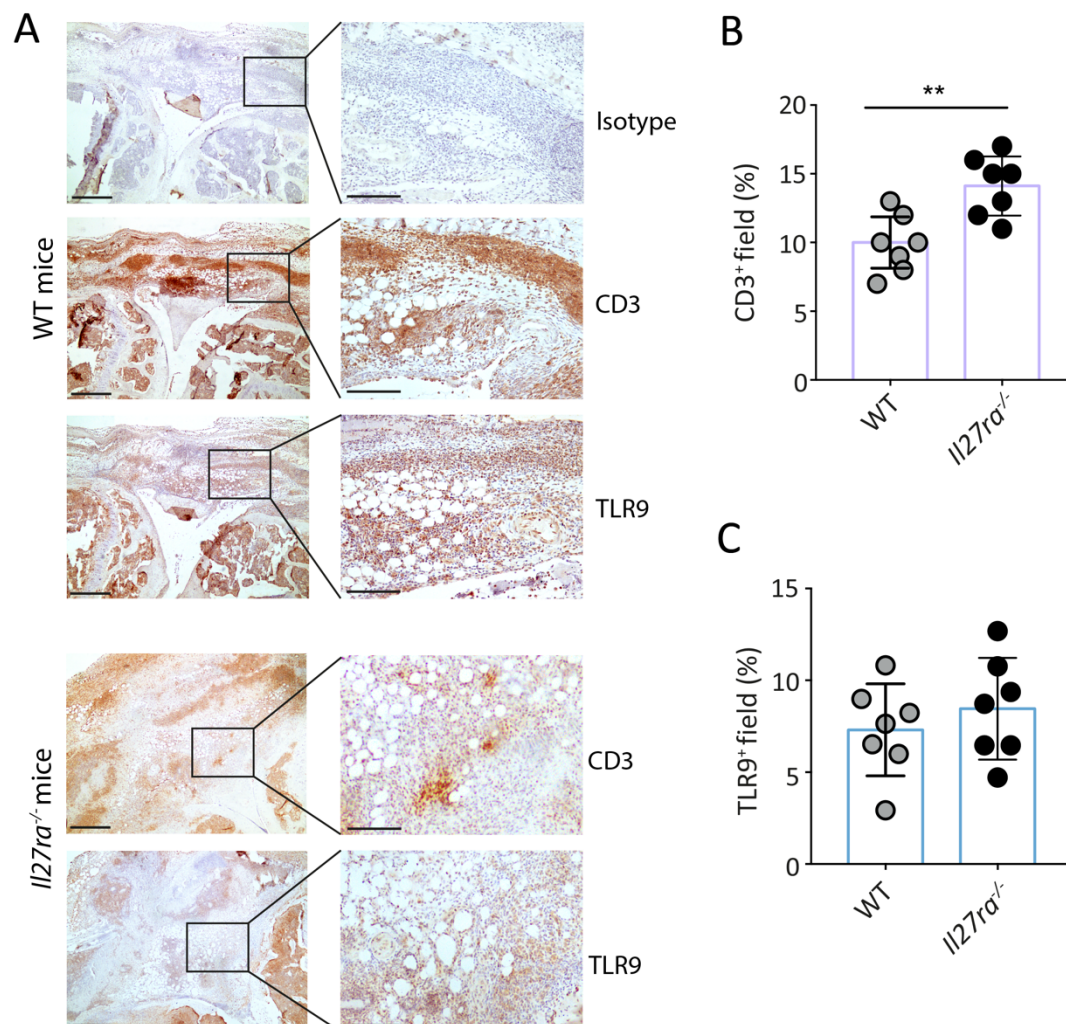


**Figure 3.2** TLR9 is expressed in the joints of WT and *Il27ra*<sup>-/-</sup> mice with AIA.

**(A)** AIA was established in WT and *Il27ra*<sup>-/-</sup> mice and histopathology assessed at day-10 post-arthritis induction. Sequential sections were stained as indicated by IHC: CD3 and TLR9. Isotype control for TLR9 is shown in the upper section. Quantification of CD3 **(B)** and TLR9 **(C)** staining (n = 7/group). Error bars indicate SEM. \*\*,  $p < 0.01$ . Shapiro-Wilk normality test and an unpaired t-test were used. Scale bars: (A) 500  $\mu$ m left, 200  $\mu$ m right. No staining was observed in non-inflamed (naïve) control joints, due to the lack of cell infiltrate within the 'healthy' synovium.

### 3.3.2 CpG-*Stat3*siRNA treatment improves arthritis severity *in vivo*

Previous studies by our laboratory have shown that CpG-*Stat3*siRNA treatment significantly reduced *Stat3* expression in *ex vivo* isolated CD19<sup>+</sup> B-cells (data not shown). To further investigate the efficacy and mode of action of CpG-*Stat3*siRNA in experimental arthritis, initial experiments tested the ability of this therapy to reduce disease activity *in vivo*. Briefly, CpG-*Stat3*siRNA (0.125 nmol/ $\mu$ L) was administered at arthritis onset by intra-articular injection, to C57BL/6 wild-type (WT) mice primed for AIA (see **Chapter 2, Section 2.3.2.1**). At day-3 and day-10 post-arthritis induction, knee joints were recovered, processed and histologically assessed as previously outlined in **Section 2.4**. Here, treatment with CpG-*Stat3*siRNA showed an improvement in disease severity at day-3 and day-10 post-arthritis induction (**Figure 3.3A, 3.4A**). CpG-*Stat3*siRNA intervention resulted in an improvement in synovial infiltrate and pannus formation (**Figure 3.3B**), and an overall reduction in joint histopathology or arthritic index (AI) at day-3 of disease (**Figure 3.3C**) as compared to the non-treatment group of WT mice with AIA.

A similar improvement in disease severity was also observed in synovial tissues for mice with established arthritis (day-10 post-AIA) (**Figure 3.4B**). Here, CpG-*Stat3*siRNA therapy also resulted in a statistically significant reduction in cartilage and bone erosion, compared to control mice (**Figure 3.4A**). Thus, CpG-*Stat3*siRNA treatment improves arthritis severity in experimental models of inflammatory arthritis – reducing synovial pannus and hyperplasia, inflammatory infiltration and joint erosion.

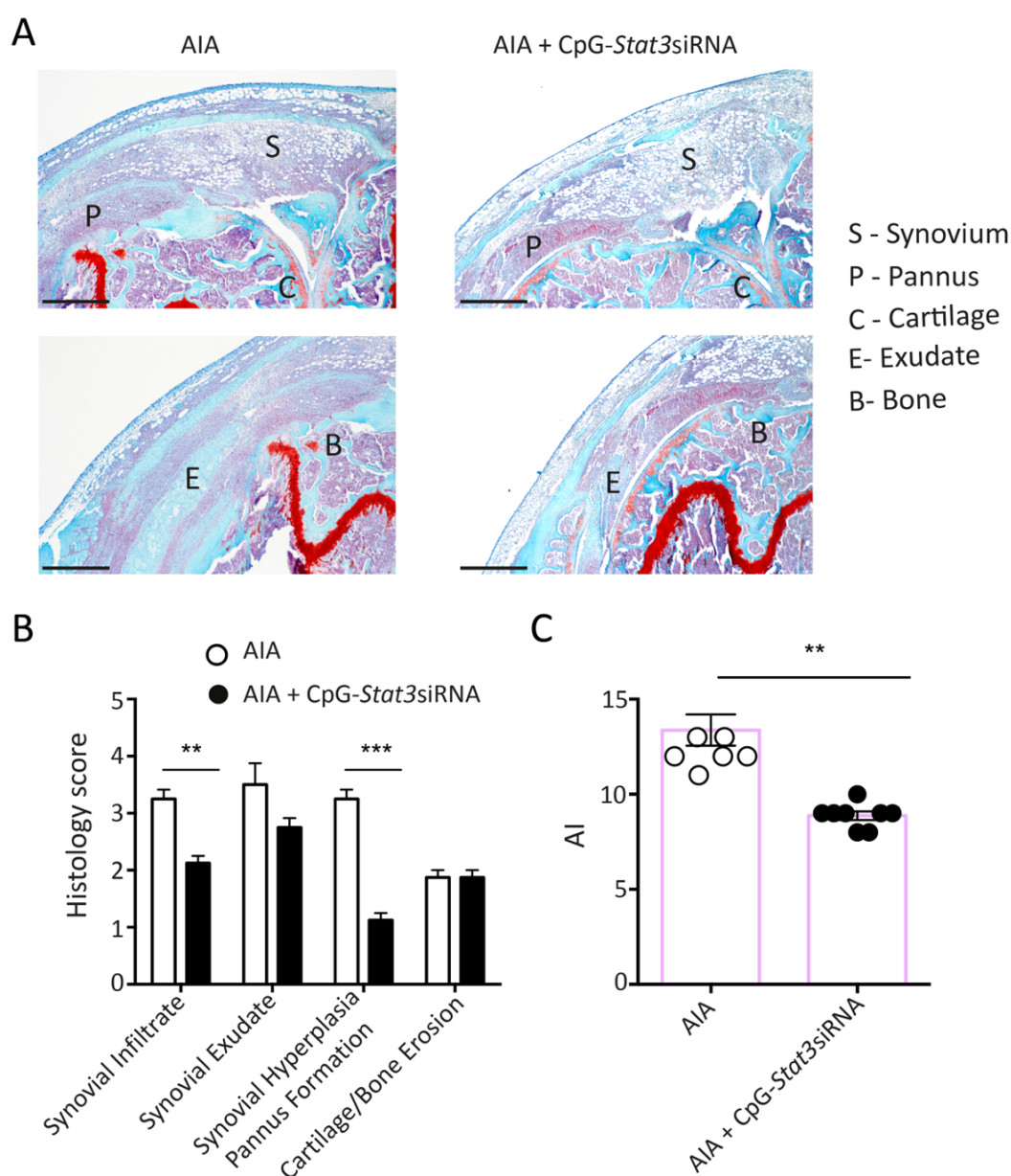


**Figure 3.3 CpG-Stat3siRNA reduces the inflammatory component in early arthritis.**

**(A)** Representative images of haematoxylin, fast green and safranin O staining of WT mouse knee joints at day-3 post-arthritis induction without any treatment (left) and treated with CpG-Stat3siRNA (right). **(B)** Histopathology scoring of AIA compared to AIA treated with CpG-Stat3siRNA in WT mice, showing synovial infiltrate, exudate, hyperplasia/pannus formation and cartilage/bone erosion at day-3 post-arthritis induction ( $n = 6-8$  mice/group). Shapiro-Wilk normality test and a two-way ANOVA, multiple comparisons. **(C)** The aggregate score for all parameters in B is presented as an arthritic index (AI) for both untreated and treated conditions ( $n = 6-8$  mice/group). Graphs indicate mean  $\pm$  SEM. \*\*,  $p < 0.01$ ; \*\*\*,  $p < 0.001$ . Shapiro-Wilk normality test and an unpaired t-test were used. Data were pulled from two independent experiments. Scale bars: (A) 500  $\mu$ m.



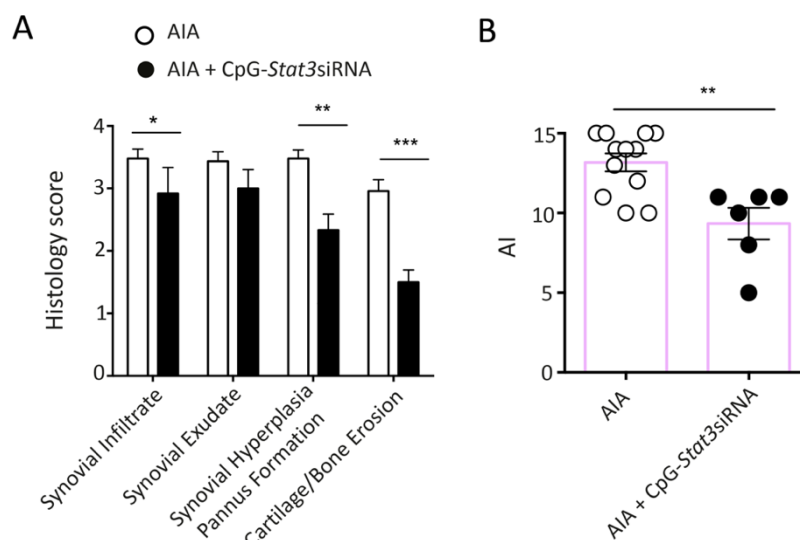


**Figure 3.4 CpG-Stat3siRNA decreases synovial infiltrate, pannus formation and cartilage/bone erosion in established arthritis.**

**(A)** Histopathology scoring of AIA compared to AIA treated with CpG-Stat3siRNA in WT mice, showing synovial infiltrate, exudate, hyperplasia/pannus formation and cartilage/bone erosion at day-10 post arthritis induction (n = 6-12 mice/group). Shapiro-Wilk normality test and a two-way ANOVA, multiple comparisons. **(B)** The aggregate score for all parameters in A is presented as an arthritic index (AI) for both untreated and treated conditions (n = 6-12 mice/group). Graphs indicate mean ± SEM. \*,  $p < 0.05$ ; \*\*,  $p < 0.01$ ; \*\*\*,  $p < 0.001$ . Shapiro-Wilk normality test and an unpaired t-test were used. Data were pulled from two independent experiments.

To verify these findings, and to further evaluate the efficacy of CpG-Stat3siRNA therapy, WT mice with AIA were treated with either CpG-Stat3siRNA, a single-stranded control variant of CpG-Stat3siRNA, a non-hybridised double-stranded CpG-Stat3siRNA (see CpG-Stat3siRNA oligonucleotide hybridisation, outlined in **Section 2.3.2.2**), or an unconjugated CpG oligonucleotide alone (CpG Class B ODN 1668, InvivoGen). Synovial joints were recovered at day-3 of AIA, processed, and tissues histologically assessed for inflammatory infiltrate, exudate, pannus formation, and cartilage and bone erosion (**Figure 3.5A**). Synovial infiltration in CpG-Stat3siRNA treated joints was considerably reduced compared to all the controls (**Figure 3.5A, B**), as well as pannus formation and cartilage and bone erosion (**Figure 3.5B**). However, CpG-Stat3siRNA treatment did not induce significant changes in the overall joint histopathology, as shown by AI (**Figure 3.5C**). Taken together, these data are consistent with prior studies on tumour microenvironment, where unconjugated Stat3 siRNA bound but did not activate TLR9<sup>351</sup> and therefore failed to internalise and silence Stat3, resulting in minor antitumour effects compared to CpG-Stat3siRNA<sup>316</sup>. Here, control conjugates had no effect in AIA compared to CpG-Stat3siRNA.



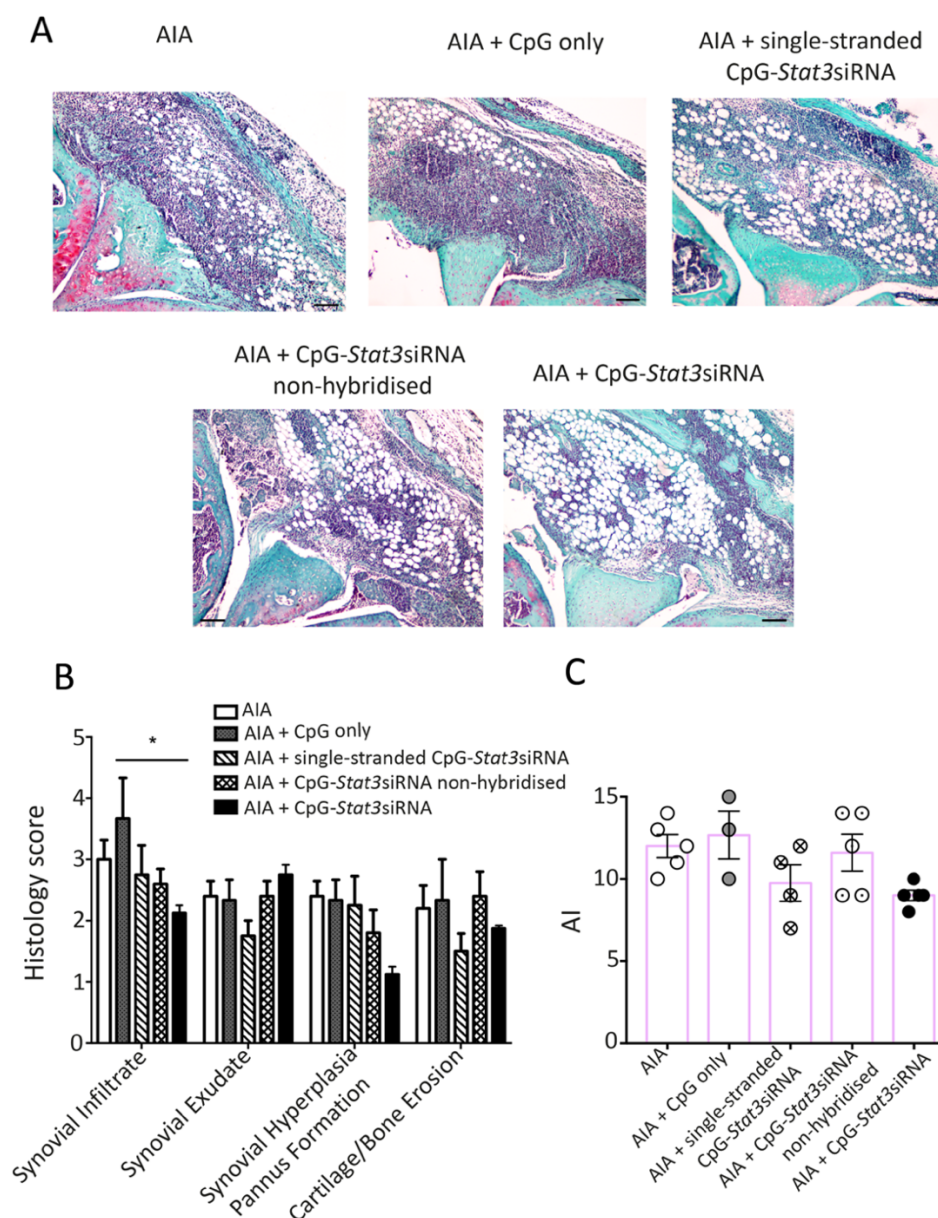


**Figure 3.5 CpG-Stat3siRNA conjugate is the only compound having a significant impact on AIA outcome compared to controls.**

AIA WT mice were treated with CpG-Stat3siRNA and different combinations of conjugates as negative controls: uncoupled CpG oligonucleotide, a single strand of CpG-Stat3siRNA and non-hybridised CpG-Stat3siRNA conjugate. Histopathology was assessed at day-3 post arthritis induction. **(A)** Representative images of haematoxylin, fast green and safranin O staining of WT mouse knee joints at day-3 post-AIA induction. **(B)** Scoring of AIA treated with CpG-Stat3siRNA and the different controls in WT mice, showing synovial infiltrate, exudate, hyperplasia/pannus formation and cartilage/bone erosion at day-3 post-arthritis induction ( $n = 3-5$  mice/group). **(C)** The aggregate score for all parameters in B is presented as an arthritic index (AI) for all conditions ( $n = 3-5$ /group). Graphs indicate mean  $\pm$  SD. \*,  $p < 0.05$ . Shapiro-Wilk normality test and a one-way ANOVA, Turkey's multiple comparisons. Scale bars: (A) 300  $\mu$ m. Graphs present data from one independent experiment.

### 3.3.3 Experimental validation of Stat3 silencing by CpG-Stat3siRNA in AIA

To test whether CpG-Stat3siRNA treatment reduced Stat3 expression within the inflamed joint of mice with AIA, quantitative PCR of Stat3 was performed on total mRNA derived from the inflamed synovium of WT and *Il27ra*<sup>-/-</sup> mice. Treatment with CpG-Stat3siRNA lowered expression of *Stat3* in both genotypes, and this reduction in expression of *Stat3* was observed at both day-3 and day-10 of AIA (**Figure 3.6**). Collectively, these data suggest that CpG-Stat3siRNA therapy successfully reduces synovial STAT3 activity in experimental arthritis in both WT and *Il27ra*<sup>-/-</sup> mice.

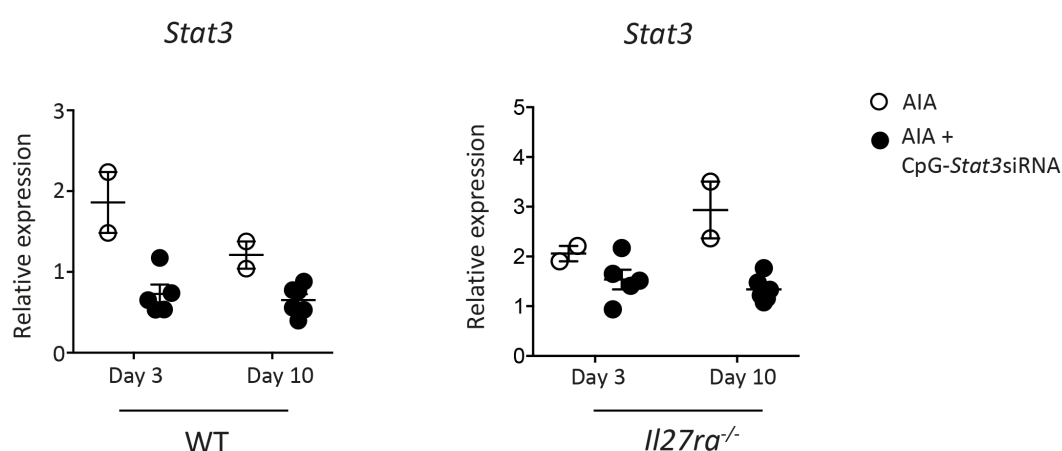


**Figure 3.6** CpG-Stat3siRNA inhibits the transcriptional activity of *Stat3*.

Synovial joint tissue from the knee joints of WT and *Il27ra*<sup>-/-</sup> mice with AIA and AIA treated with CpG-Stat3siRNA were collected at day-3 and day-10 and mRNA expression of *Stat3* gene was assessed by qPCR (n=2-6 mice/group). Graphs indicate mean ± SD. Graphs present data from one independent experiment.

### 3.3.4 CpG-Stat3siRNA treatment alters the transcriptomic profile of the inflamed synovium

RNA-seq of synovial tissue obtained from WT and *Il27ra*<sup>-/-</sup> mice with AIA treated with CpG-*Stat3*siRNA was performed to identify transcriptomic changes as a response to therapy. This provides an excellent opportunity to investigate the mode of action of CpG-*Stat3*siRNA therapy in experimental arthritis. Bulk RNA-seq datasets derived from the inflamed synovium from WT and *Il27ra*<sup>-/-</sup> mice with AIA (without any treatment), and naïve mice (without AIA) (provided as a courtesy of Dr David Hill, Cardiff University) were combined with correspondingly derived datasets from CpG-*Stat3*siRNA-treated WT and *Il27ra*<sup>-/-</sup> mice with AIA (see **Section 2.9.5**). Hierarchical cluster analysis of these transcriptomic data using one minus Pearson correlation revealed that synovial tissue mainly segregated into two distinct groups: (i) genes expressed in the non-inflamed naïve synovium across all genotypes, and (ii) genes expressed as a response to arthritis induction. Further analysis of this group of genes identified distinct sets of transcriptional gene signatures that are affected by CpG-*Stat3*siRNA treatment (**Figure 3.7**). Here, alterations in gene regulation were visible at both day 3 and day 10, and evident in WT and *Il27ra*<sup>-/-</sup> mice with AIA. Thus, CpG-*Stat3*siRNA treatment alters the transcriptional output of genes regulated as a response to arthritis onset

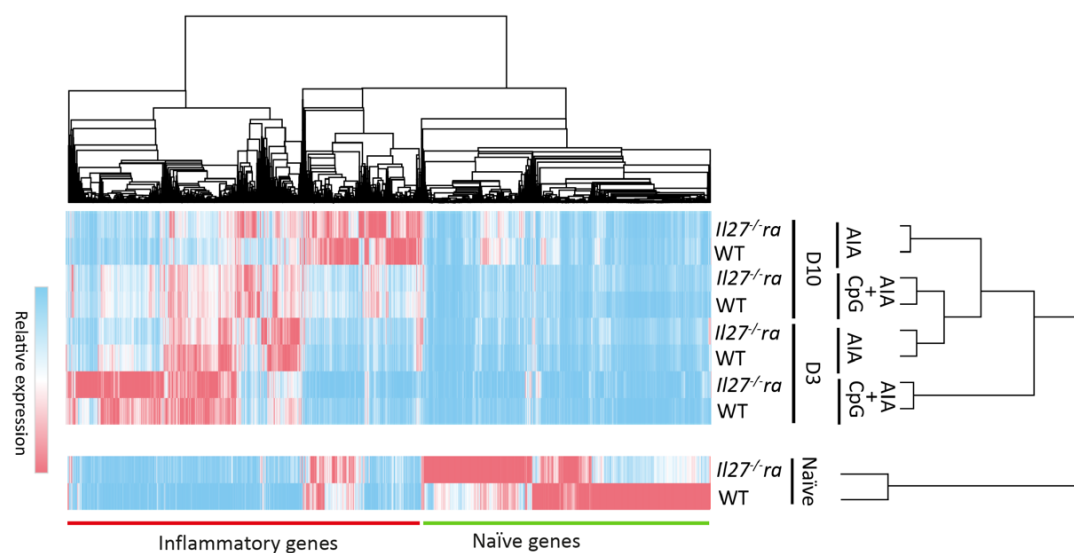
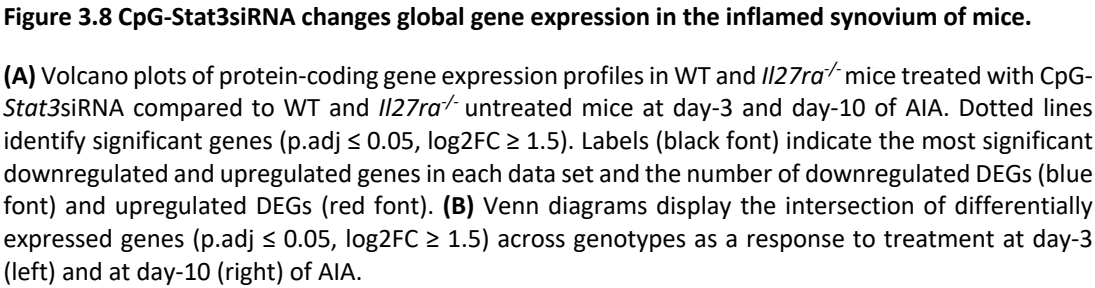


**Figure 3.7** The inflamed synovium of CpG-*Stat3*siRNA-treated mice show different transcriptional profiles compared to AIA untreated and healthy mice.

(Legend continues on the following page)

Relative expression of differentially expressed protein-coding genes in WT and *Il27ra*<sup>-/-</sup> mice in naïve synovium, at day-3 and day-10 post-induction of arthritis, untreated and treated with CpG-*Stat3*siRNA (p.adj ≤ 0.05, log2FC ≥ 1.5). Colour bars highlight clusters of genes expressed during inflammatory arthritis (red) and those expressed in naïve synovium (green). Heatmap was clustered using one minus Pearson correlation. Note that CpG refers to CpG-*Stat3*siRNA.

To identify how CpG-Stat3siRNA affected the synovial expression of genes induced as a response to arthritis onset, analysis compiled a list of all differential regulated genes as a response to therapy. Changes in gene regulation were based on the fold change expression and statistical evaluation of the response. Data were visualised using a volcano plot (see **Material and Methods, Section 2.9.7**). These studies identified a substantial number of transcripts that were affected by the drug: In WT mice, 306 and 1258 genes were differentially expressed upon treatment with CpG-Stat3siRNA at day-3 and day-10 of AIA, respectively. Of these, approximately half of the differentially expressed genes (DEGs) were upregulated in both time points by at least threefold (170 genes at day-3 and 676 genes at day-10) (**Figure 3.8A**). In *Il27ra*<sup>-/-</sup> mice, the number of DEGs at day-3 (1806) was much greater than at day-10 of AIA (617), and the vast majority were downregulated (1057 genes at day-3 and 442 at day-10). Consistent with the literature, CpG-Stat3siRNA therapy altered the expression of several genes involved in innate immunity and interferon-induced genes (e.g., *Il1a*, *Il12b*, *Gbp5*, *Gbp2*, *Gbp8*), while others were linked with immune-modulation or tissue homeostasis (e.g., *Il10*, *Slc8a2*)<sup>352</sup>. Moreover, among the downregulated genes, were transcripts encoding collagen and cellular adhesion-associated genes (e.g., *Col9a1*, *Col9a3*, *Col2a1*, *Clec3a*) (**Figure 3.8A**), which may contribute to the progression of RA, inducing proinflammatory cytokines<sup>353</sup>. To complement the above observations, analysis further examined the overlap of DEGs between genotypes at early and established disease. A substantial overlap between WT and *Il27ra*<sup>-/-</sup> data sets was found at both days-3 and -10 of AIA, with 248 genes differentially regulated by WT and *Il27ra*<sup>-/-</sup> treated mice at day-3 post-AIA, and 371 genes differentially regulated across the two genotypes at day-10 (**Figure 3.8B**).



### 3.3.5 Identification of CpG-*Stat3*siRNA-regulated genes during active synovitis

To examine how AIA onset altered the expression of genes linked with the development of synovitis in WT and *Il27ra*<sup>-/-</sup> mice, transcriptomic datasets from naïve non-challenged mice were subtracted from datasets obtained at day-3 and day-10 of arthritis induction (**Figure 3.9A**). This analysis ( $p_{\text{adj}} \leq 0.05$ ,  $\log_2\text{FC} \geq 1.5$ ) identified sets of arthritis-responsive genes at both day-3 (6071 for WT mice, 4155 for *Il27ra*<sup>-/-</sup> mice) and day-10 (4471 for WT mice, 3383 for *Il27ra*<sup>-/-</sup> mice) of AIA (**Figure 3.9A**). CpG-*Stat3*siRNA intervention substantially altered this profile of gene regulated and affected transcriptional outputs at both day 3 and day 10 of disease (**Figure 3.9B**). Here, changes to the number of regulated genes were more pronounced at day 3 for *Il27ra*<sup>-/-</sup> mice (altering the expression of a total of 1806 genes), and at day 10 for WT mice (where it influenced the expression of 1258 genes (**Figure 3.9B**)).

To investigate which of the CpG-*Stat3*siRNA-regulated genes were changed during AIA, genes differentially expressed in AIA (**Figure 3.9A**) were overlaid with CpG-*Stat3*siRNA-regulated genes (**Figure 3.9B**). At day-3, CpG-*Stat3*siRNA regulated 2.8% of the genes whose expression was changed in AIA inflamed synovium from WT mice, as opposed to the 19.8% of genes whose expression was changed in AIA inflamed synovium from *Il27ra*<sup>-/-</sup> mice (**Figure 3.9C**). In WT mice, as time post AIA increased, the proportion of CpG-*Stat3*siRNA-regulated genes increased, peaking at day-10, where CpG-*Stat3*siRNA was found to regulate 13.7% of the differentially expressed genes. Conversely, in *Il27ra*<sup>-/-</sup>, the proportion of CpG-*Stat3*siRNA-regulated genes decreased to 7.7% at day-10 post-AIA (**Figure 3.9C**). These results suggest a potentially major effect of CpG-*Stat3*siRNA treatment on established disease in WT mice, and on early disease in *Il27ra*<sup>-/-</sup> mice.

The expression of 18 genes was found to be regulated by CpG-*Stat3*siRNA treatment at all of the time points, and genotypes studied. The expression profile of these genes was also changed during AIA (**Figure 3.10A**). Genes responded to therapy with different dynamics; for example, *Tnn* and *Ccl17* were both highly downregulated in the presence of treatment, whereas *Serpib7* was strikingly upregulated in response to CpG-*Stat3*siRNA. *Tnn* has been reported to be a strong angiogenesis stimulator by elongation, migration and sprouting of endothelial cells in tumours<sup>354</sup>, while *Ccl17* plays important roles in T-cell development in the thymus as well as in trafficking and activation of mature cells. Additionally, *Serpib7*

possess protease inhibitory activity which is important in maintaining skin homeostasis<sup>355</sup>. IPA analysis revealed the top 5 upstream regulators for these 18 genes (IFNAR1, IL22, TLR9, TLR3 and CpG ODN 1668) (**Figure 3.10B**). The top 5 canonical pathways associated with these genes were granulocyte/agranulocyte adhesion and diapedesis, which are primary lines of host defence against infections, communication between innate and adaptive immune cells, cytokines mediating communication between immune cells and altered T-cell and B-cell signalling in RA (**Figure 3.10C**). Together, this data show that common CpG-*Stat3*siRNA regulated genes are associated with innate immunity and inflammation.

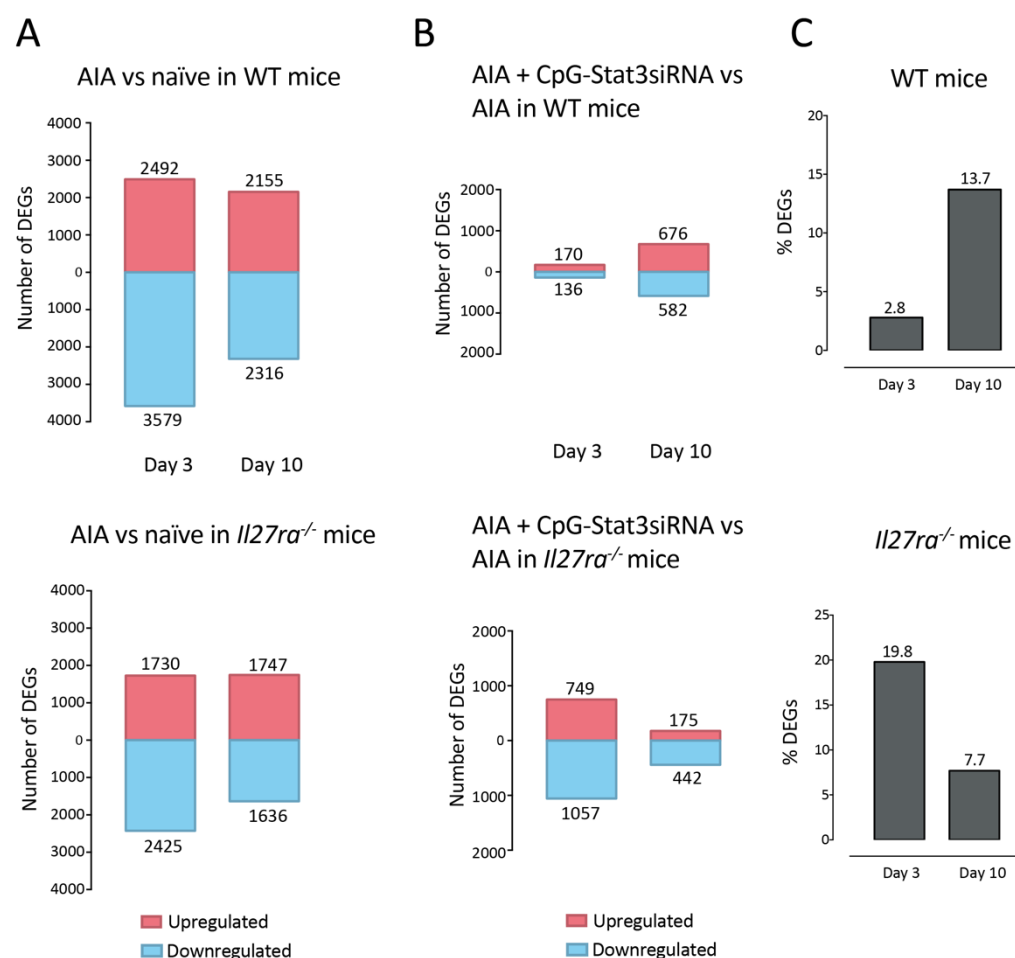


**Figure 3.9 Dynamics of CpG-*Stat3*siRNA-mediated gene expression.**

The number of differentially expressed protein-coding genes ( $p_{\text{adj}} \leq 0.05$ ,  $\log_2\text{FC} \geq 1.5$ ) during AIA (**A**) and CpG-*Stat3*siRNA-regulated genes ( $p_{\text{adj}} \leq 0.05$ ,  $\log_2\text{FC} \geq 1.5$ ) (**B**) in WT and *Il27ra*<sup>-/-</sup> mice at days-3 and day-10 of AIA. The height of a bar shows the total number of genes detected at a particular point. Upregulated genes are shown in red, and downregulated genes are shown in blue. (**C**) Proportion of genes regulated by CpG-*Stat3*siRNA therapy from all the differentially expressed genes at each time point during AIA.



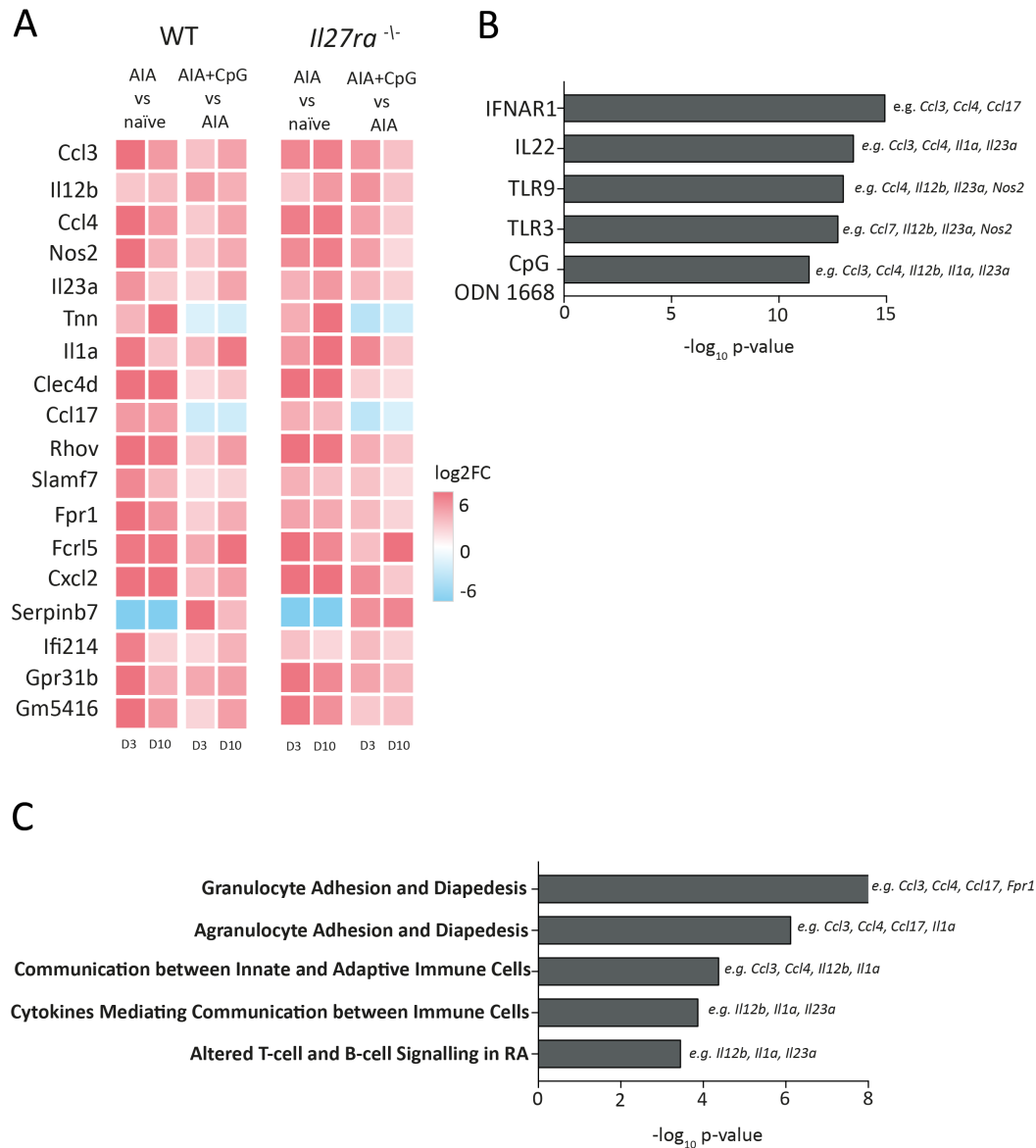


**Figure 3.10 Common CpG-Stat3siRNA-induced genes across AIA timeline and genotypes are associated with innate and adaptive immune responses and inflammation.**

(A) Heatmap of protein-coding differentially expressed genes ( $p_{\text{adj}} \leq 0.05$ ,  $\log_2\text{FC} \geq 1.5$ ) as a response to CpG-Stat3siRNA throughout the time course of AIA (day 3 and day 10) and genotypes (WT and *Il27ra*<sup>-/-</sup>). (B) The top 5 upstream regulators associated with the differentially expressed genes from panel A as predicted by IPA. (C) The top 5 canonical pathways associated with the differentially expressed genes from panel A as determined by IPA.



To further study genes that were changing in response to therapy, a more focused candidate DEG set was generated, by visualising changes in gene expression among treated and untreated mice and taking the RNA-seq data from naïve synovium into account. Here,  $\log_2FC$  values relative to baseline (naïve synovium) of mice with AIA were plotted against those with AIA treated with CpG-*Stat3*siRNA (**Figure 3.11**). Genes that remain unaltered in response to treatment are shown in yellow and can be clearly distinguished from genes that are regulated by AIA (blue) and CpG-*Stat3*siRNA therapy (green). This visualisation method enabled us to easily identify genes whose expression was modified by therapy and to focus the analysis on identifying changes specific to the treatment. Thus, genes of interest (blue, green and red) were selected for further analysis.

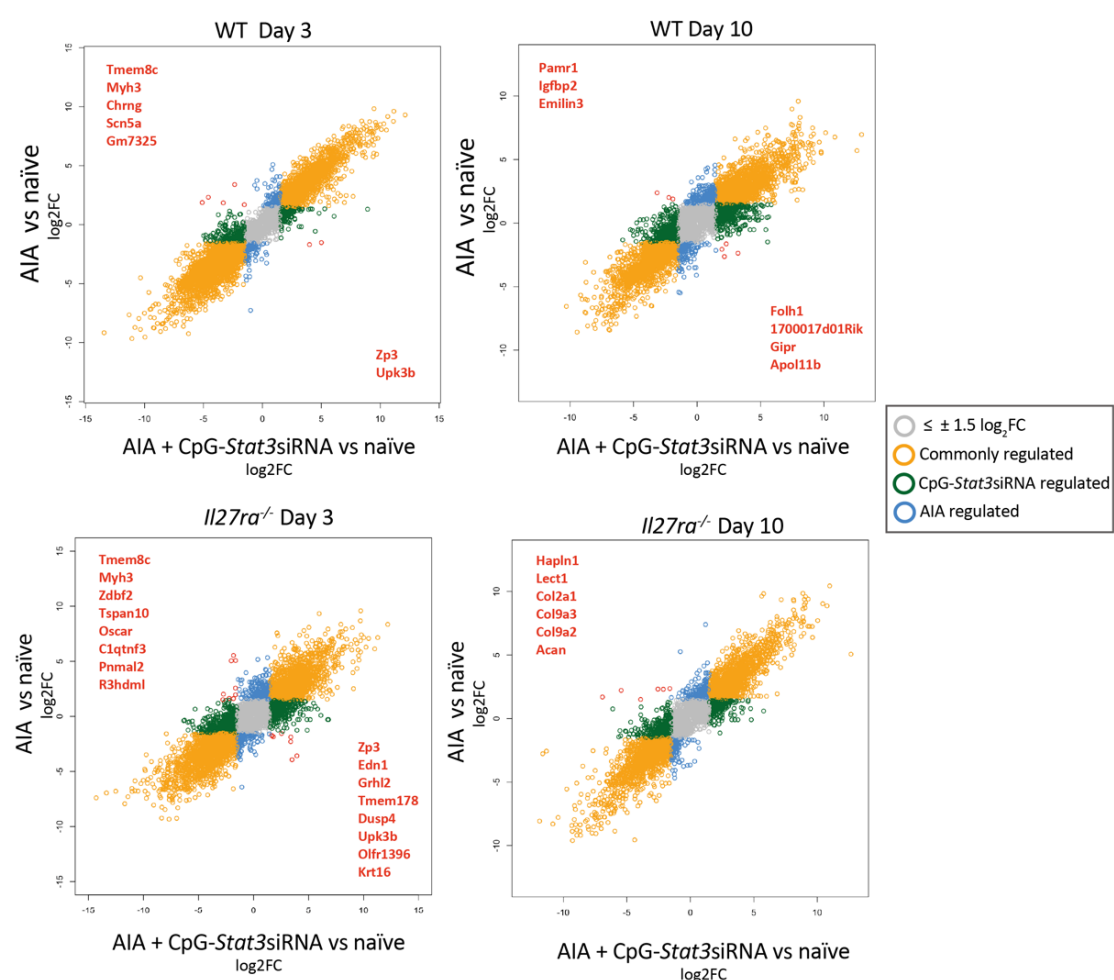


**Figure 3.11 Identification of genes that change in response to CpG-*Stat3*siRNA therapy.**

(Legend continues on the following page)

Scatterplots showing correlation between log2FC gene expression values. The X-axis corresponds to AIA + CpG-Stat3siRNA, the Y-axis to AIA. All genes were significant in at least one condition ( $p_{\text{adj}} \leq 0.05$ ). Dots correspond to DEGs: genes regulated by CpG-Stat3siRNA (green), AIA (blue), both (yellow), or neither (grey) are identified and colour-coded. Specific data point referring to genes of interest have been highlighted in red and annotated accordingly. These genes are either changing from upregulated in AIA to down-regulated in AIA + CpG-Stat3siRNA, or from down-regulated in AIA to upregulated in AIA + CpG-Stat3siRNA. There is a scatter plot for each of the timeline of AIA (Day3-right and Day10-left) and genotype (WT-at the top and Il27ra<sup>-/-</sup> at the bottom).

### 3.3.6 K-means clustering to identify temporal patterns of regulation

While the IPA analysis of RNA-seq datasets described in the previous sections provided some insight into the effects of CpG-Stat3siRNA treatment on AIA in WT and Il27ra<sup>-/-</sup> mice, the large number of DEGs observed made interpretation of the data very challenging. To resolve this, k-means clustering was used to identify groups of genes that displayed similar patterns of expression across the time course of AIA. To first gain insight into how genes behaved in disease, the optimal number of clusters was determined using statistical tests: the silhouette and Davies-Bouldin methods identified 2 or 5 gene clusters as optimal, whereas the gap statistic method identified 4 or 5 clusters as optimal (Section 2.9.7.7) (Figure 3.12).

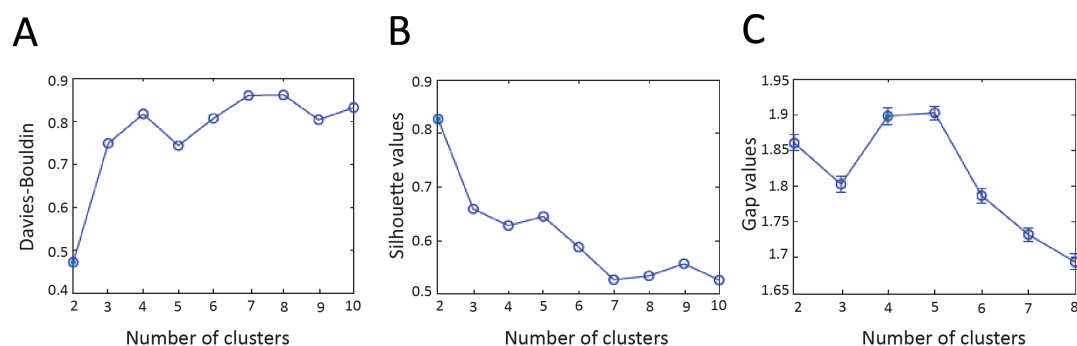


**Figure 3.12 Mathematical determination of the optimal number of clusters for the synovial transcriptome.**

The (A) Davies-Bouldin, (B) silhouette and (C) gap methods were used to determine the optimal number of clusters to use for K-means clustering of the synovial transcriptome during the time course of AIA. These statistical methods are described in more detail in Materials and methods (See Section 2.9.7.7).

Using these values as a guide, five gene clusters were selected. These broadly separated genes into three distinct patterns of genes regulation: (i) upregulated gene expression across the entire time course (clusters 2 and 5), (ii) downregulated over the time course (clusters 3 and 4), and (iii) genes that were selectively increased at day 10 (cluster 1). Corresponding patterns of gene regulation were also identified by k-means clustering in RNA-seq datasets from mice administered with CpG-*Stat3*siRNA (**Figure 3.13A, 3.14A**). Based on these analyses, clusters were statistically compared (Sign test and Wilcoxon signed-rank test) to match common patterns of regulation. This was conducted with datasets obtained from WT mice (**Table 3.1**), and *Il27ra*<sup>-/-</sup> mice (**Table 3.2**) with AIA.

AIA + CpG- <i>Stat3</i> siRNA											
	Cluster 1		Cluster 2		Cluster 3		Cluster 4		Cluster 5		
	Sign test	Wilcoxon signed-rank test	Sign test	Wilcoxon signed-rank test	Sign test	Wilcoxon signed-rank test	Sign test	Wilcoxon signed-rank test	Sign test	Wilcoxon signed-rank test	
Cluster 1	<b>4.9E-04</b>	<b>4.9E-04</b>	4.3E-01	8.2E-01	4.5E-03	1.5E-02	<b>3.4E-03</b>	<b>4.9E-04</b>	NaN	NaN	
Cluster 2	1.2E-01	1.9E-01	<b>1.6E-18</b>	<b>1.5E-22</b>	NaN	NaN	NaN	NaN	8.9E-03	3.4E-03	
AIA Cluster 3	NaN	NaN	NaN	NaN	<b>2.0E-12</b>	<b>3.8E-15</b>	4.1E-03	2.4E-04	NaN	NaN	
Cluster 4	8.2E-01	9.8E-01	NaN	NaN	3.9E-02	2.4E-03	<b>2.3E-24</b>	<b>1.1E-22</b>	NaN	NaN	
Cluster 5	<b>2.8E-09</b>	<b>7.3E-07</b>	<b>1.0E-08</b>	<b>2.6E-09</b>	NaN	NaN	NaN	NaN	<b>4.2E-15</b>	<b>1.9E-14</b>	

**Table 3.1 Sign test and Wilcoxon signed-rank test in clusters from WT genes.**

Clusters from WT AIA and WT AIA treated with CpG-*Stat3*siRNA-regulated genes were tested to assess whether the paired observations differ using the sign test and the Wilcoxon signed-rank test. The *p* value associated with each comparison is shown (significance level of 0.1%). Data outlined in red highlight clusters with the closest similarities. NaN stands for “not a number”, and it is shown when there were not any genes in common between the two clusters compared.

AIA + CpG-Stat3 siRNA										
	Cluster 1		Cluster 2		Cluster 3		Cluster 4		Cluster 5	
	Sign test	Wilcoxon signed-rank test	Sign test	Wilcoxon signed-rank test	Sign test	Wilcoxon signed-rank test	Sign test	Wilcoxon signed-rank test	Sign test	Wilcoxon signed-rank test
Cluster 1	<b>1.2E-88</b>	<b>1.5E-94</b>	6.5E-02	2.0E-02	1.1E-01	4.2E-01	<b>5.7E-38</b>	<b>1.1E-34</b>	2.2E-02	1.2E-03
Cluster 2	7.6E-02	9.9E-02	<b>2.9E-44</b>	<b>1.1E-41</b>	NaN	NaN	2.2E-02	2.2E-03	<b>2.0E-11</b>	<b>3.9E-08</b>
AIA Cluster 3	1.0E-01	6.2E-01	NaN	NaN	<b>2.8E-34</b>	<b>4.9E-33</b>	<b>9.1E-13</b>	<b>2.4E-08</b>	NaN	NaN
Cluster 4	2.1E-03	9.3E-03	NaN	NaN	3.1E-01	1.2E-02	<b>8.1E-130</b>	<b>6.0E-106</b>	NaN	NaN
Cluster 5	NaN	NaN	<b>2.4E-07</b>	<b>2.7E-05</b>	NaN	NaN	NaN	NaN	<b>6.7E-60</b>	<b>1.7E-56</b>

**Table 3.2 Sign test and Wilcoxon signed-rank test in clusters from *Il27ra*<sup>-/-</sup> genes.**

Clusters from *Il27ra*<sup>-/-</sup> AIA and *Il27ra*<sup>-/-</sup> AIA treated with CpG-Stat3siRNA-regulated genes were tested to assess whether the paired observations differ using the sign test and the Wilcoxon signed-rank test. The *p* value associated with each comparison is shown (significance level of 0.1%). Data outlined in red highlight clusters with the closest similarities. NaN stands for “not a number”, and it is shown when there were not any genes in common between the two clusters compared.

**Figure 3.13A** shows an overview of the 5 clusters of differentially expressed genes in WT AIA mice and WT AIA mice in response to treatment, relative to a healthy WT control joint previously described above. To identify specific groups of genes that changed pattern of temporal regulation as a response to CpG-Stat3siRNA therapy, we generated an alluvial diagram to observe the cluster interactions between conditions and make identification of major transitions between conditions easy. From this diagram, it can be seen that nearly all the genes in cluster 1 in AIA, changed to cluster 4 in response to treatment. Similarly, a large number of genes shifted from cluster 5 in AIA to cluster 1, and from cluster 2 in AIA to cluster 5, in response to treatment in WT synovium (**Figure 3.13B**).

A summary of the 5 clusters of differentially expressed genes obtained by k-means, in *Il27ra*<sup>-/-</sup> AIA mice and *Il27ra*<sup>-/-</sup> AIA in response to CpG-Stat3siRNA, relative to a healthy *Il27ra*<sup>-/-</sup> control joint, are displayed in **Figure 3.14A**. Alluvial diagram comparing different DEGs trajectories across clusters as a response to therapy showed that the vast majority of genes in cluster 1 in AIA moved to cluster 4 in the presence of therapy. Furthermore, a considerable number of genes in cluster 2 in AIA changed to cluster 5 (**Figure 3.14B**).

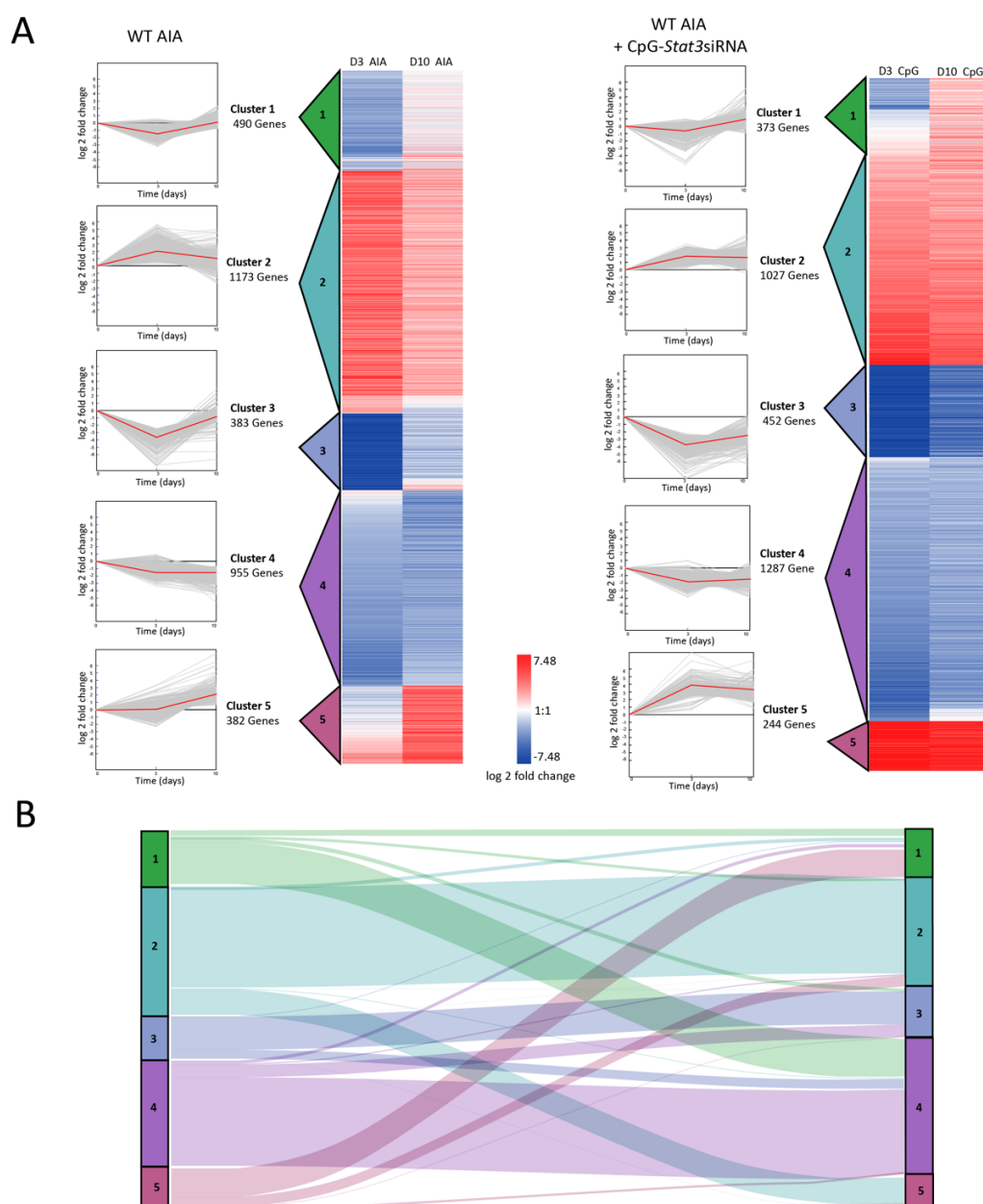


**Figure 3.13 K-means clustering analysis of the synovial transcriptome during the time course of AIA and as a response to CpG-Stat3siRNA in WT mice.**

**(A)** K-means clustering and corresponding heatmap of treatment-induced differentially expressed genes ( $p_{\text{adj}} \leq 0.05$ ,  $\log_2\text{FC} \geq 1.5$ ) in WT mice across the time course of AIA without treatment (left) and treated with CpG-Stat3siRNA (right), compared to a healthy control joint (baseline). Each cluster of genes has been given a specific colour and number. Clusters sharing similar patterns of temporal gene expression between untreated and treated mice (see **Table 3.1**) are labelled with the same number and colour. **(B)** Alluvial diagram showing the interactions between AIA and AIA + CpG-Stat3siRNA events within clusters (vertical bars, with cluster number) pairwise in each of the five patterns of gene expression. Note that CpG refers to CpG-Stat3siRNA. D3, Day-3 post-AIA; D10, Day-10 post-AIA.

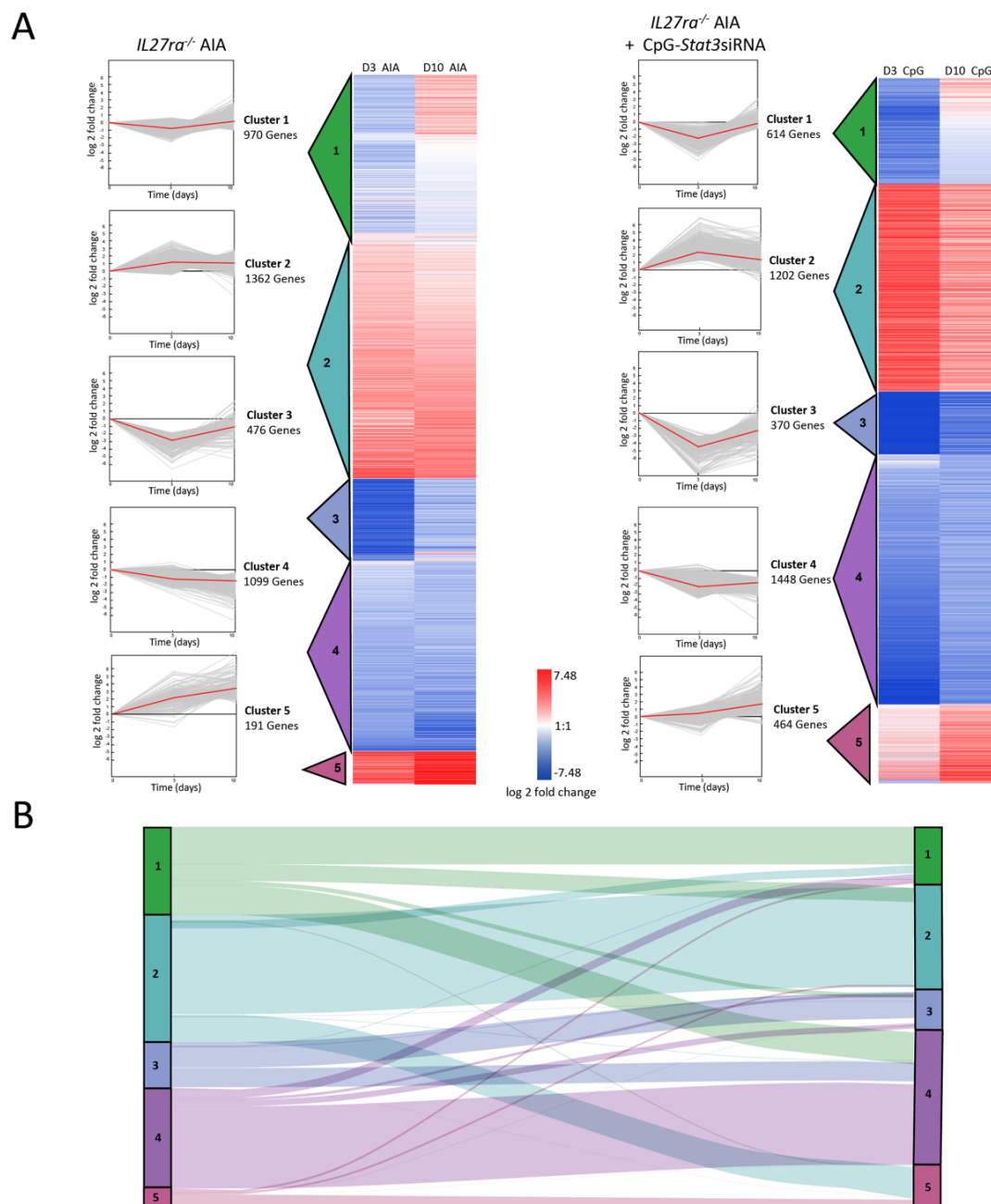


**Figure 3.14 K-means clustering analysis of the synovial transcriptome during the time course of AIA and as a response to CpG-Stat3siRNA in *IL27ra*<sup>-/-</sup> mice.**

**(A)** K-means clustering and corresponding heatmap of treatment-induced differentially expressed genes ( $p_{\text{adj}} \leq 0.05$ ,  $\log_2\text{FC} \geq 1.5$ ) in *IL27ra*<sup>-/-</sup> mice across the time course of AIA without treatment (left) and treated with CpG-Stat3siRNA (right), compared to a healthy control joint. Each cluster of genes has been given a specific colour and number. Clusters sharing similar patterns of temporal gene expression between untreated and treated mice (see **Table 3.2**) are labelled with the same number and colour. **(B)** Alluvial diagram showing the interactions between AIA and AIA + CpG-Stat3siRNA events within clusters (vertical bars, with cluster number) pairwise in each of the five patterns of gene expression. Note that CpG refers to CpG-Stat3siRNA. D3, Day-3 post-AIA; D10, Day-10 post-AIA.

Canonical pathways associated with each gene cluster in every condition were determined using IPA. Cluster 1 mainly comprised of genes associated with metabolic pathways such as protein kinase A signalling and cAMP-mediated signalling in WT mice with AIA. These pathways were downregulated in response to treatment across diffuse (WT mice) and lymphoid-rich synovitis (*Il27ra*<sup>-/-</sup> mice) (**Figure 3.15**). The most striking result to emerge from the data is that cluster 2 was highly enriched for genes involved in T-cell activation, differentiation and signalling, in WT mice during AIA when compared to those treated with CpG-*Stat3*siRNA. Cluster 3 transcripts were enriched for adrenomedullin signalling, regulation of the epithelial-mesenchymal transition and bone remodelling pathways. Cluster 4 comprised genes related to mitochondrial metabolism pathways in WT mice that were reduced in response to treatment. Interestingly, these pathways were highly upregulated in *Il27ra*<sup>-/-</sup> mice during AIA; however, their enrichment strongly decreased when these mice received treatment.

In the same manner, analysis next considered the most enriched diseases and functions linked to each gene cluster. Here, diseases and functions including leukopoiesis, proliferation of immune cells, cell movement and T-cell development, were selectively enriched in cluster 2. These diseases and function were reduced in the presence of CpG-*Stat3*siRNA, being particularly noticeable in WT mice (**Figure 3.16**). Clusters 1 and 5 comprised genes that were upregulated for abnormal morphology of bone functions in WT mice, while in *Il27ra*<sup>-/-</sup> mice, these functions were enriched in clusters 1 and 3. Thus, k-means clustering has allowed the identification of gene expression behaviours that change in response to CpG-*Stat3*siRNA during AIA, and these changes are predominantly associated with a downregulation of T-cell and mitochondrial metabolism pathways and bone and matrix remodelling pathways.

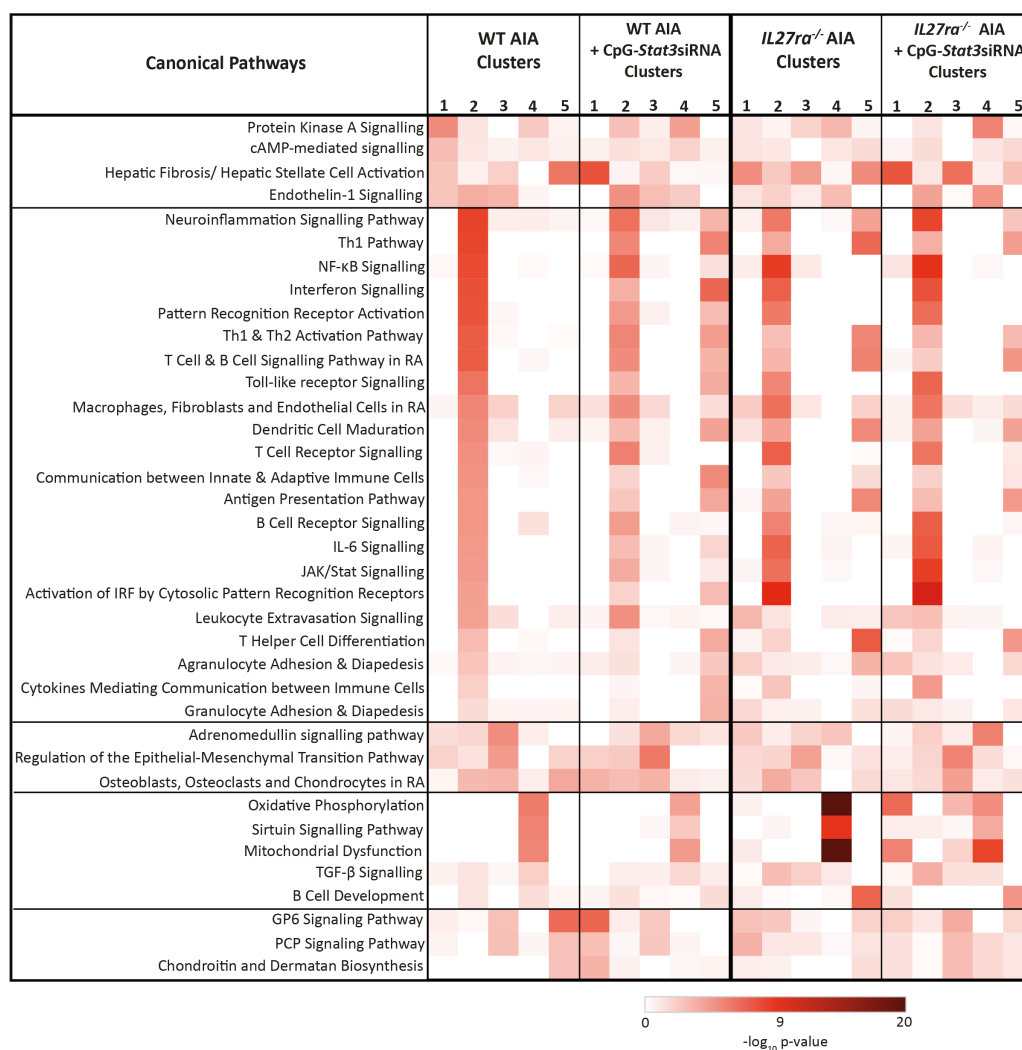


**Figure 3.15 Comparison of canonical pathways linked to individual clusters in WT and *IL27ra*<sup>-/-</sup> mice with AIA and the impact of CpG-Stat3siRNA intervention.**

The top canonical pathways, as determined by IPA, associated with each cluster of differentially expressed genes ( $p_{\text{adj}} \leq 0.05$ ,  $\log_2\text{FC} \geq 1.5$ ) in WT and *IL27ra*<sup>-/-</sup> mice across the time course of AIA without treatment and treated with CpG-Stat3siRNA, when compared to a healthy control joint.



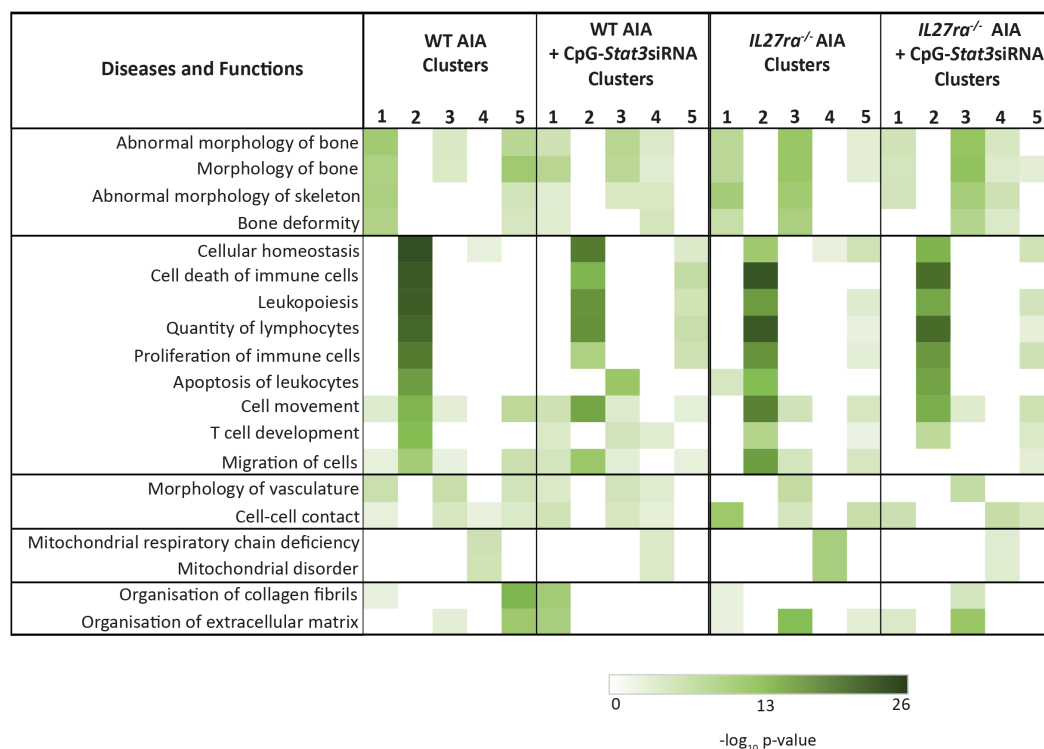


**Figure 3.16 Comparison of diseases and functions are linked to individual clusters in WT and *IL27ra*<sup>-/-</sup> mice and the impact CpG-Stat3siRNA intervention.**

The top diseases and functions, as determined by IPA, associated with each cluster of differentially expressed genes ( $p_{adj} \leq 0.05$ ,  $\log_2 FC \geq 1.5$ ) in WT and *IL27ra*<sup>-/-</sup> mice across the time course of AIA without treatment and treated with CpG-Stat3siRNA, when compared to a healthy control joint.

### 3.3.7 Canonical pathway analysis of genes that change in response to CpG-Stat3siRNA

Having established patterns of gene behaviour and their relationship between conditions (see Figures 13, 14), we next focused specifically on those genes that switched patterns of temporal expression as a response to CpG-Stat3siRNA. These groups of genes were visualised using alluvial diagrams (see Section 3.3.6), and IPA analysis was performed to identify the top 5 enriched canonical pathways in each group. In WT mice, 3 groups of genes were defined as changing their pattern of expression as a response to CpG-Stat3siRNA treatment. These genes were linked to processes associated with protein kinase A and interferon signalling, Th1 pathway, communication between innate and adaptive immune cells, and bone remodelling in RA, among others (Figure 3.17A). Corresponding analysis of data from *IL27ra*<sup>-/-</sup> mice with AIA identified 2 groups of genes that were altered by CpG-

*Stat3*siRNA. Here, IPA enrichment analysis revealed roles in RhoA signalling, macrophages, fibroblasts and endothelial cells in RA, and T-cell and B-cell signalling in RA (**Figure 3.17B**).

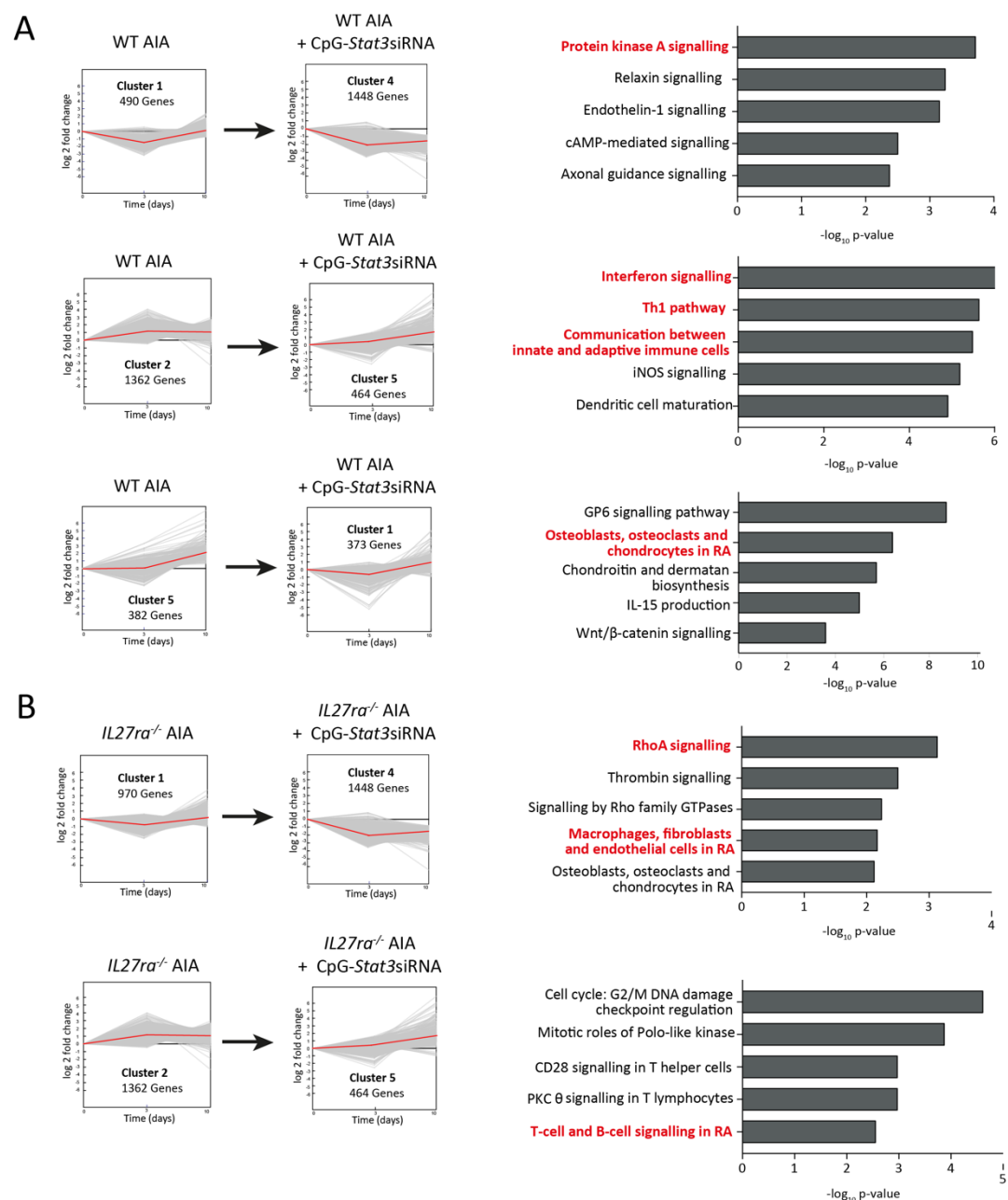


**Figure 3.17 Canonical pathway analysis of genes switching pattern of expression as a response to CpG-Stat3siRNA.**

Differentially expressed genes that change temporal pattern of expression in response to treatment and their top canonical pathways associated in AIA WT mice (**A**) and AIA *IL27ra*<sup>-/-</sup> mice (**B**) compared to a healthy control joint, extracted from previous alluvial diagrams (See figures 3.13 & 3.14). The most relevant pathways for my study are bolded in red.

### 3.3.8 STAT3 inhibition reduces cell metabolism and bone remodelling-associated pathways in diffuse-like synovitis

Cell metabolism has long been a major area of interest within the field of tumour biology, but in the past decade, its relevance has been progressively recognised in regulating inflammatory processes and immune cell function <sup>356</sup>. Recent studies have highlighted cell metabolism as a potential therapeutic target for the treatment of rheumatoid arthritis <sup>357–359</sup>. Protein kinase A (PKA) signalling was the top upregulated canonical pathway in DEGs changing from cluster 1 (AIA) to cluster 4 (AIA + treatment) in WT mice (See Figure 3.17A). The majority of these metabolism-related genes (e.g., *Akap5*, *Dusp18*, *Ptpu*, and *Myh10*) were downregulated in response to CpG-*Stat3*siRNA in WT mice at day 3 and day 10 of AIA (**Figure 3.18A**). These results seem to be consistent with research reporting that adenylate cyclase (AC)-protein kinase A (PKA) pathway may inhibit apoptosis of RA fibroblast-like synoviocytes (FLS), which contributes to synovial hyperplasia and therefore worsening disease severity <sup>360</sup>.

Pathway analysis of these group of DEGs shifting from cluster 5 (AIA) to cluster 1 (AIA + treatment) in WT mice revealed upregulation of osteoblasts, osteoclasts and chondrocytes responses in RA (See Figure 3.17A). During RA, the inflamed synovium invades cartilage and promotes bone destruction, which is facilitated by cytokines such as RANKL, essential for the differentiation of osteoclasts and subsequent resorption, or IL-17A which promotes expression of inflammatory cytokines and metalloproteinases that contribute to cartilage degradation <sup>118</sup>. The expression of these genes was also significantly suppressed in WT AIA mice treated with CpG-*Stat3*siRNA (**Figure 3.18B**). This difference in expression between treated and untreated mice was especially notable for *Bmp15*, *Nfatc4* and *Wnt10a*. Hence these data highlight a reduction in disease-related gene signature in WT AIA mice treated with CpG-*Stat3*siRNA.

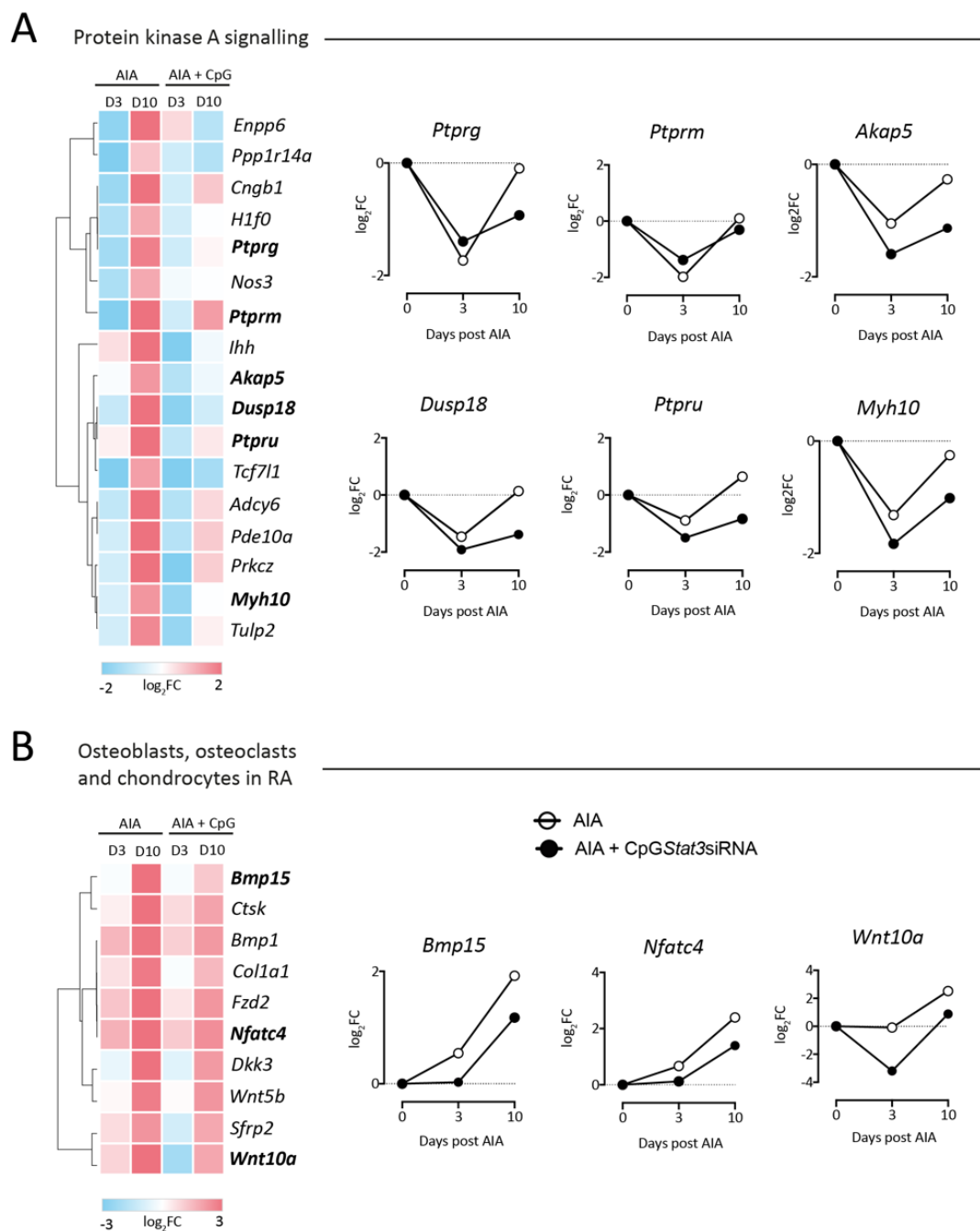


**Figure 3.18 Reduced expression of cell metabolism and bone and cartilage remodelling genes in WT mice treated with CpG-Stat3siRNA.**

**(A)** Heatmap of differentially expressed genes changing from cluster 1 in AIA to cluster 4 as a response to treatment and associated with protein kinase A, in WT mice. Selected genes are plotted for WT AIA mice with and without treatment when compared to a healthy WT control joint. **(B)** Heatmap of differentially expressed genes changing from cluster 5 in AIA to cluster 1 as a response to treatment and associated with bone and cartilage remodelling in RA, in WT mice. Selected genes are plotted for WT AIA mice with and without treatment when compared to a healthy WT control joint. Note that CpG refers to CpG-Stat3siRNA. D3, Day-3 post-AIA; D10, Day-10 post-AIA.

### 3.3.9 CpG-*Stat3*siRNA triggers interferon and Th1 pathways in diffuse-like synovitis

Analysis of transcriptomic data from inflamed synovium has so far shown that CpG-*Stat3*siRNA therapy reduced expression of genes associated with pathways that contribute to disease severity. However, it is important to note that TLR9 activation via unmethylated CpG also leads to the activation of NF- $\kappa$ B through IFN (transcription factor of the IRF family) and promotes Th1-dependent immunity<sup>316,361</sup>. Moreover, this TLR9/nuclear factor  $\kappa$ B (NF-  $\kappa$ B) signalling induces the expression of IL-6 and/or IL-10, which activates STAT3<sup>362</sup>. Indeed, interferon signalling, Th1 pathway and communication between innate and adaptive immune cells were enriched in DEGs relocating from cluster 2 (AIA) to cluster 5 (AIA + treatment) in WT mice (See Figure 3.17A). In accordance with the literature<sup>363</sup>, we observed upregulation of immune mediators, such as interferons and their targets (*Ifnb1*, *Irf1* and *Stat1*) (**Figure 3.19A**), Th1 pathway (*Cd247*, *Cd40* and *Socs1*) (**Figure 3.19B**), as well as proinflammatory cytokines (*Prf1*, *Mapk13* and *Il2*) (**Figure 3.19C**), which was more evident at day 10 of AIA. Prominently upregulated genes in response to treatment included *Cd247* (encoding for PD-L1), an essential regulator of T-cell activation that binds with the immune checkpoint inhibitor PD1 (programmed cell death protein) and whose expression in RA has been shown to be downregulated<sup>364</sup>. Interestingly, another upregulated gene, *Socs1*, has a profound role in T-cell homeostasis<sup>365</sup>.

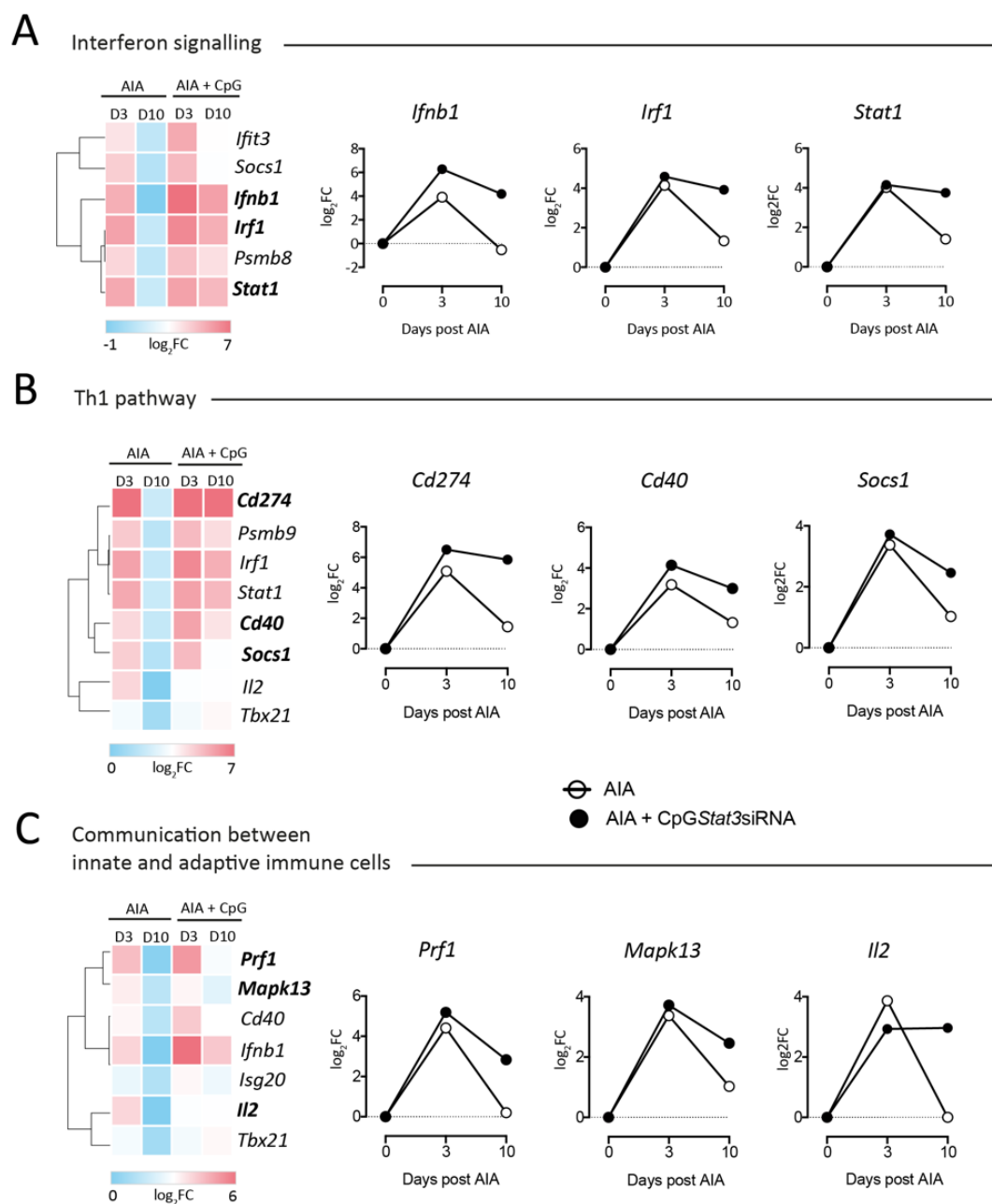


**Figure 3.19 STAT1-dependent Th1 and IFN pathways are increased in WT mice treated with CpG- Stat3siRNA.**

Heatmap of differentially expressed genes changing from cluster 2 in AIA to cluster 5 as a response to treatment and associated with **(A)** interferon signalling, **(B)** Th1 pathway and **(C)** communication between innate and adaptive immune cells, in WT mice. Selected genes from each section are plotted for WT AIA mice with and without treatment when compared to a healthy WT control joint. Note that CpG refers to CpG-Stat3siRNA. D3, Day-3 post-AIA; D10, Day-10 post-AIA.

### 3.3.10 CpG-*Stat3*siRNA treatment results in downregulation of RhoA signalling and genes involved in the pathogenesis of RA in lymphoid-rich synovitis

In *Il27ra*<sup>-/-</sup> mice, 2 main groups of DEGs changed patterns of temporal expression in response to CpG-*Stat3*siRNA treatment (See Figure 3.14B). Pathway analysis of genes linked to this group of DEGs showed an association with RhoA signalling, macrophages, fibroblasts and endothelial cells, and T-cell and B-cell signalling in RA, among others (see Figure 3.17B). Previous studies have revealed that RhoA signalling contributes to the abnormal migration and invasion of fibroblast-like synoviocytes (FLSs) in RA <sup>366</sup>. Overall, there was a prominent downregulation of these genes when compared to treated mice, at day 3 and day 10 of AIA (**Figure 3.20A**). For example, genes such as *Rtkn*, known to regulate the NF-κB pathway, playing a role in the pathogenesis of RA <sup>367</sup> or *Lpar3*, which promotes the production of inflammatory cytokines such as IL-6 <sup>368</sup>, and its blockade has been reported to reduce symptoms of RA in an animal model <sup>369</sup>. Expression of key components of Wnt signalling cascade in macrophages, including *Lrp5*, *Fzd6* and *Wnt6*, was reduced (**Figure 3.20B**). Recently, the Wnt signalling pathways have emerged as critical in the regulation of osteoblast function, being implicated in bone loss in RA <sup>370</sup>, and *Lrp5* has been associated with bone damage and radiographic progression in RA patients <sup>371</sup>.

Finally, genes associated with T-cell and B-cell signalling in RA followed a similar response pattern. Downregulated genes in response to CpG-*Stat3*siRNA included *Card11*, an activator of NF-κB and Th17 cell response, whose inhibition in inflammatory arthritis has shown to have a therapeutic effect <sup>372</sup>. Interestingly another downregulated gene, *Camk4*, has recently been implicated in Th17 cell-mediated tissue damage in inflammatory diseases <sup>373</sup> (**Figure 3.20C**). Taken together, these results suggest that treatment with CpG-*Stat3*siRNA in *Il27ra*<sup>-/-</sup> AIA mice effectively reduced expression of genes that contribute to the pathogenesis of inflammatory arthritis.

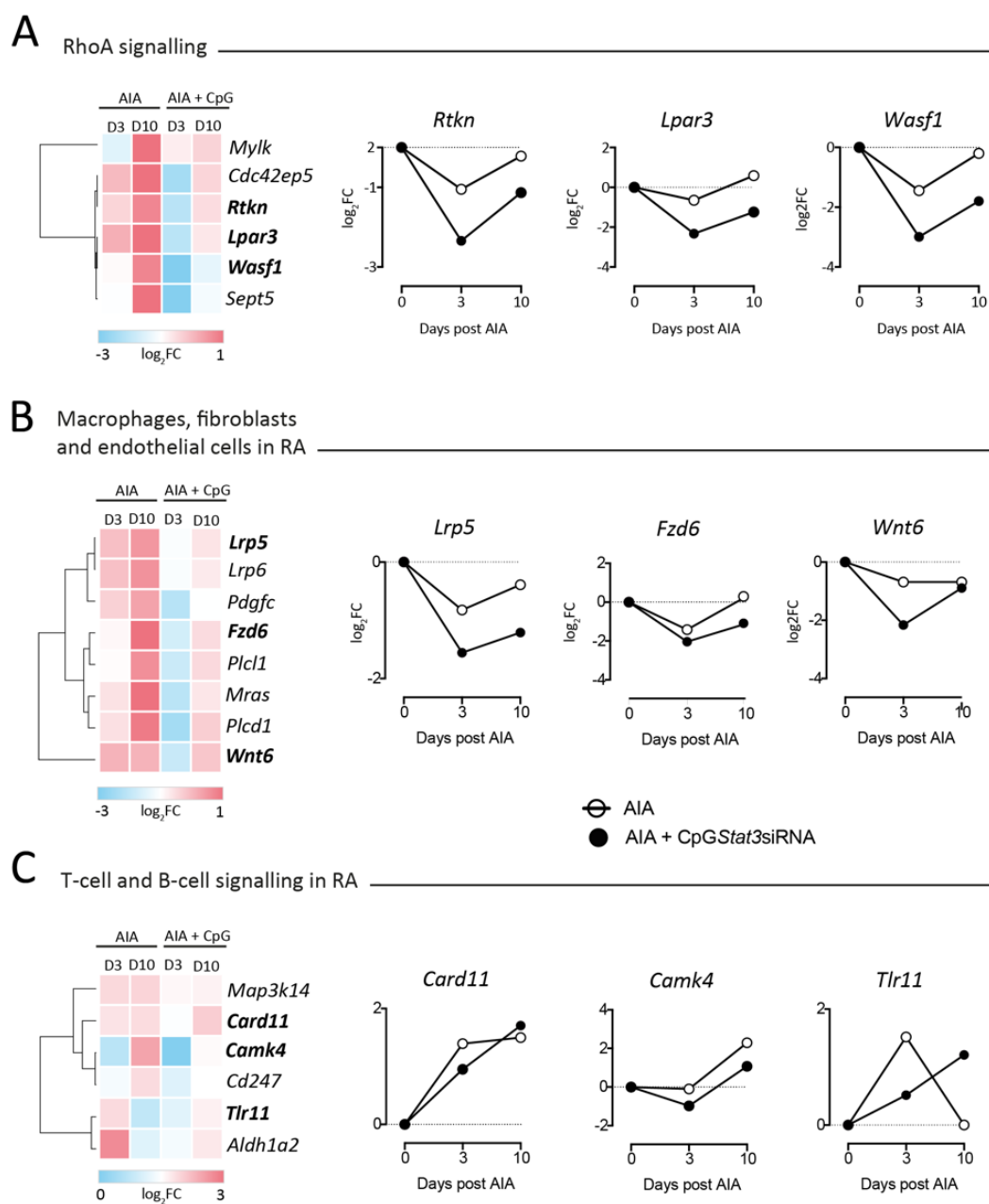


**Figure 3.20** CpG-*Stat3*siRNA inhibits expression of RhoA signalling and immune cell genes involved in RA in *Il27ra*<sup>-/-</sup> mice.

(A, B) Heatmaps of genes that comprise differentially regulated canonical pathways from genes changing from cluster 1 in AIA to cluster 4 as a response to treatment in *Il27ra*<sup>-/-</sup> mice. Selected genes are plotted for *Il27ra*<sup>-/-</sup> AIA mice with and without treatment when compared to a healthy *Il27ra*<sup>-/-</sup> control joint. (C) Heatmap of differentially expressed genes changing from cluster 2 in AIA to cluster 5 as a response to treatment and associated with T-cell and B-cell signalling in RA, in *Il27ra*<sup>-/-</sup> mice. Selected genes are plotted for WT AIA mice with and without treatment when compared to a healthy *Il27ra*<sup>-/-</sup> control joint. Note that CpG refers to CpG-*Stat3*siRNA. D3, Day-3 post-AIA; D10, Day-10 post-AIA.



### 3.3.11 CpG-*Stat3*siRNA alters the STAT1/STAT3 balance in inflammatory arthritis

The results so far obtained in this Chapter confirm the therapeutic effects of STAT3 inhibition by CpG-*Stat3*siRNA in experimental arthritis. Here, analysis confirmed the downregulation of several known STAT3 gene targets involved in matrix remodelling (e.g., *Col1a1*, *Col1a2*, *Col5a1*), connective tissue and inflammatory response-related disorders (e.g., *Ilh*, *Ldhd*, *Nes*) and cell migration and proliferation (e.g. *Cdh2*, *Snai2*) (**Figure 3.21**). Importantly, studies in cancer cells show that genetic ablation of STAT3 activities promotes an increase in STAT1 mediated responses<sup>186,189,374,375</sup>. Since synovial STAT1 responses in inflammatory arthritis often promote protective or anti-inflammatory outcomes, experiments next considered the relationship between STAT1 and STAT3 activities in AIA as a response to CpG-*Stat3*siRNA treatment. As predicted, the expression of STAT1-regulated genes as determined by IPA (e.g., *Psme2b*, *Ido1*, *Gzma*), was further enhanced when STAT3-induced genes were downregulated in response to CpG-*Stat3*siRNA in WT AIA mice (**Figure 3.21B**). Moreover, these genes were associated with cellular function, maintenance and development.

Having identified genes regulated by STAT3 and STAT1 in WT mice, transcriptomic analysis next focused on DEGs in *Il27ra*<sup>-/-</sup> mice. As shown in **Figure 3.22A**, many of the STAT3-regulated genes identified as expressed within the inflamed joint of *Il27ra*<sup>-/-</sup> mice were associated with activities relevant to the control of cell migration and proliferation, cell death and survival, cell cycle progression and fibrosis. Genes linked with these activities included STAT3 targets such as *Mras*, *Synpo* and *Notch3*, *Hoxa10*, *Cyp26a1* and *Twist1*, *Foxm*, *Klk1* and *Nr4a2*, respectively, and their expression was found to be decreased in response to therapy. Results obtained when the expression of STAT1-regulated genes was assessed in *Il27ra*<sup>-/-</sup> mice showed, however, that while *Phactr1* was upregulated, *Pdgfc* and *Slc2a2* expression was reduced in response to therapy (**Figure 3.22B**). Nevertheless, these results suggested that CpG-*Stat3*siRNA may alter the balance between STAT3 and STAT1 in our model of inflammatory arthritis, leading to a global alteration in cytokine response.

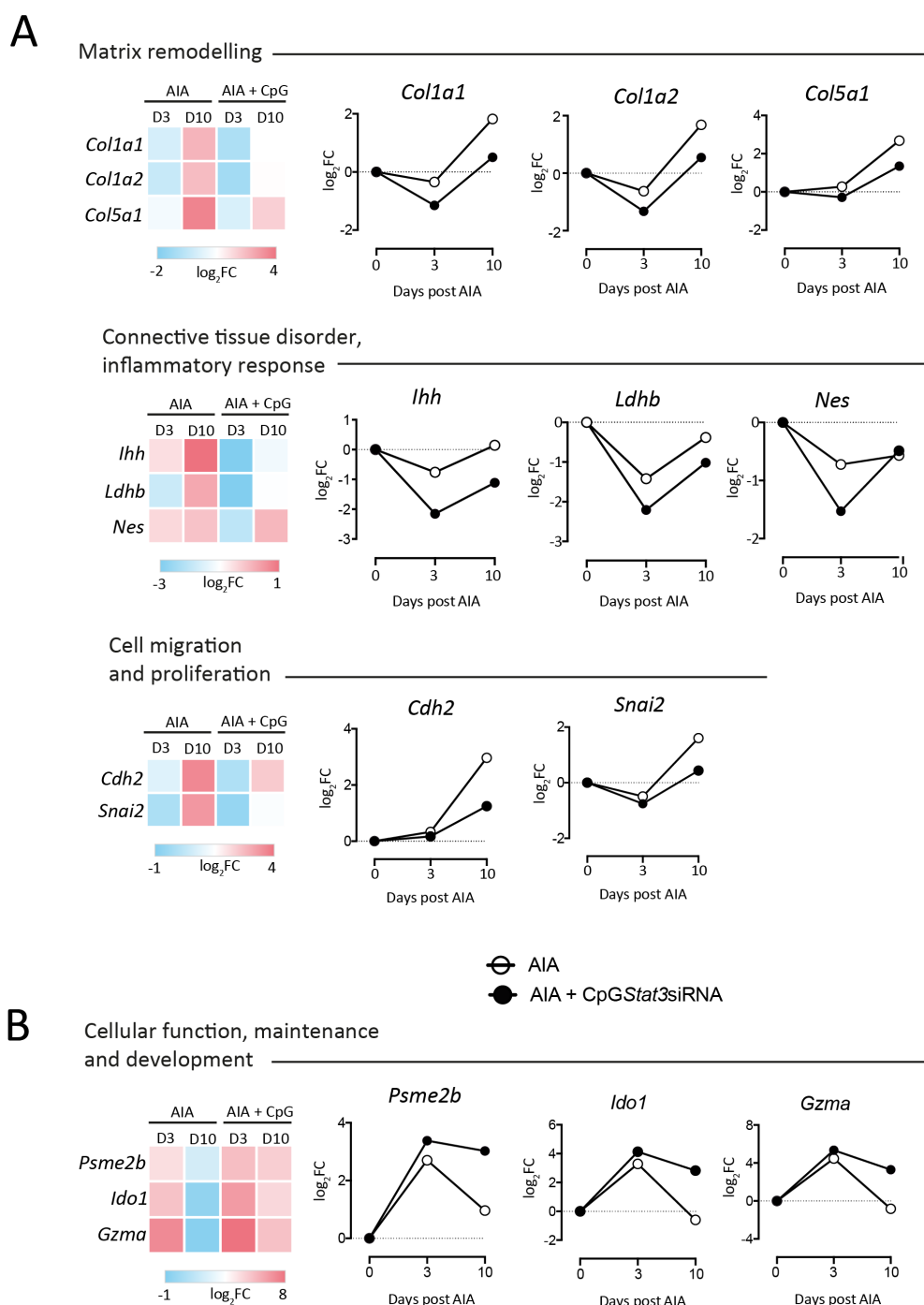


**Figure 3.21** STAT3-regulated gene expression decreases, while STAT1-associated gene expression is upregulated in WT mice in response to treatment.

(A) STAT3-regulated and (B) STAT1-regulated genes as determined by IPA in WT mice were extracted from DEGs that changed pattern of expression in response to CpG-Stat3siRNA. Heatmaps and plots of genes show gene expression relative to a healthy WT control joint at the same point expressed in  $\log_2FC$ . Note that CpG refers to CpG-Stat3siRNA. D3, Day-3 post-AIA; D10, Day-10 post-AIA.

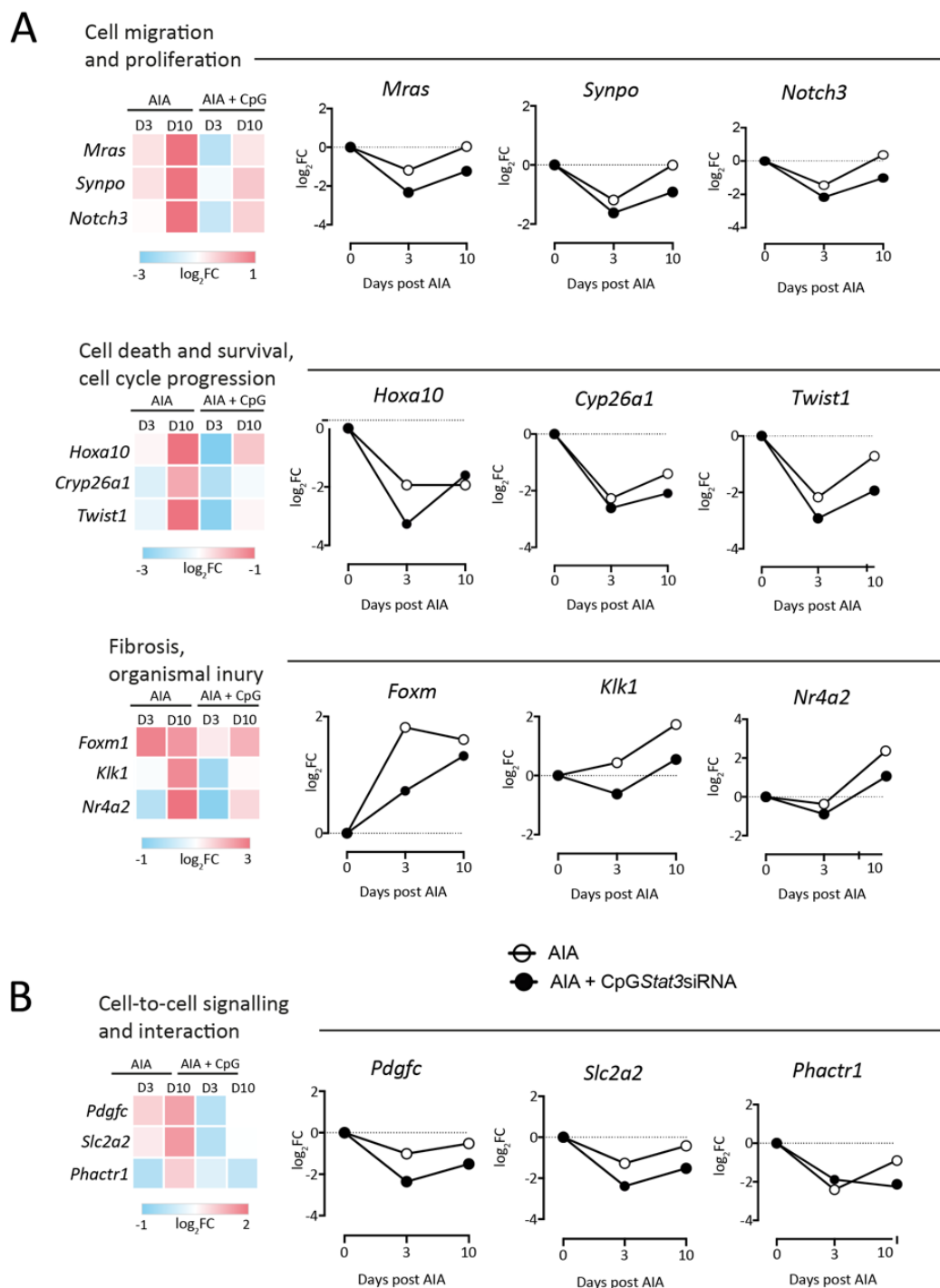


**Figure 3.22** STAT3-regulated gene expression decreases, while STAT1-associated gene expression is upregulated in *Il27ra*<sup>-/-</sup> mice, in response to treatment.

(A) STAT3-regulated and (B) STAT1-regulated genes as determined by IPA in *Il27ra*<sup>-/-</sup> mice were extracted from DEGs that changed pattern of expression in response to CpG-Stat3siRNA. Heatmaps and plots of genes show gene expression relative to a healthy *Il27ra*<sup>-/-</sup> control joint at the same point expressed in log<sub>2</sub>FC. Note that CpG refers to CpG-Stat3siRNA. D3, Day-3 post-AIA; D10, Day-10 post-AIA.

### 3.3.12 Synovial ectopic lymphoid-like structures are reduced by CpG-*Stat3*siRNA therapy

The impact of CpG-*Stat3*siRNA on STAT1 and STAT3 target genes was striking given the role these transcription factors play in their development, maintenance and activities associated with ectopic lymphoid-like structures (ELS) in autoimmunity, cancer and infection <sup>104,204</sup>. Hence, I next assessed the impact of CpG-*Stat3*siRNA treatment on the pattern of synovitis. As previously described <sup>104</sup>, AIA onset in *Il27ra*<sup>-/-</sup> mice resulted in a severe form of synovitis with evidence of ectopic lymphoid-like structures (discussed in more detail in **Chapter 1, Section 1.2.5**). Here, ELS were predominantly identified as dense accumulations of CD3<sup>+</sup> T- cells- rich accumulations within the joints of *Il27ra*<sup>-/-</sup> mice that display exacerbated disease (**Figure 3.23A**). This exacerbated synovitis has been linked with heightened STAT3 activity, development of ELS and the presence of Th17 cells in previous studies <sup>209</sup>. Synovial tissue from day-10 AIA-challenged *Il27ra*<sup>-/-</sup> mice treated with CpG-*Stat3*siRNA showed significantly fewer lymphoid aggregates and smaller in size when compared to untreated mice (**Figure 3.23B**). However, at the group size investigated this decrease in the size of these aggregates was not significant but provided rationale for a more comprehensive analysis of how the treatment affects ELS formation in *Il27ra*<sup>-/-</sup> mice *in vivo*.

To further explore CpG-*Stat3*siRNA effects on ELS, genes commonly associated with ectopic lymphoid-like structures were identified within previously selected DEGs that were switching pattern of expression in response to therapy. Most of the identified genes were strongly downregulated by CpG-*Stat3*siRNA when compared to untreated mice (**Figure 3.24**). For example, homeostatic chemokine receptors such as *Cxcl13* and *Ccl19*, involved in the activity or spatial organisation of lymphoid aggregates <sup>155</sup>, and *Vegf*, which supports cell recruitment and promotes the formation of high endothelial venules (HEVs) in ELS <sup>376,377</sup>. Similarly, other genes that were downregulated were associated with migration of cells (e.g., *Msln*, *Cd5l*, *Erdr1*) and cell adhesion (*Matn3*, *Cdh3*). Thus, CpG-*Stat3*siRNA treatment reduces the expression of genes associated with the development, maintenance and spatial organisation of ELS.

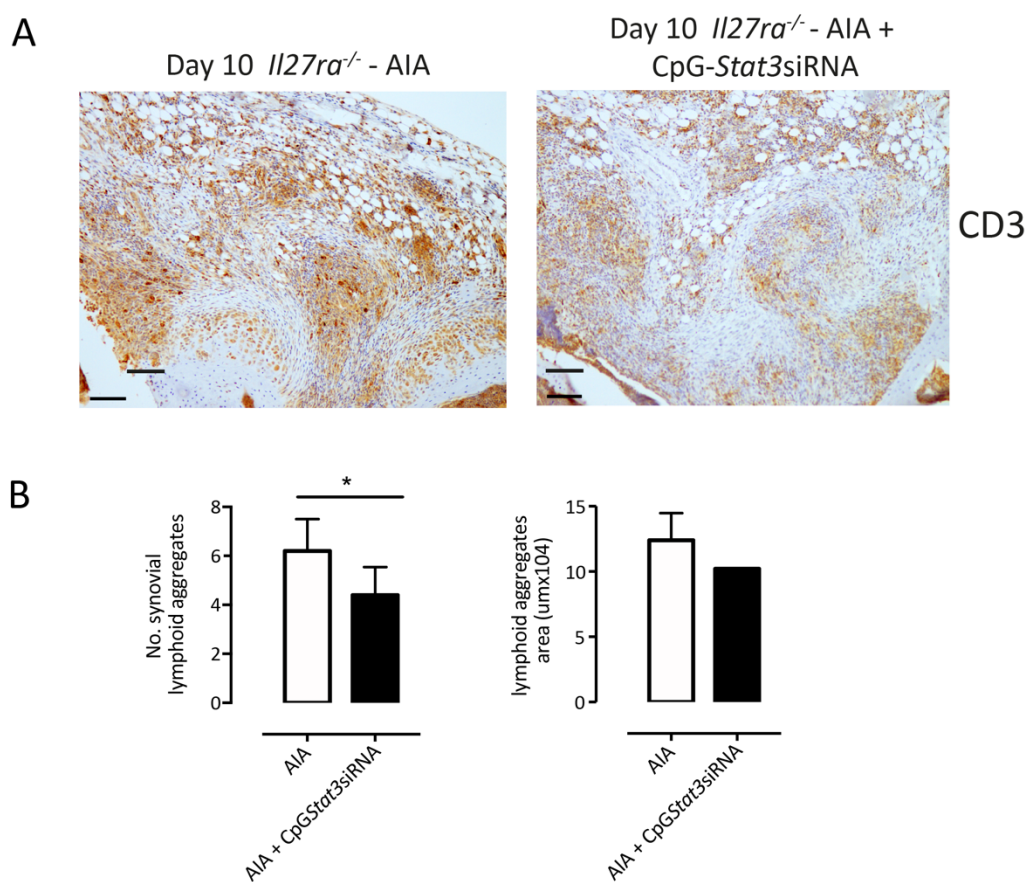
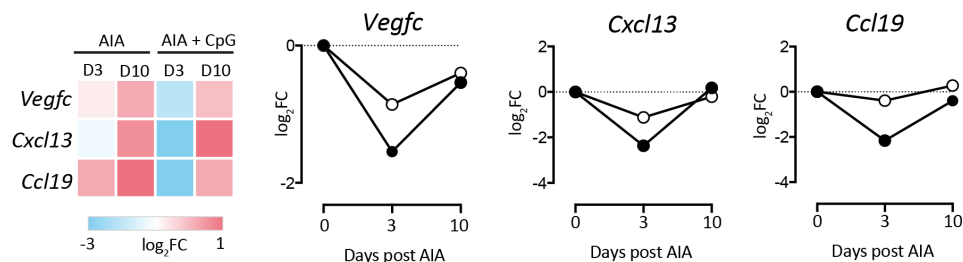


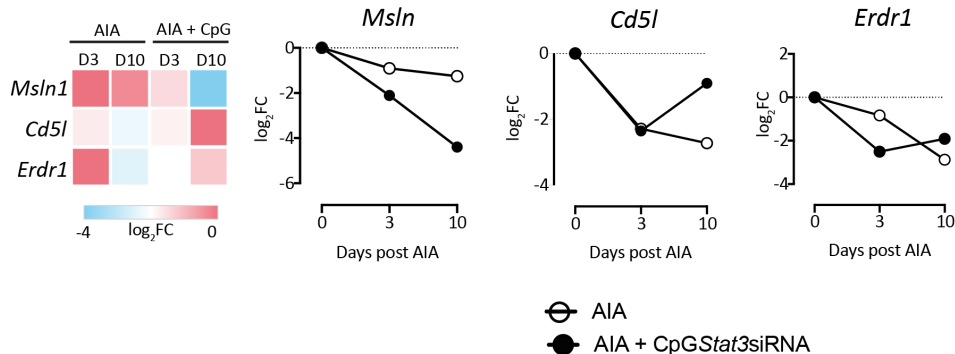
**Figure 3.23 CpG-*Stat3*siRNA treated mice show fewer ectopic lymphoid-like structures.**

**(A)** Representative IHC of CD3 in sections at day-3 and day-10 of AIA in WT and *Il27ra*<sup>-/-</sup> mice with AIA and AIA treated with CpG-*Stat3*siRNA. **(B)** The number (left) and area (right) of lymphoid aggregates were quantified in para-sagittal synovial sections ( $n = 5-10$  mice/group). Graphs indicate mean  $\pm$  SEM. \*,  $p < 0.05$  (A) 300  $\mu\text{m}$ . Data were pulled from two independent experiments.

### Immune cell trafficking, cellular infiltration by lymphocytes



### Cellular movement and migration of cells



### Cell-to-cell signalling and adhesion of connective tissue cells

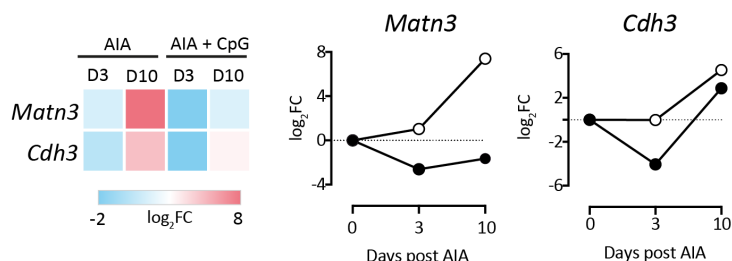


**Figure 3.24** ELS-associated genes are downregulated in the presence of CpG-Stat3siRNA.

ELS-associated genes, as determined by IPA in mice, were extracted from DEGs that changed pattern of expression in response to CpG-Stat3siRNA. Heatmaps and plots of genes show gene expression relative to a healthy WT control joint at the same point expressed in log<sub>2</sub>FC. Note that CpG refers to CpG-Stat3siRNA. D3, Day-3 post-AIA; D10, Day-10 post-AIA.

### 3.4 Discussion

In models of chronic disease, STAT3 signalling exacerbates pathology and its activities often correlate with poor prognosis or increased disease severity<sup>198,378</sup>. While an attractive target for inflammatory arthritis<sup>204,379</sup>, direct pharmacological inhibition of STAT3 has proven difficult, and despite many attempts, there are still no Food and Drug Administration (FDA)-approved small-molecule inhibitors that block STAT3s<sup>305</sup>. However, alternative strategies such as oligonucleotide-based STAT3 inhibitors, and new methods for targeted oligonucleotide delivery are in development, especially for cancer therapy<sup>316,341,363,380,381</sup>. The principle underlying the delivery of therapeutic oligonucleotides, such as STAT3 siRNA, specifically to TLR9<sup>+</sup> immune cells, has, therefore, application outside of cancer treatment and potential in autoimmune disease.

In this Chapter, I present proof-of-concept studies using a novel anti-cancer strategy based on an engineered modality that links *Stat3*siRNA to a synthetic oligonucleotide agonist of endosomal TLR9 (CpG-*Stat3*siRNA)<sup>316</sup>. Here, I showed that treatment improved arthritis severity in WT and *Il27ra*<sup>-/-</sup> mice with AIA – reducing synovial pannus and hyperplasia, inflammatory infiltration and joint erosion. Using computational analysis of whole tissue RNA-seq datasets, I explored holistic gene changes in synovial tissue at day-3 and day-10 post-arthritis induction as a response to CpG-*Stat3*siRNA, to evaluate transcriptional events controlled by STAT1 and STAT3 and identify signatures controlled by STAT1/STAT3 cross-regulation. Moreover, I determined that CpG-*Stat3*siRNA altered this STAT1/STAT3 balance and reduced the incidence of ELS and associated genes in lymphoid-rich-like synovitis in mice.

Although TLR9 is expressed in different types of mouse DCs, its expression is more selective in humans. However, consistent with the known expression of TLR9 in synovial cells during inflammatory arthritis<sup>104,155</sup>, immunohistochemical analysis demonstrated the presence of TLR9<sup>+</sup> cells in the inflamed synovium of both WT and *Il27ra*<sup>-/-</sup> mice with AIA. Interestingly, while CD3 expression correlated with disease severity, which reflects the degree of T-cell infiltration into the joint, there were no differences observed in TLR9 staining between diffuse and lymphoid-rich synovitis. Thus, TLR9 expression reflected the composition of the infiltrate across the inflamed synovium of WT and *Il27ra*<sup>-/-</sup> mice. However, a more thorough characterisation of TLR9<sup>+</sup>-secreting cells within the inflamed synovium is needed, perhaps

using flow cytometry on joint-infiltrating cells in order to identify the target cell population. CpG-*Stat3*siRNA injected locally, was effective in blocking STAT3 in experimental arthritis, as confirmed by qPCR analysis of *Stat3* mRNA from the inflamed synovium. As expected, this blockade had a therapeutic effect against established AIA, improving disease outcome when histological assessments were performed in the mice joints. These results support evidence from clinical observations and human and murine studies that show treatment with CpG-*Stat3*siRNA inhibits the transcriptional activity of *Stat3*, resulting in tumour cell apoptosis and tumour growth inhibition<sup>316,341,363,380,381</sup>. In accordance with the present results, where only double-stranded hybridised CpG-*Stat3*siRNA had a significant impact on inflammatory arthritis outcome compared to injecting controls alone – uncoupled CpG oligonucleotide, a single strand of CpG-*Stat3*siRNA and non-hybridised CpG-*Stat3*siRNA conjugate, previous studies have demonstrated that cellular uptake of both CpG oligonucleotide and the CpG-siRNA constructs can occur in the absence of TLR9. However, TLR9, at least in mouse cells, is essential for CpG-siRNA-mediated gene silencing<sup>316,346,363</sup>.

Differences in the transcriptomic output between untreated and treated WT and *Il27ra*<sup>-/-</sup> mice were observed throughout the time course of AIA. However, while CpG-*Stat3*siRNA agent targets TLR9-expressing cells, the outcomes differed between WT and *Il27ra*<sup>-/-</sup> mice. Expression of over 1,000 and 2,000 genes was found to be influenced by CpG-*Stat3*siRNA during the time course of AIA in WT and *Il27ra*<sup>-/-</sup> mice, respectively. This may mean that differences in disease heterogeneity can be potentially bypassed using this treatment, which could be very interesting since RA patients with ‘follicular’ pathology tend to show poor response to biologic therapy (e.g., the anti-TNF overall failure observed in ELS synovitis)<sup>149,153,382</sup>. Hierarchical clustering revealed the most apparent changes to be observed at day-10 in WT mice, and at day-3 in *Il27ra*<sup>-/-</sup> mice, perhaps due to a temporal inhibition of STAT3 as we observed in the previously mentioned qPCR analysis. In addition, we observed an overall decrease in ELS-associated pathways in lymphoid-rich aggregates upon treatment.

Previous studies by other groups demonstrated that CpG oligonucleotides are efficiently internalised by various APCs, such as DCs, macrophages and B-cells, and that their binding to TLR9 can initiate a cascade of innate and adaptive immune responses, such as activating NF-κB signalling, to effectively shift the tumour microenvironment from pro-oncogenic to antitumour in cancer<sup>316,343</sup>. Here, common CpG-*Stat3*siRNA-induced genes in AIA-challenged



WT and *Il27ra*<sup>-/-</sup> mice were linked with innate and adaptive immune responses in inflammation. While STAT3 has shown to be critical for regulating the synovial infiltrate in inflammatory arthritis, and thus, selective inhibition of *Stat3* may provide an effective intervention strategy for blocking IL-6-driven proarthritic activities <sup>204</sup>, activating NF-κB signalling or pathways downstream of TLR activation might have disadvantageous consequences in the context of autoimmunity. For example, the identification of IFN-related genes as risk loci in RA, or the development of RA in patients treated with IFN-α <sup>383</sup>. Type I IFN signature, induced by endosomal TLRs including TLR9, has also been recognised as an important mediator in other systemic autoimmune diseases such as systemic lupus erythematosus (SLE) <sup>384</sup>. Therefore, a potential over-activation of the innate immune system could be counterproductive in inflammatory arthritis. Further unwanted side effects of TLR9 stimulation could relate to overshooting Th1 responses combined with autoimmunity (e.g., studies in animal models showing CpG-DNA treatment can induce and exacerbate autoimmunity diseases <sup>385</sup>). Nevertheless, Katakura *et al.* showed a protective effect of TLR9-mediated IFN-α production in mice with colitis <sup>386</sup>. Thus, further studying the effect of this therapy in inflammatory arthritis can help elucidate the biological mechanisms of disease.

Transcriptomic analysis of synovial inflammation has allowed the identification of pathways associated with the delivery of CpG-*Stat3*siRNA. While many of the downregulated pathways were associated with inflammatory pathways, such as T-cell and B-cell signalling and differentiation, cell migration and proliferation, other pathways such as bone remodelling, metabolism and innate signalling and activation were also altered. Interestingly, there is evidence for a role of metabolic dysfunction in RA. Glycolytic enzymes have been shown to play an important role in the pathogenesis of RA, promoting autoimmunity by acting as autoantigens and stimulating abnormal cell proliferation, angiogenesis and pannus formation <sup>387</sup>. Additionally, analysis of serum samples from RA patients by mass spectrometry identified decreased levels of amino acids and glucose and increases levels of fatty acids and cholesterol <sup>388</sup>. Moreover, lactate, produced by immune cells in high energy demands, has been shown to be increased in RA patients, increases IL-17 expression by CD4<sup>+</sup> T-cells and has been linked with the development of ELS <sup>389</sup>. Here, downregulation of protein kinase A signalling-associated genes in response to therapy, correlated with studies describing a role for adenylate cyclase (AC)-protein kinase A (PKA) pathway in apoptosis inhibition of RA FLSs, contributing to synovial hyperplasia and therefore worsening disease severity <sup>360</sup>. Receptor activator of nuclear factor κB ligand (RANKL), a key factor for osteoclast

differentiation and activation, is critically involved in bone erosion of RA <sup>118</sup>. Our datasets show downregulation of osteoblasts, osteoclasts and chondrocytes pathways in mice treated with CpG-*Stat3*siRNA. One interesting finding is the reduction of expression in response to CpG-*Stat3*siRNA of genes associated with RhoA signalling. A strong relationship between RhoA signalling and abnormal migration and invasion of FLSs in RA has been reported in the literature <sup>366</sup>. Additionally, expression key components of Wnt signalling pathways was downregulated, consistent with their involvement in regulating osteoblast function and bone loss in inflammatory arthritis <sup>370,371</sup>. Overall, these findings may be taken to indicate that CpG-*Stat3*siRNA also improves arthritis outcome by reducing the expression of genes that contribute to disease-progression, based on transcriptomic analysis from experimental arthritis.

My laboratory has long been interested in STAT1/STAT3 cross-regulation and how it alters the profile of inflammation. Computational analysis showed that STAT3-regulated genes were predominantly downregulated in response to CpG-*Stat3*siRNA in both WT and *Il27ra*<sup>-/-</sup> mice. Importantly, these genes were involved in matrix remodelling, connective tissue disorder, inflammatory response and cell migration and proliferation. Significantly, STAT3 has been linked with regulating chemokine-directed T-cell trafficking to inflamed tissue and eliciting the early stages of the Th17 cell differentiation program <sup>390</sup>. Consistent with the often-opposing behaviour of STAT1 and STAT3, CpG-*Stat3*siRNA was shown to upregulate STAT1-regulated genes that were associated with cellular function, maintenance and development. For example, genes such as *Stat1* itself, *Irf1* – which collaborates to induce IFN $\gamma$  stimulated genes, and *Cd274* – a well-known immune checkpoint regulator, appeared to be upregulated in response to therapy in our transcriptomic analysis. As previously outlined, *Cd274* encodes an immune inhibitory ligand (PD-L1) which transmits an inhibitory signal when binding to the inhibitory checkpoint molecule PD1, reducing the proliferation of antigen-specific T-cells in lymph nodes while simultaneously reducing apoptosis in Tregs <sup>391</sup>. Interestingly, studies have shown that CpG-*Stat3*siRNA therapy has direct immunogenic effect on acute myeloid leukaemia cells *in vivo* regulating PD-L1 molecule among others <sup>392</sup>. Thus, regulation of checkpoints may then point to a model of action that explains why this therapy is effective in cancer.

Both STAT1 and STAT3 control chemokine-directed T-cell trafficking to inflamed tissue. Here, however, the proinflammatory actions of IL-6 have often been connected to STAT3, which is

essential for T-cell differentiation, recruitment, survival and maintenance of effector characteristics within inflamed tissues<sup>393</sup>. Notably, many of the immunosuppressive actions of IL-27 in T-cells have been linked to STAT1 activity, including its ability to inhibit Th17 cell differentiation, induce IL-10 secretion, and promoting co-inhibitory receptor expression<sup>246,256,394,395</sup>, creating a complex interplay between STAT1 and STAT3 that seems paradoxical, given their distinct functions. Thus, these data are in line with the previous literature and demonstrated the potential ability of this therapy to modulate the STAT1/STAT3 balance in the context of chronic inflammation.

While the presence of STAT3 in the inflamed synovium is not exclusively restricted to ELS<sup>104</sup>, it is however strongly linked synovitis in inflammatory arthritis and has been associated with the formation of ELS in the synovium as well as in other tissues in previous studies. For example, in salivary glands of 20-40% of patients with Sjögren's syndrome, ELS are associated with higher systemic disease severity<sup>139</sup>, and in gastric cancer, where *gp130<sup>F/F</sup>* mice develop ELS in gastric submucosal but in *gp130<sup>F/F</sup>:Stat3<sup>+/-</sup>* mice are not seen<sup>139,396</sup>. Our data showed that *Il27ra<sup>-/-</sup>* AIA mice treated with CpG-*Stat3*siRNA displayed a significantly reduced incidence of CD3<sup>+</sup> cell aggregates compared to untreated *Il27ra<sup>-/-</sup>* AIA mice. Similarly, transcriptomic analysis resulted in downregulation of genes associated with ELS (See Figure 3.24). For example, expression of homeostatic chemokines such as *Cxcl13* and *Ccl19*, required for lymphoid organ organisation, was prominently downregulated in the early stages of disease. Significantly, *Cxcl13* and *Ccl19* correlate with the degree of erosive bone damage in RA and have been associated with ELS development in some inflammatory diseases<sup>104,156,397</sup>. Furthermore, another downregulated ELS-associated gene at day-3 of AIA was *Erdr1*, a negative regulator of cell migration and proliferation whose overexpression in inflammatory arthritis has shown to have a therapeutic effect<sup>398</sup>. These findings suggest that CpG-*Stat3*siRNA therapy, by inhibiting STAT3 activity, may reduce the early development of ectopic lymphoid aggregates within the inflamed synovium of *Il27ra<sup>-/-</sup>* mice. However, determining whether CpG-*Stat3*siRNA alters the formation and maintenance of ELS in experimental inflammatory arthritis requires further investigation.

This study represents the first attempt to reposition a novel anti-cancer therapy, CpG-*Stat3*siRNA, in the context of inflammatory arthritis. Through the use of histological and transcriptomic approaches, the data presented in this Chapter suggest that TLR9-targeted delivery of STAT3 inhibitors offers an alternate strategy for more effective immunotherapy of inflammatory arthritis and, potentially, other autoimmune diseases. The

use of transcriptomic approaches can also help generate novel insights into the mode of action of drugs, in this case, CpG-*Stat3*siRNA therapy in the context of inflammatory arthritis. Although more studies are necessary to further understand the mechanisms of CpG-*Stat3*siRNA in inflammatory diseases and to improve CpG-siRNA gene silencing effects, our results raise the possibility of using oligonucleotide TLR agonists for siRNA delivery in RA, to specifically inhibit STAT3 activity and to further dissect the mechanism of inflammation.

## 4 Therapeutic targeting of STAT3-driven responses through the pharmacological induction of SOCS3 expression

---

### 4.1 Background

The JAK/STAT signalling pathway is tightly regulated through distinct mechanisms affecting the immediate phosphorylation of latent transcription factors (e.g., protein tyrosine phosphatases, PTPs) or negative feedback inhibitors (e.g., protein inhibitor of activated STAT, PIAS; suppressor of cytokine signalling, SOCS proteins) which restrict any sustain activation of the receptor cassette<sup>198</sup>. Suppressors of cytokine protein family consist of eight members (SOCS1-7 and CIS), which are induced following cytokine receptor activation of STAT transcription factors (discussed in more detail in **Chapter 1, Section 1.3.1.2**). They also suppress other pathways, including the NF- $\kappa$ B signalling through Toll-like receptor<sup>399</sup>. SOCS3 is a well-characterised suppressor of STAT3 activation and inhibits cytokine receptor systems, including IL-6 family members that utilise gp130 as the common  $\beta$ -signalling receptor<sup>400</sup>. Extensive evidence in the literature suggests that SOCS3 plays a significant role in RA progression and that signal inhibition of STAT3, by SOCS3, could represent an effective therapeutic strategy for clinical intervention<sup>201,401</sup>. In this Chapter, experiments will evaluate the therapeutic potential of a viral protein derived from hepatitis C virus (HCV), which triggers the transactivation of SOCS gene regulation<sup>201</sup>.

HCV infection causes cirrhosis, liver failure and hepatocellular carcinoma<sup>402,403</sup>; however, the acute phase of infection is often asymptomatic and remains undetected for many years<sup>404</sup>. The mechanisms by which pathology is limited during infection is unknown; nevertheless, this lack of clinical symptoms indicates that HCV has evolved anti-inflammatory mechanisms to effectively counteract immune responses. A role for SOCS proteins during HCV infection has been proposed<sup>405</sup>. Indeed, prior work has documented that HCV induces SOCS3 expression to suppress TNF- $\alpha$  signalling, thereby controlling proinflammatory gene regulation to counteract innate anti-viral immunity<sup>406,407</sup>. HCV p7 ion channel is vital to producing infectious viral particles during viral egress and has been shown to enhance SOCS3 mRNA and protein expression in hepatocytes<sup>408</sup>. Based on these findings, various peptides

have been derived from the HVC p7 protein to map the immunomodulatory action of HVC p7 on SOCS3 regulation. Preliminary data revealed peptide 5 (SOCS3 P) to be the most potent inducer of SOCS3 *in vitro* (unpublished work by Dr Nigel Stevenson, Trinity College Dublin). In this Chapter, I will address the hypothesis that peptide 5 (SOCS3 P) has therapeutic application for the treatment of STAT3-driven inflammatory disorders. To this end, I present pilot studies evaluating the inhibitory action of a SOCS3 P using an *in vitro* murine Th17 cell differentiation assays and an *in vivo* model of inflammatory arthritis.

## 4.2 Aims

Previous studies have demonstrated that SOCS3 plays a significant role in RA progression and that signal inhibition of STAT3 activity by SOCS3 represents an attractive strategy in the treatment of RA <sup>206,210,213,214,409</sup>. For example, Shouda *et al.* found that adenoviral gene delivery of SOCS3 in synovial tissue of mice with antigen-induced arthritis (AIA) and collagen-induced arthritis (CIA) significantly reduced arthritis severity <sup>206</sup>. However, the use of viral vectors presents significant challenges for the treatment of chronic conditions, including transient transduction and occasional undesired inflammatory responses <sup>410,411</sup>.

Thus, the overarching hypothesis for this Chapter was that SOCS3 induction as a response to HVC p7 peptide therapy would improve disease outcomes in inflammatory arthritis. In particular, the aims of the study were to:

- Investigate the therapeutic potential of the novel SOCS3-inducing peptide in a STAT3-driven experimental model of inflammatory arthritis, the antigen-induced arthritis (AIA) model.
- Determine whether the SOCS3-inducing and control peptides promote undesired proinflammatory responses in mice with AIA.
- Evaluate the ability of the SOCS3-inducing peptide to prevent STAT3-dependent Th17 cell differentiation in *in vitro* murine T-cell cultures.

## 4.3 Results

### 4.3.1 Arthritis severity and synovial infiltration are diminished by SOCS3-inducing peptide in experimental arthritis

To determine the impact of SOCS3-inducing peptide on inflammatory arthritis, AIA was established in C57BL/6 WT mice through immunisation with methylated BSA (mBSA) (see **Chapter 2, Section 2.3**). SOCS3-inducing peptide or scrambled control peptide (both at 10 ng/ $\mu$ L) was delivered by intraarticular administration in combination with mBSA (in a total volume of 10  $\mu$ L). Joint swelling was recorded over the duration of the model. At day-3 of AIA, knee joints were recovered, processed and histologically assessed as previously outlined in **Section 2.4**. Since this study represented a pilot experiment, no historical data was available for power analysis. Based on my laboratory's extensive experience of AIA, and calculations based on the resource equation <sup>332,333</sup> (**Chapter 2, Section 2.10**), 5 mice per group were chosen for this initial experiment. Here, a total of 6 experimental conditions were used (n = 15 mice): (i) 3 for evaluation of peptide therapeutic effect: mBSA-AIA, control peptide + mBSA-AIA, SOCS3-inducing peptide + mBSA-AIA; and (ii) 3 to test any proinflammatory effect of peptides: No mBSA-AIA, control peptide + no mBSA-AIA, SOCS3-inducing peptide + no mBSA-AIA (**Figure 4.1**).

Consistent with an anti-inflammatory role for the P7-derived SOCS3-inducing peptide by reducing STAT3 activity and inhibiting Th17 cell differentiation <sup>206</sup>, AIA in SOCS3-inducing peptide treated mice caused a initial delay in joint swelling compared to controls. However, by the endpoint of the experiment (day-3 of AIA), no change in knee-joint swelling was observed following treatment with control peptide (**Figure 4.2**).

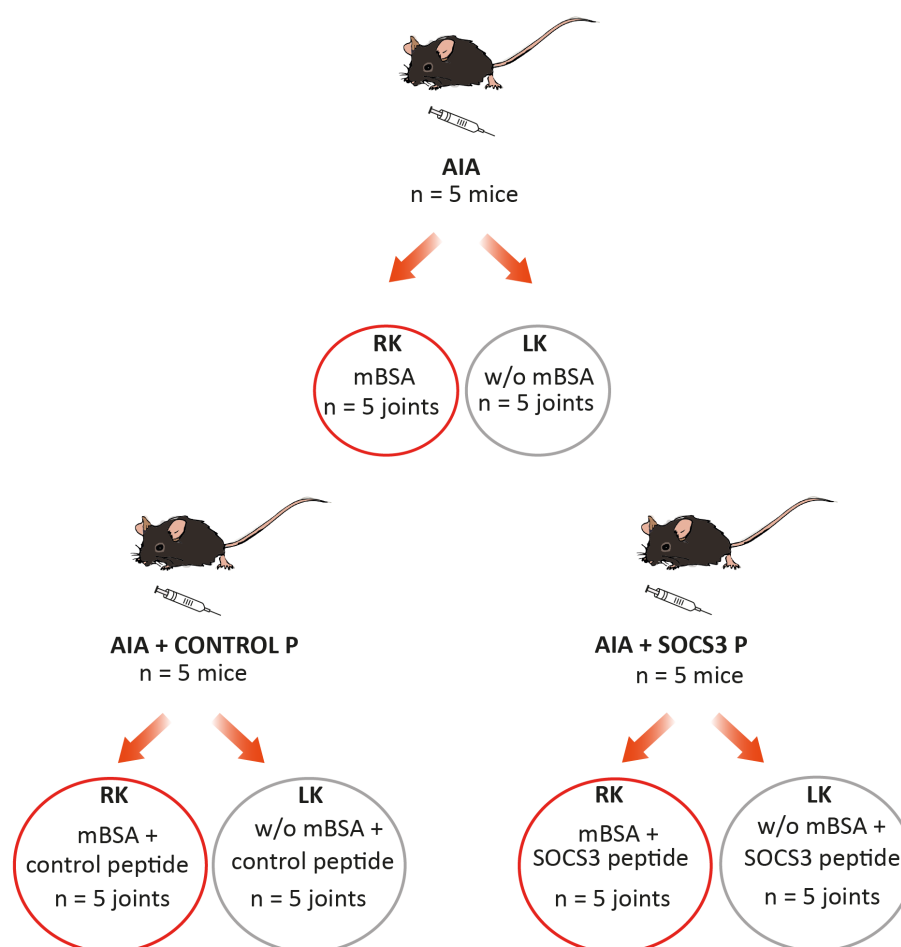


**Figure 4.1 Experimental design for *SOCS3*-inducing peptide *in vivo* experiment.**

Experiment diagram showing the number of animals per experimental group/condition. AIA was established in WT mice. On arthritis induction, knee joints in red circles received mBSA or mBSA and a combination of peptide/control peptide as shown, for evaluation of peptides therapeutic effect (3 groups); knee joints in grey circles were used as controls to test any proinflammatory effect of peptides (3 groups). Timeline for the general AIA mouse model and peptides administration is described in detail in **Materials and Methods Section 2.3.2**. AIA – Antigen Induced Arthritis; CONTROL P – control peptide; *SOCS3* P – *SOCS3*-inducing peptide; RK – right knee; LK – left knee, w/o, without.



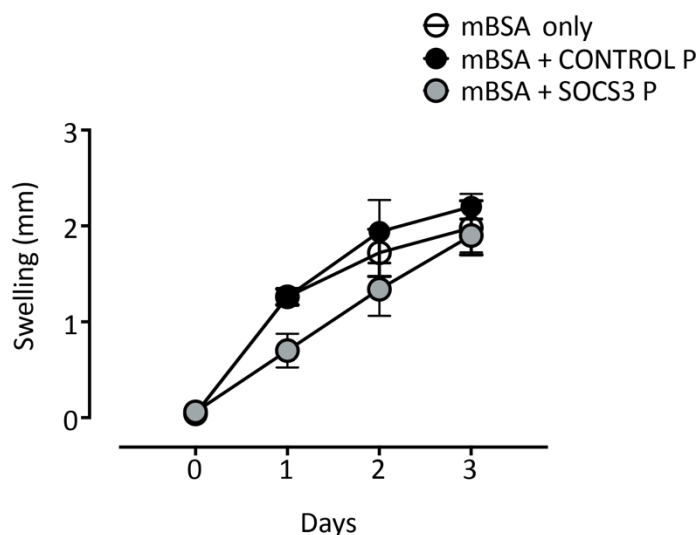


**Figure 4.2 Joint swelling is partially reduced in mice treated with SOCS3-inducing peptide.**

Graphs show joint swelling in AIA challenged WT mice in the presence or absence of control peptide and SOCS3-inducing peptide (right knees). Swelling data reflects the mean  $\pm$  SEM of knee diameters in mm;  $n = 5$ . Joint swelling was calculated as the absolute difference to the left knee diameter (without mBSA, non-inflamed joint). CONTROL P – control peptide; SOCS3 P – SOCS3-inducing peptide.

To investigate the therapeutic effect of a SOCS3-inducing peptide in experimental arthritis (AIA), histological assessment of paraffin-embedded knee-joint sections that received mBSA, mBSA + control peptide and mBSA + SOCS3-inducing peptide were compared (**Figure 4.3A**). Here, treatment with SOCS3-inducing peptide showed improvement in histopathology: SOCS3-inducing peptide contributed to marked inhibition of leukocyte infiltration, synovial exudate and synovial hyperplasia as compared to the control groups (**Figure 4.3B**). The arthritic index (AI), the composite disease score of these parameters, showed a significant reduction in the SOCS3-inducing peptide-treated group (**Figure 4.3C**).

To determine whether the SOCS3-inducing peptide or control peptide produced any undesirable proinflammatory events in mice with AIA, control knee joints that received no intra-articular injection or received control peptide/SOCS3-inducing peptide (without the arthritogenic mBSA), were evaluated (**Figure 4.4A**). Synovial joints were recovered and processed at day-3 of AIA, and tissues were histologically assessed for synovial infiltrate, exudate, pannus formation, and cartilage and bone erosion (**Figure 4.4B**). Experiments showed no signs of inflammation following administration of the SOCS3-inducing peptide or control peptide (**Figure 4.4C**).

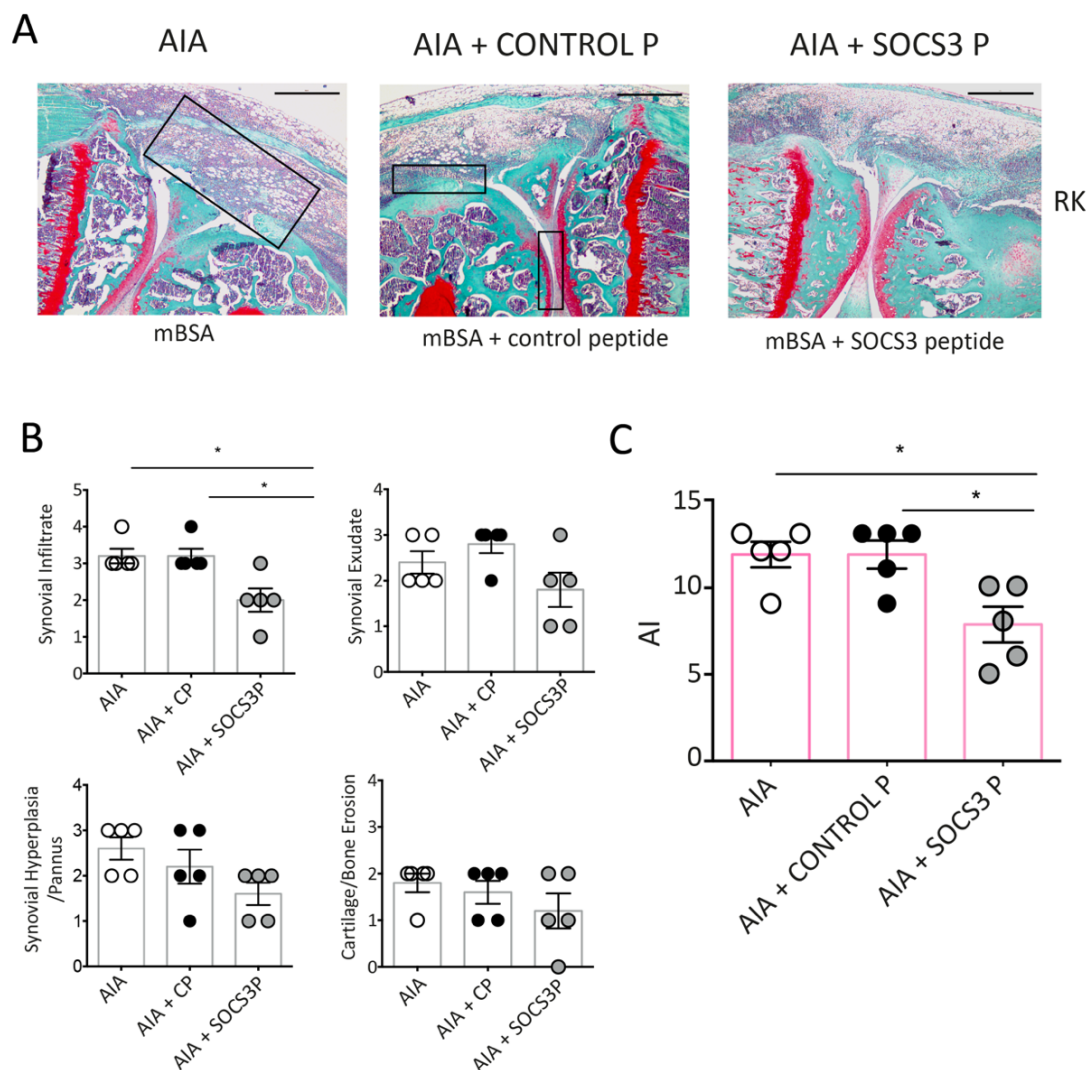


**Figure 4.3 SOCS3-inducing peptide distinctly reduces synovial infiltration and general disease activity in experimental arthritis.**

**(A)** Representative images of haematoxylin, fast green and safranin O staining of WT right knee mouse joints at day-3 post-arthritis induction in the three previously described experimental groups: knee injected only with mBSA (left), knee injected with mBSA + control peptide (middle) and knee injected with mBSA + SOCS3 peptide (right); boxed areas show extensive subsynovial inflammation (large box), focal bone erosion and cartilage degradation, seen as loss of red Safranin-O staining of the articular cartilage (small boxes) in the mBSA only and control peptide groups. **(B)** Histopathology scoring of the three conditions described in (A), showing synovial infiltrate, exudate, hyperplasia/pannus formation and cartilage/bone erosion at day-3 post-arthritis induction ( $n = 5/\text{group}$ ). **(C)** The aggregate score for all parameters in B is presented as an arthritic index (AI) for all the conditions ( $n = 5/\text{group}$ ). Error bars indicate SEM. \*,  $p < 0.05$ . Shapiro-Wilk normality test and a one-way ANOVA, Turkey's multiple comparisons test were used. Scale bars: 500  $\mu\text{m}$ . AIA, antigen-induced arthritis; CONTROL P/CP – control peptide; SOCS3 P – SOCS3-inducing peptide.

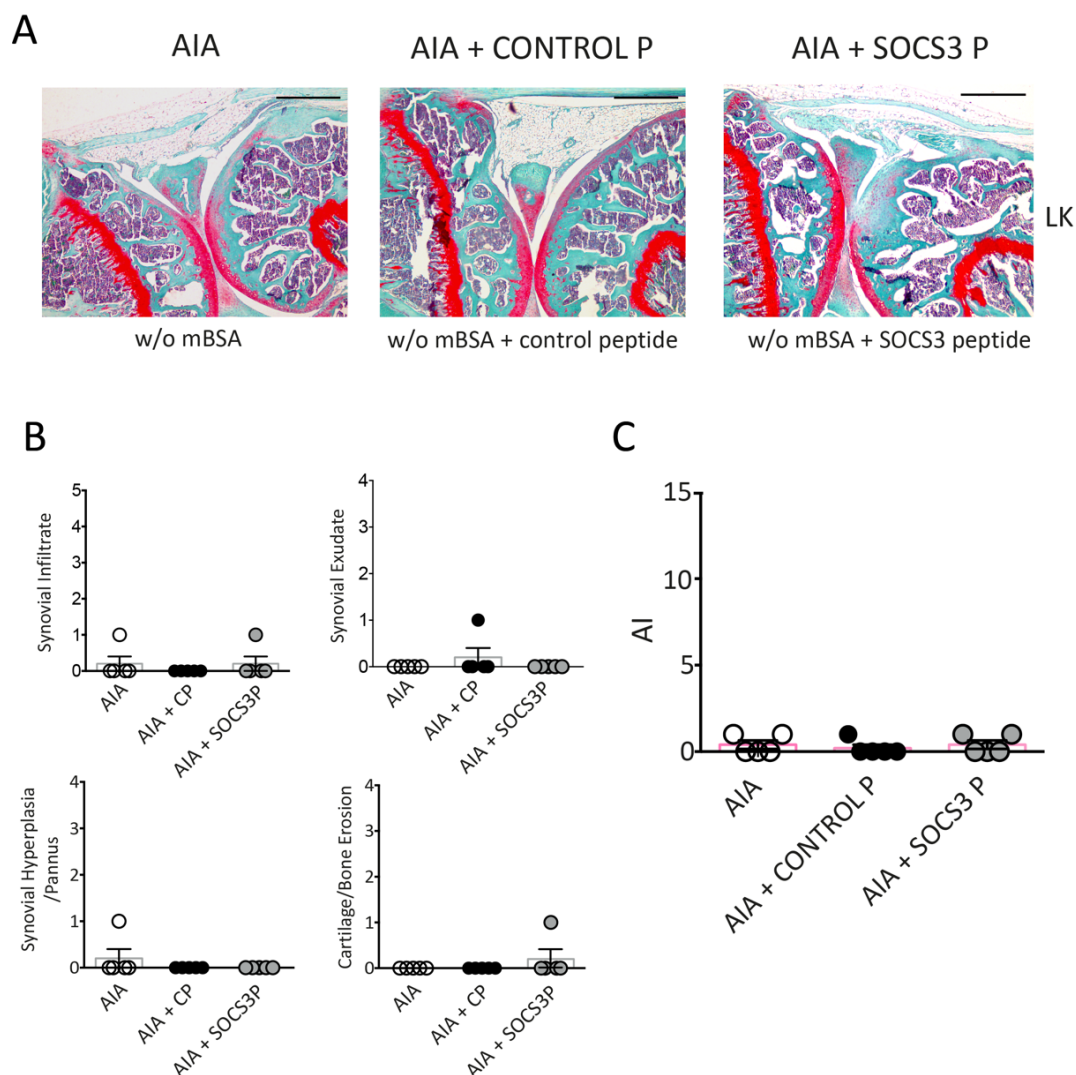


**Figure 4.4 No adverse local inflammatory effects are observed in response to SOCS3-inducing peptide or control peptide administration in mice.**

**(A)** Representative images of haematoxylin, fast green and safranin O staining of WT left knee mouse joints at day-3 post-arthritis induction in the three previously described experimental groups: without mBSA (knee not injected) (left), knee injected only with control peptide (middle) and knee injected only with SOCS3 peptide (right). **(B)** Histopathology scoring of the three conditions described above in (A), showing synovial infiltrate, exudate, hyperplasia/pannus formation and cartilage/bone erosion at day-3 post-arthritis induction ( $n = 5/\text{group}$ ). **(C)** The aggregate score for all parameters in B is presented as an arthritic index (AI) for all the conditions ( $n = 5/\text{group}$ ). Error bars indicate SEM. Shapiro-Wilk normality test and a Kruskal-Wallis test, Dunn's multiple comparisons test were used. Scale bars: 500  $\mu\text{m}$ . AIA, antigen-induced arthritis; CONTROL P/CP – control peptide; SOCS3 P – SOCS3-inducing peptide.

### 4.3.2 Local administration of SOCS3-inducing peptide does not significantly affect systemic mBSA-specific antibody titres in AIA mice

The establishment of an antigen-specific antibody response to mBSA can be confirmed prior to induction of joint inflammation by intraarticular injection of mBSA. For this, peripheral blood from all the experimental conditions was recovered by cardiac puncture blood sampling as described in **Materials and Methods Section 2.3.3**, and serum antibody titres to mBSA were determined by enzyme-linked immunosorbent assay (ELISA) as described previously (**Materials and Methods Section 2.5.2**). No changes were observed in the levels of anti-mBSA titre between the sera of the different mice (**Figure 4.5**). Here, synovitis was associated with elevated adaptive immune responses in mice receiving only mBSA without any treatment, highlighted by increased T-cell infiltrate and mBSA-specific antibody titres. However, this study will need further investigation as local administration of drug on arthritis onset may not be sufficient to affect the systemic antibody response, particularly after the establishment of mBSA-specific antibody response in previously primed mice, or to verify decreased mBSA specific serum IgG titres and therefore a reduction in adaptive immune responses in SOCS3-inducing peptide treated mice.

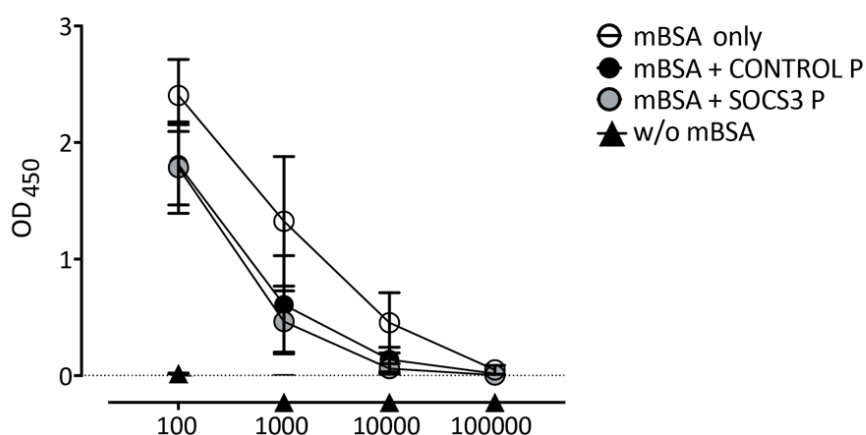


**Figure 4.5 SOCS3-inducing peptide does not significantly diminish adaptive immune responses in mice at day 3 of AIA.**

Anti-mBSA serum titre determinations. Anti-mBSA titres were measured using ELISA in sera from mice at day 3 of AIA (n= 5/group) in the 4 conditions shown. Absorbance changes were monitored at 450 nm. Values represent the mean  $\pm$  SEM. CONTROL P - control peptide; SOCS3 P; SOCS3-inducing peptide; w/o – without.

### 4.3.3 SOCS3 reduces STAT3 activity and the number of synovial infiltrating T-cells

Previous data show that inhibition of SOCS3 activity in mBSA-driven arthritis exacerbated disease severity through an increase in neutrophil infiltration and enhanced activation of T lymphocytes and macrophages<sup>213</sup>. I, therefore, assessed the impact of the therapeutic peptide on the pattern of synovial infiltration in joint sections derived from mice with AIA (**Figure 4.6**). Immunohistochemistry for synovial CD3<sup>+</sup> T-cells (see **Section 2.4.4**) demonstrated a dramatic reduction of infiltrates in SOCS3-inducing peptide group compared to both control peptide and 'only mBSA' groups (**Figure 4.6A, B**). Due to the role of STAT3 in controlling the differentiation, survival, proliferation and regulatory effector functions of T-cells, experiments also evaluated the activation of STAT3 using antibodies against a tyrosine-phosphorylated form of STAT3 (pY-STAT3)<sup>204</sup>. IHC for tyrosine-phosphorylated STAT3 (hereafter pY-STAT3) in SOCS3-inducing peptide joints revealed a much lower degree of STAT3 activity compared to controls. However, no substantial difference was observed in IHC using the generally accepted marker for murine macrophages F4/80, between the SOCS3-inducing peptide group and the control groups (**Figure 4.6A, B**). Given the fact that inflamed joints treated with SOCS3-inducing peptide showed a strong reduction in the degree of synovial CD3 and pY-STAT3 staining by IHC, I next investigated co-localisation between CD3 and pY-STAT3 in the synovium of mice treated with the SOCS3-inducing peptide. Histological joint sections from day 3 of AIA were evaluated for pY-STAT3 and CD3 using immunofluorescence. Indeed, immunofluorescence (IF) studies revealed that pY-STAT3 colocalised with CD3<sup>+</sup> T-cells throughout the synovium (**Figure 4.7**). Together, these data strongly support a role for the SOCS3-inducing peptide in negatively regulating STAT3 activity within the inflamed synovium during AIA and results in a reduction in synovial T-cell infiltration.



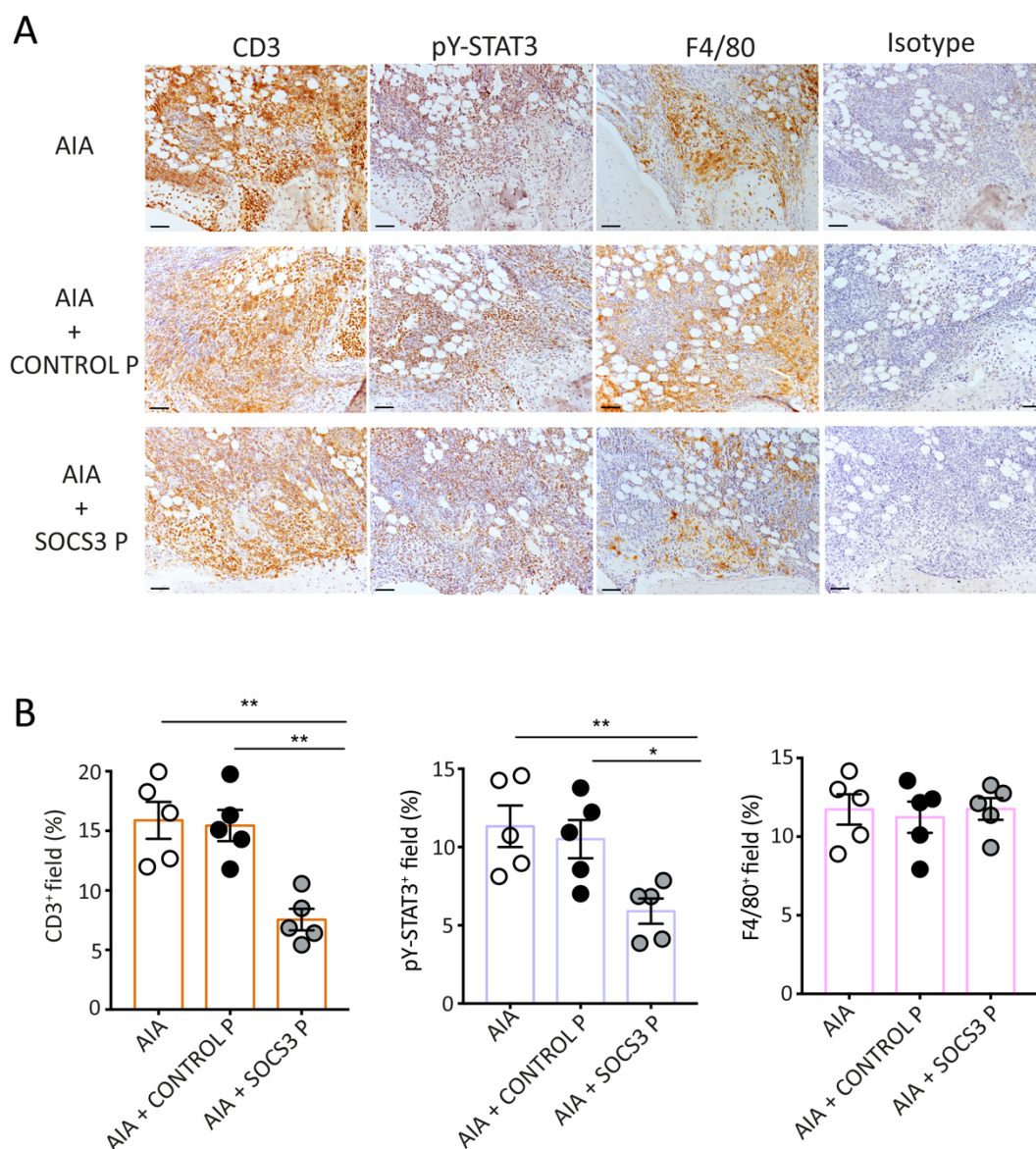


**Figure 4.6 SOCS3-inducing peptide decreases the proportion of CD3<sup>+</sup> T-cells and STAT3 activity in the inflamed synovium.**

**(A-B)** AIA was established in WT mice, with either a SOCS3-inducing peptide or control P7-derived peptide sequence and histopathology assessed at day-3 of AIA. **(A)** Representative IHC and quantification of CD3, pY-STAT3 and F4/80 staining in synovial sequential sections ( $n = 5/\text{group}$ ). Isotype control for CD3 is shown in the upper right corner. **(B)** IHC quantification of CD3, pY-STAT3 and F4/80 staining were carried out ( $n = 5/\text{group}$ ). Error bars indicate SEM. \*,  $p < 0.05$ ; \*\*,  $p < 0.01$ . Shapiro-Wilk normality test and a one-way ANOVA, Turkey's multiple comparisons test were used. Scale bars: (A) 100  $\mu\text{m}$ . AIA, antigen-induced arthritis; CONTROL P – control peptide; SOCS3 P – SOCS3-inducing peptide.

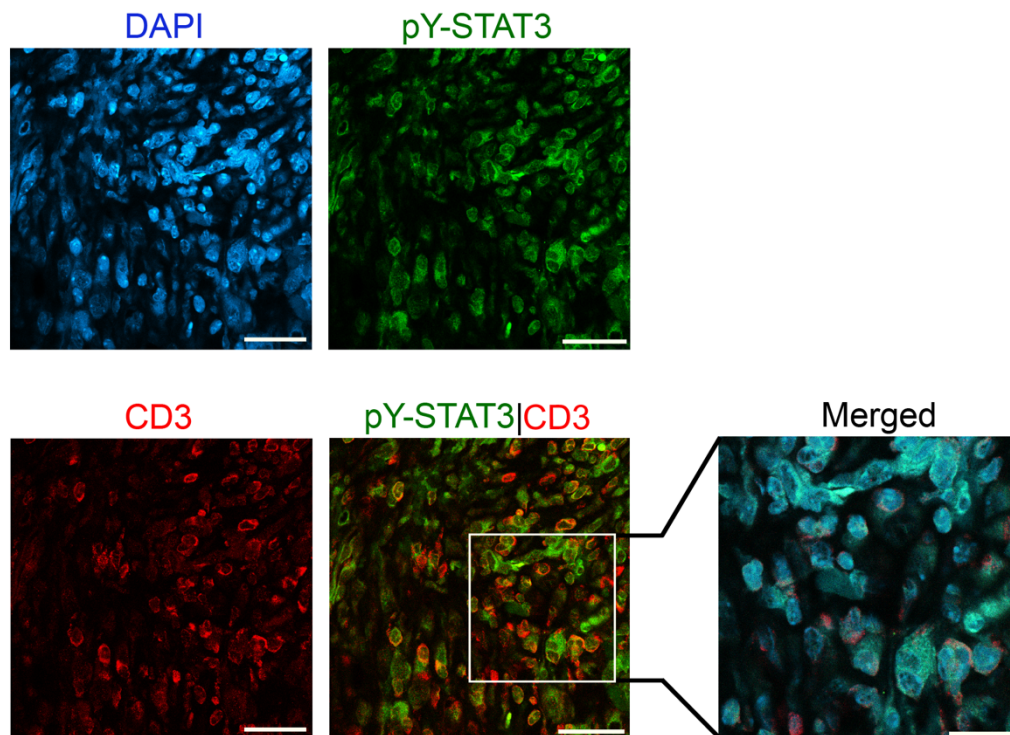


**Figure 4.7 pY-STAT3 co-localisation with CD3<sup>+</sup> T-cells in inflamed synovium treated with SOCS3-inducing peptide.**

Detection of pY-STAT3<sup>+</sup> T-cells at synovium of AIA-challenged mice treated with SOCS3-inducing peptide by confocal double-immunofluorescence with antibodies to CD3 (red), pY-STAT3 (green) and DAPI nuclear staining (blue) (Described in **Material and Methods Section 2.4.4.1**). Scale bars: 100  $\mu\text{m}$ ; 50  $\mu\text{m}$  (merged image)).

#### 4.3.4 SOCS3-inducing peptide selectively prevents differentiation of Th17 cells

SOCS3 is an important regulator of lymphokine responses relevant to the control of adaptive immunity. For example, SOCS3 plays an important role in restricting Th17 cell generation by inhibiting IL-6 and IL-23-mediated STAT3 activation <sup>412</sup>. Given the T-cell driven outcomes relating to pY-STAT3 observed in the above immunohistochemical analysis, and since Th17 cells have been associated with the pathogenesis of various autoimmune chronic inflammatory diseases and are thought to play a critical role in the pathogenesis of RA, next experiments tested whether the SOCS3-inducing peptide (SOCS3 P) affected the generation or expansion of murine Th17 cells *in vitro*. Splenic naïve CD4<sup>+</sup> T-cells (CD4<sup>+</sup>CD25<sup>-</sup>CD44<sup>lo</sup>CD62L<sup>hi</sup>) from WT mice were activated under anti-CD3 and anti-CD28 co-stimulation with Th17-polarising cytokines for 4 days, in the presence or absence of 200 ng/mL SOCS3-inducing peptide or a control P7-derived scrambled peptide. The effect of the peptides on the proportion of IL-17-secreting CD4<sup>+</sup> T-cells was assessed by flow cytometry as previously described (see **Material and Methods, Sections 2.1.2.4 and 2.2.2**). The gating strategy adopted is represented in **Figure 4.8**.

The proportion of IL-17A-secreting T-cells was significantly reduced (more than 50%) in the presence of the SOCS3-inducing peptide compared to the T-cells that were cultured with the control P7-derived peptide sequence (**Figure 4.9A, B**). To verify these findings, culture supernatants were collected for analysis of IL-17A cytokine secretion by ELISA (see **Section 2.5.1**). Here, a similar trend was observed: levels of IL-17A in the culture medium from cells cultured with SOCS3-inducing peptide were significantly decreased when compared to culture medium from cells treated with the control peptide (**Figure 4.9C**). Thus, this data highlights that treatment with SOCS3-inducing peptide *in vitro* inhibits Th17 cell differentiation.



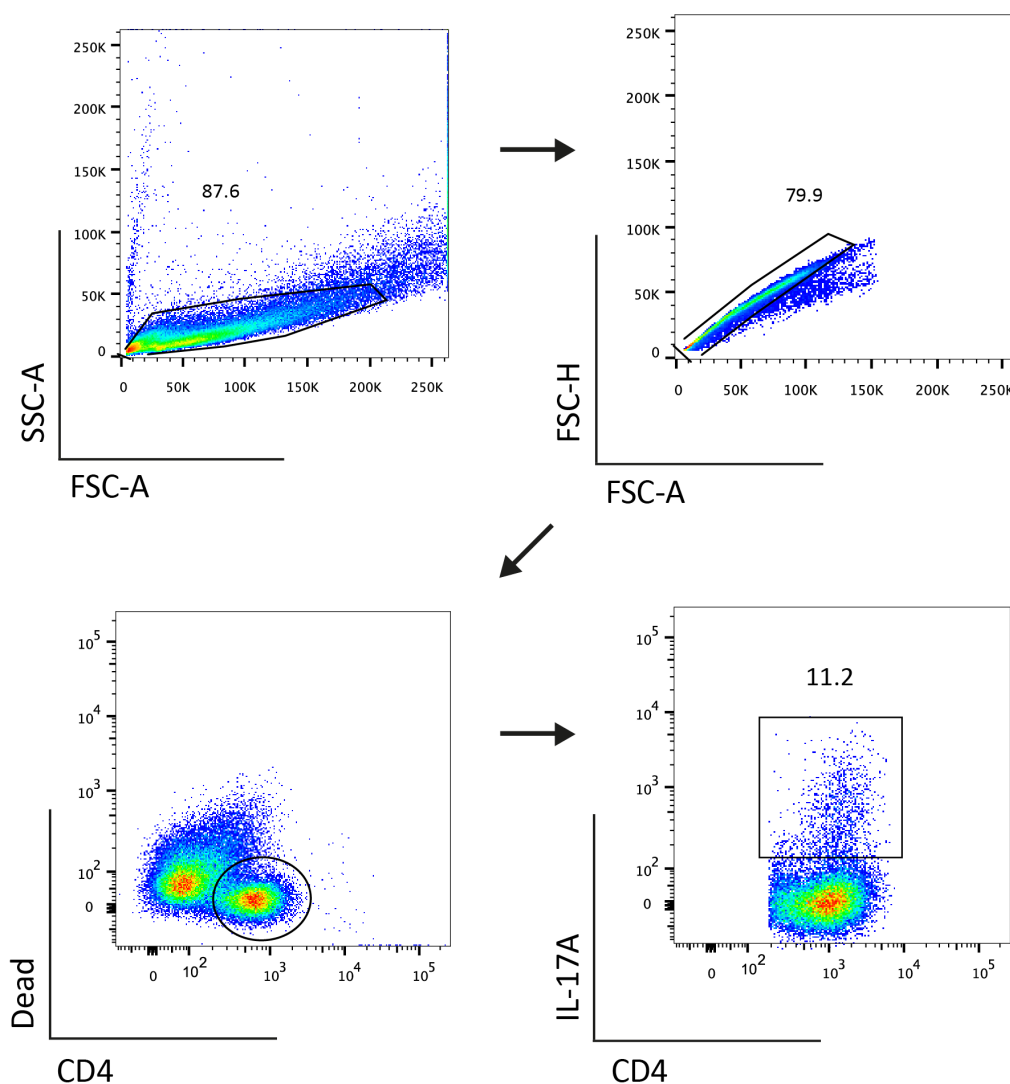


**Figure 4.8 Gating strategy for CD4<sup>+</sup> IL17A<sup>+</sup> T-cells identification using flow cytometry.**

Naïve CD4<sup>+</sup> T-cells (CD4<sup>+</sup>CD25<sup>−</sup>CD44<sup>lo</sup>CD62L<sup>hi</sup>) were plated at 1.5x10<sup>5</sup> cells/well in 96-well round-bottom plates pre-coated with anti-CD3 and anti-CD28 antibodies and cultured with TGF- $\beta$  (1 ng/mL), IL-6 (20 ng/mL) and IL-23 (20 ng/mL) in supplemented IMDM (see **Materials and Methods, Section 2.1.2.4**). After 4 days, cells were stimulated with PMA, ionomycin and monensin for 4 hours at 37 °C before intracellular cytokine staining (see **Section 2.2.2**) and flow cytometry analysis: cells were gated based on SSC and FSC, doublets were excluded, and live CD4<sup>+</sup> IL17A<sup>+</sup> T-cells were successfully identified. FSC-H – forward scatter-height, FSC-A – forward scatter-area; SSC-A – side scatter-area.

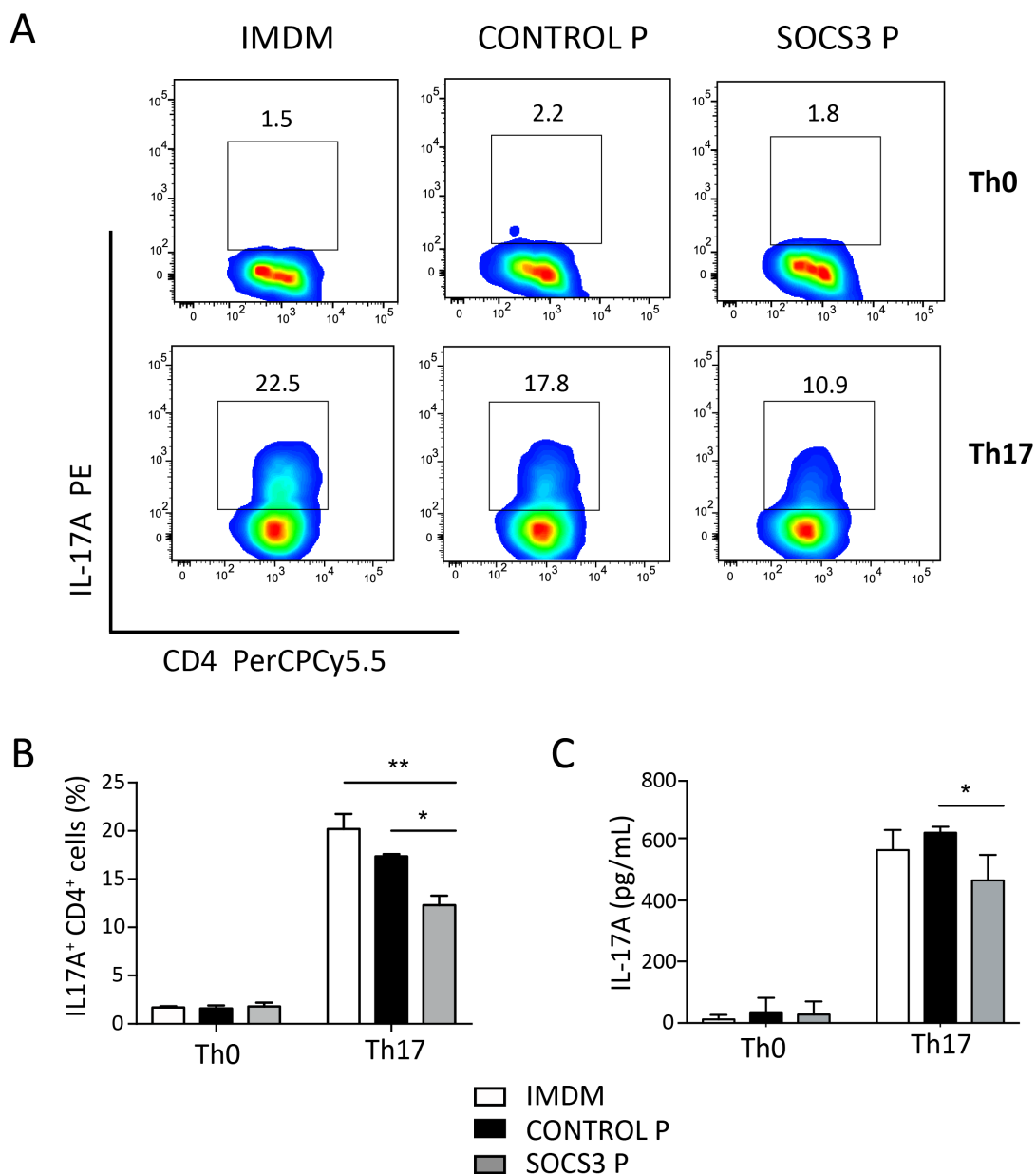


**Figure 4.9 SOCS3-inducing peptide blocks Th17 cell differentiation in vitro.**

**(A-B)** Naïve CD4<sup>+</sup> T-cells (CD4<sup>+</sup>CD25<sup>-</sup>CD44<sup>lo</sup>CD62L<sup>hi</sup>) were cultured in vitro under polarising conditions for Th17 cells in the presence or absence of 200ng/mL SOCS3-inducing peptide and control peptide for 4 days. Th17 cell differentiation was determined by flow cytometry after stimulation with PMA, ionomycin and monensin for 4 hours (see **Materials and Methods, Section 2.1.2.4**). **(A)** Representative flow cytometry plots and **(B)** percentage of cytokine IL-17A-producing effector CD4<sup>+</sup> T-cells after 4 days of culture. **(C)** Levels of IL-17A were detected in culture supernatants by ELISA. **(A- C)** n = 3/group. Data are representative of two independent experiments. IMDM- Supplemented IMDM for Th17 cells; CONTROL P – control peptide; SOCS3 P – SOCS3-inducing peptide. Graphs indicate mean ± SEM. \*, p < 0.05; \*\*, p < 0.01.

## 4.4 Discussion

SOCS3 is a key negative regulator of the JAK/STAT pathway in infection and inflammation, and more specifically, it regulates STAT3 activation in response to cytokine engagement of their receptors, such as those in the gp130-containing IL-6 receptor family<sup>413</sup>. The broad regulatory properties of SOCS3 and its direct involvement in infection and inflammatory disorders such as rheumatoid arthritis highlights its potential as a robust therapeutic target. Hence, this Chapter aims to develop a new therapeutic strategy for the treatment of RA by using a novel peptide that selectively upregulates SOCS3 and, consequently, blocks STAT3 activation. These studies build on experiments performed in Chapter 3, where selective inhibition of JAK/STAT signalling was performed in experimental arthritis by directly targeting STAT3 instead. Induction of SOCS3 by viruses such as HCV suggests a key role for SOCS3 in suppressing anti-viral signal transduction and regulating type I IFN responses during viral infection<sup>400,405</sup>. In addition, SOCS3 does not block receptor systems linked with IL-10, thereby causing no impact on anti-inflammatory immunomodulatory cytokines<sup>211,414</sup>. Therefore, therapeutic manipulation of SOCS3 expression with regulatory peptides derived from the HVC P7 protein could be a useful tool in treating disease. Indeed, in this Chapter, I show that treatment of WT mice during AIA with a SOCS3-inducing peptide led to significant improvement in disease activity *in vivo* and reduced expression of IL-17-producing T-cells *in vitro*.

SOCS3 over-expression has been previously shown to mitigate inflammatory arthritis induced by antigen (AIA) or collagen (CIA) in some inflammation mouse models<sup>210,213</sup>. Moreover, prior work has documented that adenoviral gene delivery of the SOCS3 gene into synovial tissue significantly suppressed pathological changes associated with arthritis in these mice<sup>206</sup>. The approaches taken in these studies are similar to the experiments performed in this Chapter and provided strong rationale for the experimental model chosen to investigate the therapeutic potential of a novel SOCS3-inducing peptide. Consistent with the previously mentioned recombinant adenovirus studies, where overexpression of SOCS3 showed amelioration of inflammatory arthritis development in mice, SOCS3-inducing regulatory peptide injected intraarticularly to AIA mice on disease onset, reduced arthritis severity to some extent. Particularly, treatment decreased cell infiltration in the synovium of AIA mice. Notably, Wong *et al.* reported that deletion of SOCS3 in hematopoietic and endothelial cells was associated with severe IL-1-dependent inflammatory arthritis;

characterised by a conspicuous infiltration of neutrophils and other immune cells in the synovial tissue <sup>213</sup>. Thus, prior experiments and those performed here in this Chapter highlight the critical role played by SOCS3 in inhibiting inflammation and underline the potential of inducing SOCS3 as a therapeutic approach to limit STAT3-driven chronic inflammatory conditions.

In this Chapter, I also demonstrate that upregulation of SOCS3 – indirectly showcased by the pY-STAT3 IHC – strongly diminishes STAT3 activity and consequent disease pathology in AIA joints. This behaviour agrees with the findings of previous studies performed by my group, where mice with a genetically reduced level of gp130-dependent STAT3 activation (*gp130<sup>F/F</sup>:Stat3<sup>+/-</sup>* mice, see **Chapter 2, Section 2.3.1** for more details) were reported to be protected from acute pathology <sup>204</sup>. While early anti-CD3 IHC revealed a reduction in synovial CD3<sup>+</sup> T-cells in response to SOCS3-inducing peptide treatment, the data here show that SOCS3 induction had no effect upon F4/80<sup>+</sup> myeloid cells. Thus, induction of SOCS3 expression during the early stage of the model (day-3 of AIA) does not affect macrophage recruitment.

SOCS3 plays a role in restricting Th17 cell generation, by inhibiting IL-23 and IL-6 signalling <sup>412</sup>. In this context, Th17 cell differentiation is induced by IL-6 and IL-23 in the presence of TGF- $\beta$  through the activation of STAT3, and SOCS3-mediated regulation of cytokines responses in T-cell lineages impairs Th17 differentiation <sup>415</sup>. Therefore, the reduction in Th17 cell population previously seen in this study could reflect an upregulation of SOCS3 and subsequent expected inhibition of STAT3 activity. Together, these studies confirm the therapeutic potential of SOCS3-inducing peptide in blocking Th17 cell differentiation *in vitro* and therefore, disease attenuation.

Future experiments will test SOCS3-inducing peptide in AIA-challenged mice, and disease will be evaluated at day 10 of AIA or late arthritis. Experiments will also examine the efficacy of the novel peptide during the priming phase of AIA, perhaps delivered by oral gavage at this stage, as during the priming phase, there is still no joint disease. This may potentially prevent early formation of the Th17 cell response and enable evaluation of Th17 effector cytokines expression in both the draining lymph nodes and locally within the inflamed joint. It might also be interesting to explore treatment response in other cell subtypes to see whether there is a specific effect on Th17 cells by showing no effect on Th1 or Th2 cells *in vitro*. Furthermore, another major question not addressed by these studies was whether

the findings observed for Th17 cells *in vitro* were applicable to Thf cells. These cells have shown to promote autoimmunity in RA by helping B-cells produce self-reactive Abs in germinal centres and require cytokines that activate STAT3 signalling (IL-6 and IL-21) to promote Bcl6 expression for their differentiation<sup>416,417</sup>. Thus, it would be interesting to track their response to the SOCS3-inducing peptide, as this novel therapeutic approach could potentially result in suppression of these Th subsets as well. Finally, the next stage is to trial the SOCS3 peptide in the CIA model to determine its anti-arthritic effect in a systemic model of inflammatory arthritis, as opposed to the local mono-arthritic synovitis modelled in AIA.

In summary, this Chapter represents a pilot experiment that provides *in vivo* and *in vitro* evidence for the importance of SOCS3 in modulating the development of rheumatoid arthritis. Experiments here further illustrate that virus-derived peptides from the P7 protein of hepatitis C virus (HCV) have the capacity to enhance SOCS3 expression to moderate JAK/STAT signalling. The question remains whether targeted inhibition of specific cytokines implicated in RA directly (as outlined in Chapter 3) is more effective than through the global blockade of cytokines using their respective intracellular signalling pathways as demonstrated in this Chapter. However, it is already evident that manipulation of SOCS3 could represent a novel therapeutic approach and methods of artificially regulating its expression, including regulatory peptides, may be a solution for inflammatory diseases.

## 5 Therapeutic targeting of IL-6 trans-signalling by chimeric soluble gp130 (cs-130)

---

### 5.1 Background

Current IL-6 targeted therapies display robust safety profiles and show strong efficacy in RA, where the clinically beneficial inhibition of IL-6 includes impacts on the control of adaptive immunity <sup>212</sup>. As previously discussed in **Chapter 1, Section 1.3.2**, IL-6 exerts its effects through very distinct modes of signalling on target cells: (i) Classical IL-6 receptor signalling is linked with the control of acute inflammatory processes (e.g., the acute phase response), tissue homeostasis and metabolism (e.g., epithelial regeneration, glucose, lipid and iron metabolism) and some aspects of leukocyte regulation (e.g., lymphocyte survival and proliferation) <sup>418</sup>. Binding of IL-6 to the IL-6R is followed by recruitment of the ubiquitously expressed signal-transducing co-receptor gp130 and initiation of downstream signalling cascades leading to activation of the JAK/STAT signalling pathway, ERK-MAPK signalling and various associated pathways linked with protein kinase B (Akt/PKB) and Yes-associated protein (YAP) involvement <sup>212</sup>. (ii) IL-6 trans-signalling relies on the presence of the soluble IL-6R (sIL-6R) to mediate IL-6-type responses in cells expressing gp130 alone <sup>418</sup>. This mode of IL-6 signalling also affects the overall bioavailability of IL-6 and is considered integral to the development and maintenance of immune activities within inflamed tissues, including the synovium of patients with RA <sup>241,242</sup>. Alternatively, IL-6 signal transduction can be induced by a third mechanism, namely IL-6 trans-presentation or “cluster signalling” that occurs when membrane-bound IL-6:IL-6R complexes on transmitter cells activate gp130 receptors on neighbouring receiver cells and activate signal transduction through gp130 dimerisation <sup>228,229</sup>.

IL-6 is a keystone cytokine that supports disease progression in RA and therefore, targeting its signalling should offer the best opportunity for disease remission in certain patients <sup>212</sup>. However, global IL-6 blockade (e.g., via IL-6R or IL-6 directed antibodies) targets all modes of IL-6 receptor signalling and is often associated with many side effects such as an increased risk of infections, alteration of circulating lipids and moderate increase in certain liver enzymes <sup>419</sup>. Whilst this profile of adverse outcomes is not unique to IL-6-directed intervention, and similar concerns are also seen with other biological drug regimes, any

advances that limited these deleterious consequences would significantly improve the clinical management and quality of life of patients receiving these drugs. Based on the emerging biology of IL-6 regulation and signalling in disease, second-generation biological drug therapies against this cytokine are now leading to more targeted inhibition strategies. Thus, the pioneering approach is exemplified by the clinical application of olamkicept, which is an engineered sgp130Fc protein that selectively targets IL-6 trans-signalling and IL-11 trans-signalling<sup>303</sup>.

Structure-function studies have identified regions within the IL-6 sequence essential for receptor binding. Site I for IL-6 binding to IL-6R, and sites II and III required for docking to domains D2/D3 and D1 of gp130, respectively (**Figure 5.1**). Antibodies against IL-6 (e.g., siltuximab, clazakizumab) or IL-6R (e.g., sariluman, tocilizumab), target the site I interface formed between IL-6 and the IL-6R and affect both classic and trans-signalling, while others target site II (e.g., EBI-033) or site III (e.g., olokizumab). While sgp130 is the natural inhibitor of the agonistic IL-6/sIL-6R complex, the recombinant fusion protein sgp130Fc targets sites II and III and theoretically does not affect IL-6 class-signalling, unless extremely high concentrations are used, allowing quantitative complexing of IL-6 with sIL-6R and, thus, reducing free IL-6 levels<sup>227,420</sup>. Unlike drugs that target site I, biological therapies that interact with site II and III do not cause substantive elevations in circulating IL-6 following intervention<sup>303</sup>. As a result, the control of bacterial and viral infections is not expected to be affected, which is supported by *in vivo* experiments<sup>421</sup>. However, sgp130Fc (olamkicept) is a very large protein dimer with approximately 186 kDa plus 20 glycosylation chains, leading to a total molecular weight of about 240 kDa. Efforts have been made to reduce the size of the molecule using natural sgp130 monomers (120 kDa) or the natural short sgp130-RAPS variant consisting of only the ligand-binding domains D1-D3 of gp130 (50 kDa), but the inhibitory capacities and binding affinities of such proteins are much lower than those of sgp130 dimers<sup>227,422,423</sup>.

In this Chapter, I performed proof-of-concept studies using a Th17 cell expansion assay to evaluate a novel set of sgp130-based IL-6 trans-signalling inhibitors as a more specific and effective way to block IL-6 trans-signalling and therefore prevent STAT3-driven murine Th17 cells. These inhibitors are miniaturised sgp130 variants composed of combinations of the cytokine binding domains (D1, D2, D3) of sgp130, fused with a recently described single domain antibody (sdAb, VHHH, nanobody) recognising the interface formed by IL-6 in complex with the sIL-6R (VHH6)<sup>424</sup>. The sdAb recognises only the complex of IL-6 and sIL-6,

but not the individual components, and binds to it with nanomolar affinity, stabilising the complex <sup>424</sup>. By combining the sgp130 ligand-binding domains and the sdAb, avidity effects will restore the biology activity lost through minimisation of sgp130.

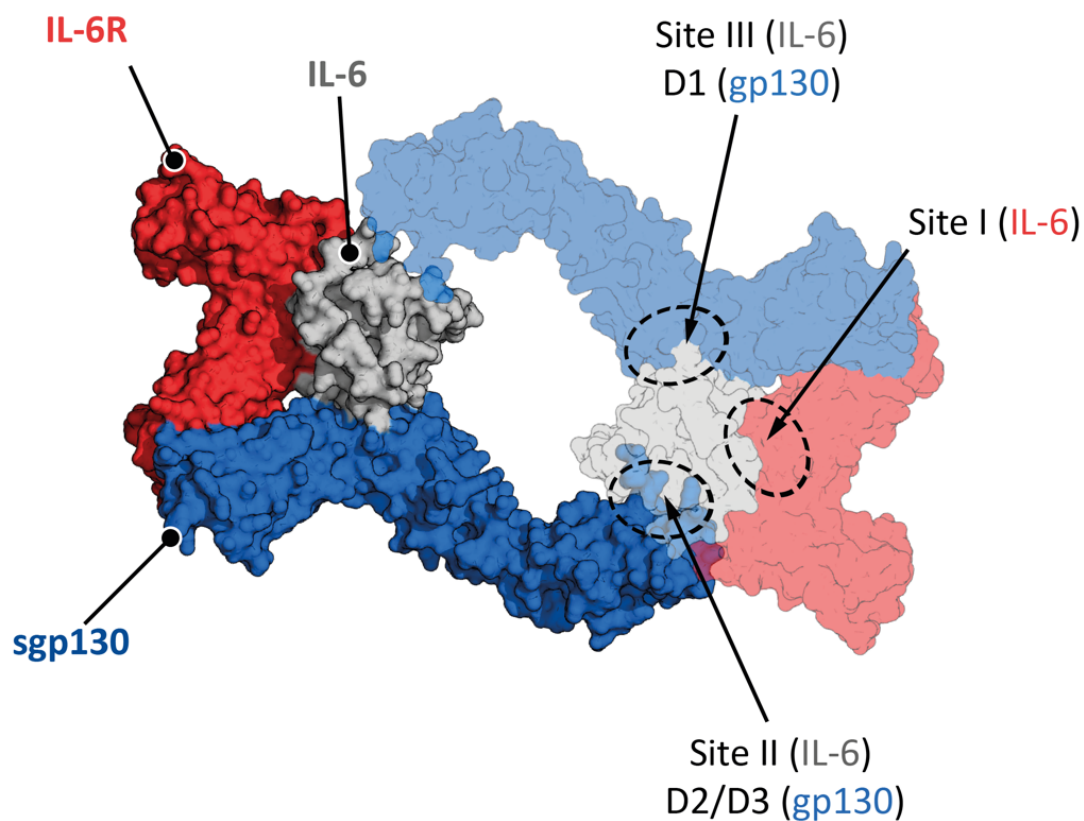


**Figure 5.1 Structure of the human IL-6/IL-6R/gp130 complex.**

Schematic view of the dimerised, hexameric signalling structure of IL-6/IL-6R/gp130 shown as a partial space-filling model with the three conserved binding sites of IL-6 (Sites I, II and III) and the three different gp130 domains (D1, D2 and D3). The shaded structures represent a schematic half of the trimeric structure to demonstrate the binding faces of the IL-6/IL-6R/gp130 complex. Molecular graphics image was produced using PyMOL 2.0 and PDB code 1P9M (see **Section 2.9.7.8**).



## 5.2 Aims

Although sgp130Fc is a very well-characterised IL-6 trans-signalling inhibitor, it is a large glycosylated molecule that may affect the pharmacokinetics or antigenicity of the drug in clinical practice. Studies have reported that the activity of sgp130-based trans-signalling inhibitors inversely correlates with their molecular weight <sup>425</sup>. The novel inhibitors utilised in this study are designed to retain the biological characteristics of olamkicept, but with increased specificity and avidity for IL-6 trans-signalling due to the linked VHH nanobody. Moreover, these constructs have a lower molecular weight than olamkicept. Therefore, it was hypothesised that these novel sgp130 variants would result in improved inhibitory capacity of IL-6 trans-signalling and consequently, STAT3-driven Th17 cell expansion *in vitro*.

In this chapter, the overall aim was to test the therapeutic potential of sgp130-based trans-signalling inhibitors, in murine naïve CD4<sup>+</sup> T-cells activated under Th17 polarising conditions *in vitro*, in collaboration with Professor Jürgen Scheller and Dr Jens Moll (Heinrich Heine University, Düsseldorf). Ablation of IL-6/STAT3 signalling axis in T-cells impairs Th17 differentiation and results to their skewing toward anti-inflammatory Treg cells <sup>426,427</sup>; I also hypothesised that following successful Th17 cells inhibition, this alternative therapy could consequently represent a useful tool in the treatment of inflammatory arthritis.

## 5.3 Results

### 5.3.1 Design of miniaturised sgp130 variants

The molecular weight of bioengineered therapeutic modalities, such as antibody-based interventions significantly affects their bioavailability and overall pharmacokinetics<sup>425</sup>. Here, pharmacological approaches have demonstrated an inverse correlation between the capacity of a drug to penetrate tissues and the molecular weight of the modality. When compared to olamkicept (an engineered sgp130-Fc construct), several smaller molecular weight variants of sgp130 (e.g., the 50 kDa sgp130- RAPS isoform) exhibit similar biological activities, but weaker efficacies<sup>226,227,422</sup>. For example, while sgp130Fc inhibited IL-6 trans- signalling with an IC<sub>50</sub> of 77 pM, the IC<sub>50</sub> of monomeric sgp130 is above 700 pM, and the IC<sub>50</sub> for sgp130-RAPS is well over 70000 pM<sup>227,422</sup>. Thus, researchers have harnessed various bioengineering strategies to enhance the efficacy of sgp130-based interventions, while improving the pharmacodynamic of the drug.

Recombinant gp130-based fusion proteins were kindly provided by Professor Jürgen Scheller and Dr Jens Moll (Heinrich Heine Universität, Düsseldorf, Germany) (see **Section 2.1.2.5**). These agents were specifically designed to combine the biological properties of sgp130 with a single domain antibody (sdAn VHH6) specific for the IL-6:sIL-6R complex. Specifically, the first three domains of sgp130 (represented in sgp130-RAPS) were connected via a flexible linker to VHH6 and a human IgG Fc domain, which is required for initial purification from cell culture supernatants. A tobacco etch virus (TEV) protease recognition site was inserted immediately prior to the IgG Fc domain to allow removal of the antibody tail ( **Figure 5.2**)<sup>422</sup>. The resulting fusion protein labelled cs-130-Fc has a theoretical molecular weight of 157 kDa compared to 186 kDa for sgp130Fc (**Figure 5.2A**). After TEV cleavage, the resultant cs-130 is reduced to a molecular weight of about 52 kDa. A variety of fusion proteins were created to examine the effects of the domains D1-D3 of sgp130 and the sdAb components with regards to inhibitory function (**Figure 5.2B**). Moreover, mutations were inserted in the D1 and D2 domains of sgp130 to reduce or increase binding affinity to the IL-6:sIL-6R complex<sup>428</sup> (**Figure 5.2B**).

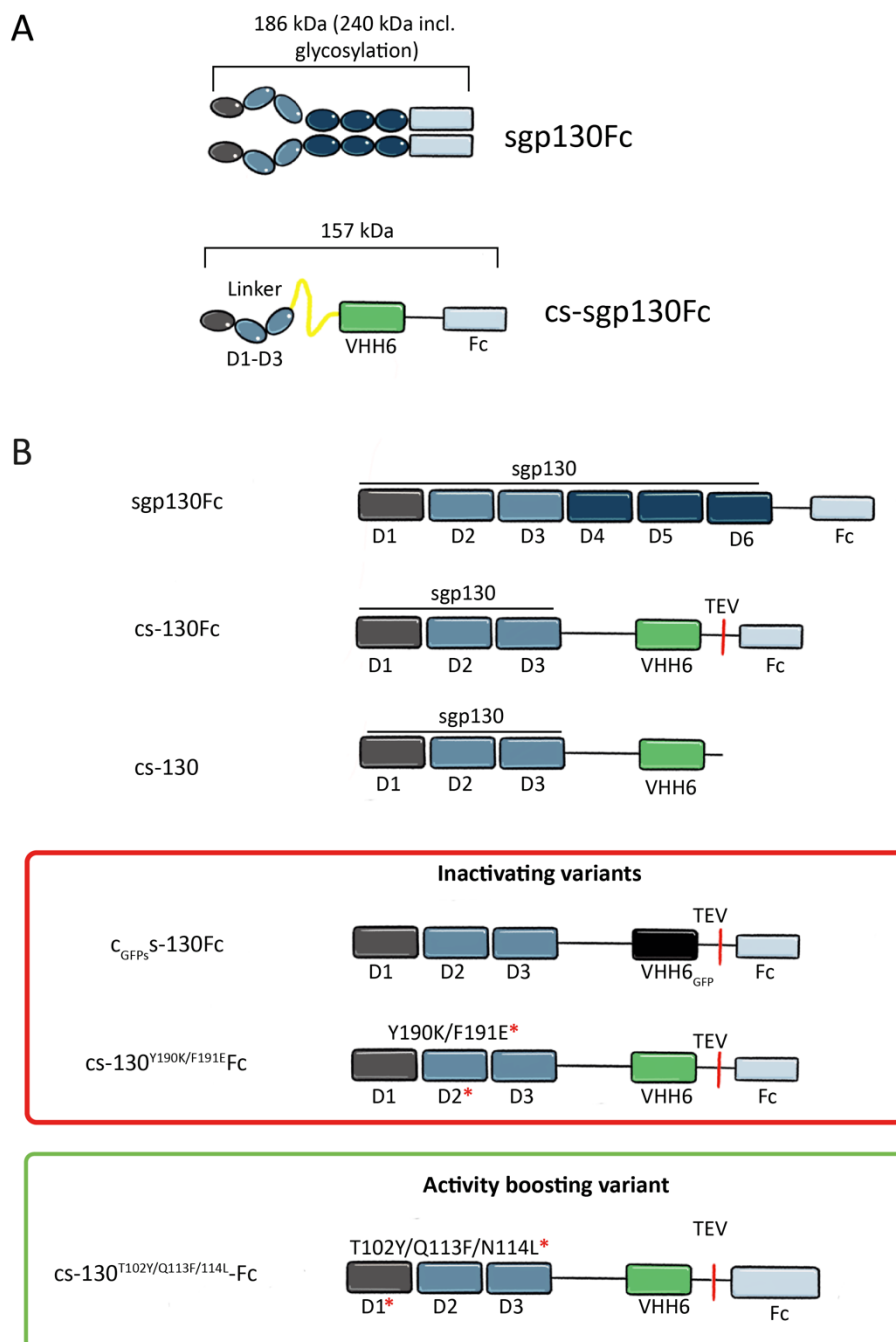


**Figure 5.2 Schematic illustration of sc-130 variant design.**

Protein domains are depicted as (not size-proportional) boxes. **(A)** Domains D1 (grey), D2-D3 (blue) of sgp130Fc, incorporating sites II and III required for cytokine binding, were fused via a long flexible linker to a single domain antibody (VHH6) recognising the complex of IL-6 and sIL-6R. A TEV protease recognition sequence connects VHH6 to the Fc fragment of a human IgG antibody. **(B)** Overview of different cs-130Fc variants. TEV protease recognition sequences (|) and positions of amino acid substitutions are indicated (\*).

### 5.3.2 cs-130Fc variants inhibit Th17 cell differentiation in a dose-dependent manner

IL-6, in combination with TGF-beta, is required for the differentiation of murine naïve CD4<sup>+</sup> T-cells into Th17 cells. Here, IL-6 activation of STAT3 promotes the expression of the transcriptional master regulator *RORγt* and the proliferative expansion of Th17 cells that secrete IL-17A and IL-17F as their signature cytokine<sup>86,237–239</sup>. To assess the effect of cs-130Fc variants on Th17 cell differentiation, naïve CD4<sup>+</sup> T-cells (CD4<sup>+</sup>CD25<sup>–</sup>CD44<sup>lo</sup>CD62L<sup>hi</sup>) cells from the spleen of WT mice were activated under anti-CD3 and anti-CD28 antibody co-stimulation with TGFβ (1 ng/mL), IL-23 (20 ng/mL), IL-6 (50 ng/mL), sIL-6R (100 ng/mL), and anti-IL-2 (10 ng/mL) for 4 days, using a modified method to that described in **Section 2.1.2**. Here, anti-IL-2 was introduced to maximise the expansion of Th17 cells, and increased concentrations of IL-6 and sIL-6R were used to match the doses utilised in Ba/F3 cell proliferation assays conducted by the team in Düsseldorf to quantify IL-6 trans-signalling. Increasing concentrations of cs-130Fc variants were added as indicated in the figure legends. Here, flow cytometry was used to monitor effector cytokine production associated with Th17 cell commitment. Under normal Th17-polarising conditions, Th17 cells accounted for about 11% ± 1.52 of the total alive CD4<sup>+</sup> T-cells; this percentage slightly increased (12.5%) when IL-6 concentration was increased to 50 ng/mL (**Figure 5.3**). Furthermore, the percentage of IL-17 expressing cells was significantly enhanced by the antibody blockade of IL-2 (22%), consistent with the known negative regulation of Th17 cells by IL-2<sup>429</sup>. To evaluate the efficiency of Th17 cell inhibition by the cs-130 derivatives, all analyses were compared against the action of IL-27, which is a potent suppressor of Th17 cell development<sup>394,430</sup> (**Figure 5.3**).

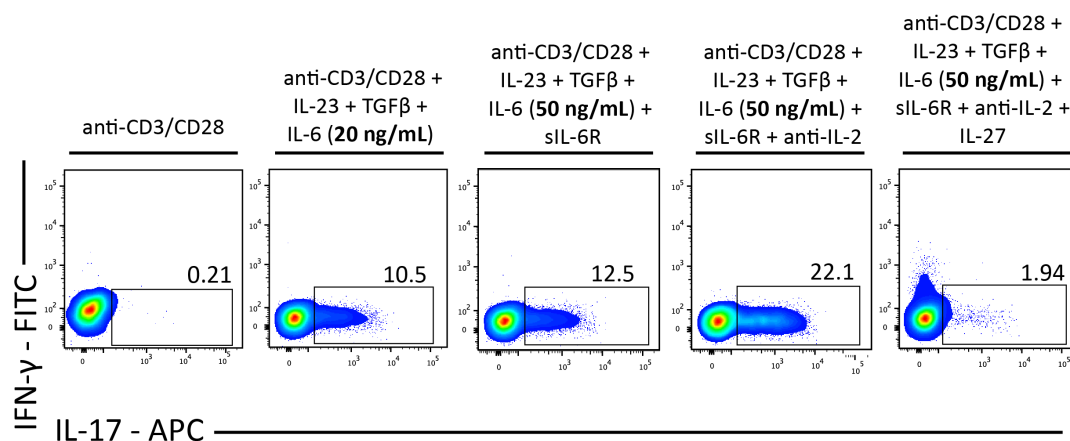


**Figure 5.3 Increasing IL-6 concentration and adding anti-IL-2 magnifies Th17 cell expansion, while IL-27 inhibits it.**

Representative flow cytometry plots of splenic naïve CD4<sup>+</sup> T-cells (CD4<sup>+</sup>CD25<sup>-</sup>CD44<sup>lo</sup>CD62L<sup>hi</sup>) cultured *in vitro* under different conditions, as indicated (n = 3). Data are representative of at least three independent experiments.

To compare the capacity of the cs-130Fc variants to block Th17 expansion, the inhibitory action of each derivative was compared against the action of sgp130Fc (olamkicept)<sup>227</sup> (**Figure 5.4**). This molecule shows no inhibitory action against IL-6 itself in controlling Th17 cell expansion, but instead selectively inhibits the development of Th17 cells expanded as a response to IL-6 trans-signalling (i.e., the IL-6:sIL-6R complex). Under these conditions, inhibition was indeed confirmed in response to 0.1-10 nM sgp130Fc with an IC<sub>50</sub> value of 1.63 nM (**Figure 5.4D**). Chimeric soluble gp130 (cs-130) variants cs-130Fc (**Figure 5.5**) and cs-130 (**Figure 5.6**) displayed comparable inhibitions of Th17 cell expansion. With an IC<sub>50</sub> value of 0.6 nM, cs-130Fc was 2.5-fold more potent than sgp130Fc; while sgp130Fc (IC<sub>50</sub>: 1.6 nM) was 1.5 times more active than cs-130 (2.5 IC<sub>50</sub>: nM). On the contrary, during control experiments using the two previously described inactivating variants of sgp130: CGFPS-130Fc and cs-<sup>130190K/F191E</sup>Fc (See Figure 5.2), no effect on Th17 expansion were observed (**Figure 5.7**). Thus, these results further support that cs-130Fc variants improve IL-6 trans-signalling inhibitory potential, which here is reflected in the inhibition of Th17 cells *in vitro*.

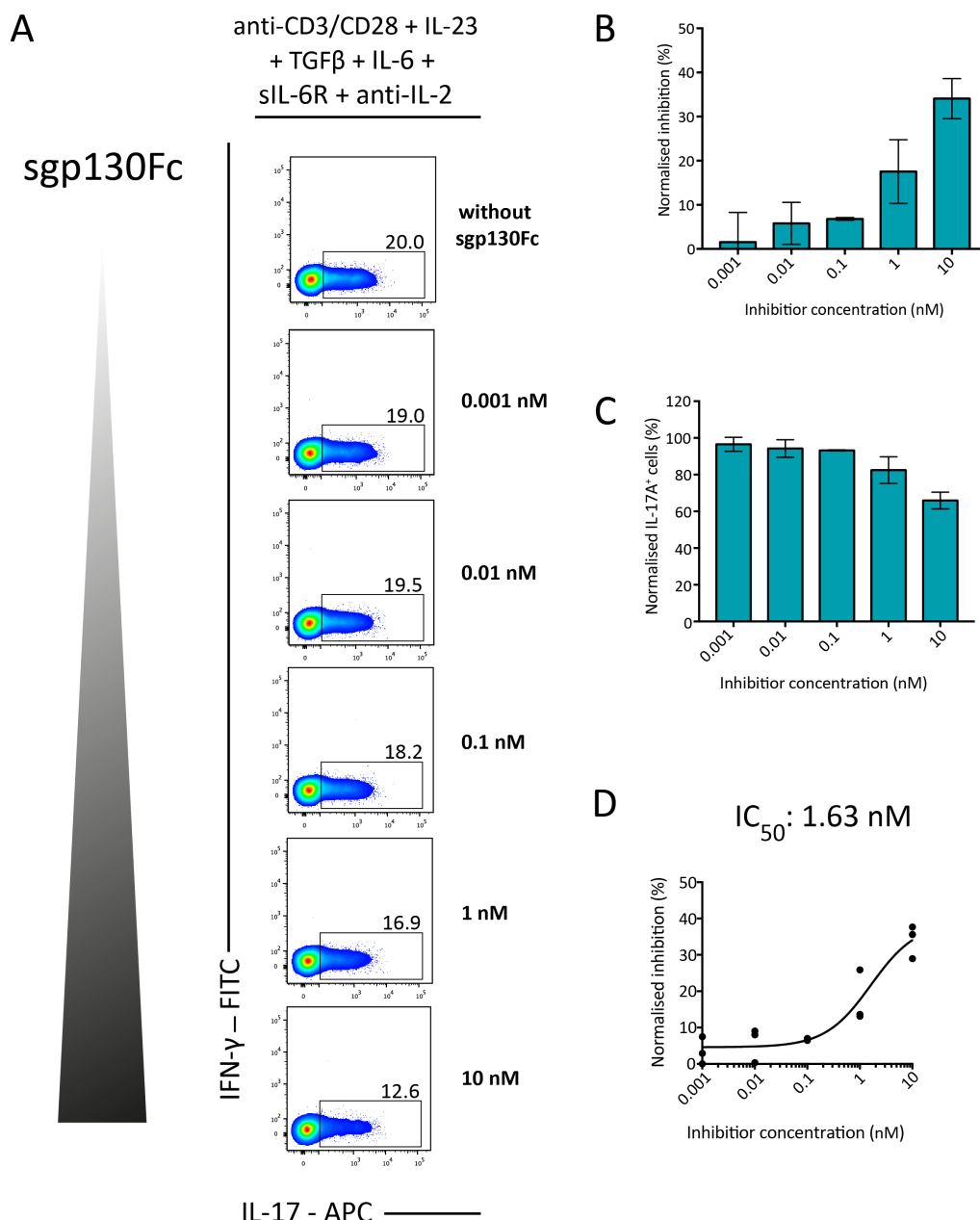


**Figure 5.4** The fusion protein sgp130Fc is able to suppress the proliferation of Th17 cells in a dose-dependent manner *in vitro*.

**(A)** Representative flow cytometry plots ( $n = 3$ ) of naïve T-cells (CD4<sup>+</sup>CD25<sup>-</sup>CD44<sup>lo</sup>CD62L<sup>hi</sup>) cultured *in vitro* under polarising conditions for Th17 cells (TGF $\beta$  (1 ng/mL), IL-23 (20 ng/mL), IL-6 (50 ng/mL), sIL-6R (100 ng/mL), and anti-IL-2 (10 ng/mL) in the presence of increasing sgp130Fc concentrations, as indicated, for 4 days. Th17 cell differentiation was determined by flow cytometry after stimulation with PMA, ionomycin and monensin for 4 hours. The % of inhibition **(B)** and IL-17A<sup>+</sup> cells **(C)**, were normalised to controls. **(D)** The concentration-dependent inhibitory dose-curve was plotted as the normalised percentage of inhibition, and effective concentration (IC<sub>50</sub>) value was calculated by nonlinear regression analysis, using the “inhibitor vs response (three parameters)” equation in Prism 7. Graphs present data from 1 independent experiment, error bars indicate SD.

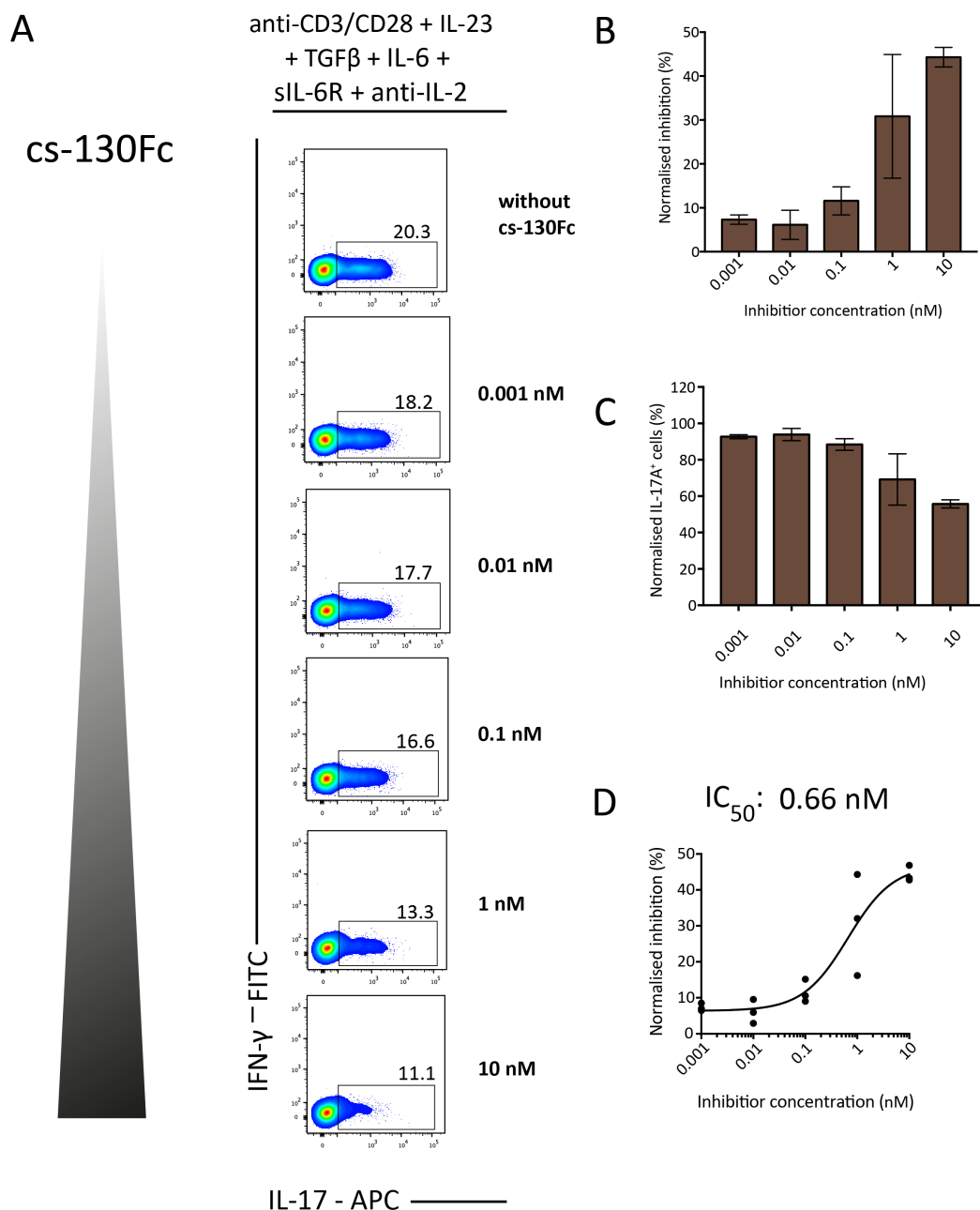


**Figure 5.5 cs-130Fc inhibits Th17 cell formation in a dose-dependent manner *in vitro*.**

**(A)** Representative flow cytometry plots ( $n = 3$ ) of naïve T-cells (CD4<sup>+</sup>CD25<sup>-</sup>CD44<sup>lo</sup>CD62L<sup>hi</sup>) cultured *in vitro* under polarising conditions for Th17 cells (TGF $\beta$  (1 ng/mL), IL-23 (20 ng/mL), IL-6 (50 ng/mL), sIL-6R (100 ng/mL), and anti-IL-2 (10 ng/mL) in the presence of increasing cs-130Fc concentrations, as indicated, for 4 days. Th17 cell differentiation was determined by flow cytometry after stimulation with PMA, ionomycin and monensin for 4 hours. The % of inhibition **(B)** and IL-17A<sup>+</sup> cells **(C)**, were normalised to controls. **(D)** The concentration-dependent inhibitory dose-curve was plotted as the normalised percentage of inhibition, and effective concentration (IC<sub>50</sub>) value was calculated by nonlinear regression analysis, using the “inhibitor vs response (three parameters)” equation in Prism 7. Graphs present data from 1 independent experiment, error bars indicate SD.

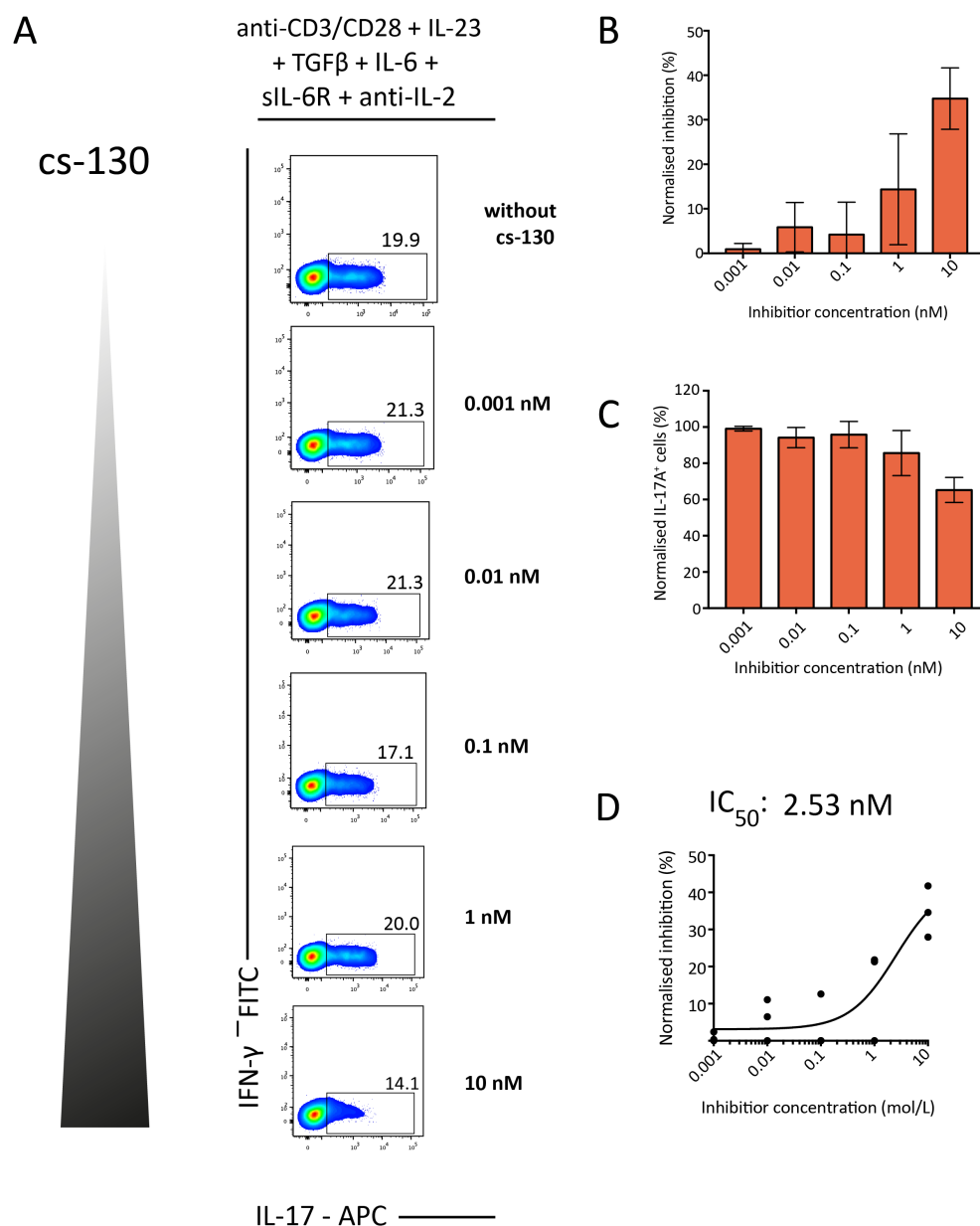


**Figure 5.6** cs-130 inhibits Th17 cell formation in a dose-dependent manner *in vitro*.

**(A)** Representative flow cytometry plots ( $n = 3$ ) of naïve T-cells (CD4<sup>+</sup>CD25<sup>-</sup>CD44<sup>lo</sup>CD62L<sup>hi</sup>) cultured *in vitro* under polarising conditions for Th17 cells (TGF $\beta$  (1 ng/mL), IL-23 (20 ng/mL), IL-6 (50 ng/mL), sIL-6R (100 ng/mL), and anti-IL-2 (10 ng/mL) in the presence of increasing cs-130 concentrations, as indicated, for 4 days. Th17 cell differentiation was determined by flow cytometry after stimulation with PMA, ionomycin and monensin for 4 hours. The % of inhibition **(B)** and IL-17A<sup>+</sup> cells **(C)**, were normalised to controls. **(D)** The concentration-dependent inhibitory dose-curve was plotted as the normalised percentage of inhibition, and effective concentration (IC<sub>50</sub>) value was calculated by nonlinear regression analysis, using the “inhibitor vs response (three parameters)” equation in Prism 7. Graphs present data from 1 independent experiment, error bars indicate SD.



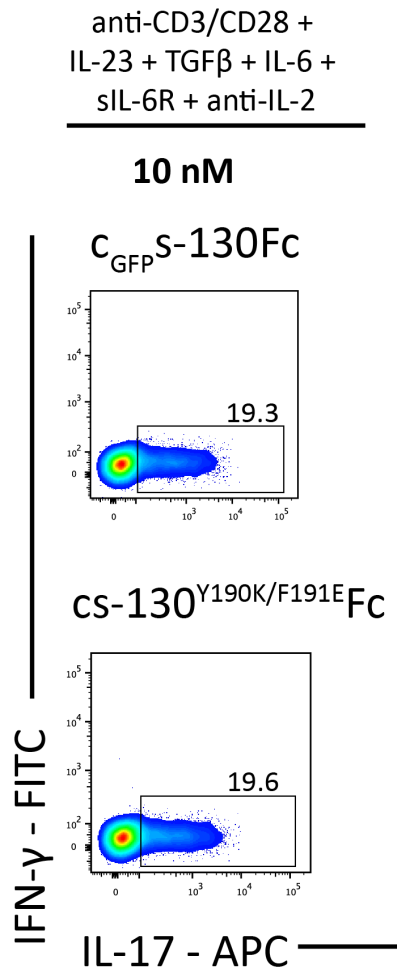


**Figure 5.7 Inactivating cs-130Fc variants did not affect Th17 differentiation *in vitro*.**

Representative flow cytometry plots (n = 3) of naïve T-cells (CD4<sup>+</sup>CD25<sup>-</sup>CD44<sup>lo</sup>CD62L<sup>hi</sup>) cultured *in vitro* under polarising conditions for Th17 cells (TGF $\beta$  (1 ng/mL), IL-23 (20 ng/mL), IL-6 (50 ng/mL), sIL-6R (100 ng/mL), and anti-IL-2 (10 ng/mL) in the presence of the two inactivating cs-130Fc variants (10 nM), as indicated, for 4 days. Th17 cell differentiation was determined by flow cytometry after stimulation with PMA, ionomycin and monensin for 4 hours.

### 5.3.3 Potency-enhancing mutations in sgp130 do not show any improvement in inhibitory selectivity towards IL-6 trans-signalling

Previous structure-function studies have identified the importance of T<sup>102</sup>, Q<sup>113</sup> and N<sup>114</sup> in recognition of IL-6/sIL-6R. These residues form part of the Site-III cytokine determinant region of gp130<sup>428</sup>. Selective mutation of these residues (T102Y, Q113F and N114L) were engineered into cs-130Fc to further improve the affinity towards IL-6/sIL-6R<sup>428</sup>. The resulting cs-130<sup>T102Y/Q113F/N114L</sup>Fc was expressed and purified by affinity chromatography by our collaborators (data not shown). Monomeric cs-130<sup>T102Y/Q113F/N114L</sup>Fc was then generated by TEV protease cleavage of the Fc fragment and isolated. To test its efficacy, I used the same approach and explored Th17 cells inhibition in the presence of cs-130<sup>T102Y/Q113F/N114L</sup>Fc (**Figure 5.8**). Monomeric cs-130<sup>T102Y/Q113F/N114L</sup>Fc efficiently inhibited murine Th17 cells *in vitro*, however, in comparison to sgp130Fc (IC<sub>50</sub>: 1.63 nM) and cs-130Fc variants (IC<sub>50</sub>: 0.66 and 2.53 nM), this inhibition was less efficient (IC<sub>50</sub>: 7.29 nM) (**Figure 5.8D**). This is a rather unexpected result, giving the success of this activity boosting variant in blocking IL-6 trans-signalling-induced proliferation of Ba/F3-sgp130 cells found in previous studies carried out by our collaborators (unpublished observations). Thus, a clear benefit of potency-enhancing sgp130 variant in preventing Th17 cells could not be identified in this system.

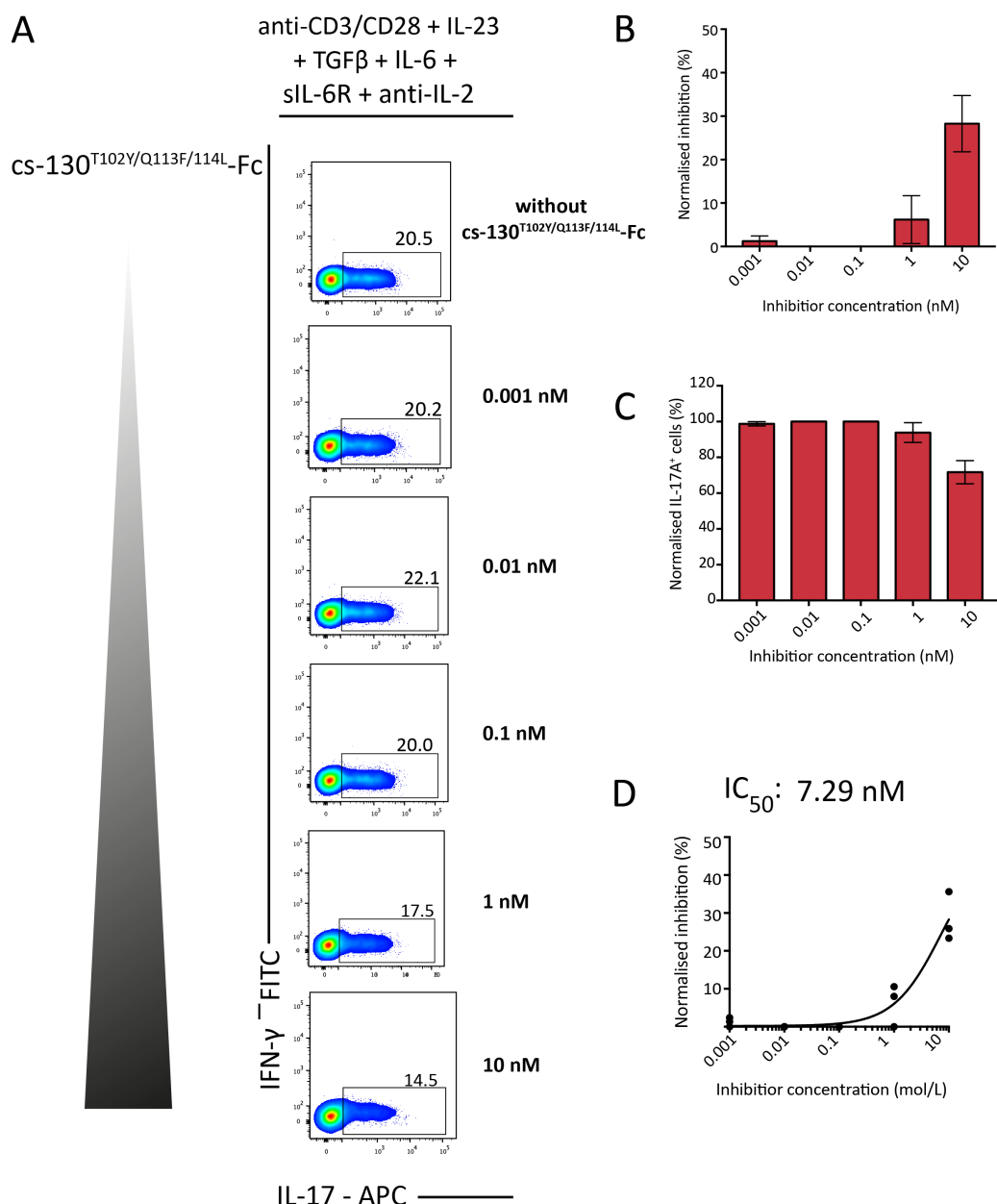


**Figure 5.8 Affinity-enhancing mutation did not improve the inhibitory capacity of cs-130Fc variants.**

**(A)** Representative flow cytometry plots ( $n = 3$ ) of naïve T-cells (CD4<sup>+</sup>CD25<sup>-</sup>CD44<sup>lo</sup>CD62L<sup>hi</sup>) cultured *in vitro* under polarising conditions for Th17 cells (TGF $\beta$  (1 ng/mL), IL-23 (20 ng/mL), IL-6 (50 ng/mL), sIL-6R (100 ng/mL), and anti-IL-2 (10 ng/mL) in the presence of increasing cs-130<sup>T102Y/Q113F/114L</sup>-Fc concentrations, as indicated, for 4 days. Th17 cell differentiation was determined by flow cytometry after stimulation with PMA, ionomycin and monensin for 4 hours. The % of inhibition **(B)** and IL-17A<sup>+</sup> cells **(C)**, were normalised to controls. **(D)** The concentration-dependent inhibitory dose-curve was plotted as the normalised percentage of inhibition, and effective concentration (IC<sub>50</sub>) value was calculated by nonlinear regression analysis, using the “inhibitor vs response (three parameters)” equation in Prism 7. Graphs present data from 1 independent experiment, error bars indicate SD.

### 5.3.4 Comparison of the effect of all the different cs-130Fc variants in preventing Th17 cell differentiation in *vitro* murine T-cell cultures

Figure 5.9 displays the summarise of the inhibitory capacity of the previously outlined miniaturised sgp130 variants in preventing the differentiation of IL-17A producing cells. Closer inspection of this figure shows that all the cs-130Fc variants inhibited Th17 cells in a dose-dependent manner, being cs-130Fc (in colour brown) the most potent inhibitor and cs-130T102Y/Q113F/114L-Fc the least. Taken together, this data highlights that novel class of chimeric soluble gp130-based IL-6 trans-signalling inhibitors successfully inhibited splenic differentiation of naïve T-cells into a Th17 phenotype *in vitro*, and that cs-130Fc was the most efficient fusion protein with an improved IC<sub>50</sub> value over sgp130Fc with regards to Th17 cells inhibition.

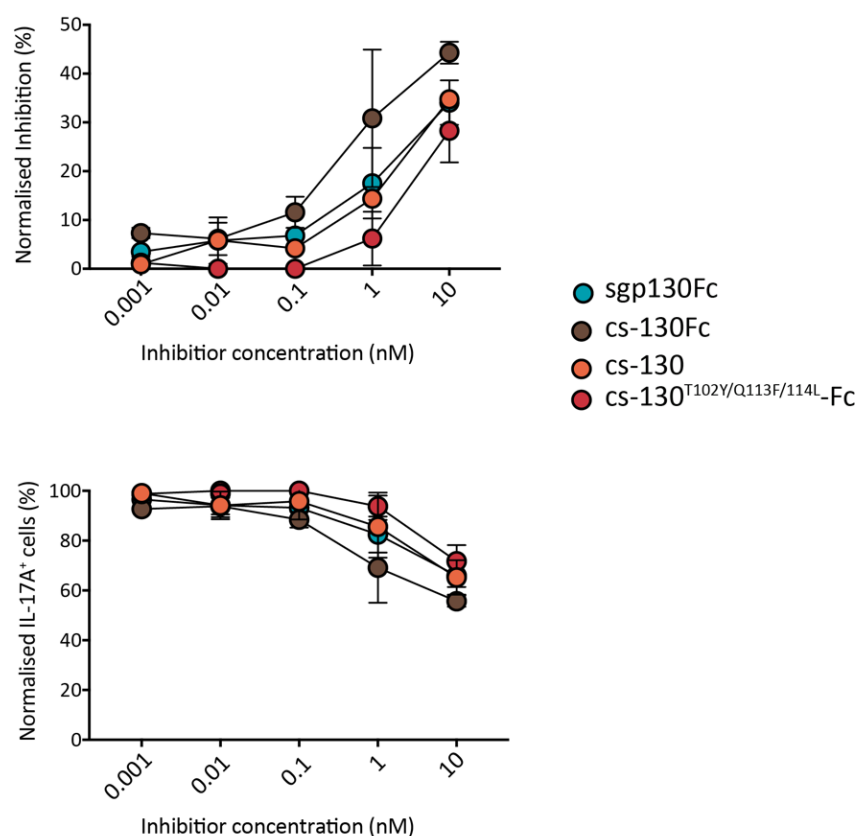


**Figure 5.9 Summary of the Th17 cells inhibitory capacity of cs-130Fc variants *in vitro*.**

Naïve CD4<sup>+</sup> T-cells (CD4<sup>+</sup>CD25<sup>-</sup>CD44<sup>lo</sup>CD62L<sup>hi</sup>) (n = 3) cultured *in vitro* under polarising conditions for Th17 cells (TGFβ (1 ng/mL), IL-23 (20 ng/mL), IL-6 (50 ng/mL), sIL-6R (100 ng/mL), and anti-IL-2 (10 ng/mL) in the presence of increasing inhibitor concentrations, as indicated, for 4 days. Th17 cell differentiation was determined by flow cytometry after stimulation with PMA, ionomycin and monensin for 4 hours. The % of inhibition and IL-17A<sup>+</sup> cells were normalised to controls. Error bars indicate SD.

## 5.4 Discussion

Therapeutic agents targeting excessive IL-6-signalling are effective in RA <sup>303</sup>. Currently, there are several monoclonal antibodies directed against IL-6 or its  $\alpha$ -receptor approved for therapeutic applications <sup>216,303</sup>. These biological drugs typically target the binding of IL-6 to IL-6R (e.g., siltuximab, tocilizumab) or target the interaction of IL-6 with sgp130 (e.g., olokizumab) and fail to distinguish between the biological activities of classical IL-6 receptor signalling and IL-6 trans-signalling. Recent advances suggest that IL-6 trans-signalling is the primary driver of IL-6 responses in local pathology (e.g., the inflamed synovium during RA) and selective targeting of this mode of signalling may help alleviate some of the confounding contradictions associated with the broader spectrum IL-6 blockers. This concept has led to the development of olamkicept, which is currently in Phase-II clinical trials and selectively targets IL-6 trans-signalling <sup>421</sup>.

Several different endogenous soluble isoforms of sgp130, implicated in the regulation of IL-6-type cytokine signal transduction, have been detected in human serum <sup>422,431–433</sup>. Sgp130Fc acts as a potent IL-6 signalling inhibitor that is mostly restricted to the trans-signalling pathway <sup>227</sup>; thereby, sgp130Fc is considered a potential therapeutic molecule for the treatment of IL-6 trans-signalling related diseases. Moreover, studies have shown that sgp130Fc does not impact the regulation of bacterial and viral infections or the control of C-reactive protein (CRP), which is recognised as the prototypical acute phase reactant <sup>421</sup>. Importantly, sgp130Fc can also have an influence on signalling induced by other IL-6 family cytokines, especially IL-11, since both IL-6 and IL-11 form a ternary complex composed of cytokines, a receptor and the sgp130 <sup>228</sup>.

Studies investigated the inhibitory effect of cs-130 variants surpassing the effect of sgp130Fc in an *in vitro* Th17 cell expansion assay. These novel inhibitors were size-reduced variants of sgp130Fc with no IL-11 trans-signalling inhibition and improved activity and selectivity for IL-6 trans-signalling, due to the previously shown inverse correlation for antibodies between tissue penetration and molecular weight <sup>425</sup>. Therefore, since the large size of sgp130Fc may limit tissue penetration, smaller variants of sgp130 were characterised regarding their inhibitory profiles <sup>226,227,422</sup>. To reconstitute sgp130Fc like activity in cs-130Fc variants, domains D1-D3 of sgp130 were fused to a sdAb recognising the IL-6/sIL-6R complex. All

miniaturised chimeric sgp130 variants were biologically active, and c<sub>GFP</sub>S-130Fc mimic the sgp130RAPS isoform.

Due to its potential in blocking IL-6 trans-signalling sgp130Fc was optimised in the past to improve stability and binding affinities for IL-6<sup>428</sup>. Several mutations at IL-6 binding sites II and III were described to improve binding affinities towards IL-6, resulting in improved biological activity<sup>428</sup>. Sgp130Fc has also been described to inhibit IL-6 mediated Th17 cell expansion in disease models of RA<sup>434</sup>. In line with these findings, we observed a more potent inhibitory effect of cs-130 variants in an in preventing Th17 cell expansion *in vitro*. Here, we show for the first time that these inhibitory proteins had a dose-dependent effect on Th17 cell proliferation. Comparison of IC<sub>50</sub> values between cs-130Fc and sgp130Fc demonstrated a 2.5-fold improvement of IC<sub>50</sub> in cs-130Fc inhibitory capacity. However, incorporation of a triple mutation at site II in cs-130<sup>T102Y/Q113F/N114L</sup>Fc variants did not further improve Th17 cells inhibition. Thus, these early studies suggest that cs-130Fc variants may be superior to sgp130Fc in terms of pharmacological inhibition of Th17 cell formation concerning activity and selectivity.

Th17 cells play a role in the pathogenesis of inflammatory arthritis. For example, IL-17A promotes the expression of inflammatory cytokines (e.g., TNF- $\alpha$ , IL-6), matrix metalloproteinases that contribute to cartilage degradation, and RANKL that is essential for the differentiation of osteoclasts and subsequent bone resorption<sup>118,435</sup>. This initial *in vitro* T-cell approach, where the efficacy of each drug was tested with a Th17 cell-based system, gave us some indications on the potential application of these agents *in vivo*. Future experiments will, therefore, evaluate the effect of these inhibitors on the severity of arthritis in a model of antigen-induced arthritis.

In summary, this chapter provides proof-of-concept studies reporting that miniaturised fusion proteins of sgp130 and a single-domain antibody against IL-6/sIL-6R displayed comparable and some even improved Th17 cell inhibition than sgp130Fc. Such variants may be beneficial for the physiological and pathophysiological dissection of IL-6 family cytokine signalling modes. Furthermore, there are possible therapeutic applications of cs-130Fc variants due to their selective inhibition of IL-6 trans-signalling and relatively small size.

## 6 Negative regulation of CRTAM by IL-6 and IL-27 in inflammatory arthritis

---

### 6.1 Background

The pathogenesis of inflammatory arthritis is multifactorial, involving complex interactions between genetic, epigenetic and environmental components. In recent years, it has become increasingly clear that many aspects of autoimmune inflammation are T-cell mediated <sup>110</sup>. Specifically, autoreactive CD4<sup>+</sup> T-cells play a dominant role in initiating and controlling specific immune responses relevant to the development of synovitis and destruction of the cartilage and bone in inflammatory arthritis <sup>274</sup>. A central function of CD4<sup>+</sup> T-cells in the pathogenesis of the disease has also been deduced from the RNA-seq analyses I performed in joints of AIA mice previously outlined in **Chapter 3**. Changes in the survival, proliferation and effector properties of T-cells are regulated by cytokines that signal through the JAK/STAT pathway (discussed in more detail in **Chapter 1, Section 1.3**).

Our research group has recently generated a transcriptomic profile of IL-6 responses in naïve, activated, and memory CD4<sup>+</sup> T-cells to determine whether T-cell subsets adopt different IL-6 signalling properties within the inflamed joint. The findings of this study have allowed us to examine the differences between these T-cell subsets in their ability to respond to antigen and to investigate the relationships between TCR activation and IL-6 signalling through STAT1 and STAT3 transcription factors, linked with the control of these responses <sup>194</sup>. These studies reiterated the importance of IL-6 as a lymphokine and also identified several genes that were negatively regulated by IL-6 in activated naïve CD4<sup>+</sup> T-cells. One target identified in this analysis was *Crtam* (**Figure 6.1**). Experiments outlined within this Chapter examined the negative regulation of *Crtam* by IL-6 and focused on the potential role *Crtam* may play in inflammatory arthritis.

Class I-restricted T-cell associated molecule (CRTAM; also known as cytotoxic and regulatory T-cell molecule or CD355) <sup>436</sup>, is an immunoglobulin-like cell surface protein that was originally identified in 2000 as one of the most abundant transcripts expressed by murine natural killer T-cells (NKT) <sup>437</sup>. Subsequent studies have since shown that CRTAM is transiently expressed on both mouse- and human- activated natural killer cells (NK), CD8<sup>+</sup>

and CD4<sup>+</sup> T-cells<sup>438–443</sup>. Whilst these studies support a prominent role for CRTAM in immune regulation by adaptive immune cells, other studies have demonstrated that CRTAM is also present on the lateral membrane of epithelial cells<sup>444</sup>. Thus, CRTAM may play essential roles in the initiation of cell-to-cell-interactions. In this respect, CRTAM displays structural features resembling proteins found within the nectin-like family of adhesion molecules. While members of the nectin-family typically contain three immunoglobulin (Ig) domains, a single transmembrane helix and an intracellular domain, CRTAM comprises two Ig domains and a class-I PDZ binding domain (which is a common structural domain of 80-90 aa found in signalling proteins); making CRTAM structurally distinct from the rest of the family<sup>445</sup>.

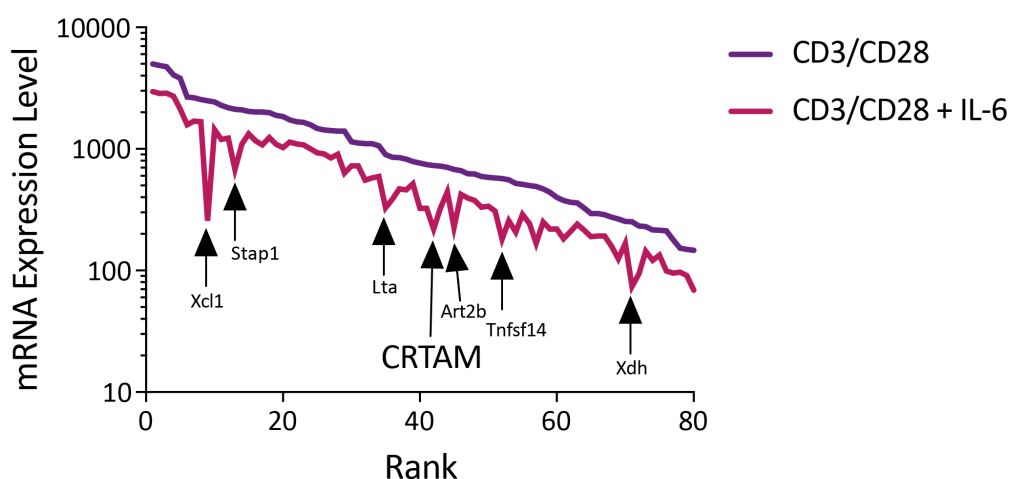


**Figure 6.1 Microarray data analysis showing downregulated genes upon IL-6 stimulation.**

Microarray expression data are presented for CD4<sup>+</sup> CD25<sup>-</sup> CD44<sup>lo</sup> CD62L<sup>hi</sup> CD127<sup>hi</sup> naïve T-cells ( $n = 3$ ) from the spleen of wild-type mice treated with anti-CD3 and anti-CD28 antibodies and 20 ng/mL IL-6 for 6 hours. The analysis was confined to the top 80 genes displaying both a relative signal intensity of  $> 150$  and  $> 1.5$ -fold alteration in expression after IL-6 treatment ( $p < 0.05$ ). All genes are ranked in decreasing order of expression at baseline under anti CD3/CD28 conditions. Data provided as a courtesy of Dr Jason Twohig, Cardiff University.

Only one CRTAM ligand has so far been described, the cell adhesion molecule 1 (CADM1; also known as nectin-like family member 2, NECL2 and tumour suppressor in lung cancer- 1, TSLC1)<sup>442</sup>. Nectin-like proteins (Necls) are immunoglobulin (Ig)-like cell adhesion molecules (CAMs) that contribute to the formation of cell-cell adhesions and have central roles regulating cellular activities such as cell movement, differentiation, proliferation and survival, and helping with the morphogenesis of numerous tissue types<sup>446</sup>. CADM1 is



expressed on epithelial cells, tumour cells, neurons and CD8 $\alpha$  DCs and functions as an immune surveillance regulator and tumour suppressor<sup>442</sup>. Binding of CRTAM to the CADM1 receptor strengthens NK cell and CD8<sup>+</sup> T-cell effector functions and is critical for the retention and proliferation of antigen-specific cytotoxic T-cells within the draining lymph nodes (LNs)<sup>447</sup>. Together with the cell-polarity protein, Scrib, CRTAM promotes activities linked to the late-phase polarisation of effector CD4<sup>+</sup> T-cells. CD4<sup>+</sup>CRTAM<sup>+</sup> T-cells have the characteristics of both CD4<sup>+</sup> and CD8<sup>+</sup> T-cells and express cytotoxic T-cell related genes, such as eomesodermin (Eomes), Granzyme B and perforin, and directly kill target cells. Moreover, CRTAM has been reported as a marker of CD4 cytotoxic T-cells (CTL)<sup>448</sup>. Furthermore, CRTAM<sup>-/-</sup> T-cells display reduced T-cell proliferation and decreased IL-22, IL-17 and IFN- $\gamma$  production<sup>449</sup>. Thus, the engagement of CRTAM supports activities linked with the control of T-cell effector characteristics.

IL-6 is essential for the generation of adaptive immunity and is therapeutically inhibited by biological drugs typically used in the treatment of inflammatory arthritis and other related diseases. However, some patients do not respond adequately to treatment and hence the urgent need to identify more reliable biomarkers to detect early stages of the disease and individualise therapy. Studying genes that change in T-cells as a response to IL-6 is, therefore, an exciting area of investigation. Although an increasing number of publications demonstrate the importance of CRTAM in regulating T-cell effector characteristics, less is currently known about how cytokines regulate CRTAM.

## 6.2 Aims

Previous studies have implicated roles of CRTAM in various inflammatory and pathogenic processes, including autoimmunity<sup>450,451</sup>. In addition, an association between CRTAM and IL-6/STAT3 signalling in the mucosa of colitic mice has also been reported<sup>452</sup>. However, at the time of conducting experiments for this thesis, no specific link of CRTAM with rheumatoid arthritis disease had been published. It was hypothesised in this Chapter that CRTAM would be present in the mouse synovium, actively participating in the regulation of inflammation.

The experiments described in this Chapter aimed to determine the role of CRTAM in synovitis. Specifically, studies:

- Characterised the presence of CRTAM<sup>+</sup> CD4<sup>+</sup> T-cells within the joint of mice with antigen-induced arthritis (AIA).
- Investigated the role of IL-6 and IL-27 on CRTAM expression in CD4<sup>+</sup> T-cells within the inflamed synovial tissue and the mechanism of CRTAM regulation.
- Examined CRTAM expression in synovial joint from patients with rheumatoid arthritis.
- Explored cell-cell interactions between CRTAM and its receptor CADM1 - specific to the engagement of T-cells with DCs, in the context of inflammatory arthritis.

## 6.3 Results

### 6.3.1 Exploring the regulation of inflammatory synovitis by IL-27 and IL-6 in AIA

IL-6 and IL-27 are members of a cytokine family (referred to as gp130-related cytokines) that signal through a cytokine receptor system containing a ligand-specific  $\alpha$ -receptor and the signal-transducing receptor gp130. Engagement of this receptor system activates the JAK/STAT pathway and the STAT1 and STAT3 transcription factors<sup>189</sup>. While IL-6 and IL-27 often elicit opposing biological activities in T-cells, their ability to control T-cell responses through STAT1 and STAT3 is essential in shaping the effector characteristics of CD4<sup>+</sup>T- cells<sup>143,189,205,375</sup> (described in more detail in **Chapter 1, Section 1.3.2**). IL-6 and IL-27 are key regulators of CD4<sup>+</sup> effector T-cell function during AIA. IL-6 deficiency protects from the development of synovitis and cartilage damage in murine models of inflammatory arthritis<sup>204,241,251</sup>. However, *Il27ra*<sup>-/-</sup> mice display exacerbated disease severity, and synovitis includes the formation of ELS<sup>104</sup>.

Based on our transcriptomic analysis of CD4<sup>+</sup> T-cells activated in the presence of IL-6, we identified *Crtam* as a gene negatively regulated by IL-6. Since IL-6 and IL-27 often counteract each other's activities, we looked at CRTAM regulation in *Il6ra*<sup>-/-</sup> and *Il27ra*<sup>-/-</sup> mice that display different forms of synovitis and therefore, provided an excellent model to assess severity of inflammation. Consequently, AIA was established in C57BL/6 WT, *Il6ra*<sup>-/-</sup>, and *Il27ra*<sup>-/-</sup> mice through immunisation with mBSA (fully described in **Chapter 2, Section 2.3**). As expected, histological assessment of the joint sections at day 10-post arthritis induction revealed exacerbated synovitis and the presence of ELS in the joints of *Il27ra*<sup>-/-</sup> mice (**Figure 6.2A**). In contrast, *Il6ra* deficient mice displayed a low level of synovial inflammation (**Figure 6.2A**). For example, the presence of leukocyte infiltrates in the inflamed synovium was notably reduced in *Il6ra*<sup>-/-</sup> mice, while joints from *Il27ra*<sup>-/-</sup> mice displayed an important increase compared to WT mice (**Figure 6.2B**). The overall joint histopathology or arthritic index (AI), which correlates to disease severity, was significantly increased in *Il27ra*<sup>-/-</sup> and decreased in *Il6ra*<sup>-/-</sup> mice. (**Figure 6.2C**). Therefore, induction of AIA in my research was consistent with formerly reported roles for IL-27 and IL-6 in synovial histopathology regulation and provided stable mouse models to investigate the presence of CRTAM in the discrete synovial pathologies observed in these mice.

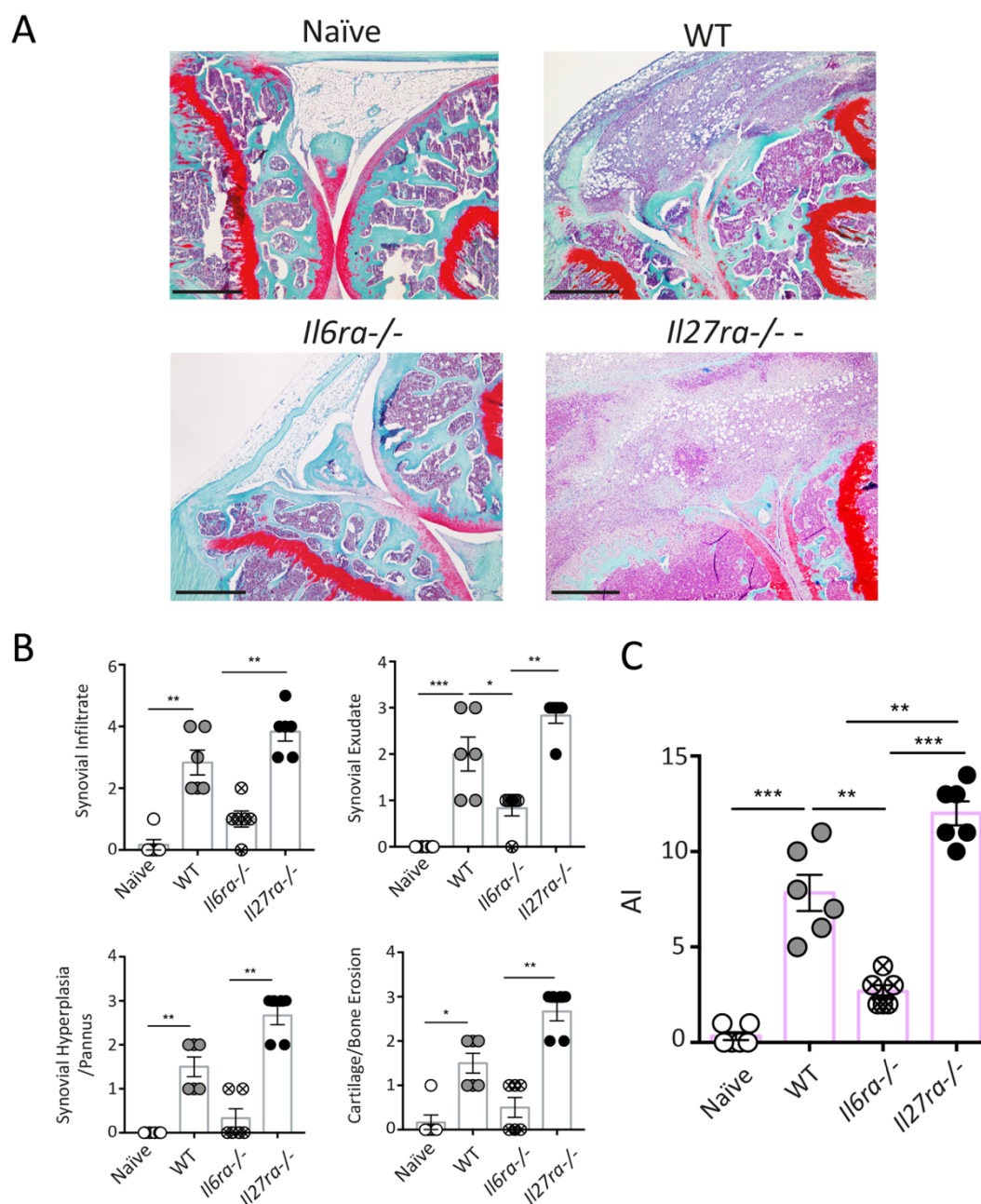


**Figure 6.2 Joint histopathology of AIA in WT, *IL27ra*<sup>-/-</sup> and *IL6ra*<sup>-/-</sup> mice.**

**(A)** Representative images of haematoxylin and safranin O staining of mouse knee joints at day-10 post-AIA induction. **(B)** Histopathology scoring of AIA in WT, *Il27ra*<sup>-/-</sup> and *Il6ra*<sup>-/-</sup> mice, showing synovial infiltrate, exudate, hyperplasia/pannus and cartilage/bone erosion at day-10 post arthritis induction ( $n = 5-6/\text{group}$ ). **(C)** The aggregate score for all parameters in B is presented as an arthritic index (AI) for each mouse genotype ( $n = 5-6/\text{group}$ ). Non-inflamed (naïve) WT control joints are shown on the left. Unchallenged joints in *Il6ra*<sup>-/-</sup> and *Il27ra*<sup>-/-</sup> mice are comparable to non-inflamed (naïve) WT. Graphs indicate mean  $\pm$  SEM. \*,  $p < 0.05$ ; \*\*,  $p < 0.01$ ; \*\*\*,  $p < 0.001$ . Shapiro-Wilk normality test and a one-way ANOVA, Turkey's multiple comparisons test (parametric tests), or a Kruskal-Wallis test, Dunn's multiple comparisons test (non-parametric tests) were used. Scale bars: (A) 600  $\mu\text{m}$ .

### 6.3.2 CRTAM expression during active arthritis is associated with disease severity

Recent studies have highlighted a correlation between CRTAM and disease outcome in pathological processes including infectious and allergic diseases, cancer and autoimmune conditions, such as type 1 diabetes (T1D), lupus, intestinal colitis or experimental autoimmune encephalomyelitis (EAE)<sup>441,448,451,453</sup>. To investigate whether CRTAM<sup>+</sup> T-cells were present in the inflamed joint, CRTAM expression was evaluated by IHC using sections derived from WT, *Il6ra*<sup>-/-</sup>, and *Il27ra*<sup>-/-</sup> mice with AIA. CRTAM<sup>+</sup> cells were detected throughout the inflamed synovium, and consistent with its expression on T-cells, CRTAM staining colocalised with the pan T-cell marker CD3 in serial sections (**Figure 6.3A, C**). Importantly, CRTAM expression was particularly evident in both WT and *Il27ra*<sup>-/-</sup> mice, while *Il6ra*<sup>-/-</sup> mice displayed a low level of synovial infiltrate with limited CRTAM expression (**Figure 6.3A**). IHC quantification of CD3 staining closely reflected the severity of joint inflammation and was most prominent within the inflamed synovium of *Il27ra*<sup>-/-</sup> mice. Consistent with previous studies where the development of synovial ELS was observed in *Il27ra*<sup>-/-</sup> mice<sup>104</sup>, dense aggregates of CD3<sup>+</sup> T-cells were identified in the inflamed synovium of these mice (**Figure 6.3A, B**). Evidence of CRTAM staining was particularly prominent within sites of ELS in synovial tissue from *Il27ra*<sup>-/-</sup> mice, which are known to be T-cell-rich<sup>104</sup>. Conversely, *Il6ra*<sup>-/-</sup> mice showed limited CRTAM expression. Here, the detection of CRTAM correlated with the degree of joint inflammation and damage in AIA (**Fig. 6.3B, C**).

CADM1, a marker for DCs, has been reported to be CRTAM natural receptor. Together they participate in the cross-talk between antigen-presenting cells and cytotoxic lymphocytes, playing a critical role in the initiation and the maintenance of immune responses<sup>442</sup>. Consistent with CRTAM immunohistochemical staining, *Crtam* mRNA transcripts in the inflamed synovium were upregulated at day-3 in WT AIA joints and were significantly increased in *Il27ra*<sup>-/-</sup> joints. Moreover, there was a significant reduction in *Crtam* expression in *Il6ra*<sup>-/-</sup> joints (**Figure 6.4A**). Interestingly, *Crtam* expression was enriched in the joint at day-3 but not at day-10 in WT AIA joints (**Figure 6.4A**). On the other side, while *Crtam* expression was elevated at the acute phase of inflammatory arthritis, *Cadm1* expression was downregulated in WT, *Il27ra*<sup>-/-</sup> and *Il6ra*<sup>-/-</sup> joints at day-3 and -10, which may be due to a proportional change in the number of resident *Cadm1* expressing cells (**Figure 6.4B**). Additionally, although *Cadm1* is also expressed in the inflamed joint, it shows no dependency on IL-6 or IL-27 control (**Figure 6.4B**). Together, these results demonstrated the presence of



CRTAM and CADM1 within the inflamed synovial tissue and suggested a regulatory role of IL-6 and IL-27 in the expression of CRTAM, but not in CADM1 expression in experimental arthritis.

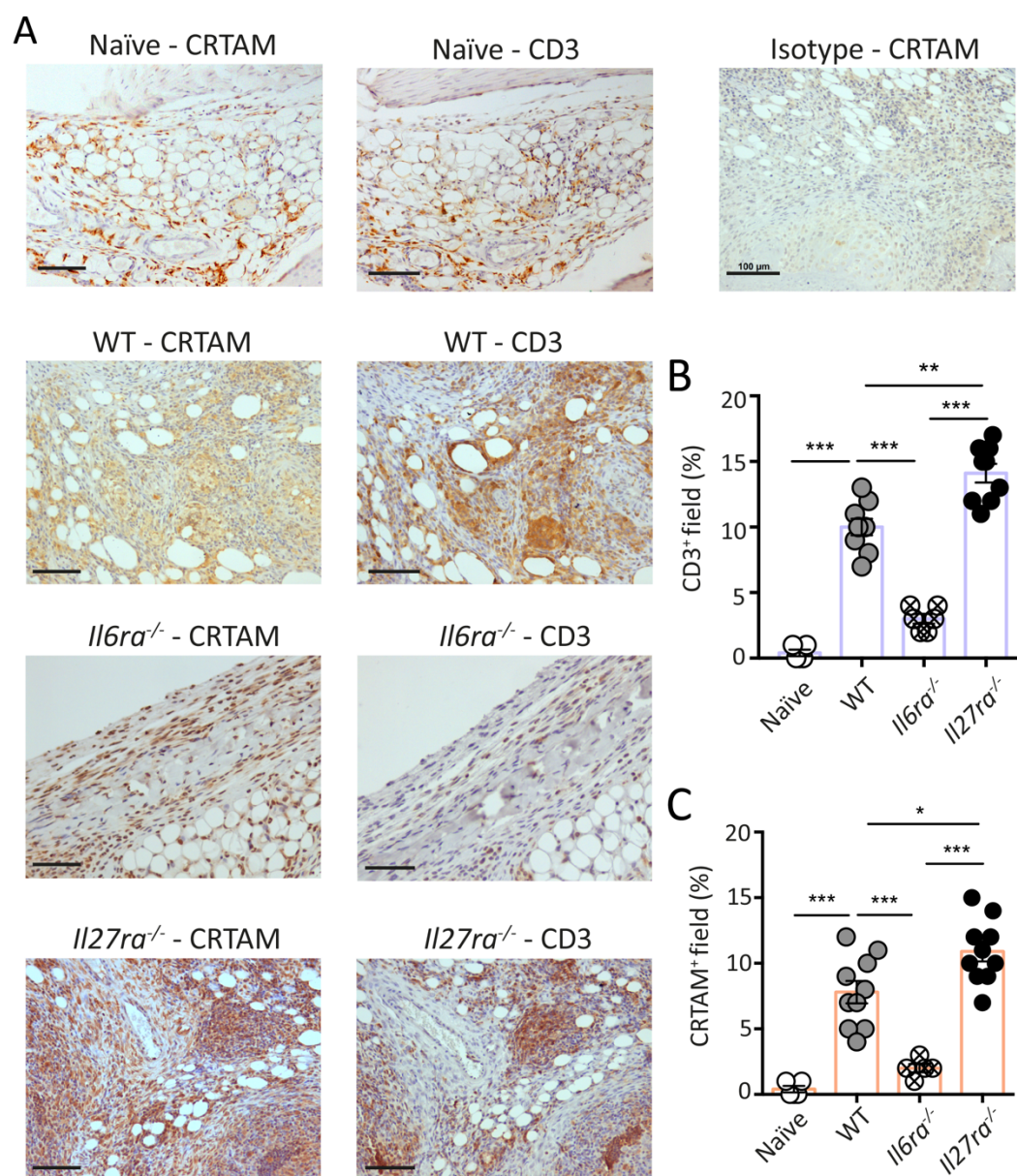


**Figure 6.3 CRTAM is expressed in the joints of mice with AIA and correlates with synovial pathology.**

**(A)** AIA was established in WT, *Il6ra*<sup>-/-</sup> and *Il27ra*<sup>-/-</sup> mice and histopathology assessed at day-10 post- arthritis induction. Sequential sections were stained as indicated by IHC: CRTAM stained sections are shown on the left column and CD3 stained sections on the right column. Isotype control for CRTAM is shown in the upper right corner. Quantification of CD3 **(B)** and CRTAM **(C)** staining was carried out ( $n = 5-11/\text{group}$ ). Sections from naïve (no AIA WT) joints were used as a negative control for both staining and scoring quantification. Error bars indicate SEM. \*,  $p < 0.05$ ; \*\*,  $p < 0.01$ ; \*\*\*,  $p < 0.001$ . Shapiro-Wilk normality test and a one-way ANOVA, Turkey's multiple comparisons test were used. Scale bars: (A) 100  $\mu\text{m}$ .

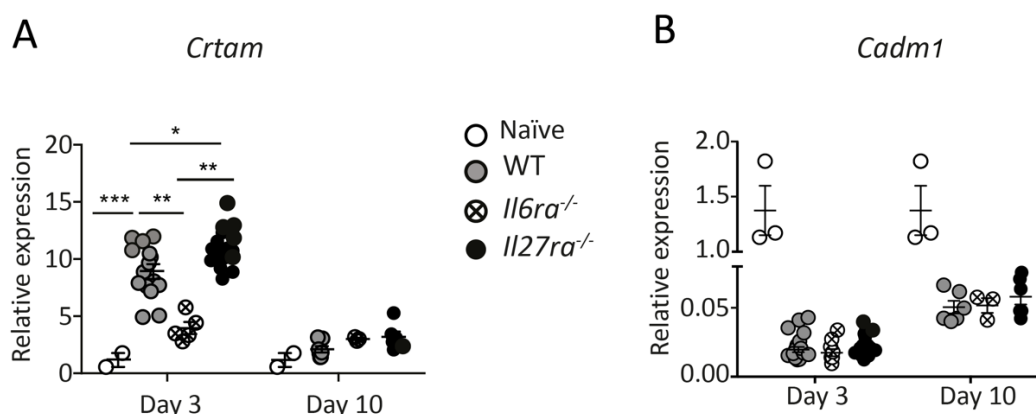


**Figure 6.4** *Crtam* and its binding molecule, *Cadm1* are expressed in the inflamed joint, but *Cadm1* shows no dependency on IL-6 or IL-27 control.

Synovial joint tissue from the knee joints of naïve (no AIA WT), WT, *Il6*<sup>-/-</sup> and *Il27ra*<sup>-/-</sup> mice with AIA were collected at day 3 and day 10, and mRNA expression of *Crtam* (**A**) and *Cadm1* (**B**) genes was assessed by qPCR. (n = 2-20/group). Graphs indicate mean ± SEM. \*,  $p < 0.05$ ; \*\*,  $p < 0.01$ ; \*\*\*,  $p < 0.001$ . Shapiro-Wilk normality test and a one-way ANOVA, Turkey's multiple comparisons test were used. Data in this figure are from three independent experiments.

### 6.3.3 Synovial CRTAM is predominantly expressed in CD3<sup>+</sup> CD4<sup>+</sup> joint infiltrating T-cells

The immunohistochemical analysis of joint sections from mice with AIA showed co-localisation on CD3 T-cells and supported the presence of CRTAM<sup>+</sup> T-cells during synovitis (see Figure 6.3). To confirm CRTAM<sup>+</sup> expression on these cells and better characterise distribution between T-cell subsets and other leukocyte infiltrates, experiments next examined the expression of CRTAM on infiltrating leukocytes derived from the inflamed synovium of mice with arthritis. Briefly, synovial tissues were excised from the joints of mice with AIA (obtained at day-3 and day-10 post AIA) and treated with collagenase IV to facilitate the extraction of inflammatory cells for analysis by flow cytometry. Details of the gating strategy for CD3<sup>+</sup>CD4<sup>+</sup> cells using flow cytometry after digestion of the synovium are shown in Figure 6.5.

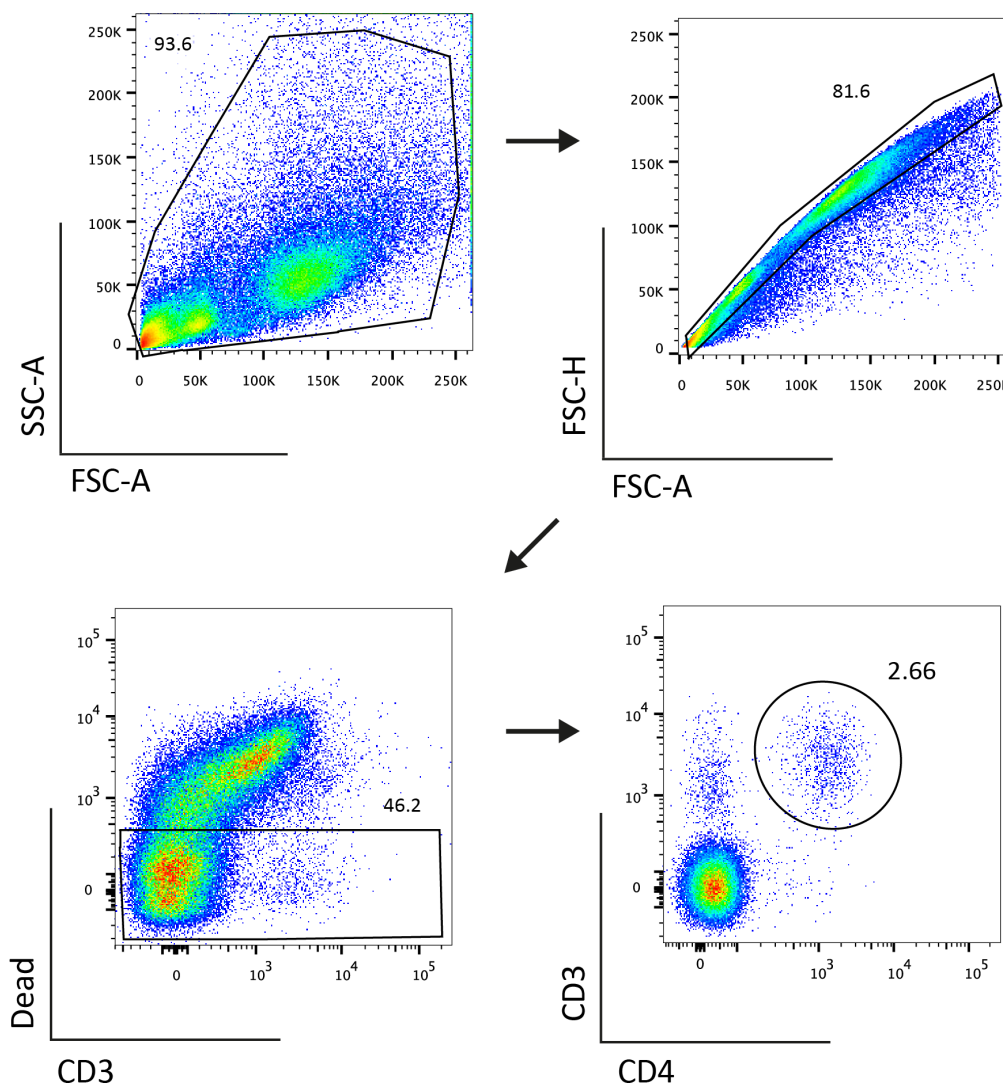


**Figure 6.5 Gating strategy for the characterisation of CRTAM secreting cells within the inflamed synovium of mice with AIA by flow cytometry.**

After collagenase digestion of the mouse synovium, all visible cells were gated based on characteristic forward, and side-scatter properties of lymphocytes, followed by exclusion of doublets, and dead cells. Subsequently, a clear and viable  $CD3^+ CD4^+$  population was identified. FSC-H – forward scatter-height; FSC-A – forward scatter-area; SSC-A – side scatter-area.



To determine the kinetics of CRTAM expression during acute experimental arthritis, CRTAM<sup>+</sup> cells in the inflamed synovium of mice were characterised at day-3 and day-10 post-AIA (**Figure 6.6**), to have a complete timeline of the expression of CRTAM in a model of experimental arthritis. At day-3 time point, approximately 3% of the total cells were CD3<sup>+</sup>CD4<sup>+</sup> compared to a 13% observed at day-10 post-AIA (**Figure 6.6A**). Similarly, the proportion of the CRTAM<sup>+</sup> population at both time points was suggestive that CRTAM<sup>+</sup> cells are more prominent within the total CD3<sup>+</sup> population at day-10 of AIA in both WT and *IL27ra*<sup>-/-</sup> mice (**Figure 6.6B**). Due to the paucity of infiltrates in *IL6ra*<sup>-/-</sup> mice, it was not possible to analyse the synovial infiltrate in these mice.

To determine which CD3<sup>+</sup> lymphocytic population expressed CRTAM within the inflamed synovium, antibodies for CD4, NK1.1, CD8 and  $\gamma\delta$ TCR were used to discriminate T-helper, natural killer, cytotoxic and  $\gamma\delta$  T-cells respectively (**Figure 6.6C**). Flow cytometric analysis identified a small subset of CRTAM<sup>+</sup> lymphocytes in the inflamed synovium of WT and *IL27ra*<sup>-/-</sup> mice with AIA. This analysis confirmed a greater proportion of CRTAM<sup>+</sup> lymphocytes in *IL27ra*<sup>-/-</sup> mice when compared to cells derived from WT mice. In both cases, the majority of CRTAM<sup>+</sup> cells were identified as CD4<sup>+</sup> T-cells (equating to 70% at day-3, and 80% at day-10 post-AIA). No other cell types were identified as expressing CRTAM (**Figure 6.7**). Overall, these data highlight CD3<sup>+</sup>CD4<sup>+</sup> T-helper cells as the main cells expressing CRTAM within the inflamed joint during AIA. This population of CD3<sup>+</sup>CD4<sup>+</sup>CRTAM<sup>+</sup> is increased at day-10 post arthritis induction as well as in the synovium of *IL-27ra*<sup>-/-</sup> mice.

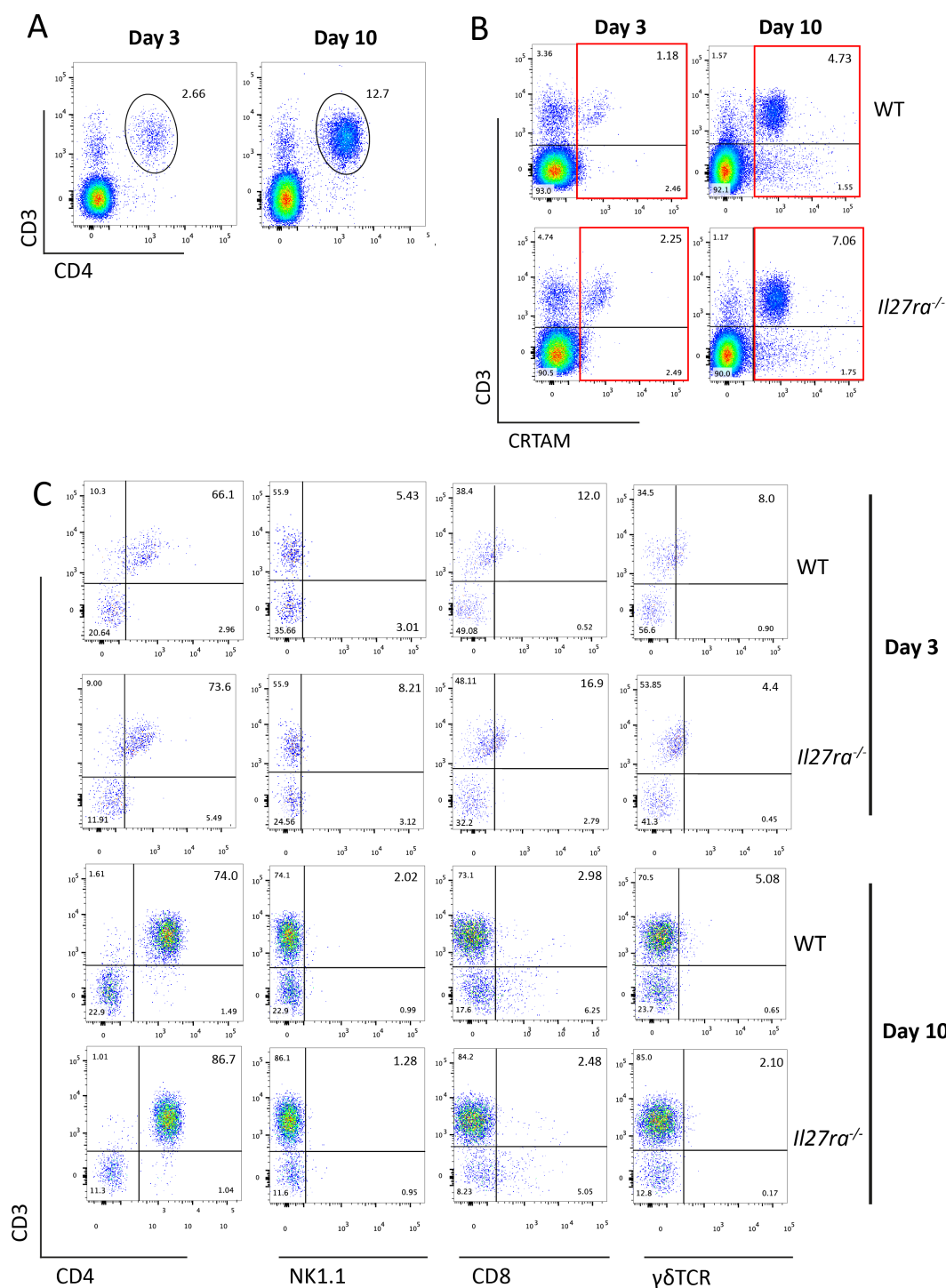


**Figure 6.6 Joint-infiltrating CD3<sup>+</sup> CD4<sup>+</sup> cells are the main CRTAM expressing cells in the synovium at day 3 and day 10 post arthritis induction.**

Flow cytometry analysis of joint infiltrating cells at day 3 and day 10 of AIA. **(A)** Inflamed synovium was digested in 1 mg/mL collagenase IV to isolate joint-infiltrating cells as described in **Material and Methods Section 2.3.4**. Successful isolation was determined by flow cytometric analysis of CD3<sup>+</sup>CD4<sup>+</sup> T-cells. **(B)** CD3<sup>+</sup>CRTAM<sup>+</sup> cells were gated in both WT and *Il27ra*<sup>-/-</sup> mice. **(C)** Representative flow cytometry plots gated on CRTAM<sup>+</sup> cells shown in a red box in panel B.

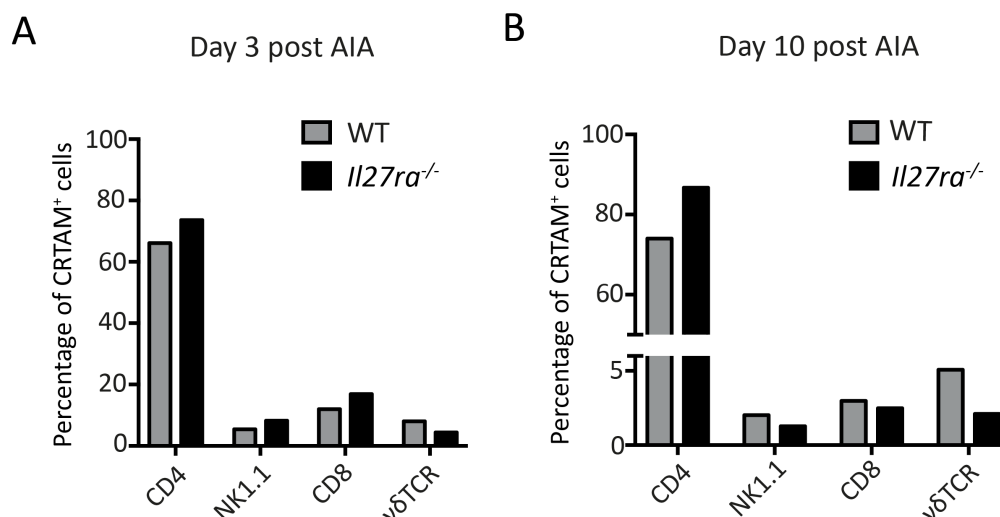


**Figure 6.7** The proportion of CD3<sup>+</sup>CD4<sup>+</sup>CRTAM<sup>+</sup> is increased at day 10 post arthritis induction as well as in the synovium of *Il27ra*<sup>-/-</sup> mice in both time points.

Cellular distribution of CRTAM-expressing cells within the inflamed joints of WT and *Il27ra*<sup>-/-</sup> mice shown as a percentage of total CRTAM<sup>+</sup> cells at day-3 (**A**) and day-10 (**B**) post-arthritis induction. WT, n = 1; *Il27ra*<sup>-/-</sup>, n = 1 (two independent biological repeats).

### 6.3.4 IL-6 and IL-27 inhibit CRTAM expression on naïve CD4<sup>+</sup> T-cells

To determine whether IL-6 and IL-27 directly regulate CRTAM in CD4<sup>+</sup> T-cells, based on our previous findings, I investigated CRTAM expression *in vitro*. Yeh, Sidhu and Chan <sup>449</sup>, initially reported that CRTAM is temporarily expressed on a subset of activated CD4<sup>+</sup> T-cells, and Takeuchi *et al.* <sup>448</sup> later confirmed that CRTAM is expressed on the surface of 2-5 % of splenic CD4<sup>+</sup> T-cells only after TCR stimulation. In fact, CRTAM protein is degraded by the proteasome in the absence of this stimulation <sup>450</sup>. To verify these observations, I purified splenic naïve CD4<sup>+</sup> T-cells (CD4<sup>+</sup>CD25<sup>-</sup>CD44<sup>lo</sup>CD62L<sup>hi</sup>) from WT mice and co-stimulated them with anti-CD3 and anti-CD28 antibodies (see **Section 2.1.2 of Material and Methods in Chapter 2** for details regarding spleen isolation and cell sorting). Cells were further stimulated in the presence and absence of 20 ng/mL IL-6 or IL-27, surface stained with a CRTAM antibody after 6, 9, 12, 18 and 24 hours of incubation, and finally assessed using flow cytometry. These time points were chosen based on the previously outlined temporal expression profile of CRTAM, which is known to be an early and transient activation molecule in CD4<sup>+</sup> T-cells, as determined by numerous research groups <sup>438,447,448,450</sup>. **Figure 6.8** provides an overview of the gating strategy for CD4<sup>+</sup> CRTAM<sup>+</sup> T-cells.

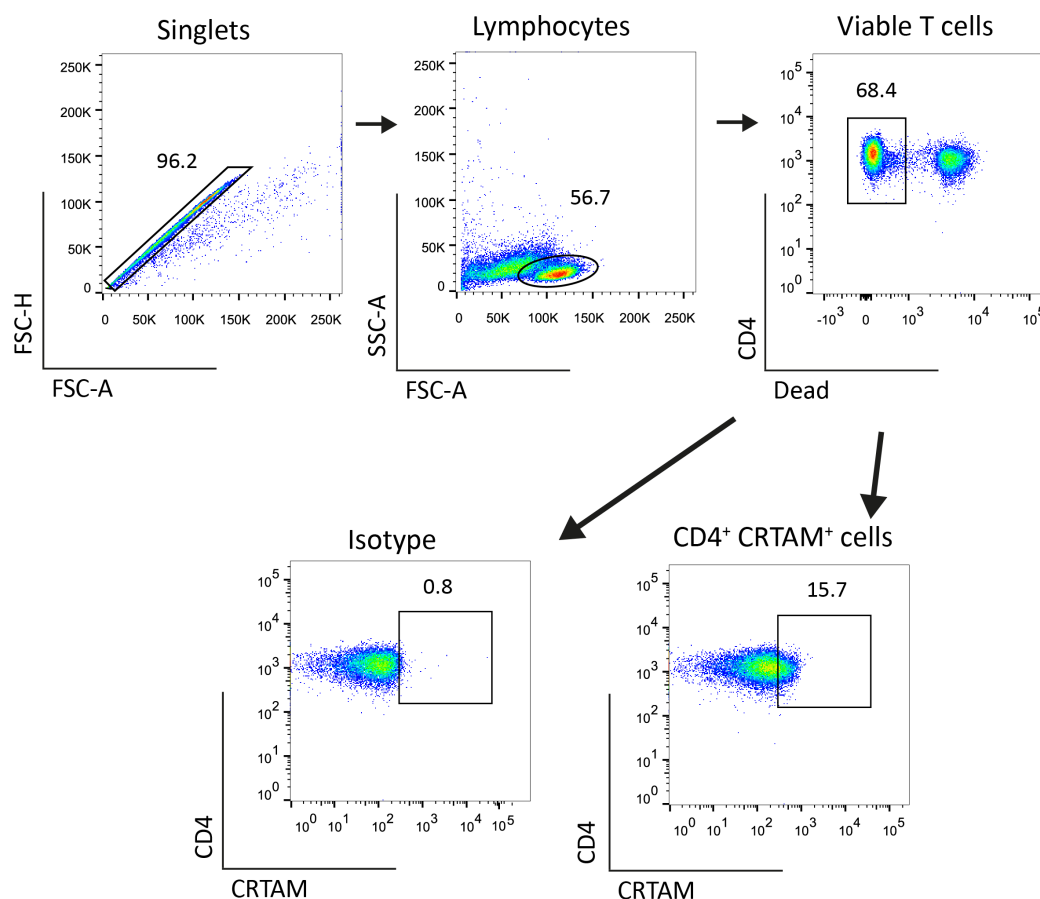


**Figure 6.8 Gating strategy for CD4<sup>+</sup> CRTAM<sup>+</sup> T-cells identification using flow cytometry.**

Naïve CD4<sup>+</sup> T-cells (CD4<sup>+</sup>CD25<sup>-</sup>CD44<sup>lo</sup>CD62L<sup>hi</sup>) were plated at  $1.5 \times 10^5$  cells/well in 96-well round-bottom plates pre-coated with anti-CD3 and anti-CD28 antibodies and were stimulated with rmlL- 6. After 18 hours, CD4<sup>+</sup> CRTAM<sup>+</sup> T-cells were assessed by flow cytometry: Doublets were excluded, and cells were then gated based on SSC and FSC. Live cells were gated, and CD4<sup>+</sup> CRTAM<sup>+</sup> T-cells were successfully identified using the isotype gating as a negative control. FSC-H – forward scatter-height, FSC-A – forward scatter-area; SSC-A – side scatter-area.

A small fraction of naïve CD4<sup>+</sup> T-cells expressed CRTAM upon stimulation (**Figure 6.9**). CRTAM was transiently expressed on naïve CD4<sup>+</sup> T-cells after TCR stimulation, which started after 6 hours post-activation, peaked at 18 hours, and by 24 hours post-activation CRTAM expression had started to dissipate (**Figure 6.9A**). CRTAM<sup>+</sup> cell population was considerably reduced after 72 hours, and there was hardly any detectable CRTAM expression on naïve CD4 T-cells after 96 hours post-TCR activation (data not shown). Co-treatment with either IL-6 or IL-27 significantly inhibited CRTAM expression. This inhibition was more prominent at 18 hours after TCR activation (approximately 50-60% inhibition compared to the unstimulated condition) (**Figure 6.9B**).

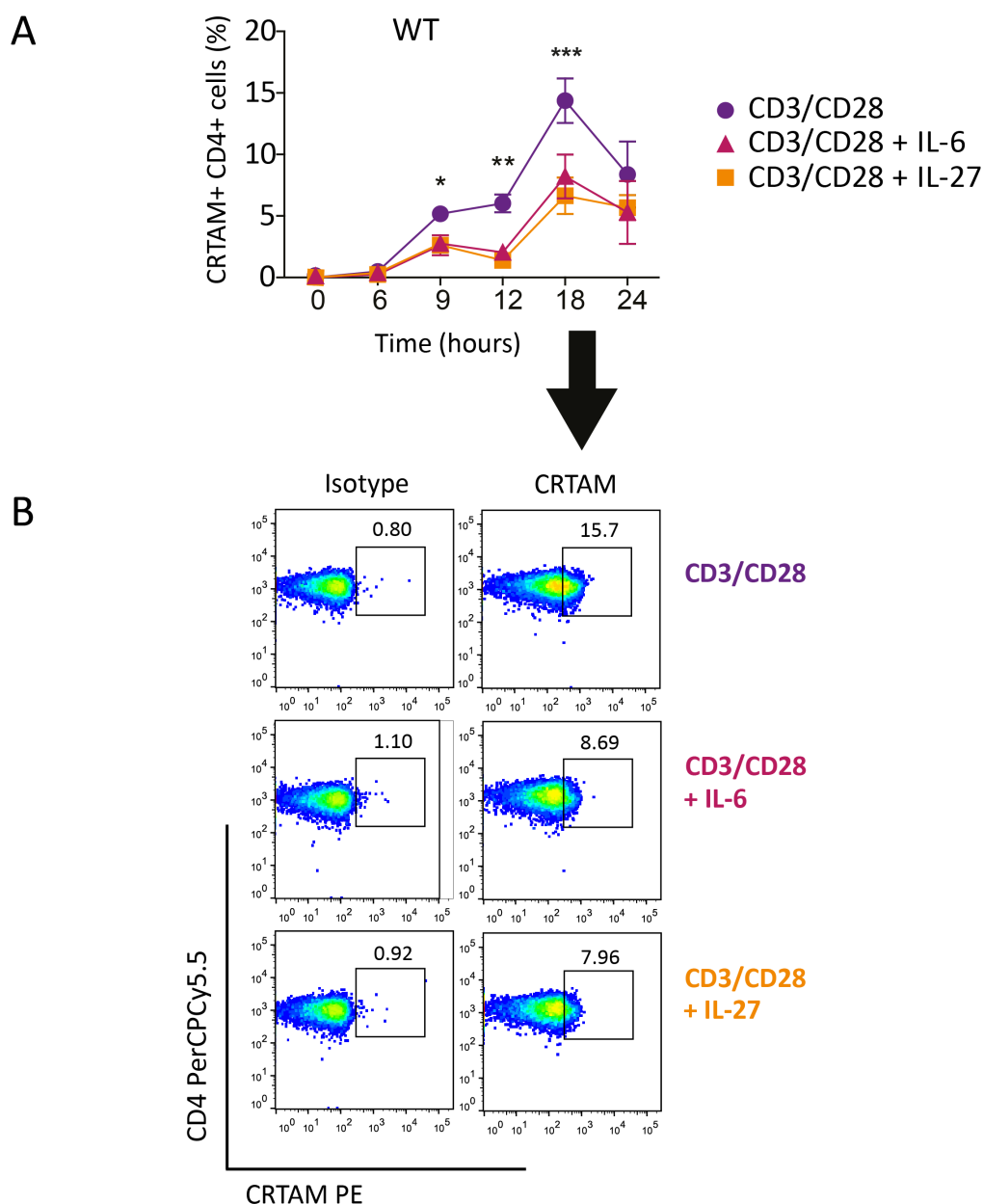


**Figure 6.9 CRTAM expression peaks at 18 hours after TCR activation in naïve CD4<sup>+</sup> T-cells from WT mice and is regulated by IL-6 and IL-27 *in vitro*.**

**(A)** Naïve CD4<sup>+</sup> T-cells (CD4<sup>+</sup>CD25<sup>-</sup>CD44<sup>lo</sup>CD62L<sup>hi</sup>) from WT mice were activated with anti-CD3 and anti-CD28 antibodies. Cells were stimulated with rIL-6, rIL-27 or neither; CRTAM expression was analysed by flow cytometry at the indicated time points (6, 9, 12, 18, 24 hours) ( $n = 3$ ). Data are from three independent experiments. Graphs indicate mean  $\pm$  SEM. \*,  $p < 0.05$ ; \*\*,  $p < 0.01$ ; \*\*\*,  $p < 0.001$ . Shapiro-Wilk normality test and a two-way ANOVA test were used. **(B)** Representative FACS plots of CD4<sup>+</sup> CRTAM<sup>+</sup> T-cells at 18 hours post-TCR activation, where CRTAM expression and IL-6 and IL-27-mediated CRTAM inhibition are the most pronounced.

To verify these findings regarding a role of IL-6/IL-27 in the regulation of CRTAM expression in naïve T-cells *in vitro*, I used the same approach with *Il6ra*<sup>-/-</sup> and *Il27ra*<sup>-/-</sup> mice and explored CRTAM inhibition 18 hours post-TCR activation (**Figure 6.10A**). Interestingly, in the absence of Interleukin 6 receptor (IL-6R) or interleukin 27 receptor (L-27RA), IL-6 and IL-27 lost their ability to block CRTAM expression. (**Figure 6.10B**).

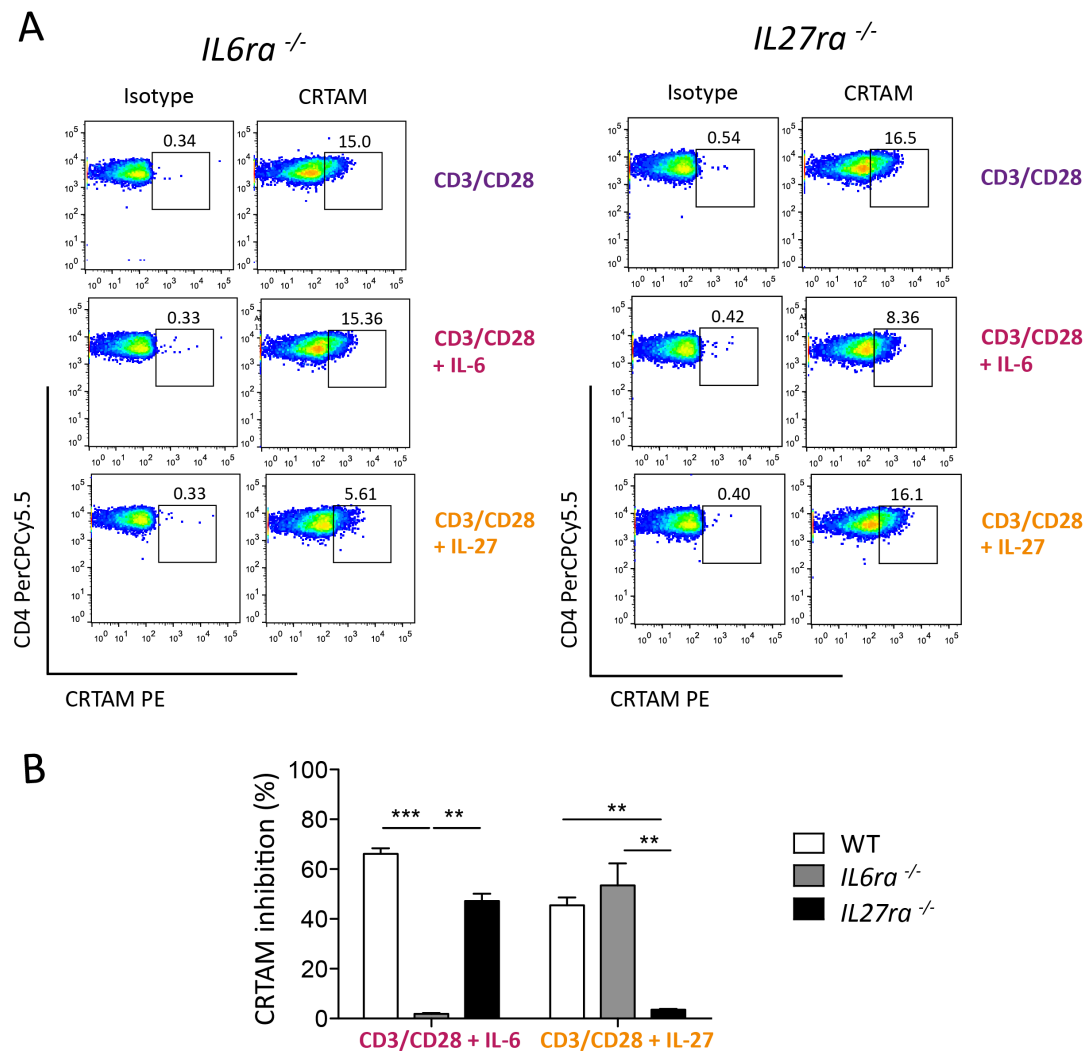


**Figure 6.10 CRTAM expression peaks at 18 hours after TCR activation in naïve CD4<sup>+</sup> T-cells from *Il6ra*<sup>-/-</sup> and *Il27ra*<sup>-/-</sup> mice and is regulated by IL-6 and IL-27 *in vitro*.**

(A) Representative FACS plots of CD4<sup>+</sup> CRTAM<sup>+</sup> T-cells from *Il6ra*<sup>-/-</sup> and *Il27ra*<sup>-/-</sup> mice at 18 hours post-TCR activation, where CRTAM expression and IL-6 and IL-27-mediated CRTAM inhibition are the most pronounced. (B) CRTAM inhibition by IL-6 and IL-27 in WT, *Il6ra*<sup>-/-</sup> and *Il27ra*<sup>-/-</sup> mice naïve CD4<sup>+</sup> T-cells, 18 hours after TCR activation, normalised against unstimulated controls (only CD3/CD8) (n = 3). Data are from two independent experiments. Graphs indicate mean ± SEM. \*, p < 0.05; \*\*, p < 0.01; \*\*\*, p < 0.001. Shapiro-Wilk normality test and a two-way ANOVA test, multiple comparisons, were used.

### 6.3.5 STAT3 signalling plays a major role in regulating CRTAM expression

IL-6/gp130 signalling through STAT3 has been shown to have a crucial role in directing leukocyte infiltration within the inflamed joint in experimental inflammatory arthritis<sup>204</sup>. Additionally, it has been demonstrated to be necessary for the survival and expansion of human synovial fibroblasts and therefore, for the pathogenesis of RA<sup>454</sup>. To identify signalling mechanisms employed by IL-6- and IL-27 to control CRTAM expression, studies were performed using naïve-CD4<sup>+</sup> T-cells derived from mice displaying enhanced gp130- mediated STAT1 and STAT3 signalling (*gp130<sup>F/F</sup>*)<sup>204,311</sup> (see **Section 2.3.1 of Material and Methods** in **Chapter 2** for details). When compared to TCR activated naïve CD4<sup>+</sup> T-cells from WT mice, naïve CD4<sup>+</sup> T-cells from *gp130<sup>F/F</sup>* mice displayed a similar profile of CRTAM expression in response to co-stimulatory anti-CD3 and anti-CD28 antibodies (**Figure 6.11A**). Treatment of activated naïve CD4<sup>+</sup> T-cells from *gp130<sup>F/F</sup>* mice with IL-6 or IL-27 contributed to a significant, stronger inhibition of CRTAM across the time course tested, and was evident at 6,9,12 and 18-hour time points (**Figure 6.11B**). Thus, enhanced gp130 receptor signalling contributes to the negative regulation of CRTAM in activated naïve CD4<sup>+</sup> T-cells.

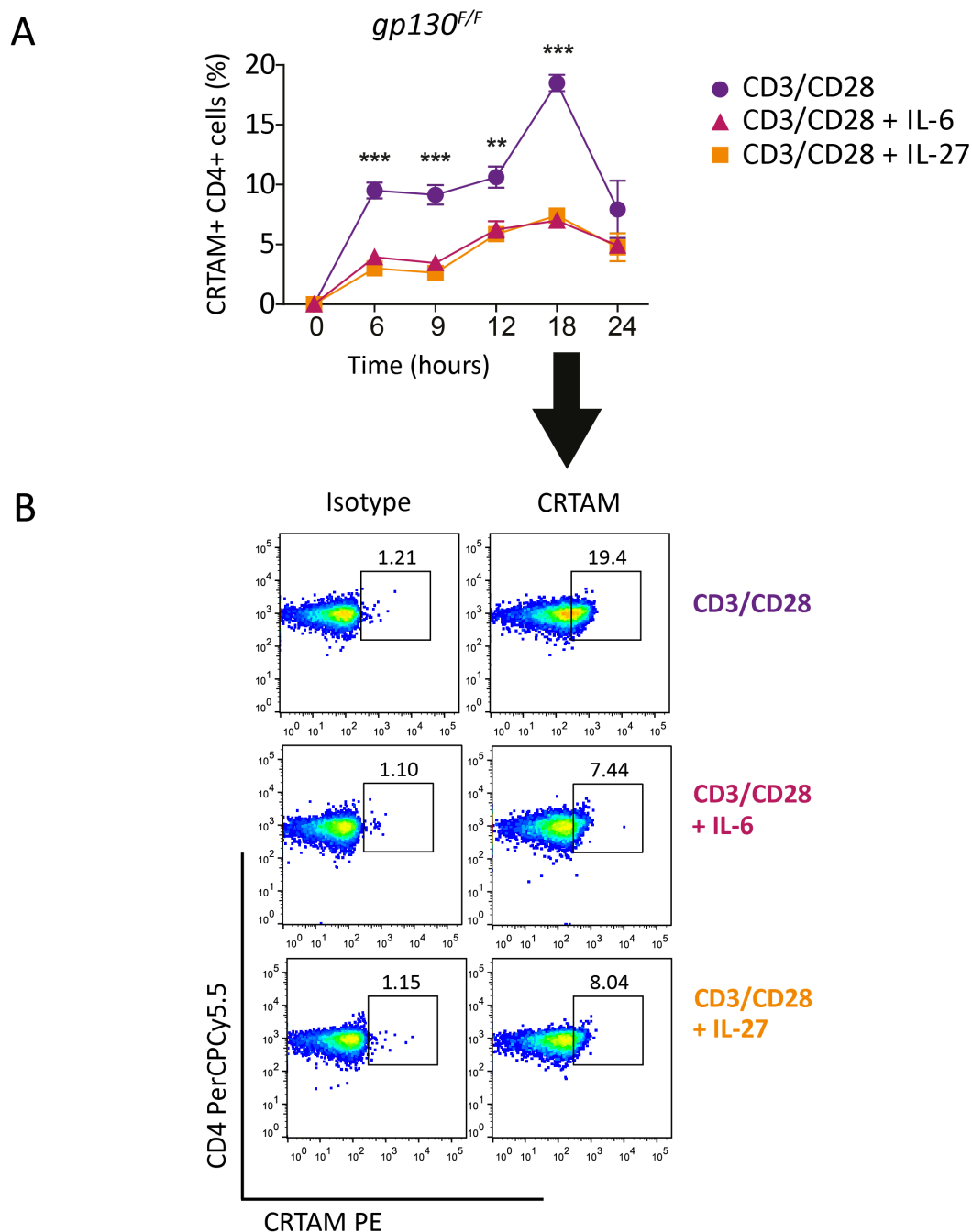


**Figure 6.11** CRTAM expression peaks at 18 hours after TCR activation in naïve CD4<sup>+</sup> T-cells from *gp130<sup>F/F</sup>* mice and is regulated by STAT3.

**(A)** Naïve CD4<sup>+</sup> T-cells (CD4<sup>+</sup>CD25<sup>-</sup>CD44<sup>lo</sup>CD62L<sup>hi</sup>) from *gp130<sup>F/F</sup>* mice were activated with anti-CD3 and anti-CD28 antibodies. Cells were stimulated with rmlIL-6, rmlIL-27 or neither; CRTAM expression was analysed by flow cytometry at the indicated time points (*n* = 3). Data are from two independent experiments. **(B)** Representative FACS plots of CD4<sup>+</sup> CRTAM<sup>+</sup> T-cells at 18 hours post-TCR activation, where CRTAM expression and IL-6 and IL-27-mediated CRTAM inhibition are the most pronounced. Graphs indicate mean ± SEM. \*\*, *p* < 0.01; \*\*\*, *p* < 0.001. Shapiro-Wilk normality test and a two-way ANOVA test were used.



To further the analysis of CRTAM regulation by gp130 receptor signalling, experiments were performed in naïve CD4<sup>+</sup> T-cells from *gp130<sup>F/F</sup>: Stat3<sup>+/-</sup>* mice, which have genetically reduced levels of gp130-dependent STAT3 activation<sup>312</sup> (see **Section 2.3.1 of Material and Methods** in **Chapter 2** for details) (**Figure 6.12A**). Whilst IL-6 and IL-27 treatment of these cells showed inhibition of CRTAM expression at 18 hours post-stimulation, the inhibition was less evident across the entire time course suggesting that the reduced cytokine signalling through STAT3 in naïve CD4<sup>+</sup> T-cells from *gp130<sup>F/F</sup>: Stat3<sup>+/-</sup>* impairs the inhibitory action of both cytokines (**Figure 6.12B**).

Comparing the results from the three different genotypes (WT, *gp130<sup>F/F</sup>* and *gp130<sup>F/F</sup>: Stat3<sup>+/-</sup>*), CRTAM expression was significantly more inhibited by IL-6 and IL-27 in naïve CD4<sup>+</sup> T-cells from *gp130<sup>F/F</sup>* compared to WT and *gp130<sup>F/F</sup>: Stat3<sup>+/-</sup>* mice, 18 hours after TCR activation. (**Figure 6.13**). Collectively, these results suggest that IL-6 or IL-27 receptor signalling inhibits CRTAM expression through a STAT3-mediated mechanism.

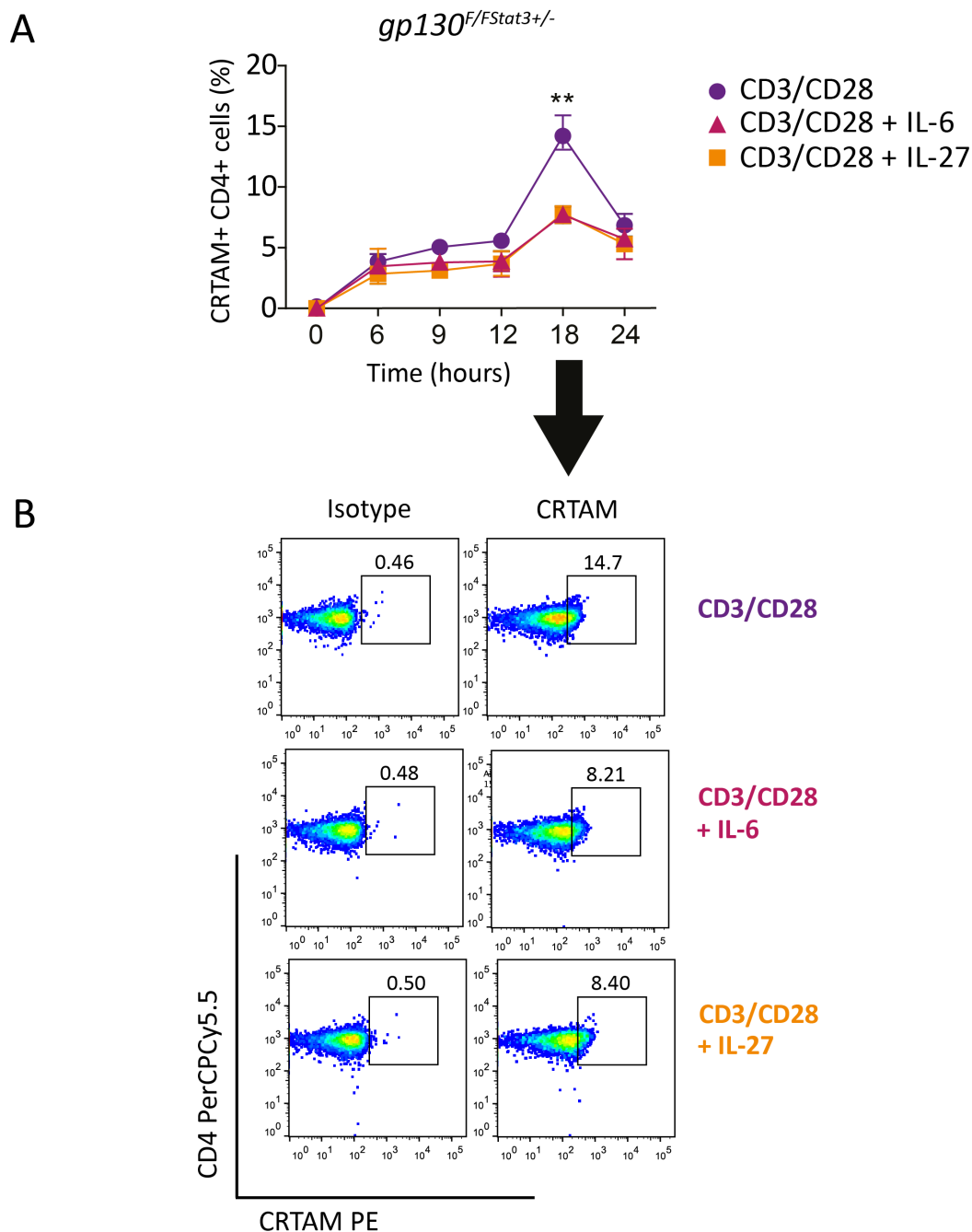


**Figure 6.12** CRTAM expression peaks at 18 hours after TCR activation in naïve CD4<sup>+</sup> T-cells from *gp130<sup>F/FStat3+/-</sup>* mice and is regulated by STAT3.

**(A)** Naïve CD4<sup>+</sup> T-cells (CD4<sup>+</sup>CD25<sup>-</sup>CD44<sup>lo</sup>CD62L<sup>hi</sup>) from *gp130<sup>F/FStat3+/-</sup>* mice were activated with anti-CD3 and anti-CD28 antibodies. Cells were stimulated with rmIL-6, rmIL-27 or neither; CRTAM expression was analysed by flow cytometry at the indicated timepoints. (n = 3). Data are from two independent experiments. **(B)** Representative FACS plots of CD4<sup>+</sup> CRTAM<sup>+</sup> T-cells at 18 hours post-TCR activation, where CRTAM expression and IL-6 and IL-27-mediated CRTAM inhibition are the most pronounced. Graphs indicate mean ± SEM. \*\*, p < 0.01. Shapiro-Wilk normality test and a two-way ANOVA test were used.

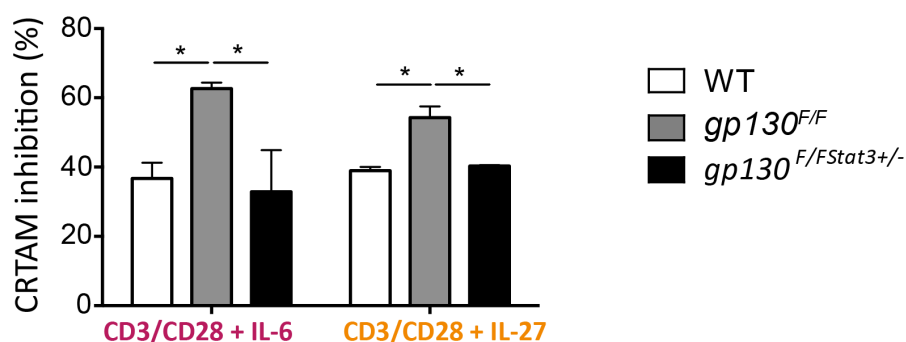


**Figure 6.13 STAT3 activation by both IL-6 and IL-27 leads to inhibition of CRTAM gene expression**

CRTAM inhibition by IL-6 and IL-27 in WT, *gp130<sup>F/F</sup>* and *gp130<sup>F/FStat3+/-</sup>* naïve CD4<sup>+</sup> T-cells (CD4<sup>+</sup>CD25<sup>-</sup>CD44<sup>lo</sup>CD62L<sup>hi</sup>), 18 hours after TCR activation, normalized against unstimulated controls (only CD3/CD8). Graphs indicate mean  $\pm$  SEM. \*,  $p < 0.05$ . (n = 3). Data are from two independent experiments. Shapiro-Wilk normality test and a two-way ANOVA test, multiple comparisons, were used.

### 6.3.6 CRTAM and its transcriptional repressor, ZEB1, colocalise in the inflamed synovium of AIA mice

The *Zeb1* (Zinc finger E-box-binding protein) homeodomain zinc finger transcription factor has been described as a negative regulator of the *Crtam* promoter in resting and activated T-cells<sup>455</sup>. To evaluate the expression of ZEB1 within the inflamed synovium of mice with AIA, confocal immunofluorescence imaging of synovial joints (see **Section 2.4.4.1 of Material and Methods**) was performed using antibodies against ZEB1. Interestingly, immunofluorescence analyses showed that ZEB1 co-localised with CRTAM within the inflamed synovium from WT mice at day-10 post-AIA (**Figure 6.14A**). The presence of synovial *Zeb1* was further confirmed by qPCR, when total mRNA was extracted from synovial joint of AIA challenged mice and the expression of *Zeb1* assessed at day-3 and day-10 post disease onset. Specifically, the relative expression of *Zeb1* was significantly increased in naïve mice at both day-3 and day-10 post-AIA, compared to the low expression observed in WT, *Il6ra<sup>-/-</sup>* and *Il27ra<sup>-/-</sup>* (**Figure 6.14B**). In naïve joint tissue, we did not observe synovial inflammation, and therefore we assume the number of leukocyte infiltrates is low, and the few existing T-cells are not TCR stimulated. These results seem to be consistent with research reporting that while unstimulated human T-cells do not express CRTAM, they have a basal ZEB1 expression<sup>455</sup>. Thus, ZEB1 is detectable within the inflamed synovium, albeit with low expression, and it colocalises with CRTAM in experimental arthritis.

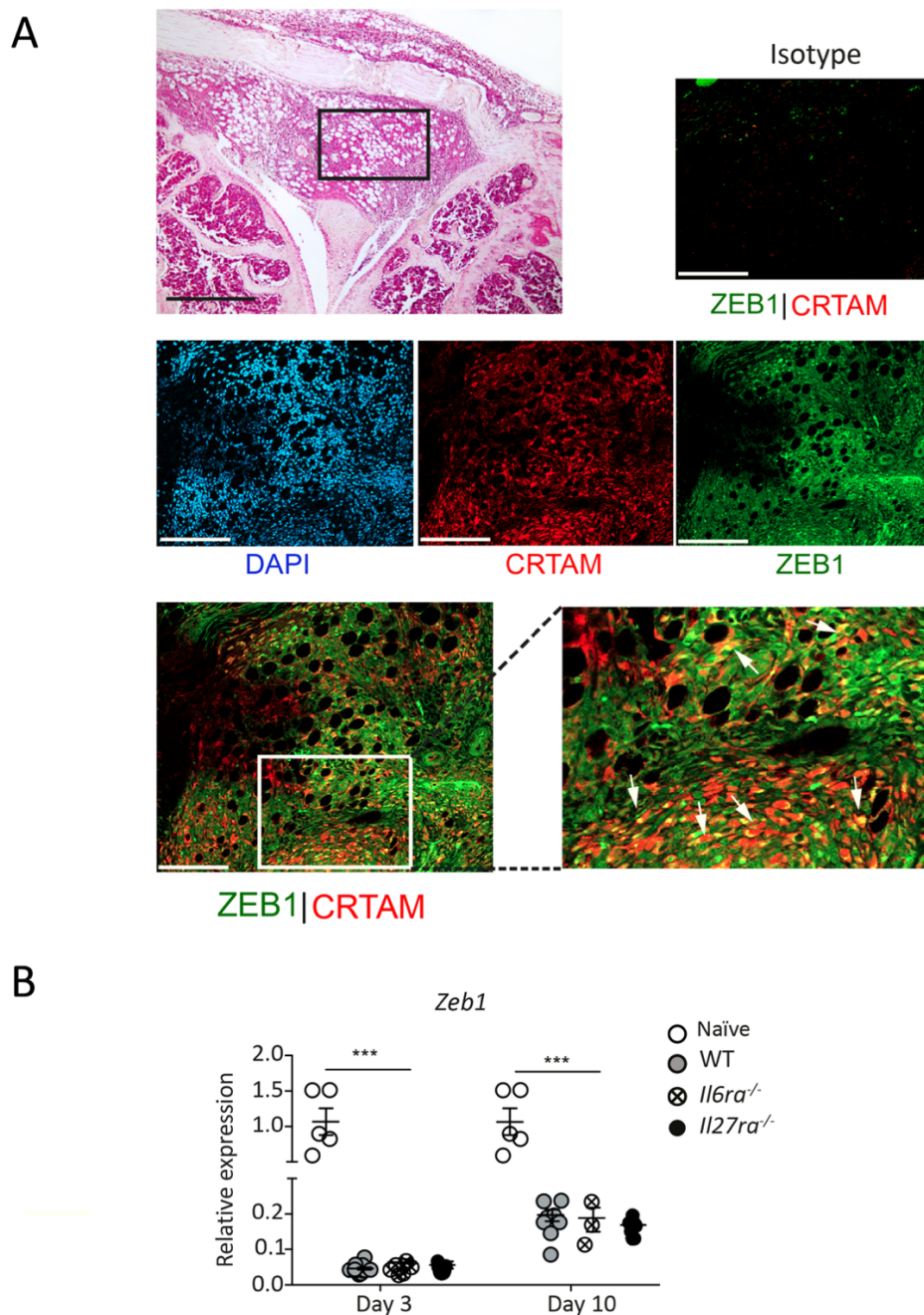


**Figure 6.14 Spatial relationship of CRTAM and ZEB1 in the inflamed synovium of AIA mice.**

**(A)** Representative image of haematoxylin & eosin staining of mouse knee joints at day 10 post AIA induction (scale bar, 500  $\mu$ m); boxed area shows the location of the immunofluorescence. Confocal double-immunofluorescence with antibodies to CRTAM (red) and ZEB1 (green) is shown with DAPI nuclear counterstaining (blue) (scale bar, 100  $\mu$ m). Co-localisation, as indicated by shades of yellow, is detectable in some areas of the synovium (arrowheads). Staining of synovium with isotype-matched controls for CRTAM and ZEB1 antibodies (upper right corner). **(B)** Synovial joint tissue from the knee joints of naïve (no AIA WT), WT, *Il6ra*<sup>-/-</sup> and *Il27ra*<sup>-/-</sup> mice with AIA were collected at day 3 and day 10, and mRNA expression of *Zeb1* was assessed by qPCR. ( $n = 3-8$ /group from 2 independent experiments). Graphs indicate mean  $\pm$  SEM. \*\*\*,  $p < 0.001$ . Shapiro-Wilk normality test and a one-way ANOVA, Turkey's multiple comparisons test were used.

### 6.3.7 CRTAM and ZEB1 exhibit a negative correlation in inflammatory arthritis

Given the fact that ZEB1 was present in the synovial tissue and colocalised with CRTAM, I next decided to compare both *Zeb1* and *Crtam* expression within the inflamed synovium to investigate their relationship at a molecular level. Quantitative PCR of previously extracted mRNA from synovial joint of AIA challenge mice (See Figure 6.4 & 6.13) at day-3 and day-10 post-disease onset, were plotted together, showing that *Crtam* and *Zeb1* displayed opposing patterns of expression (Figure 6.15A).

I next determined whether *Zeb1* and *Crtam* expression followed the same pattern of expression in the transcriptional mechanisms associated with IL-6 responses in CD4<sup>+</sup> T-cells, by analysing the microarray data previously obtained by my research group. Briefly, CD4<sup>+</sup> naïve activated and memory T-cells were stimulated for 6 hours with IL-6, then subjected to transcriptomic analysis<sup>194</sup>. Synovial CRTAM was inversely correlated with ZEB1 in IL-6 activated T-cells from WT mice (Figure 6.15B). Thus, CRTAM and ZEB1 presented an inverse relationship in both the synovial infiltrate and IL-6 stimulated T-cells.

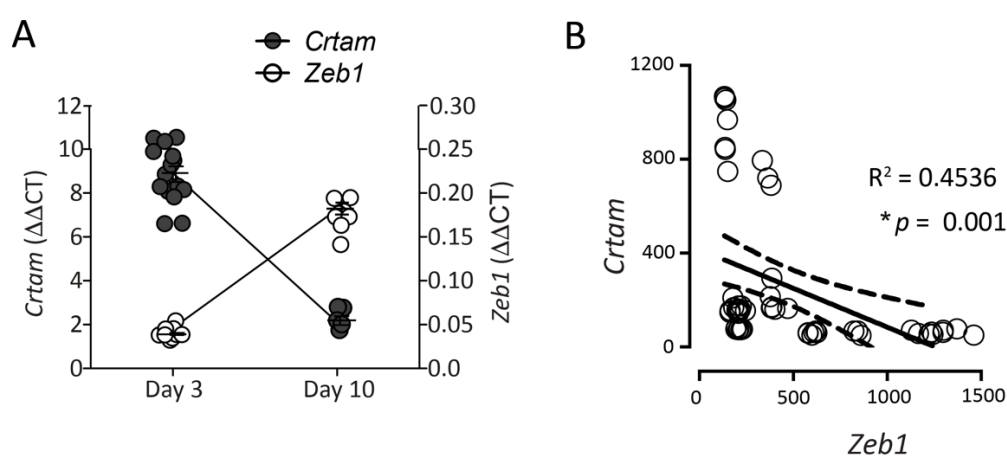


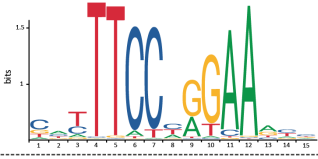
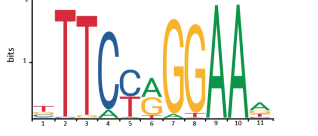
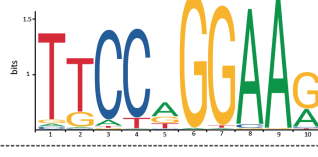

**Figure 6.15 Negative correlation between CRTAM and ZEB1 in inflammatory arthritis.**

**(A)** mRNA expression of both *Zeb1* and *Crtam* from AIA WT mouse synovium at day 3 and day 10 post arthritis induction. (n= 6-13/group). Graph indicates mean  $\pm$  SEM. **(B)** Pearson correlation analysis of the expression of *Crtam* and *Zeb1* as determined from the previous microarray expression studies: naïve, activated and memory CD4<sup>+</sup> T-cells treated with anti-CD3 and anti-CD28 antibodies and stimulated with 20 ng/mL IL-6 for 6 hours.

### 6.3.8 STAT3 interacts with *Zeb1* to regulate *Crtam* expression

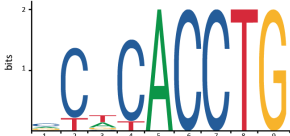
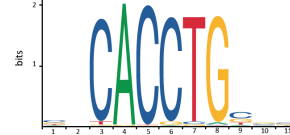
There is little information or evidence in the literature that can be used to elucidate the mechanism governing CRTAM expression. The results so far obtained in this Chapter confirm that this protein has an opposite expression pattern compared to ZEB1 and that IL-6 and/or IL-27 inhibit its expression, which is likely a mechanism driven by STAT3 and possibly STAT1. Whilst studies in CD4<sup>+</sup> T-cells from *gp130<sup>F/F</sup>* and *gp130<sup>F/F</sup>; Stat3<sup>+/-</sup>* mice support a role for JAK/STAT signalling in the regulation of CRTAM; it was unclear whether this was direct mediated by STAT1/STAT3 or controlled through STAT regulation of ZEB1. To test this hypothesis, I first used computational tools to identify consensus DNA motifs for STAT1 and STAT3 binding on *ZEB1* promoter, and ZEB1 binding on *Crtam* promoter.

To identify putative DNA binding sites for STAT1 and STAT3, the promoter sequences of *Crtam* and *Zeb1* were analysed using the bioinformatic tool JASPAR (**Appendix Figure 8.2**) (See **Material and Methods Section 2.6**). This *in silico* analysis of putative STAT1 and STAT3 binding sites on the *Zeb1* promoter revealed three binding sites for STAT1 and ten binding sites for STAT3 (**Table 6.1**). Interestingly, the identification of several more sites for STAT3 than for STAT1 on the *Zeb1* promoter suggests that STAT3 might participate more actively in ZEB1 regulation. Similarly, the same *in silico* analysis of putative ZEB1 binding sites performed on the *Crtam* promoter identified 46 binding sites for ZEB1 (**Table 6.2**); confirming previously reported binding sequences, which are consistent with the negative transcriptional regulation of *Crtam* by ZEB1 already established in the literature <sup>455</sup>.

Name	Matrix ID	Strand	Predicted sequence	Relative score	Sequence logo
Stat1	MA0137.2	+	GCTTTCCTGTGAGCG	0.81	
Stat1	MA0137.3	-	CTCACAGGAAA	0.84	
		+	TTTCTGAAAAC	0.81	
Stat3	MA0144.1	+	TGTTAGGAAG	0.83	
		-	TCACAGGAAA	0.83	
		-	GGACGGGAAG	0.80	
Stat3	MA0144.2	+	GTGTTAGGAAG	0.89	
		+	TTTCTGAAAAC	0.88	
		-	TTTTCAGAAAT	0.87	
		+	ATTTCTGAAAA	0.87	
		-	CTCACAGGAAA	0.86	
		+	CTCCTTTGAAA	0.82	
		-	CGGACGGGAAG	0.81	

**Table 6.1 Summary table of all over-represented TFBS motifs in the promoter region of ZEB1.**

*In silico* analysis of putative STAT1 and STAT3 binding sites on the *Zeb1* promoter using JASPAR (<http://jaspar.genereg.net/>), an open-access database that identifies transcription factor binding sites (TFBSs) given the promoter sequence of the transcription factor of interest. For each motif, identified by its JASPAR ID (Matrix ID), the table specifies the name of the associated transcription factor (Name), sense of DNA strand 5'-3' (Strand), Predicted sequence, Relative score, which shows the sensitivity and specificity of the prediction, and the relative consensus sequence (Sequence logo).

Name	Matrix ID	Strand	Predicted sequence	Relative score	Sequence logo
Zeb1	MA0103.2	-	CCCCACCTG	0.96	
		+	GCTCAGCTG	0.85	
		+	GGACACCTG	0.85	
		+	ACACATCTG	0.85	
		-	GCACACATG	0.85	
Zeb1	MA0103.3	-	CCCACCTGTGC	0.97	
		+	AGCACCTGCCT	0.96	
		+	GACACCTGTGG	0.95	
		+	CCCACGTGTCC	0.88	
		-	GACACGTGGGG	0.87	

**Table 6.2 Summary table of the first 10 over-represented TFBS motifs in the promoter region of CRTAM based on relative score.**

*In silico* analysis of putative Zeb1 binding sites on the *Crtam* promoter using JASPAR (<http://jaspar.genereg.net/>), an open-access database that identifies transcription factor binding sites (TFBSs) given the promoter sequence of the transcription factor of interest. For each motif, identified by its JASPAR ID (Matrix ID), the table specifies the name of the associated transcription factor (Name), sense of DNA strand (Strand), Predicted sequence, Relative score, which shows the sensitivity and specificity of the prediction, and the relative consensus sequence (Sequence logo). The complete list with all the TFBS motifs in CRTAM promoter is shown in **Appendix Table 8.1**.

To evaluate the functional significance of these putative DNA consensus motifs, chromatin immunoprecipitation (ChIP) was performed using selective antibodies to detect the binding of STAT1 and STAT3 to genome sequences derived from the promoter analyses of *Crtam* and *Zeb1*. Briefly, ChIP-qPCR analysis of STAT1 or STAT3 binding to the *Zeb1* promoter was achieved following 6 hours stimulation of WT naïve CD4<sup>+</sup> T-cells with IL-6 and IL-27. This time point was selected based on the temporal profile of pY-STAT1 and pY-STAT3 previously observed by our research group<sup>194</sup>, along with the optimal expression of STAT-target genes such as Zeb1, as determined via qPCR (data not shown). STAT1 had low or no detectable *Zeb1* binding in DNA samples from WT naïve CD4<sup>+</sup> T-cells across the different conditions, compared to binding to positive control transcription factor, *Irf1* (**Figure 6.16A**). Additionally, the binding of STAT1 to the transcription start site (TSS) regions of *Zeb1* remained unaltered upon treatment with IL-6 or IL-27 (**Figure 6.16A**). In contrast, STAT3 binding to the *Zeb1* promoter was specifically enriched in DNA samples from WT naïve CD4<sup>+</sup> T-cells treated with IL-6, compared with untreated and treated with IL-27 naïve CD4<sup>+</sup> T-cells (**Figure 6.16B**).



Thus, ChIP-qPCR results showed enhanced binding of pY-STAT3 but not pY-STAT1 to the *Zeb1* promoter, and therefore *Zeb1* is associated with STAT3-binding sites in CD4<sup>+</sup> naïve cells stimulated with IL-6. Together, these data suggest that CRTAM suppression by IL-6 and IL-27 is controlled by gp130 activation of STAT3 and reveals an inverse relationship between *Crtam* expression and its transcriptional regulator *Zeb1* in inflammatory arthritis, confirming our recently shown results so far.

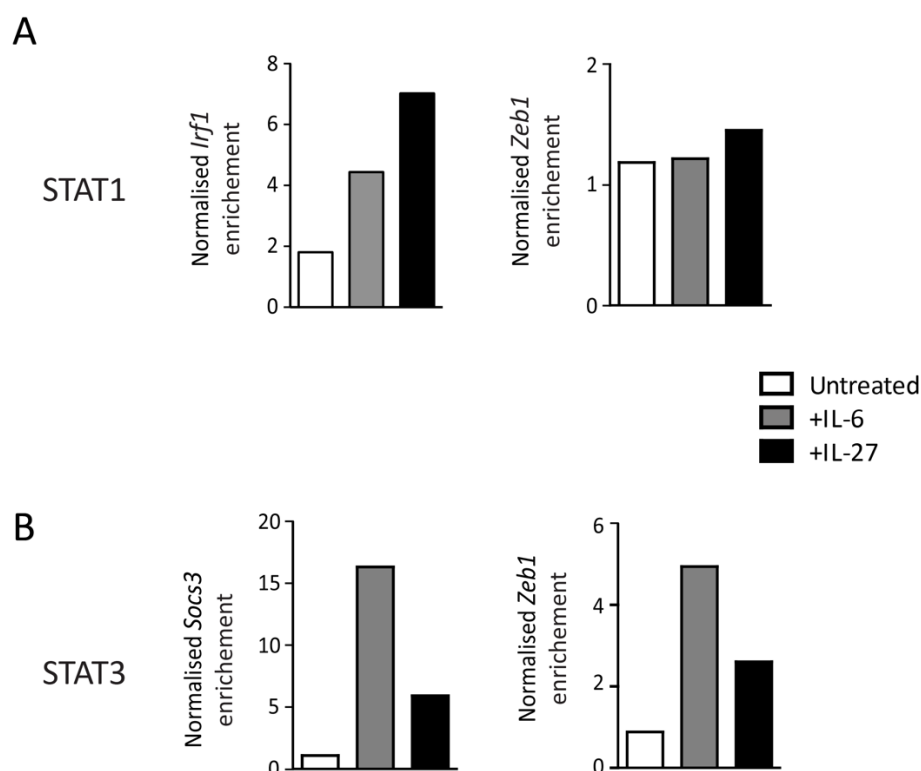


**Figure 6.16 STAT3-binding sites are associated with transcriptional repressor of CRTAM, ZEB1.**

**(A)** STAT1 binding enrichment quantification by ChIP-qPCR in naïve CD4<sup>+</sup> T-cells (CD4<sup>+</sup>CD25<sup>-</sup>CD44<sup>lo</sup>CD62L<sup>hi</sup>) from WT mice. **(B)** STAT3 binding enrichment quantification by ChIP-qPCR in naïve CD4<sup>+</sup> T-cells (CD4<sup>+</sup>CD25<sup>-</sup>CD44<sup>lo</sup>CD62L<sup>hi</sup>) from WT mice. In both cases, cells were activated for 6 hours with rIL-6, rIL-27 or neither of them in the presence of anti-CD3/CD28 antibodies (as described previously in **Chapter 2, Section 2.7**). (One experiment with pooled samples from 12 WT mice).

### 6.3.9 CRTAM is expressed in human synovial pathology and correlates with indices of synovial pathology in patients with RA.

To translate our animal studies to clinical RA, expression of CRTAM was evaluated in synovial biopsies from patients with RA and osteoarthritis (OA) using immunohistochemical methods (**Figure 6.17A**). Although RA and OA share similar characteristics and both have joint symptoms, OA is a degenerative joint disease with a multifactorial aetiology, but mainly caused by mechanical wear and tear of joints as opposed to the autoimmune nature of RA<sup>456</sup>. Hence, using biopsies from OA patients served as a reasonable negative control to investigate the role of CRTAM in shaping adaptive immune responses in chronic inflammatory disease.

CRTAM was elevated in patients with RA and colocalised with T-cell marker CD3 in serial sections. Minimal immune staining of CRTAM and CD3 was observed in joint biopsies from patients with OA (**Figure 6.17A, B**). Consistent with data presented in Figure 6.3, CRTAM positively correlated with synovial CD3 staining and joint inflammation. A lower presence of leukocyte infiltrates in OA compared to RA was expected, since OA is considered more a biomechanical process rather than a purely inflammatory disease. Nonetheless, CRTAM staining was also seen in joint biopsies from patients with OA (**Figure 6.17B**); perhaps due to the low grade of inflammation that has been increasingly recognised in this disease in recent times<sup>457</sup>.

To strengthen the link between CRTAM and inflammatory disease in patients, CRTAM expression was examined in bone marrow and blood, monocytes and leukocytes from patients with RA and OA, obtained from open access microarray datasets (GSE100786). As predicted, expression of CD3 was significantly higher in RA patients compared with patients with OA (**Figure 6.17C**). Furthermore, CRTAM showed a similar pattern of expression, with the increase in RA more significant. Finally, detection of CRTAM had a strong positive correlation with CD3 compared to a myeloid cell marker, CD14 (**Figure 6.17D**). Taken together, these results provide valuable insights into the role of CRTAM in chronic inflammation in patients with RA.

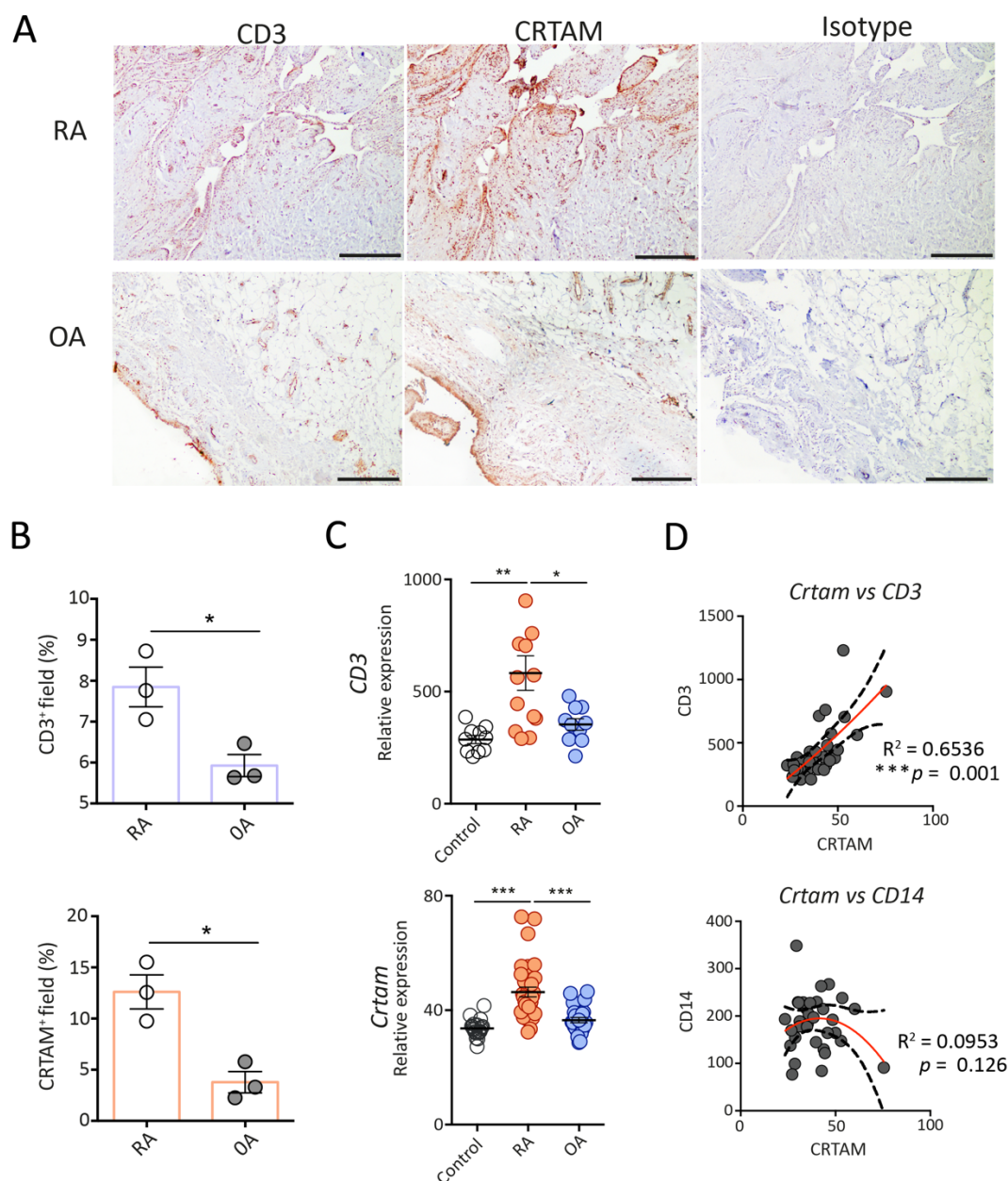


**Figure 6.17 CRTAM expression is present at higher levels in RA synovium than OA.**

**(A)** Immunohistochemical staining of CRTAM and CD3 in sequential sections of inflamed synovium from biopsies of patients with rheumatoid arthritis (RA) and osteoarthritis (OA). Isotype controls for CRTAM are shown in the upper right corner. **(B)** Quantification of CD3 and CRTAM staining was carried out ( $n = 3/\text{group}$ ) in both RA and OA sections. Shapiro-Wilk normality test and an unpaired t-test were used. **(C)** Microarray expression of CRTAM and CD3 in bone marrow and blood monocytes and leukocytes from patients with RA and OA compared to healthy controls. **(D)** Pearson correlation of CD3 and CRTAM (left) and CD14 and CRTAM (right) (Open-access data set GSE100786). Error bars indicate SEM. \*,  $p < 0.05$ ; \*\*,  $p < 0.01$ ; \*\*\*,  $p < 0.001$ . Scale bars: (A) 200  $\mu\text{m}$ .

In order to add some more clinical interpretations to the study, I next explore the association between *CRTAM*, *CADM1* and *ZEB1*, and clinical scores and pathotypes in RNA-seq datasets from synovial tissue biopsies of 87 patients with RA. Expression of *CRTAM* and *CADM1* in these biopsy samples was compared against corresponding histological staining of the inflamed synovium for the lymphocyte markers CD3 and CD20 by IHC. Analysis revealed a close relation between *CRTAM* and CD3 and CD20 (**Figure 6.18A**). This association was particularly evident in synovial biopsies displaying evidence of ELS (lymphoid-rich) and synovitis with a prominent mononuclear cell infiltrate (myeloid-rich) (**Figure 6.18B**). In contrast, *CADM1* displayed a more uniform pattern of expression within the inflamed synovium and showed no correlation with lymphocyte markers or the type of synovial pathology (**Figure 6.18A, B**).

To establish a possible link between *CRTAM* and disease activity in patients with RA, *CRTAM* was compared against some clinical scores such as patient global health visual analogue scale (VAS), used to measure the intensity or frequency of RA symptoms like pain, disease activity score 28-joint count C reactive protein (DAS28-CRP), disease activity score 28-joint erythrocyte sedimentation rate (DAS28-ESR) and tender joint count (Tender)<sup>334</sup> (see **Section 1.2.1**). Analysis of synovial RNA-seq datasets showed a correlation between *CRTAM* and disease activity scores (**Figure 6.18C**). On the other hand, no clear correlation was observed between *CADM1* and these disease characteristics (**Figure 6.18C**).

Regarding *CRTAM* transcriptional repressor, *ZEB1*, the analysis of synovial RNA-seq datasets presented a uniform pattern of expression across the different pathotypes; although there was a more obvious connection between *ZEB1* and fibroid-rich synovitis in patients with RA (**Figure 6.19 A**). This analysis showed a correlation between *ZEB1* and *STAT3*, as well as confirming previous results: a strong inverse correlation between *ZEB1* and *CRTAM*. Furthermore, within an open-access microarray dataset, comparing bone marrow and blood monocytes and leukocytes from patients with RA and OA, *ZEB1* was confirmed to be a potent negative regulator of *CRTAM* (**Figure 6.19C**). Thus, in human synovial pathology, *CRTAM* expression follows a similar pattern to that identified for *Crtam* in experimental arthritis and is associated with disease severity of joint synovitis.

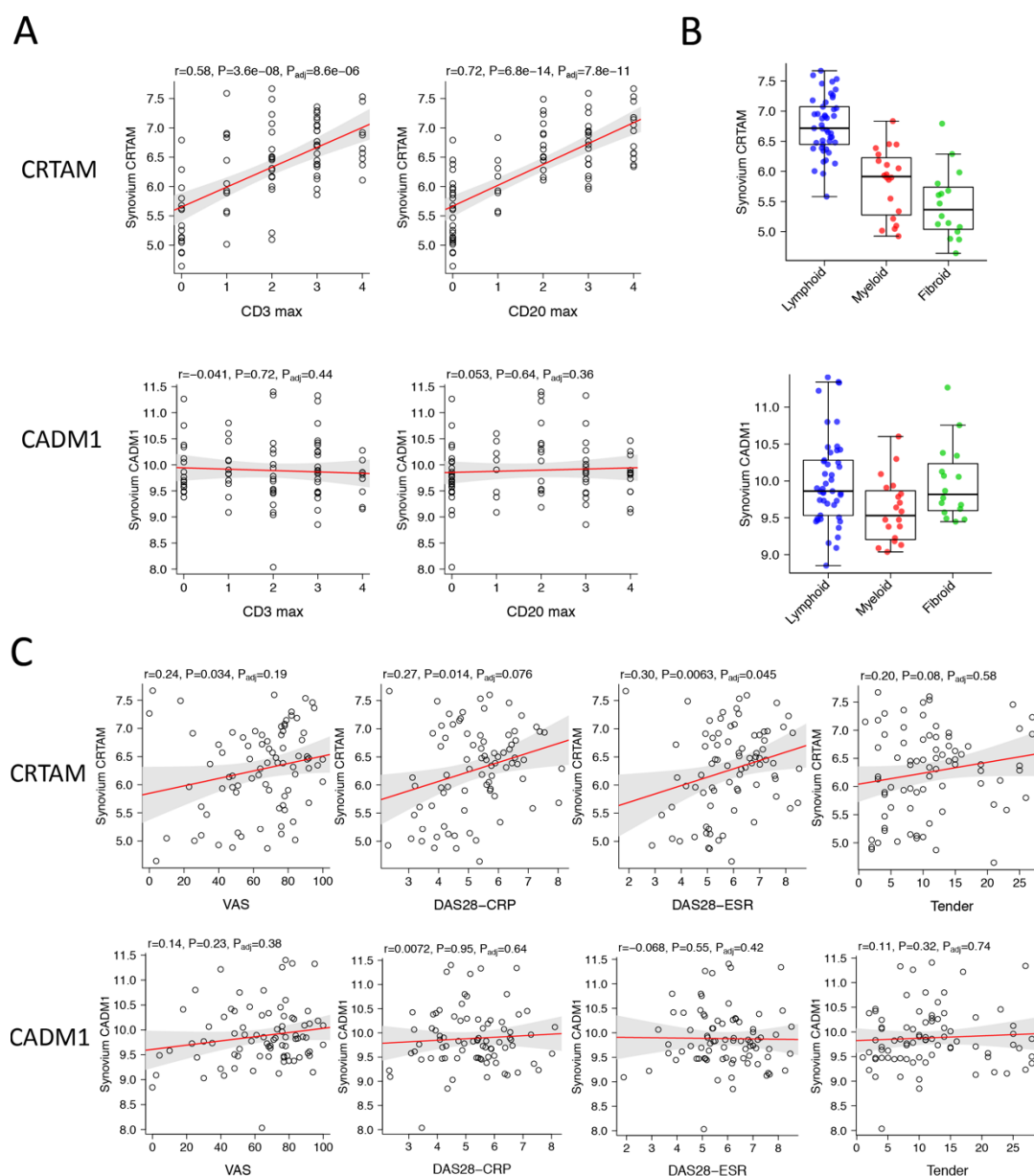


**Figure 6.18 Association of CRTAM with rheumatoid arthritis in human studies.**

**(A)** Correlations of CRTAM and CADM1 with lymphocyte cell markers CD3 and CD20 (left). **(B)** Distribution of CRTAM and CADM1 in patients stratified according to synovial pathology (lymphoid, blue; myeloid, red; fibroid, green) (right). Statistical analysis by one-way ANOVA with Bonferroni post-test. **(C)** Pearson correlations of synovium CRTAM and CADM1 with disease activity score (DAS) in patients with RA.  $P$  values were adjusted using FDR correction (Benjamini-Hochberg). VAS – visual analogue scale; DAS28-CRP – disease activity score 28-joint count C reactive protein; DAS28-ESR – disease activity score 28-joint erythrocyte sedimentation rate; Tender - tender joint count. Data provided courtesy of Professor Costantino Pitzalis (Queen Mary University of London, UK). The complete human data with other correlations are shown in **Appendix Figure 8.4**.

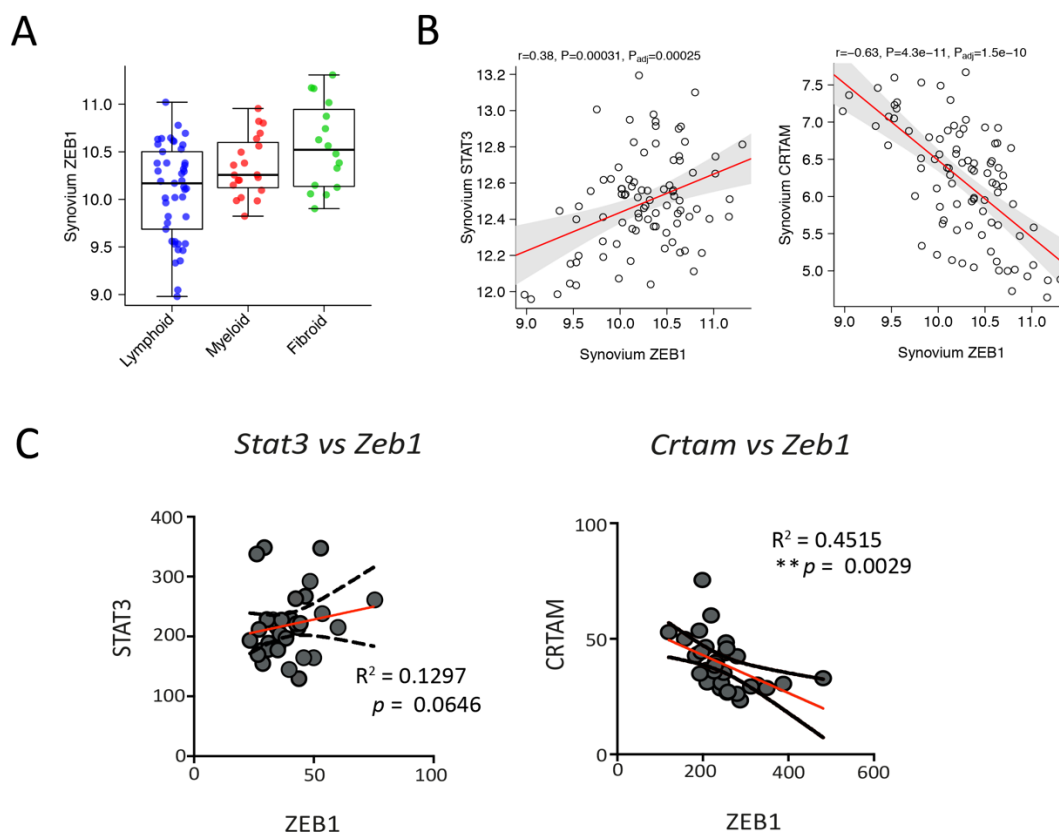


**Figure 6.19 Negative association between CRTAM and ZEB1 in patients with RA.**

**(A)** Distribution of ZEB1 in patients stratified according to synovial pathology (lymphoid, blue; myeloid, red; fibroid, green). Statistical analysis by one-way ANOVA with Bonferroni post-test. **(B)** Pearson correlation of synovium ZEB1 with STAT3 (left) and STAT1 (right). Data provided courtesy of Professor Costantino Pitzalis (Queen Mary University of London, UK). The complete human data with other correlations are shown in **Appendix Figure 8.4**. **(C)** Microarray expression of ZEB1 and STAT3 (left) and ZEB1 and CRTAM (right) in bone marrow, blood monocytes and leukocytes from patients with RA (Open-access data set GSE100786).

## 6.4 Discussion

CRTAM is a cytotoxic and regulatory T-cell molecule that was identified in our transcriptomic analysis of IL-6 stimulated CD4<sup>+</sup> T-cells as a gene target down-regulated by the action of IL-6. Importantly, CRTAM is involved in T-cell development and proliferation, with previous studies having reported its role in the establishment of Th1 and Th17 proinflammatory responses<sup>449</sup>. Exploring the function of CRTAM in inflammatory disease will undoubtedly help understand how IL-6 contributes to the underlying pathology. Thus, CRTAM holds promise as a novel biomarker of T-cell driven pathology in rheumatoid arthritis. Even though recent studies highlight roles for CRTAM in regulating these T-cell effector characteristics, the lymphokines responsible for the control of CRTAM expression remain unknown. Hence, there is considerable interest in understanding the regulatory mechanisms of CRTAM expression.

Therefore, in this Chapter, I sought to determine the role of CRTAM in synovial inflammation and its regulation. I showed that CRTAM is expressed within the synovium of mice with AIA and that it is negatively regulated by IL-6 and IL27. Using ChIP-qPCR analysis, described in **Chapter 2, Section 2.7**, I demonstrated that this regulatory mechanism involves STAT3 control of ZEB1, which acts as a transcriptional regulator of CRTAM. To complement these *in vivo* findings, I analysed clinical datasets to investigate the expression of CRTAM and its regulator molecules in patients with rheumatoid arthritis. To author's knowledge, this study represents the first attempt to investigate CRTAM regulation in a context of inflammatory arthritis.

Immunohistochemical analysis showed that CRTAM was expressed during active arthritis in the joints of mice with AIA. In models of inflammation, IL-27 deficiency is predominantly linked with more active pathology whilst IL-6 deficient mice are protected from the disease<sup>104,204,212</sup>. Interestingly, a significantly larger CRTAM<sup>+</sup> CD4<sup>+</sup> T-cell population was observed in *Il27ra*<sup>-/-</sup> mice (lymphoid-rich synovitis) as compared to WT mice (myeloid-rich synovitis). However, this was not observed in *Il6ra*<sup>-/-</sup> mice, confirming the association between CRTAM and arthritis severity. This pattern of expression suggested a potential involvement of CRTAM in the local control of adaptive immune responses.



CADM1, the ligand for CRTAM, was also observed in the inflamed joint although its expression was not dependent on IL-6 or IL-27 control. These observations also reflect those of Professor Paul Garside (Glasgow University, unpublished data). Here, transcriptomic analysis of CD4<sup>+</sup> T-cells purified from inflamed joint tissue of mice with a variation of the AIA model - using an adoptive transfer of Th1 TCR transgenic T-cells specific for ovalbumin (OVA) and challenging mice with OVA<sup>458</sup> - showed that both CRTAM and CADM1 were significantly upregulated in the joint-migrated cells. Furthermore, CD4<sup>+</sup> and CD8<sup>+</sup> T-cells were enriched in the population of cells migrating out of the inflamed tissues, supporting the hypothesis of CRTAM being expressed on some activated CD4<sup>+</sup> and CD8<sup>+</sup> T-cells<sup>447,448</sup>. In reviewing the literature, no data were found on the association between CRTAM and RA. The current study provided a functional characterisation of the CRTAM<sup>+</sup> CD4<sup>+</sup> T-cell population within the inflamed synovium at day-3 and day-10 post-AIA in both WT and *Il27ra*<sup>-/-</sup> mice. It was hypothesised that CD4<sup>+</sup>, CD8<sup>+</sup> T-cells and perhaps natural killer (NK) cells to a greater extent were the primary cell types expressing CRTAM in the joint. However, synovial CRTAM was found to be predominantly expressed in CD3<sup>+</sup>CD4<sup>+</sup> joint infiltrating T-cells, while only a small proportion of CD8<sup>+</sup> T-cells and NK expressed CRTAM. This result may be explained by the fact that the largest population of CD3<sup>+</sup> cells present in the arthritic inflamed joint is, indeed, CD4<sup>+</sup> T-cells, and that the amount of CRTAM<sup>+</sup> NK and CD8<sup>+</sup> T-cells is proportional to the percentage of total NK and CD8<sup>+</sup> T-cells within the synovium. Detailed characterisation of a total number of these cell subsets, instead of percentages, awaits further experimentation.

Prior work has documented that CRTAM is only transiently expressed upon TCR stimulation in both CD8<sup>+</sup> and CD4<sup>+</sup> T-cell<sup>447,449,450</sup>. This accords with our earlier observations, which showed that CRTAM was upregulated in naïve CD4<sup>+</sup> T-cells (CD4<sup>+</sup>CD25<sup>-</sup>CD44<sup>lo</sup>CD62L<sup>hi</sup>) 18 hours following TCR activation and downregulated within 24 hours. This transient expression is in keeping with our previous day-3-mRNA studies, which suggested a transient upregulation of CRTAM during joint inflammation. Notably, however, these data didn't fit well with the detection of CRTAM on cells into the course of the disease (day-10 post-AIA) observed in the immunohistochemical analysis. This rather contradictory result can be attributed to the differences that exist between *in vitro* and *in vivo* approaches, and mRNA and protein.

This study is the first that describes a role for cytokines in regulating CRTAM. In this context, I have demonstrated that treatment with IL-6 and IL-27 significantly impaired CRTAM expression upon naïve CD4<sup>+</sup> T-cell activation. This inhibition was significantly increased in



naïve CD4<sup>+</sup> T-cells from *gp130<sup>F/F</sup>* mice, where STAT3 is hyperactivated<sup>311,312</sup>, but remained unchanged in *gp130<sup>F/F</sup>:Stat3+/-* mice<sup>313</sup> where STAT3 expression is normalised to WT levels. It can thus be suggested that this form of suppression is controlled by gp130 activation of STAT3. This finding broadly supports the work of other studies, where CRTAM has been reported to be a key regulator CD4<sup>+</sup> cytotoxic T-cells in mice<sup>448</sup>, and it has been demonstrated that this cytotoxicity is promoted by STAT3 signalling<sup>459</sup>. Additionally, these results mirror those of a recent study which showed CRTAM conferring resistance to colitis development, in a model of inflammatory bowel disease<sup>452</sup>. Here, CRTAM-deficient mice showed a great reduction in STAT3 activation, in the secretion of IL-6 and in the presence of leukocyte infiltrate in the mucosa compared to WT animals, and therefore associated CRTAM with disease activity<sup>452</sup>.

In accordance with the present results, another group previously highlighted that CRTAM is a molecular target for ZEB1, a well-known homeodomain/Zn finger transcription factor<sup>455</sup>. This same group reported by CRTAM promoter analyses that ZEB1 is a transcriptional repressor of CRTAM. However, the mechanisms that govern CRTAM control *in vivo* are ill-defined. Our data extend this relationship by illustrating, with ChIP-qPCR analysis, that IL-6 and IL-27 stimulation-induced STAT3 binding to the *Zeb1* promoter. These findings lead us to propose a model in which IL-27 and IL-6-induced CRTAM inhibition is controlled by gp130 activation of STAT3, which promotes Zeb1 expression as a transcriptional repressor of CRTAM (**Figure 6.19**). This model corroborates the ideas of Nowell *et al.*<sup>204</sup> and work from Lionel Ivashkiv's group<sup>454</sup>, showing that STAT3 activation in inflammatory arthritis drives leukocyte infiltration and influences disease severity and is, therefore, constitutively activated in the inflamed joint tissue. Moreover, this proposed mechanism is consistent with the role of IL-6 in promoting and maintaining adaptive immune responses and regulating the recruitment and effector characteristics of joint-infiltrating T-cells<sup>204</sup>. However, it could be argued that in synovial pathology, IL-6 and IL-27 have opposing roles since the preferential activation of STATs by these cytokines differ. For example, IL-27 signals through STAT1 signalling and this pathway is associated with an anti-inflammatory outcome<sup>143</sup>. A possible explanation for this might be that in this scenario, IL-27 would mainly signal via STAT1, as it has been reported that although described as an anti-inflammatory cytokine, it can activate both STAT3 and STAT1.

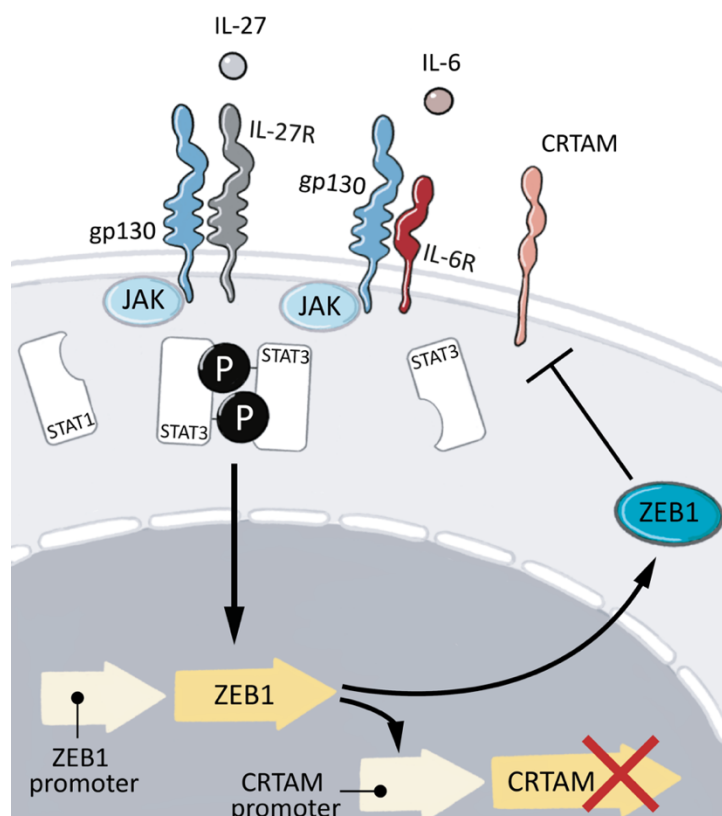


**Figure 6.20 A model of the regulation of CRTAM by a network of signalling and transcriptional pathways.**

IL-6 and IL-27 bind membrane-bound receptor complexes, which all contain the receptor subunit gp130. This binding induces receptor dimerisation, activating the associated JAKs, which phosphorylate each other and subsequently recruit STAT1 and STAT3 to the phosphorylated sites on the receptor chains. The STAT3 themselves are phosphorylated and activated by the JAKs, which enables their dimerisation and translocation to the nucleus, where they induce the transcription of ZEB1. ZEB1 functions as a transcriptional repressor of the CRTAM gene, negatively regulating its expression in synovial naïve T-cells.

In order to explain disparity between the observation of CRTAM positive cells and excess IL-6 signalling in the synovium, despite the shown negative regulation of IL-6 on CRTAM expression in other settings, it is possible that these observations are temporal and may capture the state in which IL-6 and CRTAM are both high before IL-6 can initiate negative regulation of CRTAM. However, it is also possible that we do not fully know the basal level of CRTAM expression in specific inflammatory states, therefore this expression level may be higher or lower than CRTAM expression during other states. Another potential hypothesis for this apparent discrepancy may be that in a context of a normal immune response (e.g., clearance of a bacterial infection) the negative regulatory effect is more apparent, whereas in the pathogenic scenario of inflammatory arthritis, the negative regulation of CRTAM by

IL-6 is impaired. T-cells local to the joint tend to be activated or memory T-cells; it is possible that IL-6 acting on these previously activated populations does not result in a suppression of CRTAM. Instead, the regulation by IL-6 is restricted to situations where IL-6 acts on activated naïve T-cells. Synovial CD4 T-cells tend to lack IL-6R, which suggests that the T-cells are previously activated. It can also be argued that this change in IL-6R expression may restrict IL-6 responsiveness, albeit the sIL-6R levels may circumvent this.

Another important finding was that ZEB1 colocalised with CRTAM in inflammatory arthritis. These two proteins showed strong negative correlation when assessed by qPCR. This result supports evidence from my laboratory's previous transcriptomic analyses in murine T-cells as well as from clinical observations, e.g. open access repository datasets from patients with rheumatoid arthritis and unpublished human data from Costantino Pitzalis & Myles Lewis (WHRI, London) previously shown, who also reported the same inverse correlation between the two molecules. Interestingly, CRTAM expression was significantly more visible in patients with RA compared to patients with OA. OA is contemplated as a condition whose pathogenesis implicates mechanical damage and chronic low-grade inflammation <sup>456</sup>. Moreover, based on histological and cytokine profiling, synovial membranes from patients with OA showed less leukocyte infiltrate and therefore, T-cells do not contribute to the pathophysiology as much as they do in RA <sup>460</sup>. Thus, these findings add to a growing body of evidence suggesting that CRTAM is heavily involved in T-cell-driven pathology.

In summary, this Chapter provides a distinct, yet complex mechanism to the regulatory effects of IL-6 and IL-27 on CRTAM expression in inflammatory arthritis. These findings strengthen the hypothesis that CRTAM might play a pathogenic role in inflammatory diseases. Also, it makes CRTAM a potentially suitable candidate for a novel biomarker of T-cell driven pathology and a target during inflammatory arthritis. Nevertheless, several questions remain unanswered at present. In collaboration with Professor Paul Garside (Glasgow University), we will investigate the function of the CRTAM-CADM1 interaction – specific to the engagement of T-cells with dendritic cells. Although in these studies, we characterised the relationship between T-cells and CRTAM within the joint of mice with antigen-induced arthritis (AIA), this study has been unable to examine the impact of CRTAM<sup>+</sup> CD4<sup>+</sup> T-cells in the pathogenesis of inflammatory arthritis. In future investigations, it might be necessary to use a CD4-specific CRTAM KO mouse, a CRTAM KO mouse or use antibody blockade experiments in order to address this issue. These further experiments will provide greater insight into the biology of CRTAM and its role in autoimmune diseases like RA.

## 7 General Discussion

---

### 7.1 Summary of work

The work described in my thesis has investigated several new therapeutic interventions designed to target the JAK/STAT signalling pathway for the treatment of RA. Through studies of their mode of action, my research has led to improved understanding of the inflammatory mechanisms driving arthritis progression and synovitis and has provided some insight into how the JAK/STAT pathway functions in a complex heterogeneous disease like RA. Collectively, research projects described herein highlight immunotherapies that moderate the IL-6/sgp130-associated JAK/STAT3 signalling axis and therefore cover one of the recent key advances in medicine of 2018, chosen by the magazine *Nature*, namely ‘Selective Janus kinase inhibitors come of age’<sup>461</sup>, making my work a highly current research topic.

Since its first description as interferon  $\beta$ -like protein in 1980, our understanding of the biology of IL-6 and its physiologic and pathophysiologic implications have drastically improved<sup>462</sup>. The consequences of dysregulated gp130 activation on immune homeostasis and susceptibility to infection, autoimmunity or cancer have been extensively reported, thus highlighting the importance of limiting the magnitude or duration of IL-6 cytokine family signalling in disease<sup>303</sup>. The development of biologic therapeutics that target the IL-6 family and/or STAT3-signalling cascade has widely proven the therapeutic value of inhibiting this axis and, as a result, has revolutionised the treatment of inflammatory diseases including RA<sup>119</sup>. However, many patients fail to display an adequate response to therapy, which emphasises the need for alternative therapeutic strategies or a greater understanding of how these therapies may be best applied in patients or specific indications<sup>58</sup>. Current drug strategies that target IL-6 cytokine family fall into three broad categories: (i) blocking monoclonal antibodies that directly act on either the cytokine or the cytokine receptor (e.g., tocilizumab, sarilumab, siltuximab); (ii) recombinant cytokine regimes and (iii) small molecule therapies that interfere with cytokine receptor signalling through sgp130 and/or the JAK/STAT pathway (e.g., tofacitinib, ruxolitinib, baracitinib)<sup>303</sup>. Studies presented within this thesis tested several alternative novel therapies that could potentially deliver a more selective inhibition of JAK/STAT signalling in RA (**Figure 7.1**).

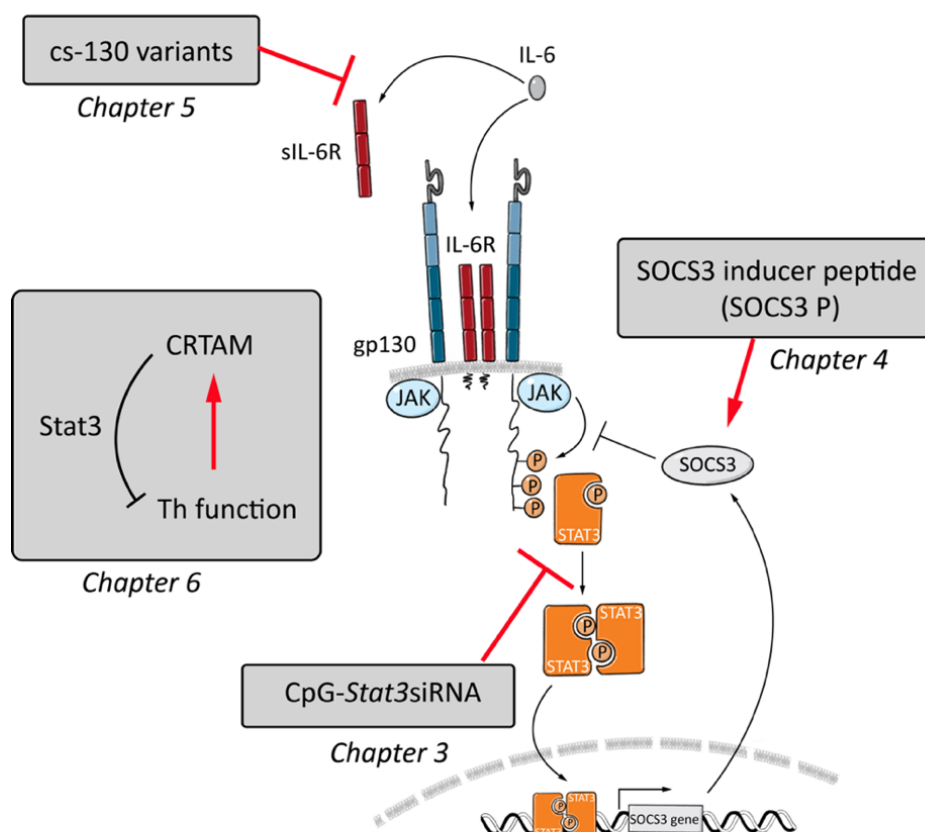


**Figure 7.1 Visual summary of the research content within this thesis.**

**Chapter 3** focused on the direct therapeutic targeting of STAT3 using CpG-Stat3siRNA therapy, while **Chapter 4** investigated the potential of a SOCS3-inducer peptide to target STAT3 signalling indirectly. **Chapter 5** aimed to use cs-130 variants that inhibited IL-6 trans-signalling and finally, **Chapter 6** explored the role of CRTAM and its negative regulation by IL-6 in synovitis.

**Chapters 3** and **4** described two small-molecule interventions that modulate receptor signalling activity or intracellular mechanisms linked to JAK/STAT3 signalling axis and thus, belong to the third class of drug intervention described above. More specifically, STAT3 is considered a central therapeutic target for RA. In **Chapter 3**, I developed an alternate strategy that directly inhibits STAT3 signalling in inflammatory cells. This novel approach developed as an anti-cancer therapy (CpG-Stat3siRNA) relies on simultaneous delivery of innate immune system activation through the TLR9 agonistic unmethylated CpG and inactivation of STAT3 via a synthetically engineered STAT3 siRNA. From histological and transcriptomic analyses, I showed that CpG-Stat3siRNA improved arthritis outcome in WT and *IL27ra*<sup>-/-</sup> mice with AIA, altered the STAT1/STAT3 balance in the inflamed synovium and reduced the presence of ELS in ELS-rich synovitis. Here, transcriptomic analysis of synovial inflammation allowed the identification of pathways associated with the delivery of

CpG- *Stat3*siRNA therapy. While many of the downregulated pathways were associated with inflammatory pathways, such as T-cell and B-cell signalling and differentiation, cell migration and proliferation, other pathways such as bone remodelling, metabolism and innate signalling and activation were also altered by treatment. Thus, RNA-sequencing is a powerful tool to investigate transcriptomic changes in response to treatment and provide mechanistic insights to the contribution of CpG-*Stat3*siRNA and the STAT3 signalling pathway in synovitis. The overall findings of this study suggested that TLR9-targeted delivery of STAT3 inhibitors may offer a new approach for more effective immunotherapy of inflammatory arthritis and, potentially, other autoimmune diseases. Conversely, **Chapter 4** focused on the indirect targeting of STAT3-driven responses through the induction of SOCS3 expression. In this study, I evaluated the therapeutic potential of a viral protein derived from hepatitis C virus, which triggers the transactivation of SOCS gene regulation and thereby ultimately suppresses STAT3 activation. The inhibitory action of this inducer of SOCS3 peptide (SOCS3 P) was initially evaluated using an *in vitro* murine Th17 cell differentiation assay and was subsequently tested in an *in vivo* model of inflammatory arthritis. This study demonstrated that this regulatory peptide had the capacity to block Th17 cell differentiation *in vitro* and reduce disease pathology in AIA joints and supports the importance of SOCS3 in modulating cytokine-driven outcomes in synovial inflammation.

In **Chapter 5**, I focussed on the first class of drugs previously mentioned, that include recombinant protein modalities for specific cytokines or cytokine receptors. Here, I used a junctional epitope nanobody that recognises the IL-6-IL-6R complex and selectively inhibits IL-6 trans-signalling. Briefly, these novel IL-6 trans-signalling inhibitors were engineered by fusion of a minimised sgp130 variant to an IL-6:sIL-6R complex-binding nanobody (VHH6), and their inhibitory capacity of STAT3-driven Th17 cell expansion *in vitro* was evaluated. I showed for the first time that these inhibitory proteins with improved activity for IL-6 trans-signalling had a dose-dependent effect on Th17 cell proliferation, demonstrating their potential therapeutic applications due to their selective inhibition of IL-6 trans-signalling and relatively small size. Although future experiments will have to evaluate the effect of these specific novel chimeric soluble gp130 (cs-130Fc) variants on the severity of arthritis in a model of antigen-induced arthritis, they remain potential therapies of interest for further investigation.

The pathogenesis of RA is complex, and it may be difficult to ever find a reliable biomarker to predict, target and monitor disease <sup>58</sup>. Consistent with formerly reported roles for autoreactive CD4<sup>+</sup> T-cells in initiating and controlling specific immune responses relevant to the development of synovitis and destruction of the cartilage and bone in inflammatory arthritis <sup>274</sup>, RNA-seq analyses from joints of AIA mice in **Chapter 3**, further demonstrated a central function of CD4<sup>+</sup> T-cells in the pathogenesis of the disease. Understanding how the expression of transcripts change during disease can provide insight into the mechanisms that underpin disease progression and has the potential to identify novel biomarkers and therapeutic targets that improve patient stratification and treatment. My research group has generated omic datasets to delineate novel mechanisms regulating T-cell fate. Through this type of approach, I identified several T-cell regulatory molecules whose expression is negatively regulated by IL-6 and gp130 cytokine receptor signalling. **Chapter 6** examined the role of CRTAM (CD355), a molecule found to be downregulated in activated naïve CD4<sup>+</sup> T-cells as a response to IL-6 and IL-27, which is essential in regulating T-cell effector characteristics and has also been previously implicated in various inflammatory and pathogenic processes, in the context of synovitis. This study provided a distinct, yet complex mechanism to the regulatory effects of IL-6 and IL-27 on CRTAM expression in inflammatory arthritis. These studies highlighted the pathogenic role for CRTAM in inflammatory disease and identified CRTAM as a novel biomarker of T-cell driven synovial pathology and a target for lymphoid-rich synovitis. The implications of these results on current knowledge, potential therapeutic relevance and application to other challenges will be discussed here.

## **7.2 Future perspectives for rheumatoid arthritis immunotherapy**

### **7.2.1 The context-dependent nature of cytokine action and the relevance to therapy**

Hardly any cytokine exerts exclusively pro-inflammatory or anti-inflammatory actions. Instead, they operate in a highly context-dependent manner that is shaped by the type of tissues involved and the course of the disease process <sup>463</sup>. Rather than boosting pathways that coordinate the suppression and resolution of inflammation and restoring immune homeostasis to enable long-term remission in patients, current treatment strategies for RA generally include targeting pro-inflammatory cytokines, and in doing so, blocking the activation process of inflammation <sup>123</sup>. However, inhibition of pro-inflammatory cytokines is

not always successful, and patients often display relapses of disease activity or changes in clinical efficacy following prolonged biological drug therapy <sup>464</sup>. The therapeutic success of TNF- $\alpha$  targeted inhibition in patients with RA in the early 1990s, revealed that chronic inflammatory diseases depend on delicate communication networks of cytokines. These networks fall apart upon deactivation of functionally vulnerable nodes such as TNF- $\alpha$ , suggesting that different chronic inflammatory diseases may share common pathophysiology <sup>129</sup>. Other cytokines that are of pivotal importance in RA are IL-6, IL-1, IL-17 and IL-23, which are required for inflammation in several different organs, including the joints, brain, gut and skin <sup>465</sup>. For example, inhibiting IL-6 receptor was shown to be effective to treat RA, yet this strategy has shown limited efficacy or even failed in most other prevalent chronic inflammatory diseases <sup>216,465</sup>. Therefore, instead of sharing similar molecular pathogenesis, chronic inflammatory diseases display quite distinct cytokine-driven activation profiles <sup>465</sup>. As a consequence, at the moment there is a need to define other cytokines that are of hierarchical importance, that drive the tissue components of RA, and that could provide additional therapeutic targets in refractory disease, where remission is difficult to achieve <sup>123</sup>. The challenge now is to determine how the specific features of these individual cytokines or cytokine networks coordinate the disease progression and the various comorbidities often associated with patients with complex chronic and illnesses.

As discussed before, IL-6 represents a keystone cytokine in infection, cancer and inflammation, supporting the maintenance of immunological reactions or driving disease progression <sup>212</sup>. One of the questions raised by the studies performed in **Chapter 5** relates to the use of IL-6 trans signalling inhibitors, which provide the opportunity to selectively target the deleterious consequences of IL-6 biology. Here, selective blockade of IL-6 trans-signalling offers a clinical advantage over a more global inhibition of IL-6 – restricting the impact of therapy on the homeostatic properties of IL-6 in health such as maintenance of barrier immunity and tissue regeneration. Cs-130Fc variants have the potential to inhibit the “danger” component of IL-6 signalling, leaving certain IL-6-regulated homeostatic processes intact <sup>216</sup>. Some studies in mice have shown, however, that inhibiting IL-6 trans-signalling does not control serum amyloid A (equivalent to C-reactive protein in humans) <sup>216</sup>. Nevertheless, experimental evidence supports the proposal of the therapeutic inhibition of IL-6 trans-signalling. For example, olamkicept (an engineered chimeric sgp130 protein that targets cytokine trans-signalling by IL-6 and IL-11), NI-1201 (an anti-IL-6R monoclonal antibody) and VHH6 (junctional epitope nanobody that recognises the IL-6–IL-6R complex),



selectively inhibit IL-6 trans-signalling and have shown considerable promise in pre-clinical studies, and early clinical trials <sup>216,303,424,466</sup>. In **Chapter 5**, we observed an inhibitory effect of cs-130Fc variants in an *in vitro* Th17 cell expansion assay when compared to olamkicept, suggesting that cs-130Fc variants may be superior to sgp130Fc in terms of pharmacological inhibition of Th17 cell formation regarding activity and selectivity.

The potential therapeutic advantage of blocking IL-6 trans-signalling without affecting classical IL-6 receptor signalling is also supported by the appearance of infections associated with global IL-6 blockade such as with tocilizumab intervention, or atopic dermatitis treatments, usually affecting tissues where IL-6 controls barrier function or tissue integrity (e.g., respiratory, urinary and gastrointestinal tracts) <sup>467–469</sup>. Thus, the challenge is to identify where and when IL-6 is active in inflammation to understand how the pleiotropic effects of IL-6 determine the progression, severity or duration of disease <sup>212</sup>. Another challenge regarding drug strategies targeting IL-6 is to understand the types of clinical indications that may benefit from these therapies and to evaluate the best approach to target these inflammatory cytokines <sup>303</sup>. For instance, does inhibition of a cytokine, its corresponding receptor or mode of cytokine receptor signalling provide optimal therapeutic opportunities or clinical outcomes? With the emergence of small molecule interventions that block specific cytokine receptor signalling systems (e.g., tofacitinib targeting of the JAK/STAT pathway), researchers and pharmaceutical companies have also begun to consider possibilities of simultaneously targeting multiple cytokines of the family as a route to therapy. Such interventions offer opportunities to either broaden the type of clinical indication that may be tractable to therapy or increase the efficacy of treatment within a given disease setting.

### 7.2.2 Safety and strategies for the optimal use of biologics in RA

Biologic therapies have improved our ability to treat RA and other autoimmune conditions. As with any drugs, however, there are risks associated with the use of these agents <sup>308</sup>. These adverse effects can be split into (i) class-specific, those that can be expected from the biological role of the target, such as a decreased in immunoglobulin associated with B-cell depletion, intracellular opportunistic infection associated with TNF inhibitors, and anaemia associated with JAK2 inhibition; and (ii) compound-specific, those unique to one compound within a class, such as infusion reactions and infliximab <sup>119</sup>. Generally, as biologic agents are larger than oral synthetic compounds, they are not metabolised by the body, and consequently, compound-specific adverse effects are less frequent with biologics <sup>119,262</sup>. To

date, it seems that all biologic DMARDs have a good benefit-to-risk-profile. Infections, however, are the primary risk (approximately 20% of the cases), as they are a direct consequence of biologic therapies suppressing the immune response <sup>58</sup>. Not surprisingly, age, smoking, comorbidities, concomitant glucocorticoid treatment and other underlying risks factors may worsen the risk of adverse effects <sup>470</sup>. However, occasionally the risk of certain infections is more common in response to specific biologics (i.e., TNF- $\alpha$  inhibitors are particularly associated with increased susceptibility to tuberculosis <sup>169</sup>). Furthermore, cytopenias (more specifically anaemias and leukopenias) are also commonly seen in patients treated with biologics. For example, neutropenia has been associated with the cytokine receptor-inhibitor tocilizumab and first-generation jakinibs, including tofacitinib and baricitinib <sup>144</sup>. Jakinibs such as tofacitinib and baricitinib, are associated with a reduction in haemoglobin levels, perhaps mediated through inhibition of JAK2, which orchestrates the response to erythropoietin. In contrast, IL-6 inhibition by tocilizumab is linked with improvement of anaemia in chronic diseases such as RA <sup>119</sup>. Elevated levels of lipids and liver transaminases have also been reported in patients with RA treated with DMARDs, biologic therapies and jakinibs <sup>144,471,472</sup>. Lower total cholesterol levels are commonly seen in patients with active RA and other inflammatory states, which is paradoxical when considering their increased risk of cardiovascular disease <sup>473</sup>. This suggests that systemic inflammation has the general effect of lowering circulating lipid levels and explains why suppressing inflammation with RA therapy seems to elevate levels of lipid fractions in patients <sup>471</sup>. This effect is more frequent in patients being treated with tofacitinib and MTX in combination and may require dose adjustment or discontinuation <sup>474</sup>. Jakinibs and some biologic agents, such as tocilizumab, might increase the risk of gastrointestinal perforation as well, highlighting the multifaced role of JAK-dependent cytokines in immune homeostasis and the importance of long-term monitoring for unexpected complications <sup>144</sup>.

Whereas the advent of biologic therapies has substantially improved the management and outcome of inflammatory arthritis, the percentage of patients achieving disease remission remains low (around 40%) <sup>34</sup>. Thus, treatment strategies that achieve higher rates of sustained disease remission are needed, and one of the options that have shown to present potential benefits for the patients is, as outlined previously, to combine different biologic therapies <sup>119</sup>. Although several studies combining therapies failed to enhanced efficacy due to the overlap of the cytokine biologic effects, the increase of our knowledge about how these cytokines and signalling pathways interact is leading to the identification and test of

new potential synergistic combinations<sup>475</sup>. Combining biologic agents successfully may also enable substantial reductions in doses of individual agents, and therefore will make them more economically viable. However, before being able to implement these combinations of biologic therapies, and given their potency and potential for immunosuppression, clinical trials need to assess their safety risk, already discussed above, and efficacy in stepwise, escalating-dose combinations<sup>119</sup>. Finally, current management of RA also aims to reduce these adverse effects by tailoring treatment to the patients by considering underlying comorbidities such as chronic kidney diseases, diabetes mellitus or previous infections<sup>58</sup>.

### 7.2.3 Towards personalised therapies

With the increasing number of biologic agents available in clinical practice (**Figure 7.2**), the choices are becoming overwhelming, and it is often difficult to choose the right treatment for each patient<sup>119</sup>. In addition, improved success in treating RA has raised the prospect of long-term drug-free clinical remission<sup>119</sup>. Rheumatology has so far relied on a trial-and-error approach, which in the UK is governed by the National Institute of Clinical Excellence (NICE) guidelines and the clinical experience of rheumatologists prescribing biological drugs<sup>58</sup>.

#### 7.2.3.1 *Identification of predictive biomarkers*

One of the major challenges associated with the treatment of RA is the lack of robust biomarkers to predict the course of inflammatory arthritis in patients whose disease is undifferentiated at presentation. Such biomarkers offer potential opportunities to stratify these patients according to their disease and inform clinical decisions on the best course of therapy for a particular patient or patient group. While disease-specific autoantibodies such as RF and ACPA correlate with disease severity, they unreliably predict underlying features of joint pathology<sup>150</sup>. Here, circulating blood markers of disease often show poor correlation with the complex histological features of synovitis<sup>151</sup>. An emerging blood biomarker of tissue inflammation is CXCL13, whose expression is increased in peripheral blood mononuclear cells from RA patients compared to healthy donors<sup>476</sup>, and in the plasma using proteomic profiling<sup>477</sup>. CXCL13 reflects a more severe pattern of RA disease; for example, levels of CXCL13 marks the presence of ELS and correlates with the degree of erosive bone damage<sup>397,476</sup>, and consequently, CXCL13 serum levels have been used as a predictive marker for lymphoid-rich synovitis<sup>128</sup>. However, further investigation to identify other blood biomarkers that reflect synovial and diseases subtypes is needed<sup>151</sup>. Moreover, CXCL13 has

also been proposed as a valuable therapeutic target in some cancers, as well as a biomarker of systemic immune activation during several infectious diseases such as Lyme disease, syphilis affecting the central nervous system, or human immunodeficiency virus (HIV) infections, where CXCL13 levels correlated both with disease progression and viral load <sup>478</sup>.

Although it is well known that clinical intervention at the earliest time point in the course of the disease allows for the best clinical outcome, current clinical assessments of RA provide limited information on the most appropriate intervention strategy or class biological drug based on their mode of action (e.g., anti-TNF inhibitor vs anti-IL-6R inhibitor vs anti-CD20 blocker) <sup>119</sup>. During my studies, I was lucky enough to be involved, for the first time, in the development and optimisation of RNA-seq methodologies of mouse synovial tissue treated with the novel anti-cancer CpG*Stat3*siRNA therapy. This approach takes advantage of high-throughput next-generation sequencing to study gene expression changes in the synovium in response to treatment within various mouse genotypes (WT and *Il27ra*<sup>-/-</sup>) with AIA (day-3 and day-10 post-AIA). The results from this study have helped improve our comprehension of the mode of action of the drug in the context of inflammatory arthritis and have identified relevant STAT3-linked pathways involved in synovitis. IL-6 (prototypical pro-tumorigenic cytokine within the IL-6 cytokine family), but also other cytokines such as IL-11, regulate various STAT3-mediated oncogenic processes by promoting chronic inflammation that supports tumour microenvironment <sup>303</sup>. For this reason, drug intervention based on blockade of the JAK/STAT3 axis has been approved or are in clinical trials for the treatment of several forms of autoimmune disease and cancer <sup>144</sup>. Given the success of CpG*Stat3*siRNA for the treatment of myeloid malignancies, as well as melanoma and lung cancer <sup>316,341–344</sup>, there are high hopes that this approach will provide an effective treatment option for autoimmune disorders such as RA. While these analyses provide some insight about the major contributing pathways that drive RA and the mechanism by which CpG*Stat3*siRNA acts, a vigorous search is currently underway to identify biomarkers that could predict response to treatment and improve patient stratification at the earliest stage of disease <sup>119</sup>.

My research group has recently generated a transcriptomic profile of IL-6 responses in naïve, activated and memory CD4<sup>+</sup> T-cells to determine whether T-cell subsets adopt different IL-6 signalling properties within the inflamed joint <sup>194</sup>. Because of the lack of reliable biomarkers for the treatment of RA, studying genes that change in T-cells as a response to IL-6 is, therefore, an interesting area of investigation. Our data showed that PTP activity controlled

the expression of genes commonly associated with ELS; for example, PTPN2 control of STAT1 phosphorylation was shown to affect the transactivation of inflammatory cytokines such as IL-21, and immune checkpoint regulators such as CD274<sup>194</sup>. The gene signature identified through this screen may, therefore, predict the efficacy of adoptive immunotherapy strategies, or response to biological drug therapies.

In **Chapter 6**, CRTAM was demonstrated to be a potentially suitable candidate for a novel biomarker of T-cell driven pathology and a target during inflammatory arthritis. It was highlighted the importance of CRTAM in regulating T-cell effector characteristics and perhaps a pathogenic role in inflammatory disease. Furthermore, based on the success of initial histological assessments and mice work using different therapies presented in this thesis (i.e. SOCS3 peptide in **Chapter 4**), RNA-seq and ATAC-seq of the inflamed synovium will be used to generate novel insights into the therapeutic mode of action of these novel drugs in the near future. Here, approaches will benefit from archived datasets obtained from WT, *Il6ra*<sup>-/-</sup> and *Il27ra*<sup>-/-</sup> mice with AIA within my own laboratory.

Conversely, specific biological outcomes of targeted therapies may not explain the differences in response and, consequently, the search of biomarkers allowing one to target specific populations at risk might be less revealing than one might think<sup>43</sup>. While the search for biomarkers needs to be continued in a more innovative way than hitherto, at present clinical markers, rather than biological markers, appear to be most predictive of outcome and response to therapy, hence the focus of clinicians on clinical disease activity assessment and targeting remission or low disease activity promptly<sup>43</sup>.

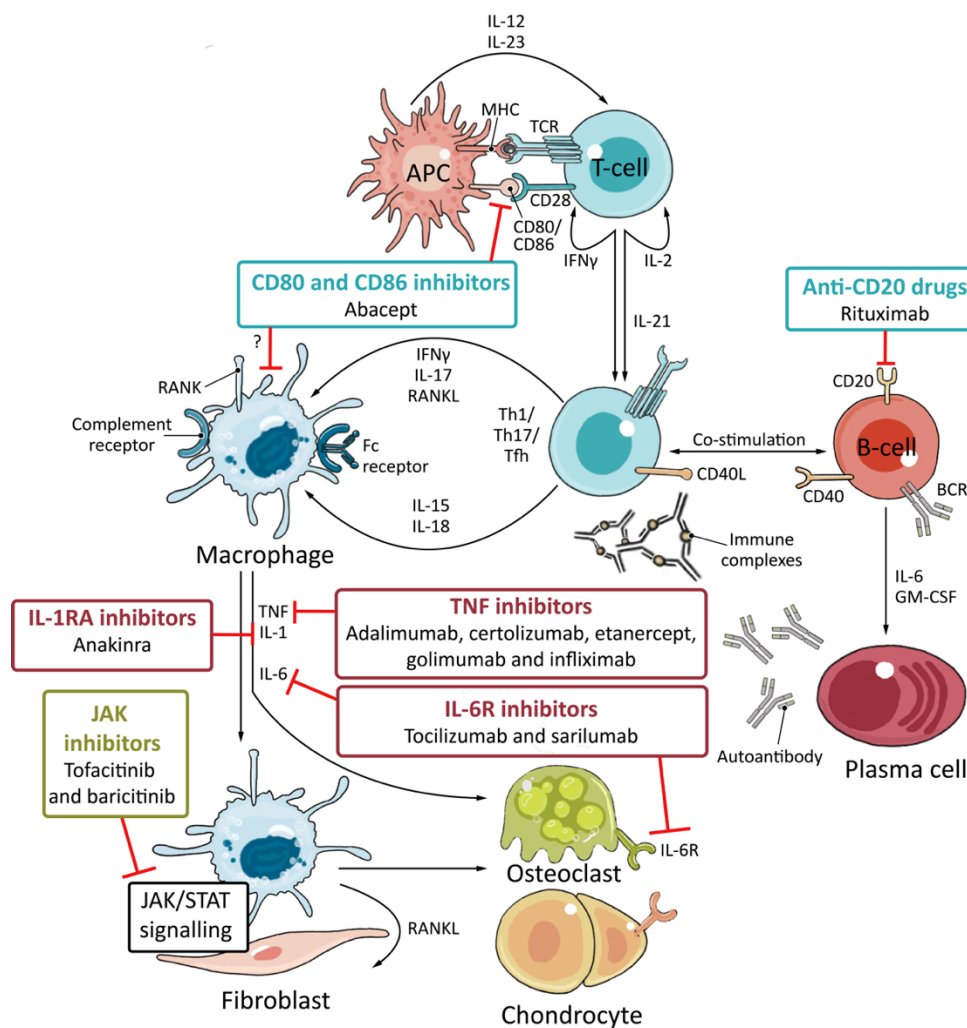


**Figure 7.2 Summary of the main disease-modifying antirheumatic drugs for RA treatment**

Examples of lymphocyte-targeting agents are highlighted in turquoise; cytokine/receptor blockers in dark red, and small molecule inhibitors of signal transduction pathways in dark green. APC, antigen-presenting cell; BCR, B-cell receptor; CD40L, CD40 ligand; GM-CSF, granulocyte-macrophage colony-stimulating factor; MHC, major histocompatibility complex; RANK, receptor activator of nuclear factor; RANKL, RANK ligand; MHC, major histocompatibility complex; TCR, T-cell receptor; Tfh, T-follicular helper cell; Th, T-helper cell. (Adapted from Smolen *et al.*, 2018).

### 7.2.3.2 Population-wide studies – how do you classify a patient with complex disease?

Current advances are already providing information on the course of disease progression and are aiming at identifying the most appropriate therapy for a particular patients group. Genome-wide analysis studies (GWAS), together with epigenetic studies, clearly implicate the JAK/STAT signalling pathway and cognate cytokines in common human immune-mediated diseases<sup>185</sup>. Importantly, GWAS have led to an explosion of loci associated with risk of these disorders<sup>195</sup>. Together, these studies shed light on fundamental

genes, pathways and cell types that contribute to RA pathogenesis, and provide empirical evidence that GWAs can provide valuable information for direct identification of therapeutic targets and drug discovery in RA<sup>479</sup>. Indeed, some existing therapies target genes and/or pathways have already been highlighted by such studies. An example of approved RA therapies identified by this analysis is abatacept (CTLA-4-Ig), and CTLA-4 polymorphisms are associated with RA risk<sup>60,479</sup>.

Among the more encouraging developments, a recent study that developed cellular and molecular pathway-driven/stratified approaches to patients with RA, by determining their relationship with clinical phenotypes and treatment outcomes, stands out<sup>334</sup>. Here, despite the ambiguity of how RA heterogeneity relates to disease activity, prognosis and therapeutic response and outcome in patients, diverse synovial pathotypes were shown to be present at an early disease stage prior to DMARDs, and it was demonstrated that specific synovial pathotypes and related molecular signatures were associated with clinical phenotypes and disease prognosis<sup>334</sup>. Importantly, while these approaches are mainly associated with the observed pathology within the inflamed joint, the implications of cytokine network modulation on systemic homeostatic processes – such as cardiovascular risk, mood, depression, fatigue and infection – and haematologic processes, are as well key components of biologic intervention<sup>119</sup>.

As discussed in **Section 1.2.4**, 30-40% of patients with RA present follicular pathology featuring ELS, remain challenging to treat and typically respond poorly to anti-TNF treatment<sup>104,151</sup>. Indeed, studies suggest that ELS can affect the response to biologic therapy, although it can be a controversial subject, and thus, a greater understanding is needed in this area. For example, recent research reported the presence of lymphoid aggregates within the synovium of RA patients to be a negative predictor of the response to anti-TNF therapy, revealing a significant decline in DAS28 scores, despite the elevated levels of TNF $\alpha$  within the synovium of patients with follicular pathology<sup>149,153</sup>. However, ELS have also been associated with a better clinical response to anti-TNF $\alpha$  treatment in other studies<sup>480</sup>. A more comprehensive evaluation of ELS, for example utilising RNA-seq, as I have done in my studies, may offer an opportunity to identify transcriptomic signatures that include markers of ELS activity and to develop more robust markers with prognostic value. Although a whole- tissue RNA-seq approach was taken here, advances in sequencing technologies such as single-cell RNA-seq could provide more information regarding ELS composition and

regulation. In this regard, the investigation of major inflammatory pathways linked with synovial ELS development during experimental inflammatory arthritis and gastric cancer was the focus of another PhD project (D.Hill, 2019) within my research group. Moreover, single-cell transcriptome profiling of synovial tissue has been used to identify cellular subpopulations present in RA <sup>481</sup>.

### **7.3 Concluding remarks**

Our understanding of epidemiology, genetics, pathogenesis, clinical assessment and therapy of RA is becoming increasingly refined as the field strides into its second quarter-century, with the incorporation of recent discoveries and technological advances which should ultimately lead to increased development and implementation of pathway-targeting drugs. Consequently, the treatment of RA has seen tremendous advances, but many challenges still exist. A key focus of my research was to study the immunotherapeutic potential of the IL-6/JAK/STAT3 signalling axis in inflammatory arthritis, thus hopefully paving the way for the discovery of novel therapeutically relevant targets and uncover the cause or causes of RA to attempt a cure or at least prevention, as aspirational and ambitious as these goals may be.



# 8 Appendix

**Figure 8.1** Flow cytometry gating strategy to determine purity of naïve CD4<sup>+</sup> T-cells.

Population purity of sorted naïve CD4<sup>+</sup> T-cells was calculated by running a sample of the cell population after sorting. In this example, CD4<sup>+</sup>CD25<sup>-</sup>CD44<sup>lo</sup>CD62L<sup>hi</sup> cell purity (p5) was 95.7%. SSC-A – side scatter-area; FSC-A – forward scatter-area; FSC-H – forward scatter-height.

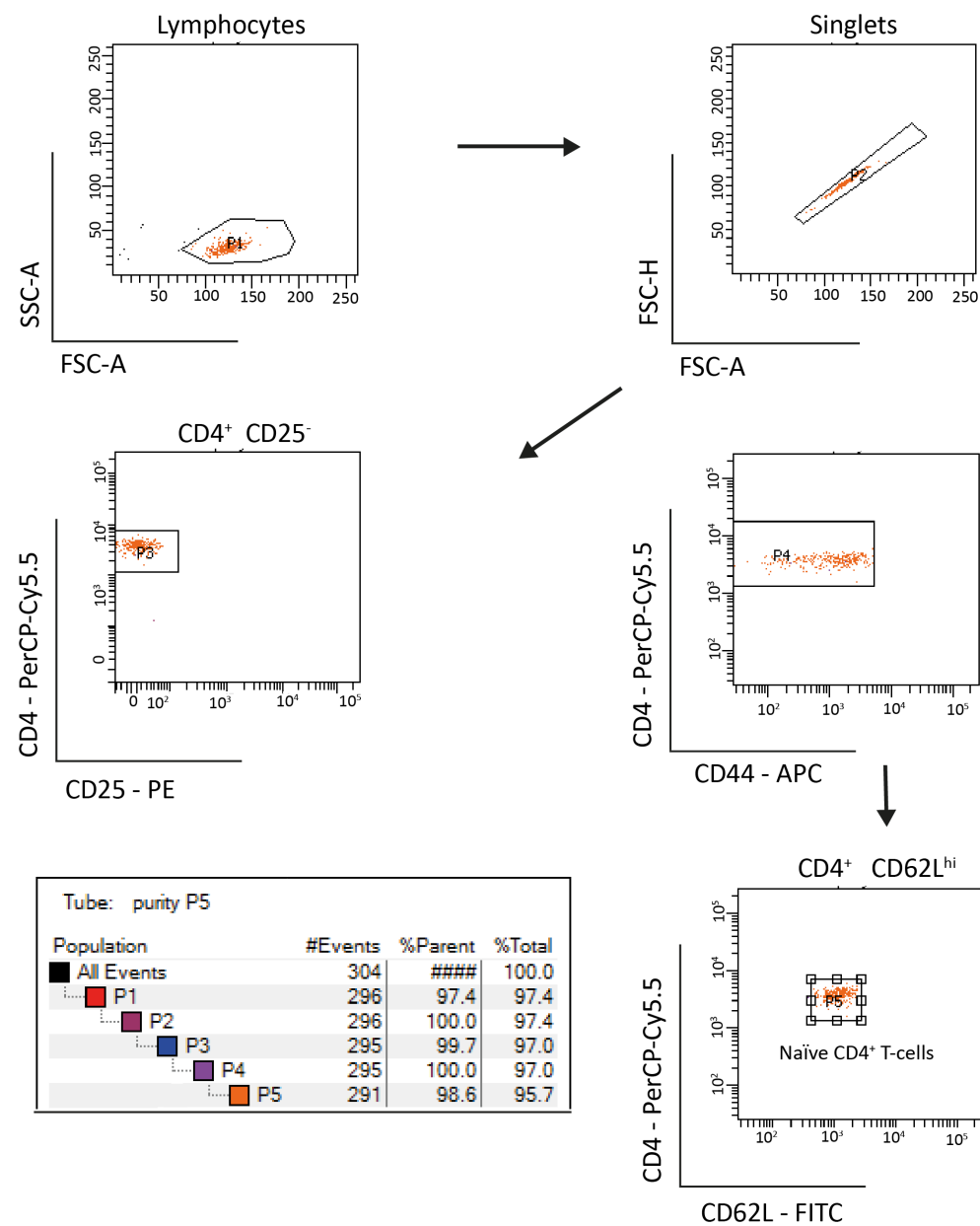


**Figure 8.2 Promoter sequence of Crtam and negative regulator Zeb1**

**(A)** *Crtam* and **(B)** *Zeb1* promoter sequences. The exons are high-lighted in yellow background and red text, promoter sequences are usually the sequence immediately upstream the transcription start site (TSS) or first exon. By default, 600 bp 5'-flanking sequence of the gene is displayed when using Ensembl software (<http://www.ensembl.org/index.html>).

**Exons** Crtam exons All exons in this region

**Markup** loaded

>chromosome:GRCh38:9:40969091:41005228:-1  
CACATTTTTCCTAAAAACAACAACAGCAGAGAAGGACATTTTGTGTGATGTCTGATCATCT  
TAGTGAGGCATGTAAAGATGTTGGATGTAGAGAGAGAGAGAGAGGTGTGCACAGCTGGG  
GAGATTAATAGTAGACATGAAGAAGACATAGTAGATAAATGGGAAGATTTCGAAGTGAA  
TGAATGAATCAATACATCTAATAACCATAGATATTGTTGGCTCCAAAGTCAGAAATACAAA  
TATCCAGAAGGTGGGACAAAAAATACCTAGCTATTGTTGCTTAGTAAAGATAGAAAAGC  
TAAAAACAATGTCCAGACAGGATGATTACTCTCTCTGCGCTCTCTCTTCCCCCAAGAT  
CTCATGTCTACTCTTGCCATAGGCTACCCACTTGTGGCTGCCAGTGGTTGTCCAGAACAC  
CTCGTTCACACCTTCCCAATGATAGGACAGCTGGTGTCCCAAGATGTTCCACAG  
GAGGTGTTTACGGGCAGCTAACTAAAGAGGGGGCTCAGAGAAGGTGAGAGAGGTGACACA  
GGCAAGGTCCAGAGCTACAGCCTTCCCCCTTCAAAGGCTGTGTTGATTAGAACCC  
**ACAGGAAGCTGTGCAGAGACTCCCTCCGTTCAAGCAGAGCAGCATGTGGTGGGGAGCCCTC**  
**AGTTTGCCTGTTCGGGTCCGGGTCAAG**GTAAAGCATTAGATAAATGGATATTGTTGCT  
CAGCTGACTTTTAGGGCTTTTGTGTAAACCTACTGTGCAGCAACTGTGCTTGGAGG  
TCGTA CTCTGGAAGATAACTCAGTAACTTGTCTAACTCTCTGGCTGTGCTCAACC  
ACACGCTCCAAGGCGATTA CTCTGCTCTCTTAATTGAACCTCTCTTCAGGGGTGAGCGGAG  
CTCGGATGCATCTTGGAATGTGTGTGATGAATAAAACAGCGCCCTAAGTCTATCT  
TTTGAAGGTTTATCAGTTGAAGGACATCTATTTAGATTCAAAATGTCTTGTATGAGA  
AGTCTTTGTCAAAATACCCATATTTCTCTAAATTCAGTTTTCGATTTTTCAGGCTGAG  
ATCTCGGACCTCATTTCTATAGATTAGGCTGGCTCAACCTACAGAGATCCACTCTCTGA  
GTACTGGGATCAAAGGCTGTCACCAACGCCCATCCGACTCAATTTTTCATCTTTATAGAT  
AGGATGTTAAGAAATGACCTGTCTCAAACTGCTCATATAAGAAATATCTCAAAATTTACATG  
CTTTTGAAGTGAAGTAGGATTAATCAATTCGAATTTAGTTCGAGGAATAAGAACCCAG  
TAAAAAGCTTTTCAATTTAAACATGTGCTTTATTTATCTATGTGATGAGTGTGTGCGCTG  
CTTAGGTGTGTGGCGGTGTGTGTGCTGCTGCTCAAGGGGCTCAGAGAGAGATGGGGG  
TTTGGAGCTGCAGTTATCCAGATGGCCAGGAGCTGCCATGTGGGTGCCGGGGAATGAGCT  
GGAGTCTCTCGCGGAGCAGGAGTGCCCTTAACCATGAGCCATCTCTCCGCGCCCGAA  
AGCTACTTGTGTTTGTAGAAATCAGTCTCTATTTTTCACATTTGCTATCTTGGTTTGGGA

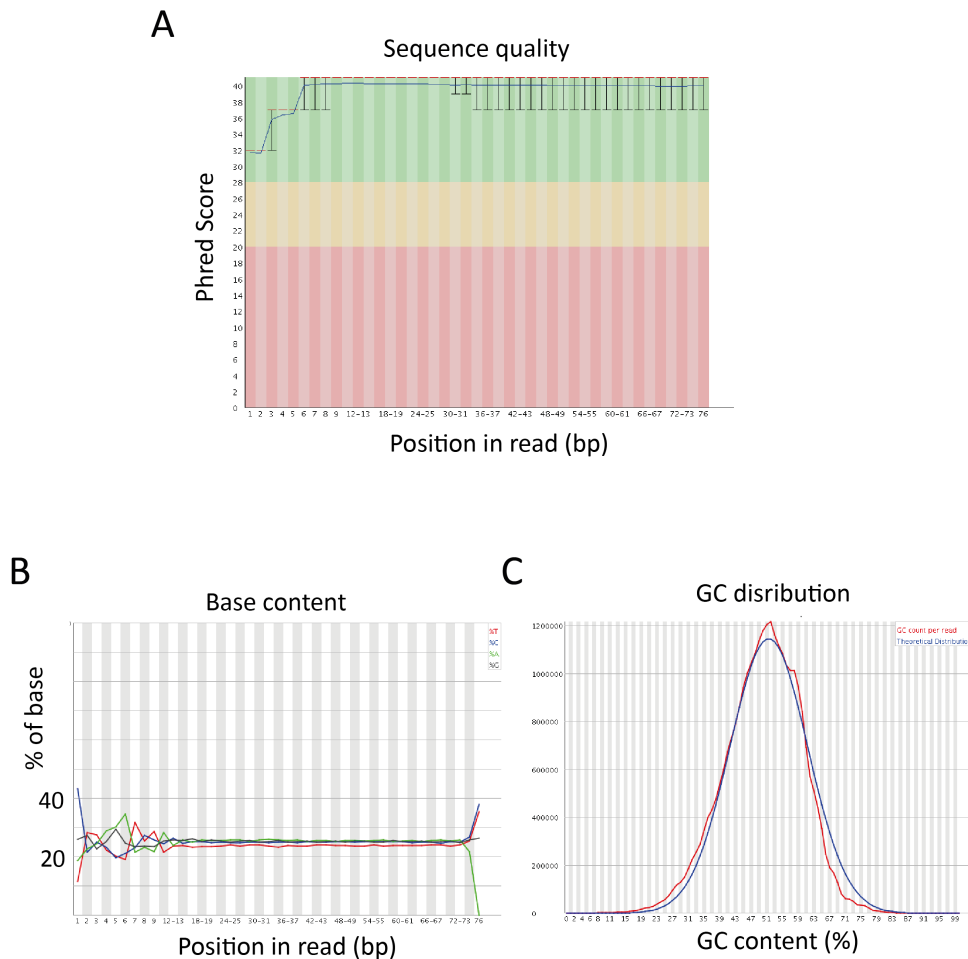
**Exons**    **Zeb1 exons**    All exons in this region

**Markup**    loaded

>chromosome:GRCh38:18:5591260:5776067:1  
GGGGATTACTCATGCTGCTTTCCTGTGAGCGGAAATTTCGTGCGGGCCTCTCTGTGCTGCTT  
GAAGTTCAACCTAACTCAGCAGTACTCCCGTCGGGTAGGCTGGGGAAACCCGCGCTGC  
TGGGAGGGGGGAGGAGGACAGAACGACGAGGTAGCTGCGGACGACGCGTCCCGGCT  
GTCCAGCTCCCGCGCGCAGCTCGGGGTCCGCCACCAACAGACGAGCGGCGCGGGT  
CCGCAAGTGCACCAATCGTCTGCTGGGGATGACGGGCTGTGCCCATGTCCGCGCAGCT  
CAACCTGGCCTAGGAAGCCACGCTGTGCCTCCCATTCTGTCCCCAGAGCCCCAGCACT  
ATTCTCCGCTATCTCACACCACTGAGCAAAACTTTCCCTCGCCTTCAAGATTCAAACT  
CTGCGAGGTCFAAGGCTGCGCGAAACACCCCGGCCCTAGCAAAAGGTTTCGGCGCGTAG  
AGCGAGCGCGCGCTAGGTGTTAGGAAGGTGATGTCGTAAGGCTCGAGTGTCTGTA AACAG  
TGTGCGTGGGAGGGGGAGGAGGTGGAGCGCCGGGTGGGGGGGGGAGGGGAGGAGGGA  
**GGGAGGGAGGGAGGAGGTCTGCGACTTATGACACAGGACGAGGATCATGGCGGATG**  
**GCCCCAGGTGTAAAGCGCAAGAAAGCGGACACCCCGCGCGCAATTACG**GTGAGTGGCGGA  
GGGCGCCGGTGCGGCGCGGGCAGCGGGCGCGCGGCGAGGGGCGCAGGGGCCAAGCGGGC  
CGGGGCGCGCGCGGGCGCGGGCCGAGTAGAGTGGGAAAGTAAAGTAGTCGCCCCCGTGT  
CCGCTGCCGCGCGCGCTGCCGCGCGCGCGCGGCTGTGTCGAGTGGACCGCTTATGTCTTAC  
TCTGCTCTCGCCTAGCGGCTCCCGCGCGCCCGCGGGAGCGTGTAGCTGCGCGCTCCG  
CCGCGCGCGCGGCCACTTTTCGCGCCGGGTGGAGCGGCTGTGCTCTTTTCGCACT  
TTCTCACTTCTGTGTCGCTTCGGCGCTCCCGCGCGGCGATCTCTCTCCGCGACGGCC  
CGACGCGGGGGAACAAACTTTCGCGCGGCGGGCGCGGGCTGTGCGGCGGGCGCGGCGG  
GAGAGGACGGGCGCGCGGGCTGGTTGCGTGTGCGGTGTGCGGCTGTGCGGCGTGGCGGCTG  
TGCGCGGAGAGCGGCGCTGCGCGCCGGTTCGGGCGCCCGCGGGAGAGTGGCGCGCGCGC  
GCTCGCGGCGCGGGGATGGGACGCGGCGCGGCGTGTGAGTGGCGCGCCAGGGGCG  
TGAAACCCGCGCCTGCGGTGCCGTGCCGTGCGGCGCGGGCACGCTCTAGTGCTCTAGCTG  
CTGCCACGGGGCGGTTGTGTCGTGAATCTCGGCTCGCGGCGGGAAATAGCAGCAGAC  
AGGTTCGGGACCGCGGCGACCGAGTCCGGCGGGCAGCGGGTGTGTGATCGCCTCT

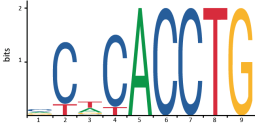

**Figure 8.3 Quality of sequencing determined by FastQC report.**

Representative traces from a FastQC report showing the quality of the sequencing. **(A)** Box and whisker plot of Phred quality scores of each base called at each point within a read. The red line represents the median value and upper and lower lines represent the 90% and 10% values. The blue line is the mean quality score. A Phred score of 30 means there is 99.9% accuracy in the base called. A Phred score of 40 gives 99.99% accuracy. **(B)** Trace showing the percentage of each base at a position in the read that has been called. For a random library an equal proportion of each base is expected. **(C)** Comparison of the GC content of a library (red), compared to a normal GC distribution (blue).



**Table 8.1 Summary table of all over-represented TFBS motifs in the promoter region of CRTAM based on relative score.**

*In silico* analysis of putative Zeb1 binding sites on the *Crtam* promoter using JASPAR (<http://jaspar.genereg.net/>), an open-access database that identifies transcription factor binding sites (TFBSs) given the promoter sequence of the transcription factor of interest. For each motif, identified by its JASPAR ID (Matrix ID), the table specifies the name of the associated transcription factor (Name), sense of DNA strand (Strand), Predicted sequence, Relative score, which shows the sensitivity and specificity of the prediction, and the relative consensus sequence (Sequence logo).

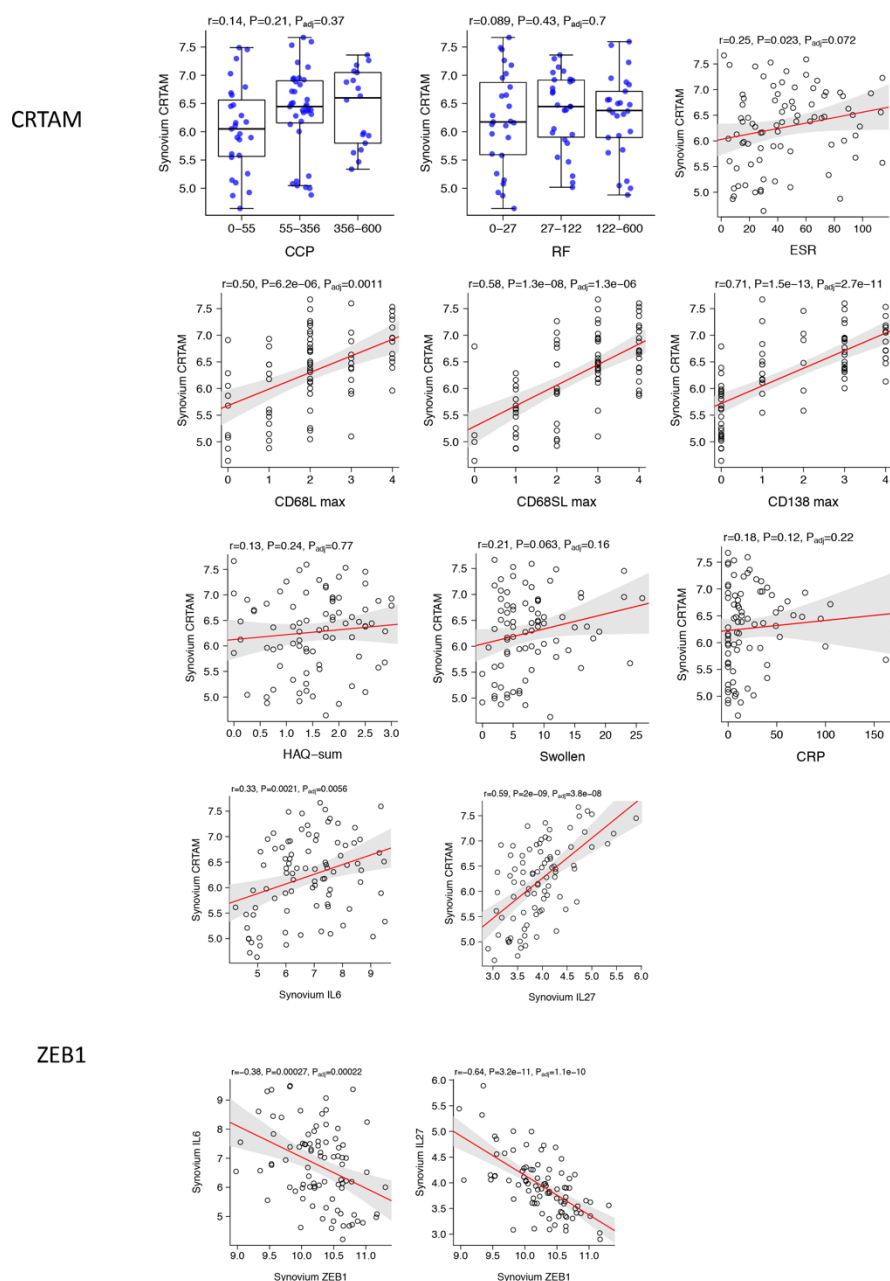
Name	Matrix ID	Strand	Predicted sequence	Relative score	Sequence logo
Zeb1	MA0103.2	-	CCCCACCTG	0.96	
		+	GCTCAGCTG	0.85	
		+	GGACACCTG	0.85	
		+	ACACATCTG	0.85	
		-	GCACACATG	0.85	
		+	CAGCACCTG	0.84	
		+	TCTCTCCTG	0.84	
		+	TCACACCTC	0.83	
		+	CCCCACGTG	0.83	
		-	CTTCAACTG	0.83	
		+	ACCCACTTG	0.82	
		-	CCTTGCCTG	0.81	
		-	CCTTACCTT	0.81	
		+	ATTACAGCTG	0.81	
		-	AGTTACCTG	0.81	
		-	ATACACATG	0.81	
		-	ACTTATCTG	0.80	
		-	GCTTAGCTG	0.80	
Zeb1	MA0103.3	-	CCCACCTGTGC	0.97	
		+	AGCACCTGCCT	0.96	
		+	GACACCTGTGG	0.95	
		+	CCCACGTGTCC	0.88	
		-	GACACGTGGGG	0.87	
		-	TGCACCGGCAC	0.86	
		+	CACACCTCTCC	0.85	
		-	GTCACCTCCTC	0.84	
		-	GTTACCTGAGT	0.84	
		+	CACATCTGCAA	0.84	
		-	ACCACATGCTG	0.83	
		-	TCCACCTTCTC	0.83	
		-	AACACCTCCTG	0.83	
		+	GTCAGCTGCTG	0.83	
		+	ACCAGETGCAG	0.83	
		+	CTCTCCTGCCC	0.83	
		-	CACACATGTAT	0.82	
		+	AGGACCTGGGT	0.82	
		+	GCCTCCTGCCC	0.82	
		-	TACACATGTAC	0.82	

+	TGCATCTGTGG	0.82
+	CCCACTTGTGG	0.82
+	TTCAGCTGTCC	0.81
-	GTCAGCTGAGC	0.81
+	CTCAGCTGACT	0.80
+	ATGACCTGTCA	0.80
+	AACACCTCGTT	0.80
+	ATCACTTGCCA	0.80

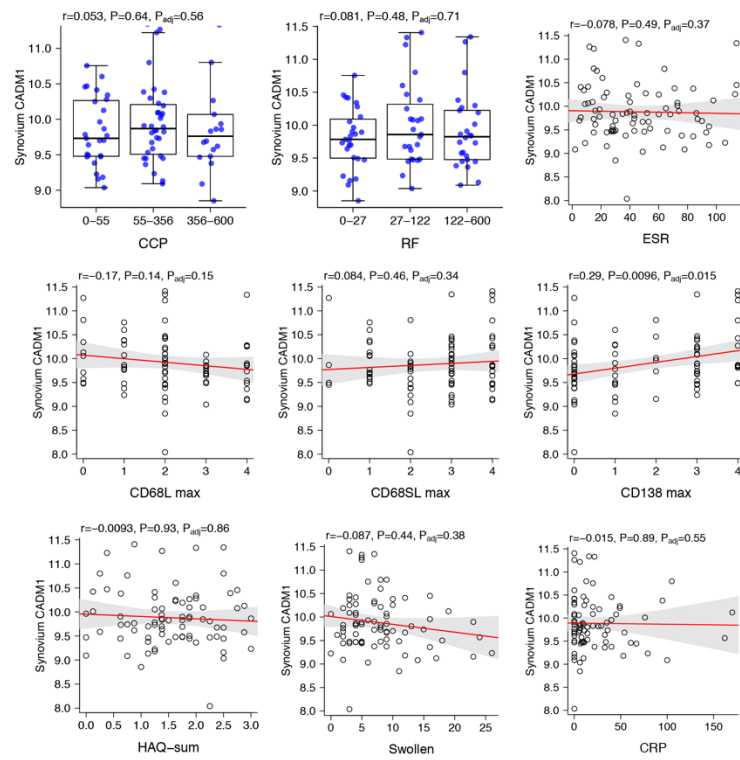
---

**Figure 8.4 Association of CRTAM, ZEB1 and CADM1 with RA in human studies.**

CCP – anti-cyclic citrullinated peptide titre; RF – rheumatoid factor titre; ESR – erythrocyte sedimentation rate; CD68L – monocytes or macrophages (CD68<sup>+</sup>) in the synovial lining; CD68SL – monocytes or macrophages (CD68<sup>+</sup>) in sublining layers; CD138 – CD138<sup>+</sup> plasma cells; HAQ – health assessment questionnaire; Swollen – swollen joints scores; CRP – C-reactive protein. Statistical analysis by one-way ANOVA with Bonferroni post-test. *P* values were adjusted using FDR correction (Benjamini-Hochberg). Data provided courtesy of Professor Costantino Pitzalis (Queen Mary University of London, UK).



CADM1



1. Sattler, S. The role of the immune system beyond the fight against infection. in *Advances in Experimental Medicine and Biology* **1003**, 3–14 (Adv Exp Med Biol, 2017).
2. Davis, D. M. *The Beautiful Cure: Harnessing Your Body's Natural Defences*. (The Bodley Head, 2018).
3. Lodish, H. *et al. Molecular Cell Biology*. (W. H. Freeman, 2016).
4. Lanier, L. L. Shades of grey-the blurring view of innate and adaptive immunity. *Nature Reviews Immunology* **13**, 73–74 (2013).
5. Cooper, M. D. & Alder, M. N. The evolution of adaptive immune systems. *Cell* **124**, 815–822 (2006).
6. Erturk-Hasdemir, D. & Kasper, D. L. Resident commensals shaping immunity. *Current Opinion in Immunology* **25**, 450–455 (2013).
7. Janeway, C. A. & Medzhitov, R. Innate Immune Recognition. *Annu. Rev. Immunol.* **20**, 197–216 (2002).
8. Janeway, C. A. Approaching the asymptote? Evolution and revolution in immunology. in *Cold Spring Harbor Symposia on Quantitative Biology* **54**, 1–13 (1989).
9. Medzhitov, R. Approaching the Asymptote: 20 Years Later. *Immunity* **30**, 766–775 (2009).
10. Iwasaki, A. & Medzhitov, R. Control of adaptive immunity by the innate immune system. *Nature Immunology* **16**, 343–353 (2015).
11. Rock, K. L. & Kono, H. The Inflammatory Response to Cell Death. *Annu. Rev. Pathol. Mech. Dis.* **3**, 99–126 (2008).
12. Medzhitov, R., Preston-Hurlburt, P. & Janeway, C. A. A human homologue of the Drosophila toll protein signals activation of adaptive immunity. *Nature* **388**, 394–397 (1997).
13. Barton, G. M. & Kagan, J. C. A cell biological view of toll-like receptor function: Regulation through compartmentalization. *Nature Reviews Immunology* **9**, 535–541 (2009).
14. Motta, V., Soares, F., Sun, T. & Philpott, D. J. Nod-like receptors: Versatile cytosolic sentinels. *Physiol. Rev.* **95**, 149–178 (2015).
15. Guo, H., Callaway, J. B. & Ting, J. P.-Y. Inflammasomes: Mechanism of action, role in disease, and therapeutics. *Nature Medicine* **21**, 677–687 (2015).
16. Tabas, I. & Glass, C. K. Anti-Inflammatory Therapy in Chronic Disease: Challenges and Opportunities. *Science (80-. )* **339**, 166–172 (2013).
17. Morgan, B. P. & Kavanagh, D. Introduction to complement in health and disease: novel aspects and insights. *Seminars in Immunopathology* **40**, 1–2 (2018).
18. Nathan, C. Neutrophils and immunity: Challenges and opportunities. *Nature Reviews Immunology* **6**, 173–182 (2006).
19. Bianchi, M. E. DAMPs, PAMPs and alarmins: all we need to know about danger. *J. Leukoc. Biol.* **81**, 1–5 (2007).
20. Patel, S. Danger-Associated Molecular Patterns (DAMPs): the Derivatives and Triggers of Inflammation. *Current Allergy and Asthma Reports* **18**, 63 (2018).
21. Murphy, Kenneth & Weaver, C. *Janeway's Immunobiology*. (Garland Science, 2016).
22. Hirano, M. *et al.* Evolutionary implications of a third lymphocyte lineage in lampreys. *Nature* **501**, 435–438 (2013).
23. Oettinger, M. A., Schatz, D. G., Gorka, C. & Baltimore, D. RAG-1 and RAG-2, adjacent genes that synergistically activate V(D)J recombination. *Science (80-. )* **248**, 1517–1523 (1990).
24. Schatz, D. G., Oettinger, M. A. & Baltimore, D. The V(D)J recombination activating gene, RAG-1. *Cell* **59**, 1035–1048 (1989).
25. Tonegawa, S. Reiteration frequency of immunoglobulin light chain genes: further evidence for somatic generation of antibody diversity. *Proc. Natl. Acad. Sci. U. S. A.* **73**, 203–207 (1976).
26. Mombaerts, P. *et al.* RAG-1-deficient mice have no mature B and T lymphocytes. *Cell* **68**, 869–877 (1992).
27. Steinman, R. M. & Banchereau, J. Taking dendritic cells into medicine. *Nature* **449**, 419–426 (2007).
28. June, C. H., Ledbetter, J. A., Gillespie, M. M., Lindsten, T. & Thompson, C. B. T-cell proliferation involving the CD28 pathway is associated with cyclosporine-resistant interleukin 2 gene expression. *Mol. Cell. Biol.* **7**, 4472–4481 (1987).
29. Muramatsu, M. *et al.* Class switch recombination and hypermutation require activation-induced cytidine deaminase (AID), a potential RNA editing enzyme. *Cell* **102**, 553–563 (2000).
30. Burnet, F. M. A Modification of Jerne's Theory of Antibody Production using the Concept of Clonal Selection. *CA. Cancer J. Clin.* **26**, 119–121 (1976).
31. Hoffman, W., Lakkis, F. G. & Chalasani, G. B cells, antibodies, and more. *Clin. J. Am. Soc. Nephrol.* **11**, 137–154 (2016).



32. Wang, L., Wang, F. S. & Gershwin, M. E. Human autoimmune diseases: A comprehensive update. *Journal of Internal Medicine* **278**, 369–395 (2015).
33. Banchereau, R., Cepika, A.-M., Banchereau, J. & Pascual, V. Understanding Human Autoimmunity and Autoinflammation Through Transcriptomics. (2017). doi:10.1146/annurev-immunol
34. Smolen, J. S., Aletaha, D. & McInnes, I. B. Rheumatoid arthritis. *The Lancet* **388**, 2023–2038 (2016).
35. Firestein, G. S. Evolving concepts of rheumatoid arthritis. *Nature* **423**, 356–361 (2003).
36. Gabriel, S. & Michaud, K. Epidemiological studies in incidence, prevalence, mortality, and comorbidity of the rheumatic diseases. *Arthritis Res. Ther.* **11**, Arte Number: 229. ate of Pubaton: 19 May 2009 (2009).
37. Peschken, C. A. & Esdaile, J. M. Rheumatic diseases in North America's indigenous peoples. *Semin. Arthritis Rheum.* **28**, 368–391 (1999).
38. Tobón, G. J., Youinou, P. & Saraux, A. The environment, geo-epidemiology, and autoimmune disease: Rheumatoid arthritis. *J. Autoimmun.* **35**, 10–14 (2010).
39. Radner, H., Lesperance, T., Accortt, N. A. & Solomon, D. H. Incidence and Prevalence of Cardiovascular Risk Factors Among Patients With Rheumatoid Arthritis, Psoriasis, or Psoriatic Arthritis. *Arthritis Care Res. (Hoboken)*. **69**, 1510–1518 (2017).
40. Sparks, J. A. *et al.* Rheumatoid Arthritis and Mortality Among Women During 36 Years of Prospective Follow-Up: Results From the Nurses' Health Study. *Arthritis Care Res. (Hoboken)*. **68**, 753–762 (2016).
41. Markuse, I. M. *et al.* Long-Term Outcomes of Patients With Recent-Onset Rheumatoid Arthritis After 10 Years of Tight Controlled Treatment. *Ann. Intern. Med.* **164**, 523 (2016).
42. Abhishek, A. *et al.* Rheumatoid arthritis and excess mortality: down but not out. A primary care cohort study using data from Clinical Practice Research Datalink. *Rheumatology* (2018). doi:10.1093/rheumatology/key013
43. Smolen, J. S. & Aletaha, D. Forget personalised medicine and focus on abating disease activity. *Annals of the Rheumatic Diseases* **72**, 3–6 (2013).
44. Prevoo, M. L. L. *et al.* Modified disease activity scores that include twenty-eight-joint counts development and validation in a prospective longitudinal study of patients with rheumatoid arthritis. *Arthritis Rheum.* **38**, 44–48 (1995).
45. Fransen, J. & van Riel, P. L. C. M. The Disease Activity Score and the EULAR Response Criteria. *Rheumatic Disease Clinics of North America* **35**, 745–757 (2009).
46. Felson, D. T. *et al.* The American college of rheumatology preliminary core set of disease activity measures for rheumatoid arthritis clinical trials. *Arthritis Rheum.* **36**, 729–740 (1993).
47. Felson, D. T. *et al.* American College of Rheumatology/European League Against Rheumatism provisional definition of remission in rheumatoid arthritis for clinical trials. *Annals of the Rheumatic Diseases* **70**, 404–413 (2011).
48. Frisell, T., Saevarsdottir, S. & Askling, J. Family history of rheumatoid arthritis: An old concept with new developments. *Nature Reviews Rheumatology* **12**, 335–343 (2016).
49. MacGregor, A. J. *et al.* Characterizing the quantitative genetic contribution to rheumatoid arthritis using data from twins. *Arthritis Rheum.* **43**, 30–37 (2000).
50. Gregersen, P. K., Silver, J. & Winchester, R. J. The shared epitope hypothesis. an approach to understanding the molecular genetics of susceptibility to rheumatoid arthritis. *Arthritis Rheum.* **30**, 1205–1213 (1987).
51. Begovich, A. B. *et al.* A Missense Single-Nucleotide Polymorphism in a Gene Encoding a Protein Tyrosine Phosphatase (PTPN22) Is Associated with Rheumatoid Arthritis. *Am. J. Hum. Genet.* **75**, 330–337 (2004).
52. Van Der Helm-van Mil, A. H. M., Wesoly, J. Z. & Huizinga, T. W. J. Understanding the genetic contribution to rheumatoid arthritis. *Current Opinion in Rheumatology* **17**, 299–304 (2005).
53. Fishman, D. *et al.* The effect of novel polymorphisms in the interleukin-6 (IL-6) gene on IL-6 transcription and plasma IL-6 levels, and an association with systemic-onset juvenile chronic arthritis. *J. Clin. Invest.* **102**, 1369–1376 (1998).
54. Krabben, A., Huizinga, T. W. J. & Mil, A. H. M. Biomarkers for Radiographic Progression in Rheumatoid Arthritis. *Curr. Pharm. Des.* **21**, 147–169 (2014).
55. Paradowska-Gorycka, A. *et al.* Association of Single Nucleotide Polymorphisms in the IL27 Gene with Rheumatoid Arthritis. *Scand. J. Immunol.* **80**, 298–305 (2014).
56. Ngo, S. T., Steyn, F. J. & McCombe, P. A. Gender differences in autoimmune disease. *Frontiers in Neuroendocrinology* **35**, 347–369 (2014).
57. Alpizar-Rodríguez, D., Pluchino, N., Canny, G., Gabay, C. & Finckh, A. *The role of female hormonal factors*

- in the development of rheumatoid arthritis. Rheumatology (United Kingdom)* **56**, 1254–1263 (Oxford University Press, 2017).
58. Smolen, J. S. *et al.* Rheumatoid arthritis. *Nat. Rev. Dis. Prim.* **4**, 18001 (2018).
  59. Benson, R. A., McInnes, I. B., Brewer, J. M. & Garside, P. Cellular imaging in rheumatic diseases. *Nature Reviews Rheumatology* **11**, 357–367 (2015).
  60. Viatte, S., Plant, D. & Raychaudhuri, S. Genetics and epigenetics of rheumatoid arthritis. *Nature reviews. Rheumatology* **9**, 141–53 (2013).
  61. Hammaker, D. & Firestein, G. S. Epigenetics of inflammatory arthritis. *CE Alpana; BOR* **300205**, (2017).
  62. VanderBorgh, A., Geusens, P., Raus, J. & Stinissen, P. The autoimmune pathogenesis of rheumatoid arthritis: Role of autoreactive T cells and new immunotherapies. *Semin. Arthritis Rheum.* **31**, 160–175 (2001).
  63. Steiner, G. Auto-antibodies and autoreactive T-cells in rheumatoid arthritis. *Clin. Rev. Allergy Immunol.* **32**, 23–35 (2007).
  64. Monach, P. A., Mathis, D. & Benoist, C. The K/BxN arthritis model. *Current Protocols in Immunology* **Chapter 15**, Unit 15.22 (2008).
  65. Muller, S. & Radic, M. Citrullinated Autoantigens: From Diagnostic Markers to Pathogenetic Mechanisms. *Clinical Reviews in Allergy and Immunology* **49**, 232–239 (2015).
  66. De Rycke, L. *et al.* Rheumatoid factor and anticitrullinated protein antibodies in rheumatoid arthritis: Diagnosis value, associations with radiological progression rate, and extra-articular manifestations. *Ann. Rheum. Dis.* **63**, 1587–1593 (2004).
  67. Makrygiannakis, D. *et al.* Smoking increases peptidylarginine deiminase 2 enzyme expression in human lungs and increases citrullination in BAL cells. *Ann. Rheum. Dis.* **67**, 1488–1492 (2008).
  68. Dissick, A. *et al.* Association of Periodontitis With Rheumatoid Arthritis: A Pilot Study. *J. Periodontol.* **81**, 223–230 (2010).
  69. Konig, M. F. *et al.* Aggregatibacter actinomycetemcomitans-induced hypercitrullination links periodontal infection to autoimmunity in rheumatoid arthritis. *Sci. Transl. Med.* **8**, 369ra176 (2016).
  70. Trouw, L. A., Huizinga, T. W. J. & Toes, R. E. M. Autoimmunity in rheumatoid arthritis: Different antigens - Common principles. *Ann. Rheum. Dis.* **72**, ii132–6 (2013).
  71. Holers, V. M. Autoimmunity to citrullinated proteins and the initiation of rheumatoid arthritis. *Current Opinion in Immunology* **25**, 728–735 (2013).
  72. Nielen, M. M. J. *et al.* Specific Autoantibodies Precede the Symptoms of Rheumatoid Arthritis: A Study of Serial Measurements in Blood Donors. *Arthritis Rheum.* **50**, 380–386 (2004).
  73. De Hair, M. J. H. *et al.* Features of the synovium of individuals at risk of developing rheumatoid arthritis : Implications for understanding preclinical rheumatoid arthritis. *Arthritis Rheumatol.* **66**, 513–522 (2014).
  74. Orr, C. *et al.* Synovial tissue research: A state-of-the-art review. *Nature Reviews Rheumatology* **13**, 463–475 (2017).
  75. Castor, C. W. The microscopic structure of normal human synovial tissue. *Arthritis Rheum.* **3**, 140–151 (1960).
  76. Bartok, B. & Firestein, G. S. Fibroblast-like synoviocytes: key effector cells in rheumatoid arthritis. *Immunol Rev.* **233**, 233–255 (2011).
  77. Kiener, H. P., Lee, D. M., Agarwal, S. K. & Brenner, M. B. Cadherin-11 induces rheumatoid arthritis fibroblast-like synoviocytes to form lining layers in vitro. *Am. J. Pathol.* **168**, 1486–1499 (2006).
  78. Kiener, H. P. *et al.* Cadherin 11 promotes invasive behavior of fibroblast-like synoviocytes. *Arthritis Rheum.* **60**, 1305–1310 (2009).
  79. Lefèvre, S. *et al.* Synovial fibroblasts spread rheumatoid arthritis to unaffected joints. *Nat. Med.* **15**, 1414–1420 (2009).
  80. Stanczyk, J. *et al.* Altered expression of microRNA in synovial fibroblasts and synovial tissue in rheumatoid arthritis. *Arthritis Rheum.* **58**, 1001–1009 (2008).
  81. Croft, A. *et al.* Distinct fibroblast subsets drive inflammation and damage in arthritis. *Nature* **570**, 246–251 (2019).
  82. Mizoguchi, F. *et al.* Functionally distinct disease-associated fibroblast subsets in rheumatoid arthritis. *Nat. Commun.* **9**, (2018).
  83. Hsieh, C. S. *et al.* Development of TH1 CD4+ T cells through IL-12 produced by Listeria-induced macrophages. *Science (80-. )*. **260**, 547–549 (1993).
  84. Swain, S. L., Weinberg, A. D., English, M. & Huston, G. IL-4 directs the development of Th2-like helper

- effectors. *J. Immunol.* **145**, 3796–806 (1990).
85. Stritesky, G. L., Yeh, N. & Kaplan, M. H. IL-23 Promotes Maintenance but Not Commitment to the Th17 Lineage. *J. Immunol.* **181**, 5948–5955 (2008).
86. Veldhoen, M., Hocking, R. J., Atkins, C. J., Locksley, R. M. & Stockinger, B. TGF $\beta$  in the context of an inflammatory cytokine milieu supports de novo differentiation of IL-17-producing T cells. *Immunity* **24**, 179–189 (2006).
87. Nurieva, R. I. *et al.* Generation of T Follicular Helper Cells Is Mediated by Interleukin-21 but Independent of T Helper 1, 2, or 17 Cell Lineages. *Immunity* **29**, 138–149 (2008).
88. Zhu, J., Yamane, H. & Paul, W. E. Differentiation of Effector CD4 T Cell Populations. *Annu. Rev. Immunol.* **28**, 445–489 (2010).
89. Dienz, O. *et al.* The induction of antibody production by IL-6 is indirectly mediated by IL-21 produced by CD4 + T cells. *J. Exp. Med.* **206**, 69–78 (2009).
90. Chen, W. J. *et al.* Conversion of Peripheral CD4+CD25- Naive T Cells to CD4+CD25+ Regulatory T Cells by TGF- $\beta$  Induction of Transcription Factor Foxp3. *J. Exp. Med.* **198**, 1875–1886 (2003).
91. Eyerich, S. *et al.* Th22 cells represent a distinct human T cell subset involved in epidermal immunity and remodeling. *J. Clin. Invest.* **119**, 3573–3585 (2009).
92. Rauber, S. *et al.* Resolution of inflammation by interleukin-9-producing type 2 innate lymphoid cells. *Nat. Med.* **23**, 938–944 (2017).
93. Gagliani, N. *et al.* TH17 cells transdifferentiate into regulatory T cells uring resolution of inflammation. *Nature* **523**, 221–225 (2015).
94. Carrier, Y., Yuan, J., Kuchroo, V. K. & Weiner, H. L. Th3 Cells in Peripheral Tolerance. I. Induction of Foxp3-Positive Regulatory T Cells by Th3 Cells Derived from TGF- $\beta$  T Cell-Transgenic Mice. *J. Immunol.* **178**, 179–185 (2007).
95. Dardalhon, V. *et al.* IL-4 inhibits TGF- $\beta$ -induced Foxp3+ T cells and, together with TGF- $\beta$ , generates IL-9+ IL-10+ Foxp3- effector T cells. *Nat. Immunol.* **9**, 1347–1355 (2008).
96. Veldhoen, M. *et al.* Transforming growth factor- $\beta$  ‘reprograms’ the differentiation of T helper 2 cells and promotes an interleukin 9-producing subset. *Nat. Immunol.* **9**, 1341–1346 (2008).
97. Yamane, H. & Paul, W. E. Memory CD4 + T Cells: Fate determination, positive feedback and plasticity. *Cellular and Molecular Life Sciences* **69**, 1577–1583 (2012).
98. Addey, C. *et al.* Functional Plasticity of Antigen-Specific Regulatory T Cells in Context of Tumor. *J. Immunol.* **186**, 4557–4564 (2011).
99. Zhou, L., Chong, M. M. W. & Littman, D. R. Plasticity of CD4+ T Cell Lineage Differentiation. *Immunity* **30**, 646–655 (2009).
100. Hirota, K. *et al.* Autoimmune Th17 Cells Induced Synovial Stromal and Innate Lymphoid Cell Secretion of the Cytokine GM-CSF to Initiate and Augment Autoimmune Arthritis. *Immunity* **48**, 1220–1232.e5 (2018).
101. Pöllinger, B. *et al.* Th17 Cells, Not IL-17 +  $\gamma\delta$  T Cells, Drive Arthritic Bone Destruction in Mice and Humans. *J. Immunol.* **186**, 2602–2612 (2011).
102. Frederique Ponchel\*, Edward Vital, S. R. K. & Yasser. Evidence for roles of T cells in rheumatoid arthritis. *Int. J. Clin. Rheumatol* **7**, 37–53 (2012).
103. Peters, A. *et al.* Th17 cells induce ectopic lymphoid follicles in central nervous system tissue inflammation. *Immunity* **35**, 986–996 (2011).
104. Jones, G. W. *et al.* Interleukin-27 inhibits ectopic lymphoid-like structure development in early inflammatory arthritis. *J. Exp. Med.* **212**, 1793–802 (2015).
105. Cooles, F. A. H., Isaacs, J. D. & Anderson, A. E. Treg cells in rheumatoid arthritis: An update. *Curr. Rheumatol. Rep.* **15**, 352 (2013).
106. Komatsu, N. *et al.* Pathogenic conversion of Foxp3 + T cells into TH17 cells in autoimmune arthritis. *Nat. Med.* **20**, 62–68 (2014).
107. Humby, F. *et al.* Ectopic lymphoid structures support ongoing production of class-switched autoantibodies in rheumatoid synovium. *PLoS Med.* **6**, 0059–0075 (2009).
108. Henkart, P. A. Lymphocyte-mediated cytotoxicity: Two pathways and multiple effector molecules. *Immunity* **1**, 343–346 (1994).
109. Andersen, M. H., Schrama, D., Thor Straten, P. & Becker, J. C. Cytotoxic T cells. *Journal of Investigative Dermatology* **126**, 32–41 (2006).
110. Skapenko, A., Leipe, J., Lipsky, P. E. & Schulze-Koops, H. The role of the T cell in autoimmune inflammation. *Arthritis Res. Ther.* **7 Suppl 2**, S4–14 (2005).

111. Samuels, J., Ng, Y. S., Coupillaud, C., Paget, D. & Meffre, E. Impaired early B cell tolerance in patients with rheumatoid arthritis. *J. Exp. Med.* **201**, 1659–1667 (2005).
112. Barr, T. A. *et al.* B cell depletion therapy ameliorates autoimmune disease through ablation of IL-6-producing B cells. *J. Exp. Med.* **209**, 1001–1010 (2012).
113. Yeo, L. *et al.* Cytokine mRNA profiling identifies B cells as a major source of RANKL in rheumatoid arthritis. *Ann. Rheum. Dis.* **70**, 2022–2028 (2011).
114. Weyand, C. M. & Goronzy, J. J. Ectopic germinal center formation in rheumatoid synovitis. in *Annals of the New York Academy of Sciences* **987**, 140–149 (John Wiley & Sons, Ltd, 2003).
115. Randen, I. *et al.* Clonally related IgM rheumatoid factors undergo affinity maturation in the rheumatoid synovial tissue. *J. Immunol.* **148**, 3296–301 (1992).
116. Catrina, A. I., Jimmy Ytterberg, A., Reynisdottir, G., Malmström, V. & Klareskog, L. Lungs, joints and immunity against citrullinated proteins in rheumatoid arthritis. *Nature Reviews Rheumatology* **10**, 645–653 (2014).
117. Haringman, J. J. *et al.* Synovial tissue macrophages: A sensitive biomarker for response to treatment in patients with rheumatoid arthritis. *Ann. Rheum. Dis.* **64**, 834–838 (2005).
118. McInnes, I. B. & Schett, G. Cytokines in the pathogenesis of rheumatoid arthritis. *Nat. Rev. Immunol.* **7**, 429–442 (2007).
119. Choy, E. H., Kavanaugh, A. F. & Jones, S. A. The problem of choice: current biologic agents and future prospects in RA. *Nat. Rev. Rheumatol.* **9**, 154–163 (2013).
120. Feldmann, M. & Maini, R. N. Anti-TNF $\alpha$  therapy of Rheumatoid Arthritis: What Have We Learned? *Annu. Rev. Immunol.* **19**, 163–196 (2001).
121. Feldmann, M. & Maini, S. R. N. Role of cytokines in rheumatoid arthritis: An education in pathophysiology and therapeutics. *Immunological Reviews* **223**, 7–19 (2008).
122. Zhang, Y. H., Heulsmann, A., Tondravi, M. M., Mukherjee, A. & Abu-Amer, Y. Tumor necrosis factor- $\alpha$  (TNF) stimulates RANKL-induced osteoclastogenesis via coupling of TNF type 1 receptor and RANK signaling pathways. *J. Biol. Chem.* **276**, 563–568 (2001).
123. McInnes, I. B., Buckley, C. D. & Isaacs, J. D. Cytokines in rheumatoid arthritis — shaping the immunological landscape. *Nat. Rev. Rheumatol.* **12**, 63–68 (2015).
124. Jones, S. A. *et al.* Interleukin 6: The biology behind the therapy. *Considerations Med.* **2**, 2–6 (2018).
125. McInnes, I. B. *et al.* Effect of interleukin-6 receptor blockade on surrogates of vascular risk in rheumatoid arthritis: MEASURE, a randomised, placebo-controlled study. *Ann. Rheum. Dis.* **74**, 694–702 (2015).
126. Tanaka, T., Narazaki, M. & Kishimoto, T. IL-6 in inflammation, Immunity, And disease. *Cold Spring Harb. Perspect. Biol.* **6**, a016295 (2014).
127. Gabay, C. *et al.* Tocilizumab monotherapy versus adalimumab monotherapy for treatment of rheumatoid arthritis (ADACTA): A randomised, double-blind, controlled phase 4 trial. *Lancet* **381**, 1541–1550 (2013).
128. Dennis, G. *et al.* Synovial phenotypes in rheumatoid arthritis correlate with response to biologic therapeutics. *Arthritis Res. Ther.* **16**, R90 (2014).
129. McInnes, I. B. & Schett, G. The pathogenesis of rheumatoid arthritis. *The New England journal of medicine* **365**, 2205–2219 (2011).
130. Garlanda, C., Dinarello, C. A. & Mantovani, A. The Interleukin-1 Family: Back to the Future. *Immunity* **39**, 1003–1018 (2013).
131. Schett, G., Dayer, J. M. & Manger, B. Interleukin-1 function and role in rheumatic disease. *Nat. Rev. Rheumatol.* **12**, 14–24 (2016).
132. Mertens, M. & Singh, J. A. Anakinra for rheumatoid arthritis. *Cochrane Database of Systematic Reviews* (2009). doi:10.1002/14651858.CD005121.pub3
133. Van Nieuwenhuijze, A. *et al.* GM-CSF as a therapeutic target in inflammatory diseases. *Molecular Immunology* **56**, 675–682 (2013).
134. Burmester, G. R. *et al.* Efficacy and safety of mavrilimumab in subjects with rheumatoid arthritis. *Ann. Rheum. Dis.* **72**, 1445–1452 (2013).
135. Lubberts, E. Th17 cytokines and arthritis. *Seminars in Immunopathology* **32**, 43–53 (2010).
136. Benedetti, G. & Miossec, P. Interleukin 17 contributes to the chronicity of inflammatory diseases such as rheumatoid arthritis. *Eur. J. Immunol.* **44**, 339–347 (2014).
137. Ferretti, E., Ponzoni, M., Doglioni, C. & Pistoia, V. IL-17 superfamily cytokines modulate normal germinal center B cell migration. *J. Leukoc. Biol.* **100**, 913–918 (2016).

138. Pfeifle, R. *et al.* Regulation of autoantibody activity by the IL-23-T H 17 axis determines the onset of autoimmune disease. *Nat. Immunol.* **18**, 104–113 (2017).
139. Hill, D. G. *et al.* Hyperactive gp130/STAT3-driven gastric tumourigenesis promotes submucosal tertiary lymphoid structure development. *Int. J. Cancer* **143**, 167–178 (2018).
140. Robert, M. & Miossec, P. IL-17 in rheumatoid arthritis and precision medicine: From synovitis expression to circulating bioactive levels. *Frontiers in Medicine* **6**, 364 (2019).
141. Lubberts, E. The IL-23-IL-17 axis in inflammatory arthritis. *Nature Reviews Rheumatology* **11**, 415–429 (2015).
142. Vignali, D. A. A. & Kuchroo, V. K. IL-12 family cytokines: immunological playmakers. *Nature Immunology* **13**, 722–728 (2012).
143. Jones, G. W., Hill, D. G., Cardus, A. & Jones, S. A. IL-27: a double agent in the IL-6 family. *Clin. Exp. Immunol.* **193**, 37–46 (2018).
144. Schwartz, D. M. *et al.* JAK inhibition as a therapeutic strategy for immune and inflammatory diseases. *Nat. Rev. Drug Discov.* nrd.2017.201 (2017). doi:10.1038/nrd.2017.201
145. Hermann, J. A., Hall, M. A., Maini, R. N., Feldmann, M. & Brennan, F. M. Important immunoregulatory role of interleukin-11 in the inflammatory process in rheumatoid arthritis. *Arthritis Rheum.* **41**, 1388–1397 (1998).
146. Kim, H. R., Hwang, K. A., Park, S. H. & Kang, I. IL-7 and IL-15: Biology and roles in T-cell immunity in health and disease. *Critical Reviews in Immunology* **28**, 325–339 (2008).
147. Deshpande, P. *et al.* IL-7– and IL-15–Mediated TCR Sensitization Enables T Cell Responses to Self-Antigens. *J. Immunol.* **190**, 1416–1423 (2013).
148. Krishnamurthy, A. *et al.* Identification of a novel chemokine-dependent molecular mechanism underlying Rheumatoid arthritis-associated autoantibody-mediated bone loss. *Ann. Rheum. Dis.* **75**, 721–729 (2016).
149. Klimiuk, P. A., Goronzy, J. J., Björ nsson, J., Beckenbaugh, R. D. & Weyand, C. M. Tissue cytokine patterns distinguish variants of rheumatoid synovitis. *Am. J. Pathol.* **151**, 1311–9 (1997).
150. Pitzalis, C., Kelly, S. & Humby, F. New learnings on the pathophysiology of RA from synovial biopsies. *Curr. Opin. Rheumatol.* **25**, 334–344 (2013).
151. Bugatti, S. *et al.* Synovial tissue heterogeneity and peripheral blood biomarkers. *Curr. Rheumatol. Rep.* **13**, 440–448 (2011).
152. Kavanaugh, A. *et al.* Assessment of rituximab’s immunomodulatory synovial effects (ARISE trial). 1: Clinical and synovial biomarker results. *Ann. Rheum. Dis.* **67**, 402–408 (2008).
153. Cañete, J. D. *et al.* Clinical significance of synovial lymphoid neogenesis and its reversal after anti-tumour necrosis factor therapy in rheumatoid arthritis. *Ann. Rheum. Dis.* **68**, 751–756 (2009).
154. Lewis, M. J. *et al.* Molecular Portraits of Early Rheumatoid Arthritis Identify Clinical and Treatment Response Phenotypes. *Cell Rep.* **28**, 2455–2470.e5 (2019).
155. Pitzalis, C., Jones, G. W., Bombardieri, M. & Jones, S. A. Ectopic lymphoid-like structures in infection, cancer and autoimmunity. *Nat. Rev. Immunol.* **14**, 447–62 (2014).
156. Jones, G. W., Hill, D. G. & Jones, S. A. Understanding immune cells in tertiary lymphoid organ development: It is all starting to come together. *Frontiers in Immunology* **7**, 401 (2016).
157. Mebius, R. E., Rennert, P. & Weissman, I. L. Developing lymph nodes collect CD4+CD3- LTβ+ cells that can differentiate to APC, NK cells, and follicular cells but not T or B cells. *Immunity* **7**, 493–504 (1997).
158. Bombardieri, M., Lewis, M. & Pitzalis, C. Ectopic lymphoid neogenesis in rheumatic autoimmune diseases. *Nature Reviews Rheumatology* **13**, 141–154 (2017).
159. Peduto, L. *et al.* Inflammation Recapitulates the Ontogeny of Lymphoid Stromal Cells. *J. Immunol.* **182**, 5789–5799 (2009).
160. Browning, J. L. *et al.* Lymphotoxin-β receptor signaling is required for the homeostatic control of HEV differentiation and function. *Immunity* **23**, 539–550 (2005).
161. Kim, K. W. *et al.* Up-regulation of stromal cell-derived factor 1 (CXCL12) production in rheumatoid synovial fibroblasts through interactions with T lymphocytes: Role of interleukin-17 and CD40L-CD40 interaction. *Arthritis Rheum.* **56**, 1076–1086 (2007).
162. Grogan, J. L. & Ouyang, W. A role for Th17 cells in the regulation of tertiary lymphoid follicles. *European Journal of Immunology* **42**, 2255–2262 (2012).
163. Smolen, J. S., Aletaha, D., Grisar, J. C., Stamm, T. A. & Sharp, J. T. Estimation of a numerical value for joint damage-related physical disability in rheumatoid arthritis clinical trials. *Ann. Rheum. Dis.* **69**, 1058–1064



- (2010).
164. Van der Heijde, D. M. F. M. *et al.* Validity of single variables and composite indices for measuring disease activity in rheumatoid arthritis. *Ann. Rheum. Dis.* **51**, 177–181 (1992).
  165. Smolen, J. S. *et al.* Treating rheumatoid arthritis to target: 2014 update of the recommendations of an international task force. *Ann. Rheum. Dis.* **75**, 3–15 (2016).
  166. De Stefano, R. *et al.* Comparison of combination therapies in the treatment of rheumatoid arthritis: Leflunomide-anti-TNF-alpha versus methotrexate-anti-TNF-alpha. *Clin. Rheumatol.* **29**, 517–524 (2010).
  167. Benedek, T. G. History of the development of corticosteroid therapy. *Clin. Exp. Rheumatol.* **29**, S-5-12 (2011).
  168. Visser, K. & Van Der Heijde, D. Optimal dosage and route of administration of methotrexate in rheumatoid arthritis: A systematic review of the literature. *Annals of the Rheumatic Diseases* **68**, 1094–1099 (2009).
  169. Smolen, J. S. *et al.* EULAR recommendations for the management of rheumatoid arthritis with synthetic and biological disease-modifying antirheumatic drugs: 2016 update. *Ann. Rheum. Dis.* **76**, 960–977 (2017).
  170. Elliott, M. J. *et al.* Randomised double-blind comparison of chimeric monoclonal antibody to tumour necrosis factor  $\alpha$  (cA2) versus placebo in rheumatoid arthritis. *Lancet* **344**, 1105–1110 (1994).
  171. Scott, L. J. Tocilizumab: A Review in Rheumatoid Arthritis. *Drugs* **77**, 1865–1879 (2017).
  172. Edwards, J. C. W., Leandro, M. J. & Cambridge, G. B lymphocyte depletion in rheumatoid arthritis: targeting of CD20. *Curr. Dir. Autoimmun.* **8**, 175–192 (2005).
  173. Mierau, M. *et al.* Assessing remission in clinical practice. *Rheumatology* **46**, 975–979 (2007).
  174. Weinblatt, M. E. *et al.* A trial of etanercept, a recombinant tumor necrosis factor receptor:Fc fusion protein, in patients with rheumatoid arthritis receiving methotrexate. *N. Engl. J. Med.* **340**, 253–259 (1999).
  175. Weinblatt, M. E. *et al.* Adalimumab, a fully human anti-tumor necrosis factor  $\alpha$  monoclonal antibody, for the treatment of rheumatoid arthritis in patients taking concomitant methotrexate: The ARMADA trial. *Arthritis Rheum.* **48**, 35–45 (2003).
  176. Lipsky, P. E. *et al.* Infliximab and methotrexate in the treatment of rheumatoid arthritis. *N. Engl. J. Med.* **343**, 1594–1602 (2000).
  177. Liongue, C. & Ward, A. C. Evolution of the JAK-STAT pathway. *JAK-STAT* **2**, e22756 (2013).
  178. Darnell, J. E., Kerr, I. M. & Stark, G. R. Jak-STAT Pathways and Transcriptional Activation in Response to IFNs and Other Extracellular Signaling Proteins. *Adv. Sci.* **264**, 1415–1421 (2008).
  179. Aggarwal, B. B. Signalling pathways of the TNF superfamily: A double-edged sword. *Nature Reviews Immunology* **3**, 745–756 (2003).
  180. Lawrence, T. The nuclear factor NF-kappaB pathway in inflammation. *Cold Spring Harbor perspectives in biology* **1**, a001651 (2009).
  181. Braicu, C. *et al.* A comprehensive review on MAPK: A promising therapeutic target in cancer. *Cancers* **11**, (2019).
  182. Weber, A., Wasiliew, P. & Kracht, M. Interleukin-1 (IL-1) pathway. *Science Signaling* **3**, cm1 (2010).
  183. O'shea, J. J., Kontzias, A., Yamaoka, K., Tanaka, Y. & Laurence, A. Janus kinase Inhibitors in autoimmune diseases Role of Type I/II cytokines in RA and related diseases. *Ann. Rheum. Dis.* **72**, 1–11 (2013).
  184. Heinrich, P. C. *et al.* Principles of interleukin (IL)-6-type cytokine signalling and its regulation. *Biochem. J.* **374**, 1–20 (2003).
  185. O'shea, J. J. *et al.* The JAK-STAT Pathway: Impact on Human Disease and Therapeutic Intervention \*. *Annu. Rev. Med* **66**, 311–28 (2015).
  186. Villarino, A. V., Kanno, Y. & O'Shea, J. J. Mechanisms and consequences of Jak-STAT signaling in the immune system. *Nature Immunology* **18**, 374–384 (2017).
  187. Takeda, A. *et al.* Cutting Edge: Role of IL-27/WSX-1 Signaling for Induction of T-Bet Through Activation of STAT1 During Initial Th1 Commitment. *J. Immunol.* **170**, 4886–4890 (2003).
  188. Takeda, K. *et al.* Correction: Stat3 Activation Is Responsible for IL-6-Dependent T Cell Proliferation through Preventing Apoptosis: Generation and Characterization of T Cell-Specific Stat3-Deficient Mice. *J. Immunol.* **194**, 3526–3526 (2015).
  189. Hirahara, K. *et al.* Asymmetric Action of STAT Transcription Factors Drives Transcriptional Outputs and Cytokine Specificity. *Immunity* **42**, 877–889 (2015).
  190. Vahedi, G. *et al.* STATs shape the active enhancer landscape of T cell populations. *Cell* **151**, 981–993

- (2012).
191. Lu, D. *et al.* The phosphatase DUSP2 controls the activity of the transcription activator STAT3 and regulates T H 17 differentiation. *Nat. Immunol.* **16**, 1263–1273 (2015).
  192. Böhmer, F.-D. & Friedrich, K. Protein tyrosine phosphatases as wardens of STAT signaling. *JAK-STAT* **3**, e28087 (2014).
  193. Wu, T. R. *et al.* SHP-2 is a dual-specificity phosphatase involved in Stat1 dephosphorylation at both tyrosine and serine residues in nuclei. *J. Biol. Chem.* **277**, 47572–47580 (2002).
  194. Twohig, J. P. *et al.* Activation of naïve CD4 + T cells re-tunes STAT1 signaling to deliver unique cytokine responses in memory CD4 + T cells. *Nat. Immunol.* **20**, 458–470 (2019).
  195. O’Shea, J. J. & Plenge, R. JAK and STAT Signaling Molecules in Immunoregulation and Immune-Mediated Disease. *Immunity* **36**, 542–550 (2012).
  196. Hilton, D. J. *et al.* Twenty proteins containing a C-terminal SOCS box form five structural classes. *Proc. Natl. Acad. Sci. U. S. A.* **95**, 114–119 (1998).
  197. Piessevaux, J., Lavens, D., Peelman, F. & Tavernier, J. The many faces of the SOCS box. *Cytokine and Growth Factor Reviews* **19**, 371–381 (2008).
  198. Shuai, K. & Liu, B. Regulation of JAK–STAT signalling in the immune system. *Nat. Rev. Immunol.* **3**, 900–911 (2003).
  199. Babon, J. J. & Nicola, N. A. The biology and mechanism of action of suppressor of cytokine signaling 3. *Growth Factors* **30**, 207–219 (2012).
  200. Babon, J. J., Sabo, J. K., Zhang, J. G., Nicola, N. A. & Norton, R. S. The SOCS Box Encodes a Hierarchy of Affinities for Cullin5: Implications for Ubiquitin Ligase Formation and Cytokine Signalling Suppression. *J. Mol. Biol.* **387**, 162–174 (2009).
  201. Mahony, R., Ahmed, S., Diskin, C. & Stevenson, N. J. *SOCS3 revisited: a broad regulator of disease, now ready for therapeutic use? Cellular and Molecular Life Sciences* **73**, 3323–3336 (Springer International Publishing, 2016).
  202. Wang, F., Sengupta, T. K., Zhong, Z. & Ivashkiv, L. B. Regulation of the balance of cytokine production and the signal transducer and activator of transcription (STAT) transcription factor activity by cytokines and inflammatory synovial fluids. *J. Exp. Med.* **182**, 1825–1831 (1995).
  203. Sengupta, T. K., Chen, A., Zhong, Z., Darnell, J. E. & Ivashkiv, L. B. Activation of monocyte effector genes and STAT family transcription factors by inflammatory synovial fluid is independent of interferon  $\gamma$ . *J. Exp. Med.* **181**, 1015–1025 (1995).
  204. Nowell, M. A. *et al.* Therapeutic targeting of IL-6 trans signaling counteracts STAT3 control of experimental inflammatory arthritis. *J. Immunol.* **182**, 613–22 (2009).
  205. Jones, G. W. *et al.* Exacerbated inflammatory arthritis in response to hyperactive gp130 signalling is independent of IL-17A. *Ann. Rheum. Dis.* **72**, 1738–42 (2013).
  206. Shouda, T. *et al.* Induction of the cytokine signal regulator SOCS3/CIS3 as a therapeutic strategy for treating inflammatory arthritis. *J. Clin. Invest.* **108**, 1781–1788 (2001).
  207. Croker, B. A. *et al.* SOCS3 negatively regulates IL-6 signaling in vivo. *Nat. Immunol.* **4**, 540–545 (2003).
  208. Oike, T. *et al.* Stat3 as a potential therapeutic target for rheumatoid arthritis. *Sci. Rep.* **7**, 10965 (2017).
  209. Svensson, M. N. *et al.* Reduced expression of phosphatase PTPN2 promotes pathogenic conversion of Tregs in autoimmunity. *Journal of Clinical Investigation* **129**, 1193–1210 (2019).
  210. Veenbergen, S. *et al.* Splenic suppressor of cytokine signaling 3 transgene expression affects T cell responses and prevents development of collagen-induced arthritis. *Arthritis Rheum.* **58**, 3742–3752 (2008).
  211. Yasukawa, H. *et al.* IL-6 induces an anti-inflammatory response in the absence of SOCS3 in macrophages. *Nat. Immunol.* **4**, 551–556 (2003).
  212. Hunter, C. A. & Jones, S. A. IL-6 as a keystone cytokine in health and disease. *Nat. Immunol.* **16**, 448–57 (2015).
  213. Wong, P. K. K. *et al.* SOCS-3 negatively regulates innate and adaptive immune mechanisms in acute IL-1-dependent inflammatory arthritis. *J. Clin. Invest.* **116**, 1571–1581 (2006).
  214. Van De Loo, F. A. J. *et al.* Enhanced suppressor of cytokine signaling 3 in arthritic cartilage dysregulates human chondrocyte function. *Arthritis Rheum.* **64**, 3313–3323 (2012).
  215. Hirano, T. *et al.* Complementary DNA for a novel human interleukin (BSF-2) that induces B lymphocytes to produce immunoglobulin. *Nature* **324**, 73–76 (1986).
  216. Jones, S. A., Scheller, J. & Rose-John, S. Therapeutic strategies for the clinical blockade of IL-6/gp130

- signaling. *J. Clin. Invest.* **121**, 3375–83 (2011).
217. Hibi, M. *et al.* Molecular cloning and expression of an IL-6 signal transducer, gp130. *Cell* **63**, 1149–1157 (1990).
  218. Taga, T. *et al.* Interleukin-6 triggers the association of its receptor with a possible signal transducer, gp130. *Cell* **58**, 573–581 (1989).
  219. Tosato, G. *et al.* Monocyte-derived human B-cell growth factor identified as Interferon- $\beta$ 2 (BSF-2, IL-6). *Science* (80-. ). **239**, 502–504 (1988).
  220. Skiniotis, G., Boulanger, M. J., Garcia, K. C. & Walz, T. Signaling conformations of the tall cytokine receptor gp130 when in complex with IL-6 and IL-6 receptor. *Nat. Struct. Mol. Biol.* **12**, 545–551 (2005).
  221. Rose-John, S. Interleukin-6 biology is coordinated by membrane-bound and soluble receptors: role in inflammation and cancer. *J. Leukoc. Biol.* **80**, 227–236 (2006).
  222. Scheller, J. & Rose-John, S. Interleukin-6 and its receptor: From bench to bedside. *Medical Microbiology and Immunology* **195**, 173–183 (2006).
  223. Matthews, V. *et al.* Cellular cholesterol depletion triggers shedding of the human interleukin-6 receptor by ADAM10 and ADAM17 (TACE). *J. Biol. Chem.* **278**, 38829–38839 (2003).
  224. Jones, S. A. Directing Transition from Innate to Acquired Immunity: Defining a Role for IL-6. *J. Immunol.* **175**, 3463–3468 (2005).
  225. Campbell, I. L. *et al.* Trans-signaling is a dominant mechanism for the pathogenic actions of interleukin-6 in the brain. *J. Neurosci.* **34**, 2503–2513 (2014).
  226. Richards, P. J. *et al.* Functional characterization of a soluble gp130 isoform and its therapeutic capacity in an experimental model of inflammatory arthritis. *Arthritis Rheum.* **54**, 1662–1672 (2006).
  227. Jostock, T. *et al.* Soluble gp130 is the natural inhibitor of soluble interleukin-6 receptor transsignaling responses. *Eur. J. Biochem.* **268**, 160–167 (2001).
  228. Lamertz, L. *et al.* Soluble gp130 prevents interleukin-6 and interleukin-11 cluster signaling but not intracellular autocrine responses. *Sci. Signal.* **11**, 1–14 (2018).
  229. Heink, S. *et al.* Trans-presentation of IL-6 by dendritic cells is required for the priming of pathogenic T H 17 cells. *Nat. Immunol.* **18**, 74–85 (2017).
  230. Kingsolver, M. B. & Hardy, R. W. Making connections in insect innate immunity. *Proceedings of the National Academy of Sciences of the United States of America* **109**, 18639–18640 (2012).
  231. McLoughlin, R. M. *et al.* Interplay between IFN- $\gamma$  and IL-6 signaling governs neutrophil trafficking and apoptosis during acute inflammation. *J. Clin. Invest.* **112**, 598–607 (2003).
  232. Hurst, S. M. *et al.* IL-6 and its soluble receptor orchestrate a temporal switch in the pattern of leukocyte recruitment seen during acute inflammation. *Immunity* **14**, 705–714 (2001).
  233. Mauer, J. *et al.* Signaling by IL-6 promotes alternative activation of macrophages to limit endotoxemia and obesity-associated resistance to insulin. *Nat. Immunol.* **15**, 423–430 (2014).
  234. Silver, J. S., Stumhofer, J. S., Passos, S., Ernst, M. & Hunter, C. A. IL-6 Mediates the Susceptibility of Glycoprotein 130 Hypermorphs to *Toxoplasma gondii*. *J. Immunol.* **187**, 350–360 (2011).
  235. Jin, J. O., Han, X. & Yu, Q. Interleukin-6 induces the generation of IL-10-producing Tr1 cells and suppresses autoimmune tissue inflammation. *J. Autoimmun.* **40**, 28–44 (2013).
  236. Harker, J. A., Lewis, G. M., Mack, L. & Zuniga, E. I. Late interleukin-6 escalates T follicular helper cell responses and controls a chronic viral infection. *Science* (80-. ). **334**, 825–829 (2011).
  237. Harrington, L. E. *et al.* Interleukin 17-producing CD4+ effector T cells develop via a lineage distinct from the T helper type 1 and 2 lineages. *Nat. Immunol.* **6**, 1123–1132 (2005).
  238. Zhou, L. *et al.* IL-6 programs TH-17 cell differentiation by promoting sequential engagement of the IL-21 and IL-23 pathways. *Nat. Immunol.* **8**, 967–974 (2007).
  239. Acosta-Rodriguez, E. V., Napolitani, G., Lanzavecchia, A. & Sallusto, F. Interleukins 1 $\beta$  and 6 but not transforming growth factor- $\beta$  are essential for the differentiation of interleukin 17-producing human T helper cells. *Nat. Immunol.* **8**, 942–949 (2007).
  240. O'Connor, R. A., Floess, S., Huehn, J., Jones, S. A. & Anderton, S. M. Foxp3 + Treg cells in the inflamed CNS are insensitive to IL-6-driven IL-17 production. *Eur. J. Immunol.* **42**, 1174–1179 (2012).
  241. Ohshima, S. *et al.* Interleukin 6 plays a key role in the development of antigen-induced arthritis. *Immunology* **95**, 8222–8226 (1998).
  242. Alonzi, T. *et al.* Interleukin 6 is required for the development of collagen-induced arthritis. *J. Exp. Med.* **187**, 461–8 (1998).
  243. Pflanz, S. *et al.* IL-27, a heterodimeric cytokine composed of EBI3 and p28 protein, induces proliferation



- of naive CD4<sup>+</sup>T cells. *Immunity* **16**, 779–790 (2002).
244. Chen, Q. *et al.* Development of Th1-type immune responses requires the type I cytokine receptor TCCR. *Nature* **407**, 916–920 (2000).
  245. Yoshida, H. *et al.* WSX-1 Is Required for the Initiation of Th1 Responses and Resistance to L. major Infection. *Immunity* **15**, 569–578 (2001).
  246. Villarino, A. V *et al.* IL-27 Limits IL-2 Production during Th1 Differentiation. *J. Immunol.* **176**, 237–247 (2006).
  247. Hall, A. O. *et al.* The Cytokines Interleukin 27 and Interferon- $\gamma$  Promote Distinct Treg Cell Populations Required to Limit Infection-Induced Pathology. *Immunity* **37**, 511–523 (2012).
  248. Clement, M. *et al.* Cytomegalovirus-Specific IL-10-Producing CD4<sup>+</sup>T Cells Are Governed by Type-I IFN-Induced IL-27 and Promote Virus Persistence. *PLoS Pathog.* **12**, e1006050 (2016).
  249. Stumhofer, J. S. *et al.* Interleukin 27 negatively regulates the development of interleukin 17-producing T helper cells during chronic inflammation of the central nervous system. *Nat. Immunol.* **7**, 937–945 (2006).
  250. Yoshida, H. & Hunter, C. A. The Immunobiology of Interleukin-27. *Annu. Rev. Immunol.* **33**, 417–443 (2015).
  251. Nowell, M. A. *et al.* Soluble IL-6 Receptor Governs IL-6 Activity in Experimental Arthritis: Blockade of Arthritis Severity by Soluble Glycoprotein 130. *J. Immunol.* **171**, 3202–3209 (2003).
  252. Hirano, T. *et al.* Excessive production of interleukin 6/B cell stimulatory factor-2 in rheumatoid arthritis. *Eur. J. Immunol.* **18**, 1797–1802 (1988).
  253. Thurlings, R. M. *et al.* Synovial lymphoid neogenesis does not define a specific clinical rheumatoid arthritis phenotype. *Arthritis Rheum.* **58**, 1582–1589 (2008).
  254. Lucchesi, D. *et al.* Impaired IL-27 Mediated Control of CD4<sup>+</sup> T Cell Function Impacts on Ectopic Lymphoid Structure Formation in Patients with Sjögren's Syndrome. *Arthritis Rheumatol.* art.41289 (2020).
  255. Cañete, J. D. *et al.* Ectopic lymphoid neogenesis is strongly associated with activation of the IL-23 pathway in rheumatoid synovitis. *Arthritis Res. Ther.* **17**, 173 (2015).
  256. Niedbala, W. *et al.* Interleukin 27 attenuates collagen-induced arthritis. *Ann. Rheum. Dis.* **67**, 1474–1479 (2008).
  257. Shukla, P. *et al.* Interleukin 27 (IL-27) alleviates bone loss in estrogen-deficient conditions by induction of early growth response-2 gene. *J. Biol. Chem.* **292**, 4686–4699 (2017).
  258. Kondo, Y. *et al.* Pre-treatment interleukin-6 levels strongly affect bone erosion progression and repair detected by magnetic resonance imaging in rheumatoid arthritis patients. *Rheumatol. (United Kingdom)* **56**, 1089–1094 (2017).
  259. Kalliolias, G. D., Zhao, B., Triantafyllopoulou, A., Park-Min, K. H. & Ivashkiv, L. B. Interleukin-27 inhibits human osteoclastogenesis by abrogating RANKL-mediated induction of nuclear factor of activated T cells c1 and suppressing proximal RANK signaling. *Arthritis Rheum.* **62**, 402–413 (2010).
  260. Amarasekara, D. S. *et al.* Regulation of osteoclast differentiation by cytokine networks. *Immune Network* **18**, e8 (2018).
  261. Sasaguri, T. *et al.* Interleukin-27 controls basal pain threshold in physiological and pathological conditions. *Sci. Rep.* **8**, 11022 (2018).
  262. Aaltonen, K. J. *et al.* Systematic review and meta-analysis of the efficacy and safety of existing TNF blocking agents in treatment of rheumatoid arthritis. *PLoS ONE* **7**, (2012).
  263. Singh, J. A. *et al.* Tocilizumab for rheumatoid arthritis: a Cochrane systematic review. *J. Rheumatol.* **38**, 10–20 (2011).
  264. Busso, N. & So, A. Mechanisms of inflammation in gout. *Arthritis Research and Therapy* **12**, 206 (2010).
  265. Dinarello, C. A. The IL-1 family of cytokines and receptors in rheumatic diseases. *Nature Reviews Rheumatology* **15**, 612–632 (2019).
  266. Silke, J. The regulation of TNF signalling: What a tangled web we weave. *Current Opinion in Immunology* **23**, 620–626 (2011).
  267. Hayden, M. S. & Ghosh, S. NF- $\kappa$ B, the first quarter-century: Remarkable progress and outstanding questions. *Genes Dev.* **26**, 203–234 (2012).
  268. Cheon, H. J., Yang, J. & Stark, G. R. The functions of signal transducers and activators of transcriptions 1 and 3 as cytokine-inducible proteins. *Journal of Interferon and Cytokine Research* **31**, 33–40 (2011).
  269. Hueber, W. *et al.* Effects of AIN457, a fully human antibody to interleukin-17A, on psoriasis, rheumatoid arthritis, and uveitis. *Sci. Transl. Med.* **2**, 52ra72 (2010).

270. Papp, K. A. *et al.* Brodalumab, an anti-interleukin-17-receptor antibody for psoriasis. *N. Engl. J. Med.* **366**, 1181–1189 (2012).
271. Gandhi, M., Alwawi, E. & Gordon, K. B. Anti-p40 Antibodies Ustekinumab and Briakinumab: Blockade of Interleukin-12 and Interleukin-23 in the Treatment of Psoriasis. *Seminars in Cutaneous Medicine and Surgery* **29**, 48–52 (2010).
272. Hunter, C. A. New IL-12-family members: IL-23 and IL-27, cytokines with divergent functions. *Nature Reviews Immunology* **5**, 521–531 (2005).
273. Burmester, G. R. *et al.* Mavrilimumab, a human monoclonal antibody targeting GM-CSF receptor- $\alpha$ , in subjects with rheumatoid arthritis: A randomised, double-blind, placebo-controlled, phase I, first-in-human study. *Ann. Rheum. Dis.* **70**, 1542–1549 (2011).
274. Guo, Q. *et al.* Rheumatoid arthritis: Pathological mechanisms and modern pharmacologic therapies. *Bone Research* **6**, 15 (2018).
275. Cragg, M. S., Walshe, C. A., Ivanov, A. O. & Glennie, M. J. The biology of CD20 and its potential as a target for mAb therapy. *Current directions in autoimmunity* **8**, 140–174 (2005).
276. Vos, K. *et al.* Early effects of rituximab on the synovial cell infiltrate in patients with rheumatoid arthritis. *Arthritis Rheum.* **56**, 772–778 (2007).
277. Teng, Y. K. O. *et al.* Immunohistochemical analysis as a means to predict responsiveness to rituximab treatment. *Arthritis Rheum.* **56**, 3909–3918 (2007).
278. Isaacs, J. D. *et al.* Effect of baseline rheumatoid factor and anticitrullinated peptide antibody serotype on rituximab clinical response: A meta-analysis. *Ann. Rheum. Dis.* **72**, 329–336 (2013).
279. Tak, P. P. *et al.* Inhibition of joint damage and improved clinical outcomes with rituximab plus methotrexate in early active rheumatoid arthritis: The IMAGE trial. *Ann. Rheum. Dis.* **70**, 39–46 (2011).
280. Chatzidionysiou, K. *et al.* Effectiveness of disease-modifying antirheumatic drug co-therapy with methotrexate and leflunomide in rituximab-treated rheumatoid arthritis patients: Results of a 1-year follow-up study from the CERERRA collaboration. *Ann. Rheum. Dis.* **71**, 374–377 (2012).
281. Kausar, F. *et al.* Ocrelizumab: A step forward in the evolution of B-cell therapy. *Expert Opinion on Biological Therapy* **9**, 889–895 (2009).
282. Goldenberg, D. M., Morschhauser, F. & Wegener, W. A. Veltuzumab (humanized anti-CD20 monoclonal antibody): Characterization, current clinical results, and future prospects. *Leukemia and Lymphoma* **51**, 747–755 (2010).
283. Taylor, P. C. *et al.* Ofatumumab, a fully human anti-CD20 monoclonal antibody, in biological-naïve, rheumatoid arthritis patients with an inadequate response to methotrexate: A randomised, double-blind, placebo-controlled clinical trial. *Ann. Rheum. Dis.* **70**, 2119–2125 (2011).
284. Emery, P. *et al.* Safety with ocrelizumab in rheumatoid arthritis: Results from the ocrelizumab phase III program. *PLoS One* **9**, e87379 (2014).
285. Wallace, D. J. *et al.* Efficacy and safety of epratuzumab in patients with moderate/severe active systemic lupus erythematosus: Results from EMBLEM, a phase IIb, randomised, double-blind, placebo-controlled, multicentre study. *Ann. Rheum. Dis.* **73**, 183–190 (2014).
286. Stohl, W. *et al.* Efficacy and safety of belimumab in patients with rheumatoid arthritis: A phase II, randomized, double-blind, placebo-controlled, dose-ranging study. *J. Rheumatol.* **40**, 579–589 (2013).
287. Tak, P. P. *et al.* Atacicept in patients with rheumatoid arthritis: Results of a multicenter, phase Ib, double-blind, placebo-controlled, dose-escalating, single- and repeated-dose study. *Arthritis Rheum.* **58**, 61–72 (2008).
288. Genovese, M. C., Kinnman, N., De La Bourdonnaye, G., Pena Rossi, C. & Tak, P. P. Atacicept in patients with rheumatoid arthritis and an inadequate response to tumor necrosis factor antagonist therapy: Results of a phase II, randomized, placebo-controlled, dose-finding trial. *Arthritis Rheum.* **63**, 1793–1803 (2011).
289. Genovese, M. C. *et al.* Tabalumab, an anti-BAFF monoclonal antibody, in patients with active rheumatoid arthritis with an inadequate response to TNF inhibitors. *Ann. Rheum. Dis.* **72**, 1461–1468 (2013).
290. Lenschow, D. J. & Bluestone, J. A. T cell co-stimulation and in vivo tolerance. *Curr. Opin. Immunol.* **5**, 747–752 (1993).
291. Buch, M. H. *et al.* Mode of action of abatacept in rheumatoid arthritis patients having failed tumour necrosis factor blockade: a histological, gene expression and dynamic magnetic resonance imaging pilot study. *Ann. Rheum. Dis.* **68**, 1220–1227 (2009).
292. Choy, E. H. Selective modulation of T-cell co-stimulation: A novel mode of action for the treatment of

- rheumatoid arthritis. *Clinical and Experimental Rheumatology* **27**, 510–518 (2009).
293. Remans, P. H. J. *et al.* CTLA-4Ig suppresses reactive oxygen species by preventing synovial adherent cell-induced inactivation of Rap1, a Ras family GTPase mediator of oxidative stress in rheumatoid arthritis T cells. *Arthritis Rheum.* **54**, 3135–3143 (2006).
  294. Álvarez-Quiroga, C. *et al.* CTLA-4-Ig therapy diminishes the frequency but enhances the function of treg cells in patients with rheumatoid arthritis. *J. Clin. Immunol.* **31**, 588–595 (2011).
  295. Platt, A. M. *et al.* Abatacept Limits Breach of Self-Tolerance in a Murine Model of Arthritis via Effects on the Generation of T Follicular Helper Cells. *J. Immunol.* **185**, 1558–1567 (2010).
  296. Choy, E. H. S. *et al.* Repeat-cycle study of high-dose intravenous 4162W94 anti-CD4 humanized monoclonal antibody in rheumatoid arthritis. A randomized placebo-controlled trial. *Rheumatology (Oxford)*. **41**, 1142–8 (2002).
  297. Yocum, D. E. *et al.* Clinical and immunologic effects of a PRIMATIZED anti-CD4 monoclonal antibody in active rheumatoid arthritis: results of a phase I, single dose, dose escalating trial. *J. Rheumatol.* **25**, 1257–62 (1998).
  298. Gizinski, A. M. & Fox, D. A. T cell subsets and their role in the pathogenesis of rheumatic disease. *Current Opinion in Rheumatology* **26**, 204–210 (2014).
  299. Chan, A. C. & Carter, P. J. Therapeutic antibodies for autoimmunity and inflammation. *Nature Reviews Immunology* **10**, 301–316 (2010).
  300. Morgan, M. E. *et al.* Effective treatment of collagen-induced arthritis by adoptive transfer of CD25+ regulatory T cells. *Arthritis Rheum.* **52**, 2212–2221 (2005).
  301. Van Herwijnen, M. J. C. *et al.* Regulatory T cells that recognize a ubiquitous stress-inducible self-antigen are long-lived suppressors of autoimmune arthritis. *Proc. Natl. Acad. Sci. U. S. A.* **109**, 14134–14139 (2012).
  302. Lamba, M. *et al.* Extended-Release Once-Daily Formulation of Tofacitinib: Evaluation of Pharmacokinetics Compared With Immediate-Release Tofacitinib and Impact of Food. *J. Clin. Pharmacol.* **56**, 1362–1371 (2016).
  303. Jones, S. A. & Jenkins, B. J. Recent insights into targeting the IL-6 cytokine family in inflammatory diseases and cancer. *Nature Reviews Immunology* **18**, 773–789 (2018).
  304. Shkhyan, R. *et al.* Drug-induced modulation of gp130 signalling prevents articular cartilage degeneration and promotes repair. *Ann. Rheum. Dis.* **77**, 760–769 (2018).
  305. Sen, M. & Grandis, J. R. Nucleic acid-based approaches to STAT inhibition. *JAK-STAT* **1**, 285–291 (2012).
  306. Miklossy, G., Hilliard, T. S. & Turkson, J. Therapeutic modulators of STAT signalling for human diseases. *Nature Reviews Drug Discovery* **12**, 611–629 (2013).
  307. Toffalini, F. & Demoulin, J. B. New insights into the mechanisms of hematopoietic cell transformation by activated receptor tyrosine kinases. *Blood* **116**, 2429–2437 (2010).
  308. Woodrick, R. S. & Ruderman, E. M. Safety of biologic therapy in rheumatoid arthritis. *Nature Reviews Rheumatology* **7**, 639–652 (2011).
  309. Jones, G. W., Hill, D. G., Sime, K. & Williams, A. S. In vivo models for inflammatory arthritis. *Methods Mol. Biol.* **1725**, 101–118 (2018).
  310. Jones, G. W. *et al.* Loss of CD4<sup>+</sup> T Cell IL-6R Expression during Inflammation Underlines a Role for IL-6 Trans Signaling in the Local Maintenance of Th17 Cells. *J. Immunol.* **184**, 2130–2139 (2010).
  311. Tebbutt, N. C. *et al.* Reciprocal regulation of gastrointestinal homeostasis by SHP2 and STAT-mediated trefoil gene activation in gp130 mutant mice. *Nat. Med.* **8**, 1089–1097 (2002).
  312. Jenkins, B. J. *et al.* Hyperactivation of Stat3 in gp130 mutant mice promotes gastric hyperproliferation and desensitizes TGF- $\beta$  signaling. *Nat. Med.* **11**, 845–852 (2005).
  313. Takeda, K. *et al.* Targeted disruption of the mouse Stat3 gene leads to early embryonic lethality. *Proc. Natl. Acad. Sci.* **94**, 3801–3804 (1997).
  314. Hawkins, P. *et al.* Applying refinement to the use of mice and rats in rheumatoid arthritis research. *Inflammopharmacology* **23**, 131–150 (2015).
  315. Van den Berg, W. B., Joosten, L. A. B. & Van Lent, P. L. E. M. Murine Antigen-Induced Arthritis. in *Arthritis Research: Methods and Protocols Volume 2* (ed. Cope, A. P.) 243–253 (Humana Press, 2007).
  316. Kortylewski, M. *et al.* In vivo delivery of siRNA to immune cells by conjugation to a TLR9 agonist enhances antitumor immune responses. *Nat. Biotechnol.* **27**, 925–32 (2009).
  317. Hyc, A., Osiecka-Iwan, A., Dziunycz, P. & Moskalewski, S. Preparation of rat synovial membrane for studies of cytokine secretion. *Folia Histochem. Cytobiol.* **45**, 57–60 (2007).

318. Inukai, S., Kock, K. H. & Bulyk, M. L. Transcription factor–DNA binding: beyond binding site motifs. *Current Opinion in Genetics and Development* **43**, 110–119 (2017).
319. Khan, A. *et al.* JASPAR 2018: Update of the open-access database of transcription factor binding profiles and its web framework. *Nucleic Acids Res.* **46**, D260–D266 (2018).
320. Mathelier, A. *et al.* JASPAR 2016: A major expansion and update of the open-access database of transcription factor binding profiles. *Nucleic Acids Res.* **44**, D110–D115 (2016).
321. Wasserman, W. W. & Sandelin, A. Applied bioinformatics for the identification of regulatory elements. *Nature Reviews Genetics* **5**, 276–287 (2004).
322. Schmittgen, T. D. & Livak, K. J. Analyzing real-time PCR data by the comparative CT method. *Nat. Protoc.* **3**, 1101–1108 (2008).
323. Livak, K. J. & Schmittgen, T. D. Analysis of relative gene expression data using real-time quantitative PCR and the 2- $\Delta\Delta$ CT method. *Methods* **25**, 402–408 (2001).
324. Schurch, N. J. *et al.* How many biological replicates are needed in an RNA-seq experiment and which differential expression tool should you use? *RNA* **22**, 839–851 (2016).
325. ENCODE. ENCODE Guidelines and Best Practices for RNA-Seq: Revised December 2016. 1–5 (2016). doi:10.1101/044578
326. Sayols, S., Scherzinger, D. & Klein, H. dupRadar: A Bioconductor package for the assessment of PCR artifacts in RNA-Seq data. *BMC Bioinformatics* **17**, 428 (2016).
327. Davies, D. L. & Bouldin, D. W. A Cluster Separation Measure. *IEEE Trans. Pattern Anal. Mach. Intell.* **PAMI-1**, 224–227 (1979).
328. Rousseeuw, P. J. Silhouettes: A graphical aid to the interpretation and validation of cluster analysis. *J. Comput. Appl. Math.* **20**, 53–65 (1987).
329. Tibshirani, R., Walther, G. & Hastie, T. Estimating the number of clusters in a data set via the gap statistic. *J. R. Stat. Soc. Ser. B Stat. Methodol.* **63**, 411–423 (2001).
330. Boulanger, M. J., Chow, D. chone, Brevnova, E. E. & Garcia, K. C. Hexameric structure and assembly of the interleukin-6/IL-6  $\alpha$ -receptor/gp130 complex. *Science (80- )*. **300**, 2101–2104 (2003).
331. Faul, F., Erdfelder, E., Lang, A. G. & Buchner, A. G\*Power 3: A flexible statistical power analysis program for the social, behavioral, and biomedical sciences. in *Behavior Research Methods* **39**, 175–191 (Springer-Verlag, 2007).
332. Arifin, W. N. & Zahiruddin, W. M. Sample size calculation in animal studies using resource equation approach. *Malaysian J. Med. Sci.* **24**, 101–105 (2017).
333. Charan, J. & Kantharia, N. How to calculate sample size in animal studies? *Journal of Pharmacology and Pharmacotherapeutics* **4**, 303–306 (2013).
334. Humby, F. *et al.* Synovial cellular and molecular signatures stratify clinical response to csDMARD therapy and predict radiographic progression in early rheumatoid arthritis patients. *Ann. Rheum. Dis.* **78**, 761–772 (2019).
335. Avalle, L., Pensa, S., Regis, G., Novelli, F. & Poli, V. STAT1 and STAT3 in tumorigenesis. *JAK-STAT* **1**, 65–72 (2012).
336. Yu, H., Pardoll, D. & Jove, R. STATs in cancer inflammation and immunity: A leading role for STAT3. *Nat. Rev. Cancer* **9**, 798–809 (2009).
337. Bromberg, J. Stat proteins and oncogenesis. *Journal of Clinical Investigation* **109**, 1139–1142 (2002).
338. Zhang, H. F. & Lai, R. STAT3 in cancer-friend or foe? *Cancers* **6**, 1408–1440 (2014).
339. Schwartz, D. M., Bonelli, M., Gadina, M. & O'Shea, J. J. Type I/II cytokines, JAKs, and new strategies for treating autoimmune diseases. *Nat. Rev. Rheumatol.* **12**, 25–36 (2016).
340. Akira, S., Uematsu, S. & Takeuchi, O. Pathogen recognition and innate immunity. *Cell* **124**, 783–801 (2006).
341. Zhang, Q. *et al.* Serum-resistant CpG-STAT3 decoy for targeting survival and immune checkpoint signaling in acute myeloid leukemia. *Blood* **127**, 1687–1700 (2016).
342. Zhang, Q. *et al.* STAT3 induces transcription of the DNA methyltransferase 1 gene (DNMT1) in malignant T lymphocytes. *Blood* **108**, 1058–1064 (2006).
343. Krieg, A. M. Toll-like receptor 9 (TLR9) agonists in the treatment of cancer. *Oncogene* **27**, 161–167 (2008).
344. Klinman, D. M., Curie, D., Gursel, I., Verthely & Daniela. Use of CpG oligodeoxynucleotides as immune adjuvants. *Immunol. Rev.* **199**, 201–216 (2004).
345. Kortylewski, M. *et al.* Inhibiting Stat3 signaling in the hematopoietic system elicits multicomponent antitumor immunity. *Nat. Med.* **11**, 1314–1321 (2005).



346. Zhang, Q. *et al.* TLR9-mediated siRNA delivery for targeting of normal and malignant human hematopoietic cells in vivo. *Blood* **121**, 1304 (2013).
347. Iwasaki, A. & Medzhitov, R. Toll-like receptor control of the adaptive immune responses. *Nature Immunology* **5**, 987–995 (2004).
348. Suzuki, K. *et al.* The sensing of environmental stimuli by follicular dendritic cells promotes immunoglobulin A generation in the gut. *Immunity* **33**, 71–83 (2010).
349. Hu, F. *et al.* Toll-like receptors expressed by synovial fibroblasts perpetuate Th1 and Th17 cell responses in rheumatoid arthritis. *PLoS One* **9**, e100266 (2014).
350. Lacerte, P. *et al.* Overexpression of TLR2 and TLR9 on monocyte subsets of active rheumatoid arthritis patients contributes to enhance responsiveness to TLR agonists. *Arthritis Res. Ther.* **18**, 10 (2016).
351. Latz, E. *et al.* TLR9 signals after translocating from the ER to CpG DNA in the lysosome. *Nat. Immunol.* **5**, 190–198 (2004).
352. Samarasinghe, R. *et al.* Induction of an anti-inflammatory cytokine, IL-10, in dendritic cells after toll-like receptor signaling. *J. Interf. Cytokine Res.* **26**, 893–900 (2006).
353. Ham, S. *et al.* Epigenetic analysis in rheumatoid arthritis synoviocytes. *Exp. Mol. Med.* **51**, 22 (2019).
354. Martina, E. *et al.* Tenascin-W is a specific marker of glioma-associated blood vessels and stimulates angiogenesis in vitro. *FASEB J.* **24**, 778–787 (2010).
355. Kubo, A. *et al.* Mutations in SERPINB7, encoding a member of the serine protease inhibitor superfamily, cause nagashima-type palmoplantar keratosis. *Am. J. Hum. Genet.* **93**, 945–956 (2013).
356. McGarry, T. & Fearon, U. Cell metabolism as a potentially targetable pathway in RA. *Nature Reviews Rheumatology* **15**, 70–72 (2019).
357. Bustamante, M. F. *et al.* Hexokinase 2 as a novel selective metabolic target for rheumatoid arthritis. *Ann. Rheum. Dis.* **77**, 1636–1643 (2018).
358. Li, Y. *et al.* Succinate induces synovial angiogenesis in rheumatoid arthritis through metabolic remodeling and HIF-1 $\alpha$ /VEGF axis. *Free Radic. Biol. Med.* **126**, 1–14 (2018).
359. Zeisbrich, M. *et al.* Hypermetabolic macrophages in rheumatoid arthritis and coronary artery disease due to glycogen synthase kinase 3 $\beta$  inactivation. *Ann. Rheum. Dis.* **77**, 1053–1062 (2018).
360. Uzan, B. *et al.* A Critical Role for Adrenomedullin-Calcitonin Receptor-Like Receptor in Regulating Rheumatoid Fibroblast-Like Synoviocyte Apoptosis. *J. Immunol.* **176**, 5548–5558 (2006).
361. Tsujimura, H. *et al.* Toll-Like Receptor 9 Signaling Activates NF- $\kappa$ B through IFN Regulatory Factor-8/IFN Consensus Sequence Binding Protein in Dendritic Cells. *J. Immunol.* **172**, 6820–6827 (2004).
362. Kortylewski, M. *et al.* Toll-like receptor 9 activation of signal transducer and activator of transcription 3 constrains its agonist-based immunotherapy. *Cancer Res.* **69**, 2497–2505 (2009).
363. Zhao, X. *et al.* B Cell Lymphoma Immunotherapy Using TLR9-Targeted Oligonucleotide STAT3 Inhibitors. *Mol. Ther.* **26**, 695–707 (2018).
364. Guo, Y. *et al.* Immune checkpoint inhibitor PD-1 pathway is down-regulated in synovium at various stages of rheumatoid arthritis disease progression. *PLoS One* **13**, e0192704 (2018).
365. Sharma, J. & Larkin, J. Therapeutic implication of SOCS1 modulation in the treatment of autoimmunity and cancer. *Frontiers in Pharmacology* **10**, 324 (2019).
366. Xiao, Y. *et al.* Inhibitory effects of simvastatin on migration and invasion of rheumatoid fibroblast-like synoviocytes by preventing geranylgeranylation of RhoA. *Rheumatol. Int.* **33**, 389–399 (2013).
367. Myouzen, K. *et al.* Functional Variants in NFKBIE and RTKN2 Involved in Activation of the NF- $\kappa$ B Pathway Are Associated with Rheumatoid Arthritis in Japanese. *PLoS Genet.* **8**, e1002949 (2012).
368. Hwang, Y. S., Lee, S. K., Park, K. K. & Chung, W. Y. Secretion of IL-6 and IL-8 from lysophosphatidic acid-stimulated oral squamous cell carcinoma promotes osteoclastogenesis and bone resorption. *Oral Oncol.* **48**, 40–48 (2012).
369. Orosa, B. *et al.* Lysophosphatidic acid receptor inhibition as a new multipronged treatment for rheumatoid arthritis. *Ann. Rheum. Dis.* **73**, 298–305 (2014).
370. Baum, R. & Gravallese, E. M. Bone as a Target Organ in Rheumatic Disease: Impact on Osteoclasts and Osteoblasts. *Clinical Reviews in Allergy and Immunology* **51**, 1–15 (2016).
371. Bernardes, M. *et al.* LRP5 gene polymorphisms and radiographic joint damage in rheumatoid arthritis patients. *Osteoporos. Int.* **29**, 2355–2368 (2018).
372. Wang, H. *et al.* CARD11 blockade suppresses murine collagen-induced arthritis via inhibiting CARD11/Bcl10 assembly and T helper type 17 response. *Clin. Exp. Immunol.* **176**, 238–245 (2014).
373. Koga, T. *et al.* Calcium/Calmodulin-Dependent Kinase IV Facilitates the Recruitment of Interleukin-17–

- Producing Cells to Target Organs Through the CCR6/CCL20 Axis in Th17 Cell–Driven Inflammatory Diseases. *Arthritis Rheumatol.* **68**, 1981–1988 (2016).
374. Costa-Pereira, A. P. *et al.* Mutational switch of an IL-6 response to an interferon- $\gamma$ -like response. *Proc. Natl. Acad. Sci. U. S. A.* **99**, 8043–8047 (2002).
  375. Peters, A. *et al.* IL-27 Induces Th17 Differentiation in the Absence of STAT1 Signaling. *J. Immunol.* **195**, 4144–4153 (2015).
  376. Webster, B. *et al.* Regulation of lymph node vascular growth by dendritic cells. *J. Exp. Med.* **203**, 1903–1913 (2006).
  377. Chyou, S. *et al.* Fibroblast-Type Reticular Stromal Cells Regulate the Lymph Node Vasculature. *J. Immunol.* **181**, 3887–3896 (2008).
  378. Haddad, E. (University of M. STAT3: Too much may be worse than not enough! *Blood* **125**, 583–584 (2015).
  379. Poli, G. *et al.* Identification of a new STAT3 dimerization inhibitor through a pharmacophore-based virtual screening approach. *J. Enzyme Inhib. Med. Chem.* **31**, 1011–1017 (2016).
  380. Kortylewski, M. & Nechaev, S. Cancer therapy using oligonucleotide-based STAT3 inhibitors: Will they deliver? *Therapeutic Delivery* **5**, 239–242 (2014).
  381. Hong, D. *et al.* AZD9150, a next-generation antisense oligonucleotide inhibitor of STAT3 with early evidence of clinical activity in lymphoma and lung cancer. *Sci. Transl. Med.* **7**, 314ra185 (2015).
  382. Klimiuk, P. A. *et al.* Circulating tumour necrosis factor  $\alpha$  and soluble tumour necrosis factor receptors in patients with different patterns of rheumatoid synovitis. *Ann. Rheum. Dis.* **62**, 472–475 (2003).
  383. Passos de Souza, E., Teles Evangelista Segundo, P., Freire José, F., Lemaire, D. & Santiago, M. Rheumatoid arthritis induced by  $\alpha$ -interferon therapy. *Clin. Rheumatol.* **20**, 297–299 (2001).
  384. Crow, M. K., Olfieriev, M. & Kirou, K. A. Type I Interferons in Autoimmune Disease. *Annu. Rev. Pathol. Mech. Dis.* **14**, 369–393 (2019).
  385. Deng, G. M., Nilsson, I. M., Verdrengh, M., Collins, L. V. & Tarkowski, A. Intra-articularly localized bacterial DNA containing CpG motifs induces arthritis. *Nat. Med.* **5**, 702–705 (1999).
  386. Katakura, K. *et al.* Toll-like receptor 9-induced type I IFN protects mice from experimental colitis. *J. Clin. Invest.* **115**, 695–702 (2005).
  387. Chang, X. & Wei, C. Glycolysis and rheumatoid arthritis. *International Journal of Rheumatic Diseases* **14**, 217–222 (2011).
  388. Zhou, J. *et al.* Exploration of the serum metabolite signature in patients with rheumatoid arthritis using gas chromatography–mass spectrometry. *J. Pharm. Biomed. Anal.* **127**, 60–67 (2016).
  389. Haas, R. *et al.* Lactate regulates metabolic and proinflammatory circuits in control of T cell migration and effector functions. *PLoS Biol.* **13**, e1002202 (2015).
  390. Tripathi, S. K. *et al.* Genome-wide Analysis of STAT3-Mediated Transcription during Early Human Th17 Cell Differentiation. *Cell Rep.* **19**, 1888–1901 (2017).
  391. Van Der Vlist, M., Kuball, J., Radstake, T. R. D. & Meyaard, L. Immune checkpoints and rheumatic diseases: What can cancer immunotherapy teach us? *Nature Reviews Rheumatology* **12**, 593–604 (2016).
  392. Hossain, D. M. S. *et al.* Leukemia cell-targeted STAT3 silencing and TLR9 triggering generate systemic antitumor immunity. *Blood* **123**, 15–25 (2014).
  393. Teague, T. K. *et al.* Activation-induced inhibition of interleukin 6-mediated T cell survival and signal transducer and activator of transcription 1 signaling. *J. Exp. Med.* **191**, 915–925 (2000).
  394. Neufert, C. *et al.* IL-27 controls the development of inducible regulatory T cells and Th17 cells via differential effects on STAT1. *Eur. J. Immunol.* **37**, 1809–1816 (2007).
  395. Villarino, A. V., Gallo, E. & Abbas, A. K. STAT1-Activating Cytokines Limit Th17 Responses through Both T-bet–Dependent and –Independent Mechanisms. *J. Immunol.* **185**, 6461–6471 (2010).
  396. Timmer, T. C. G. *et al.* Inflammation and ectopic lymphoid structures in rheumatoid arthritis synovial tissues dissected by genomics technology: Identification of the interleukin-7 signaling pathway in tissues with lymphoid neogenesis. *Arthritis Rheum.* **56**, 2492–2502 (2007).
  397. Bugatti, S. *et al.* High expression levels of the B cell chemoattractant CXCL13 in rheumatoid synovium are a marker of severe disease. *Rheumatol. (United Kingdom)* **53**, 1886–1895 (2014).
  398. Kim, K. E. *et al.* Therapeutic effect of erythroid differentiation regulator 1 (Erdr1) on collagen-induced arthritis in DBA/1J mouse. *Oncotarget* **7**, 76354–76361 (2016).
  399. Yoshimura, A., Nishinakamura, H., Matsumura, Y. & Hanada, T. Negative regulation of cytokine signaling

- and immune responses by SOCS proteins. *Arthritis Res. Ther.* **7**, 100–10 (2005).
400. Malemud, C. J. Negative regulators of JAK/STAT signaling in rheumatoid arthritis and osteoarthritis. *International Journal of Molecular Sciences* **18**, 484 (2017).
  401. Krebs, D. L. & Hilton, D. J. SOCS proteins: negative regulators of cytokine signaling. *Stem Cells* **19**, 378–387 (2001).
  402. Toshikuni, N., Arisawa, T. & Tsutsumi, M. Hepatitis C-related liver cirrhosis - strategies for the prevention of hepatic decompensation, hepatocarcinogenesis, and mortality. *World J. Gastroenterol.* **20**, 2876–2887 (2014).
  403. Goossens, N. & Hoshida, Y. Hepatitis C virus-induced hepatocellular carcinoma. *Clinical and molecular hepatology* **21**, 105–114 (2015).
  404. Deutsch, M., Papadopoulos, N., Hadziyannis, E. & Koskinas, J. Clinical characteristics, spontaneous clearance and treatment outcome of acute hepatitis C: A single tertiary center experience. *Saudi J. Gastroenterol.* **19**, 81–85 (2013).
  405. Yoshimura, A., Suzuki, M., Sakaguchi, R., Hanada, T. & Yasukawa, H. SOCS, inflammation, and autoimmunity. *Frontiers in Immunology* **3**, 20 (2012).
  406. Collins, A. S. *et al.* Hepatitis C virus (HCV)-induced suppressor of cytokine signaling (SOCS) 3 regulates proinflammatory TNF- responses. *J. Leukoc. Biol.* **96**, 255–263 (2014).
  407. Convery, O. *et al.* The hepatitis C virus (HCV) protein, p7, suppresses inflammatory responses to tumor necrosis factor (TNF)- $\alpha$  via signal transducer and activator of transcription (STAT)3 and extracellular signal-regulated kinase (ERK)-mediated induction of suppressor of cy. *FASEB J.* **33**, 8732–8744 (2019).
  408. Bentham, M. J., Foster, T. L., McCormick, C. & Griffin, S. Mutations in hepatitis C virus p7 reduce both the egress and infectivity of assembled particles via impaired proton channel function. *J. Gen. Virol.* **94**, 2236–2248 (2013).
  409. Atsumi, T. *et al.* A point mutation of Tyr-759 in interleukin 6 family cytokine receptor subunit gp130 causes autoimmune arthritis. *J. Exp. Med.* **196**, 979–990 (2002).
  410. Byrnes, A. P., Rusby, J. E., Wood, M. J. A. & Charlton, H. M. Adenovirus gene transfer causes inflammation in the brain. *Neuroscience* **66**, 1015–1024 (1995).
  411. Varley, A. W., Coulthard, M. G., Meidell, R. S., Gerard, R. D. & Munford, R. S. Inflammation-induced recombinant protein expression in vivo using promoters from acute-phase protein genes. *Proc. Natl. Acad. Sci. U. S. A.* **92**, 5346–5350 (1995).
  412. Chen, Z. *et al.* Selective regulatory function of Socs3 in the formation of IL-17-secreting T cells. *Proc. Natl. Acad. Sci. U. S. A.* **103**, 8137–8142 (2006).
  413. Yadav, A., Kalita, A., Dhillon, S. & Banerjee, K. JAK/STAT3 pathway is involved in survival of neurons in response to insulin-like growth factor and negatively regulated by suppressor of cytokine signaling-3. *J. Biol. Chem.* **280**, 31830–31840 (2005).
  414. Camporeale, A. & Poli, V. IL-6, IL-17 and STAT3: A holy trinity in auto-immunity? *Front. Biosci.* **17**, 2306–2326 (2011).
  415. Ivanov, I. I. *et al.* The Orphan Nuclear Receptor ROR $\gamma$ t Directs the Differentiation Program of Proinflammatory IL-17+ T Helper Cells. *Cell* **126**, 1121–1133 (2006).
  416. Liu, S. M. & King, C. IL-21–Producing Th Cells in Immunity and Autoimmunity. *J. Immunol.* **191**, 3501–3506 (2013).
  417. Wu, H. *et al.* An Inhibitory Role for the Transcription Factor Stat3 in Controlling IL-4 and Bcl6 Expression in Follicular Helper T Cells. *J. Immunol.* **195**, 2080–2089 (2015).
  418. Scheller, J., Garbers, C. & Rose-John, S. Interleukin-6: From basic biology to selective blockade of pro-inflammatory activities. *Semin. Immunol.* **26**, 2–12 (2014).
  419. Lang, V. R. *et al.* Risk of infections in rheumatoid arthritis patients treated with tocilizumab. *Rheumatology* **51**, 852–857 (2012).
  420. Garbers, C. *et al.* Inhibition of classic signaling is a novel function of soluble glycoprotein 130 (sgp130), which is controlled by the ratio of interleukin 6 and soluble interleukin 6 receptor. *J. Biol. Chem.* **286**, 42959–42970 (2011).
  421. Hoge, J. *et al.* IL-6 Controls the Innate Immune Response against *Listeria monocytogenes* via Classical IL-6 Signaling. *J. Immunol.* **190**, 703–711 (2013).
  422. Sommer, J. *et al.* Alternative intronic polyadenylation generates the interleukin-6 trans-signaling inhibitor sgp130-E10. *J. Biol. Chem.* **289**, 22140–22150 (2014).
  423. Lin, M., Rose-John, S., Grötzinger, J., Conrad, U. & Scheller, J. Functional expression of a biologically

- active fragment of soluble gp130 as an ELP-fusion protein in transgenic plants: Purification via inverse transition cycling. *Biochem. J.* **398**, 577–583 (2006).
424. Adams, R. *et al.* Discovery of a junctional epitope antibody that stabilizes IL-6 and gp80 protein:protein interaction and modulates its downstream signaling. *Sci. Rep.* **7**, 37716 (2017).
  425. Li, Z. *et al.* Influence of molecular size on tissue distribution of antibody fragments. *MAbs* **8**, 113–119 (2016).
  426. Harris, T. J. *et al.* Cutting Edge: An In Vivo Requirement for STAT3 Signaling in TH17 Development and TH17-Dependent Autoimmunity. *J. Immunol.* **179**, 4313–4317 (2007).
  427. Nurieva, R. *et al.* Essential autocrine regulation by IL-21 in the generation of inflammatory T cells. *Nature* **448**, 480–483 (2007).
  428. Tenhumberg, S. *et al.* Structure-guided optimization of the interleukin-6 trans-signaling antagonist sgp130. *J. Biol. Chem.* **283**, 27200–27207 (2008).
  429. Luo, J. *et al.* IL-2 inhibition of Th17 generation rather than induction of treg cells is impaired in primary Sjögren's syndrome patients. *Front. Immunol.* **9**, 1–9 (2018).
  430. Liu, H. & Rohowsky-Kochan, C. Interleukin-27-mediated suppression of human Th17 cells is associated with activation of STAT1 and suppressor of cytokine signaling protein 1. *J. Interf. Cytokine Res.* **31**, 459–469 (2011).
  431. Zhang, J. G. *et al.* Identification and characterization of two distinct truncated forms of gp130 and a soluble form of leukemia inhibitory factor receptor  $\alpha$ -chain in normal human urine and plasma. *J. Biol. Chem.* **273**, 10798–10805 (1998).
  432. Tanaka, M. *et al.* Cloning of novel soluble gp130 and detection of its neutralizing autoantibodies in rheumatoid arthritis. *J. Clin. Invest.* **106**, 137–144 (2000).
  433. Narazaki, M. *et al.* Soluble forms of the interleukin-6 signal-transducing receptor component gp130 in human serum possessing a potential to inhibit signals through membrane-anchored gp130. *Blood* **82**, 1120–1126 (1993).
  434. Fujimoto, M., Serada, S. & Naka, T. [Role of IL-6 in the development and pathogenesis of CIA and EAE]. *Nihon Rinsho Meneki. Gakkai Kaishi* **31**, 78–84 (2008).
  435. Miossec, P. & Kolls, J. K. Targeting IL-17 and T H 17 cells in chronic inflammation. *Nature Reviews Drug Discovery* **11**, 763–776 (2012).
  436. Matesanz-Isabel, J. *et al.* New B-cell CD molecules. *Immunol. Lett.* **134**, 104–112 (2011).
  437. Kennedy J, Vicari AP, Saylor V, Zurawski SM, Copeland NG, Gilbert DJ, Jenkins NA, Z. *et al.* A molecular analysis of NKT cells: identification of a class-I restricted T cell-associated molecule (CRTAM). *J. Leukoc. Biol.* **67**, 725–734 (2000).
  438. Arase, N. *et al.* Heterotypic interaction of CRTAM with Nect2 induces cell adhesion on activated NK cells and CD8+ T cells. *Int. Immunol.* **17**, 1227–1237 (2005).
  439. Boles, K. S., Barchet, W., Diacovo, T., Cella, M. & Colonna, M. The tumor suppressor TSLC1/NECL-2 triggers NK-cell and CD8+ T-cell responses through the cell-surface receptor CRTAM. *Blood* **106**, 779–786 (2005).
  440. Chan, C. J., Andrews, D. M. & Smyth, M. J. Receptors that interact with nectin and nectin-like proteins in the immunosurveillance and immunotherapy of cancer. *Current Opinion in Immunology* **24**, 246–251 (2012).
  441. Patiño-Lopez, G. *et al.* Human class-I restricted T cell associated molecule is highly expressed in the cerebellum and is a marker for activated NKT and CD8+ T lymphocytes. *J. Neuroimmunol.* **171**, 145–155 (2006).
  442. Galibert, L. *et al.* Nectin-like protein 2 defines a subset of T-cell zone dendritic cells and is a ligand for Class-I-restricted T-cell-associated molecule. *J. Biol. Chem.* **280**, 21955–21964 (2005).
  443. Valle-Rios, R. *et al.* Characterization of CRTAM gene promoter: AP-1 transcription factor control its expression in human T CD8 lymphocytes. *Mol. Immunol.* **46**, 3379–3387 (2009).
  444. Garay, E. *et al.* CRTAM: A molecule involved in epithelial cell adhesion. *J. Cell. Biochem.* **111**, 111–122 (2010).
  445. Zhang, S. *et al.* Competition of cell adhesion and immune recognition: Insights into the interaction between CRTAM and nectin-like 2. *Structure* **21**, 1430–1439 (2013).
  446. Takai, Y., Miyoshi, J., Ikeda, W. & Ogita, H. Nectins and nectin-like molecules: Roles in contact inhibition of cell movement and proliferation. *Nature Reviews Molecular Cell Biology* **9**, 603–615 (2008).
  447. Takeuchi, A. *et al.* CRTAM confers late-stage activation of CD8+ T cells to regulate retention within lymph



- node. *J. Immunol.* **183**, 4220–4228 (2009).
448. Takeuchi, A. *et al.* CRTAM determines the CD4 + cytotoxic T lymphocyte lineage. *J. Exp. Med.* **213**, 123–138 (2016).
  449. Yeh, J. H., Sidhu, S. S. & Chan, A. C. Regulation of a Late Phase of T Cell Polarity and Effector Functions by Crtam. *Cell* **132**, 846–859 (2008).
  450. Takeuchi, A. & Saito, T. CD4 CTL, a cytotoxic subset of CD4+ T cells, their differentiation and function. *Front. Immunol.* **8**, 194 (2017).
  451. Beristain-Covarrubias, N. *et al.* Class I-Restricted T Cell-Associated Molecule Is a Marker for IFN- $\gamma$ -Producing iNKT Cells in Healthy Subjects and Patients with Type 1 Diabetes. *J. Interf. Cytokine Res.* **37**, 39–49 (2017).
  452. Serrano, C. *et al.* Compartmentalized Response of IL-6/STAT3 Signaling in the Colonic Mucosa Mediates Colitis Development. *J. Immunol.* **202**, 1239–1249 (2019).
  453. Cortez, V. S. *et al.* CRTAM controls residency of gut CD4+CD8+ T cells in the steady state and maintenance of gut CD4+ Th17 during parasitic infection. *J. Exp. Med.* **211**, 623–33 (2014).
  454. Krause, A., Scaletta, N., Ji, J.-D., Ivashkiv, L. B. & Ivashkiv, L. B. Rheumatoid arthritis synoviocyte survival is dependent on Stat3. *J. Immunol.* **169**, 6610–6616 (2002).
  455. Rojas-Marquez, C., Valle-Rios, R., Lopez-Bayghen, E. & Ortiz-Navarrete, V. CRTAM is negatively regulated by ZEB1 in T cells. *Mol. Immunol.* **66**, 290–8 (2015).
  456. Chen, D. *et al.* Osteoarthritis: toward a comprehensive understanding of pathological mechanism. *Bone Res.* **5**, 16044 (2017).
  457. Orlowsky, E. W. & Kraus, V. B. The role of innate immunity in osteoarthritis: When our first line of defense goes on the offensive. *Journal of Rheumatology* **42**, 363–371 (2015).
  458. Maffia, P. *et al.* Inducing Experimental Arthritis and Breaking Self-Tolerance to Joint-Specific Antigens with Trackable, Ovalbumin-Specific T Cells. *J. Immunol.* **173**, 151–156 (2004).
  459. Alshekaili, J. *et al.* STAT3 regulates cytotoxicity of human CD57+ CD4+ T cells in blood and lymphoid follicles. *Sci. Rep.* **8**, 3529 (2018).
  460. Penatti, A. *et al.* Differences in serum and synovial CD4+ T cells and cytokine profiles to stratify patients with inflammatory osteoarthritis and rheumatoid arthritis. *Arthritis Res. Ther.* **19**, 103 (2017).
  461. O'Shea, J. J. & Gadina, M. Selective Janus kinase inhibitors come of age. *Nat. Rev. Rheumatol.* **15**, 74–75 (2019).
  462. Garbers, C., Aparicio-Siegmund, S. & Rose-John, S. The IL-6/gp130/STAT3 signaling axis: Recent advances towards specific inhibition. *Current Opinion in Immunology* **34**, 75–82 (2015).
  463. Chen, Z., Bozec, A., Ramming, A. & Schett, G. Anti-inflammatory and immune-regulatory cytokines in rheumatoid arthritis. *Nature Reviews Rheumatology* **15**, 9–17 (2019).
  464. Haschka, J. *et al.* Relapse rates in patients with rheumatoid arthritis in stable remission tapering or stopping antirheumatic therapy: Interim results from the prospective randomised controlled RETRO study. *Ann. Rheum. Dis.* **75**, 45–51 (2016).
  465. Schett, G., Elewaut, D., McInnes, I. B., Dayer, J. & Neurath, M. F. How Cytokine Networks Fuel Inflammation: Toward a cytokine-based disease taxonomy. *Nat. Med.* **19**, 822–826 (2013).
  466. Baran, P. *et al.* The balance of interleukin (IL)-6, IL-6soluble IL-6 receptor (sIL-6R), and IL-6sIL-6Rsgp130 complexes allows simultaneous classic and trans-signaling. *J. Biol. Chem.* **293**, 6762–6775 (2018).
  467. Barkhausen, T. *et al.* Selective blockade of interleukin-6 trans-signaling improves survival in a murine polymicrobial sepsis model. *Crit. Care Med.* **39**, 1407–1413 (2011).
  468. Grivennikov, S. *et al.* IL-6 and Stat3 Are Required for Survival of Intestinal Epithelial Cells and Development of Colitis-Associated Cancer. *Cancer Cell* **15**, 103–113 (2009).
  469. Spehlmann, M. E. *et al.* Trp53 Deficiency Protects against Acute Intestinal Inflammation. *J. Immunol.* **191**, 837–847 (2013).
  470. Burmester, G. R. *et al.* Adalimumab long-term safety: Infections, vaccination response and pregnancy outcomes in patients with rheumatoid arthritis. *Ann. Rheum. Dis.* **76**, 414–417 (2017).
  471. Robertson, J., Peters, M. J., McInnes, I. B. & Sattar, N. Changes in lipid levels with inflammation and therapy in RA: A maturing paradigm. *Nature Reviews Rheumatology* **9**, 513–523 (2013).
  472. Winthrop, K. L. The emerging safety profile of JAK inhibitors in rheumatic disease. *Nature Reviews Rheumatology* **13**, 234–243 (2017).
  473. Gabay, C. *et al.* Comparison of lipid and lipid-associated cardiovascular risk marker changes after treatment with tocilizumab or adalimumab in patients with rheumatoid arthritis. *Ann. Rheum. Dis.* **75**,

- 1806–1812 (2016).
474. Conaghan, P. G. *et al.* Comparing the effects of tofacitinib, methotrexate and the combination, on bone marrow oedema, synovitis and bone erosion in methotrexate-naïve, early active rheumatoid arthritis: Results of an exploratory randomised MRI study incorporating semiquantitative. *Ann. Rheum. Dis.* **75**, 1024–1033 (2016).
  475. Liu, X., Jones, G. W., Choy, E. H. & Jones, S. A. The biology behind interleukin-6 targeted interventions. *Curr. Opin. Rheumatol.* (2016). doi:10.1097/BOR.0000000000000255
  476. Rioja, I. *et al.* Potential novel biomarkers of disease activity in rheumatoid arthritis patients: CXCL13, CCL23, transforming growth factor  $\alpha$ , tumor necrosis factor receptor superfamily member 9, and macrophage colony-stimulating factor. *Arthritis Rheum.* **58**, 2257–2267 (2008).
  477. Manzo, A. *et al.* Mature antigen-experienced T helper cells synthesize and secrete the B cell chemoattractant CXCL13 in the inflammatory environment of the rheumatoid joint. *Arthritis Rheum.* **58**, 3377–3387 (2008).
  478. Kazanietz, M. G., Durando, M. & Cooke, M. CXCL13 and its receptor CXCR5 in cancer: Inflammation, immune response, and beyond. *Frontiers in Endocrinology* **10**, 471 (2019).
  479. Okada, Y. *et al.* Genetics of rheumatoid arthritis contributes to biology and drug discovery. *Nature* **506**, 376–381 (2014).
  480. Klaasen, R. *et al.* The relationship between synovial lymphocyte aggregates and the clinical response to infliximab in rheumatoid arthritis: A prospective study. *Arthritis Rheum.* **60**, 3217–3224 (2009).
  481. Stephenson, W. *et al.* Single-cell RNA-seq of rheumatoid arthritis synovial tissue using low-cost microfluidic instrumentation. *Nat. Commun.* **9**, (2018).